



# Iterative Decoding and Detection for Physical Layer Network Coding

Alaa Abdulameer Saeed Al-Rubaie

---

A thesis submitted to the School of Electrical and Electronic  
Engineering in partial fulfilment of the requirements for the degree of

*Doctor of Philosophy*

---

Newcastle University

United Kingdom

April 2015

---

## Declaration

I declare that this thesis is my own work and it has not been previously submitted, either by me or by anyone else, for a degree or diploma at any educational institute, school or university. To the best of my knowledge, this thesis does not contain any previously published work, except where another person's work used has been cited and included in the list of references.

Alaa Abdulameer Saeed Al-Rubaie

I dedicate this thesis to my precious wife and children, Abdullah, Ranya and Dalya, who have supported me throughout the years of my study.

# Acknowledgements

Foremost, my thanks go to the almighty **Allah** for his graces at every stage of my life.

It has been my privilege to work closely with my supervision team, Dr. Charalampos Tsimenidis, Dr. Martin Johnston, and Prof. Bayan Sharif. I have enjoyed the opportunity to watch and learn from their knowledge and experience. Their frequent insights and patience with me are always appreciated. Their guidance helped me throughout the period of research. I am very proud of what we have achieved together, and I really owe my deepest gratitude and appreciation to them, thank you all. I am also grateful to Prof. Said Boussakta for his help and encouragement.

Gratefulness and gratitude go to my parents, who deserve far more credit than I can ever give them. I am grateful to them from the bottom of my heart for everything they have given me throughout my life. I would also like to show my gratitude to my brother, Walaa, and my sisters, Lamyaa and Lykaa, for their moral support.

Lastly, I would like to thank my sponsor *the Iraqi Ministry of Higher Education and Scientific Research*. My deep thanks to the Department of Ages and Projects for offering me this great study opportunity. It is a pleasure to thank all my colleagues in the Engineering Section.

# Abstract

Wireless networks comprising multiple relays are very common and it is important that all users are able to exchange messages via relays in the shortest possible time. A promising technique to achieve this is physical layer network coding (PNC), where the time taken to exchange messages between users is achieved by exploiting the interference at the relay due to the multiple incoming signals from the users. At the relay, the interference is demapped to a binary sequence representing the exclusive-OR of both users' messages. The time to exchange messages is reduced because the relay broadcasts the network coded message to both users, who can then acquire the desired message by applying the exclusive-OR of their original message with the network coded message. However, although PNC can increase throughput it is at the expense of performance degradation due to errors resulting from the demapping of the interference to bits.

A number of papers in the literature have investigated PNC with an iterative channel coding scheme in order to improve performance. However, in this thesis the performance of PNC is investigated for end-to-end (E2E) the three most common iterative coding schemes: turbo codes, low-density parity-check (LDPC) codes and trellis bit-interleaved coded modulation with iterative decoding (BICM-ID). It is well known that in most scenarios turbo and LDPC codes perform similarly and can achieve near-Shannon limit performance, whereas BICM-ID does not perform quite as well but has a lower complexity. However, the results in this thesis show that on a two-way relay channel (TWRC) employing PNC, LDPC codes do not perform well and BICM-ID actually outperforms them while also performing comparably with turbo codes. Also presented in this thesis is an extrinsic information transfer (ExIT) chart analysis of the iterative decoders for each coding scheme, which is used

to explain this surprising result. Another problem arising from the use of PNC is the transfer of reliable information from the received signal at the relay to the destination nodes. The demapping of the interference to binary bits means that reliability information about the received signal is lost and this results in a significant degradation in performance when applying soft-decision decoding at the destination nodes. This thesis proposes the use of traditional angle modulation (frequency modulation (FM) and phase modulation (PM)) when broadcasting from the relay, where the real and imaginary parts of the complex received symbols at the relay modulate the frequency or phase of a carrier signal, while maintaining a constant envelope. This is important since the complex received values at the relay are more likely to be centred around zero and it undesirable to transmit long sequences of low values due to potential synchronisation problems at the destination nodes. Furthermore, the complex received values, obtained after angle demodulation, are used to derive more reliable log-likelihood ratios (LLRs) of the received symbols at the destination nodes and consequently improve the performance of the iterative decoders for each coding scheme compared with conventionally coded PNC.

This thesis makes several important contributions: investigating the performance of different iterative channel coding schemes combined with PNC, presenting an analysis of the behaviour of different iterative decoding algorithms when PNC is employed using EXIT charts, and proposing the use of angle modulation at the relay to transfer reliable information to the destination nodes to improve the performance of the iterative decoding algorithms. The results from this thesis will also be useful for future research projects in the areas of PNC that are currently being addressed, such as synchronisation techniques and receiver design.

# Contents

<b>Nomenclature</b>	<b>xvii</b>
<b>List of Symbols</b>	<b>xx</b>
<b>1 Introduction</b>	<b>1</b>
1.1 Background . . . . .	2
1.2 Challenges and Motivation . . . . .	2
1.3 Literature Review . . . . .	3
1.3.1 Overview . . . . .	3
1.3.2 Classification . . . . .	4
1.3.3 Relay Network . . . . .	6
1.3.4 Error Detection and Correction . . . . .	7
1.3.5 Iterative Decoding . . . . .	8
1.3.6 Joint PNC and Error Correction Coding . . . . .	8
1.3.7 PNC and ExIT Chart Analysis . . . . .	9
1.3.8 PNC and the Modulation Technique . . . . .	10
1.4 Research Contribution and Publications . . . . .	11
1.4.1 Related publications . . . . .	12
1.5 Organization of the Thesis . . . . .	12
<b>2 Theoretical Background and System Model</b>	<b>14</b>
2.1 Introduction . . . . .	15
2.2 Two Way Communication Systems . . . . .	15
2.2.1 Cooperative Communication Systems . . . . .	15
2.2.2 Two Way Relay Channels . . . . .	16
2.2.3 Relaying Schemes . . . . .	17
2.2.3.1 Decode and Forward . . . . .	17

2.2.3.2	Amplify and Forward . . . . .	17
2.2.3.3	Estimate and Forward . . . . .	18
2.2.4	Physical Layer Network Coding . . . . .	18
2.3	Bandpass Signals and Systems Representation . . . . .	19
2.3.1	Baseband Equivalent of Bandpass Signals . . . . .	19
2.3.2	Baseband Equivalent of Bandpass Systems . . . . .	20
2.4	A Measure of Information . . . . .	22
2.4.1	Entropy . . . . .	22
2.4.2	Mutual Information . . . . .	23
2.4.2.1	Mutual Information for Real-Values . . . . .	24
2.4.2.2	Mutual Information for Complex-Values . . . . .	25
2.5	System Model . . . . .	26
2.5.1	Transmitter . . . . .	27
2.5.2	Channel Model and Characterization . . . . .	29
2.5.3	The Relay . . . . .	30
2.5.3.1	Consideration of Noise . . . . .	35
2.5.3.2	Consideration of Rayleigh flat-Fading Channels . . . . .	37
2.5.4	The Receiver . . . . .	39
2.5.5	Simulation Results . . . . .	40
2.6	Chapter Summary . . . . .	42
<b>3 Error Control Coding and Iterative Decoding Schemes Combined</b>		
<b>with E2E PNC</b>		<b>43</b>
3.1	Introduction . . . . .	44
3.2	Convolutional Codes . . . . .	44
3.2.1	Convolutional Encoder Structure . . . . .	45
3.2.2	Representation of Convolutional Code . . . . .	45
3.2.3	BCJR Decoding Algorithm . . . . .	47
3.2.4	BCJR Algorithm in Logarithm Domain . . . . .	49
3.3	Bit-Interleaved Coded Modulation with Iterative Decoding . . . . .	50
3.3.1	BICM Encoder Structure . . . . .	52
3.3.2	Iterative Demapper and Decoder Structure . . . . .	52
3.4	Turbo Code . . . . .	52
3.4.1	Turbo Encoder Structure . . . . .	53

3.4.2	Turbo Decoder Structure . . . . .	54
3.5	Low-Density Parity-Check Code . . . . .	55
3.5.1	Tanner Graph . . . . .	56
3.5.2	Quasi-cyclic codes . . . . .	56
3.5.3	Repeat-accumulate codes . . . . .	57
3.5.4	The Sum-Product Algorithm . . . . .	58
3.6	Channel Coding with Physical Layer Network Coding . . . . .	61
3.6.1	BICM-ID with PNC . . . . .	62
3.6.2	Turbo Codes with PNC . . . . .	63
3.6.3	LDPC codes with PNC . . . . .	63
3.7	Simulation Results and Discussions . . . . .	65
3.8	Chapter Summary . . . . .	77
<b>4</b>	<b>ExIT Chart Analysis of Iterative Decoding Schemes with E2E PNC</b>	<b>79</b>
4.1	Introduction . . . . .	80
4.2	Extrinsic Information Transfer Charts . . . . .	81
4.2.1	The Gaussian Approximation . . . . .	81
4.2.2	Mutual Information . . . . .	82
4.3	ExIT Charts Construction and Properties . . . . .	84
4.3.1	ExIT Charts for BICM-ID Code with PNC . . . . .	84
4.3.2	ExIT Charts for LDPC Code with PNC . . . . .	87
4.3.3	ExIT Charts for Turbo Code with PNC . . . . .	92
4.4	Iterative Decoder Behaviour with E2E PNC . . . . .	94
4.4.1	Analysis for BICM-ID Code with PNC . . . . .	98
4.4.2	Analysis for LDPC Code with PNC . . . . .	100
4.4.3	Analysis for Turbo Code with PNC . . . . .	103
4.5	Summary . . . . .	106
<b>5</b>	<b>Constant Envelope PNC Angle Modulation</b>	<b>107</b>
5.1	Introduction . . . . .	108
5.2	Angle Modulation . . . . .	108
5.2.1	Frequency Modulation . . . . .	110
5.2.2	Phase Modulation . . . . .	111
5.3	Analytic Technique . . . . .	112

5.3.1	Fourier Transform . . . . .	113
5.3.2	Hilbert Transform . . . . .	113
5.4	Joint Constant Envelope Technique and PNC . . . . .	114
5.4.1	CE-PNC System Model . . . . .	114
5.4.2	Transmitter and Signal Structures . . . . .	115
5.4.3	CE-PNC Relay Structure . . . . .	116
5.4.3.1	Passband Quadrature Modulation Schemes . . . . .	116
5.4.3.2	Constant Envelope Scheme . . . . .	118
5.4.4	The Structure of CE-PNC Receiver and Signal Detection Tech- niques . . . . .	118
5.4.4.1	Effect of Noise on Angle Modulation . . . . .	120
5.4.4.2	Hilbert Transform Based Demodulation . . . . .	124
5.4.4.3	Passband Quadrature Demodulation Schemes . . . . .	127
5.4.4.4	Decoding Process . . . . .	128
5.5	Systems performance . . . . .	129
5.5.1	Simulation Setup . . . . .	129
5.5.2	Simulation Study . . . . .	130
5.5.3	Simulation Results . . . . .	139
5.6	Chapter Summary . . . . .	146
<b>6</b>	<b>Concluding Remarks</b>	<b>148</b>
<b>A</b>	<b>Soft Demapping of 9-Point Constellation at the Relay with LLRs</b>	<b>152</b>
<b>B</b>	<b>The Signal Power and Symbol Energy</b>	<b>156</b>
	<b>References</b>	<b>159</b>

# List of Figures

1.1	Transmission Schemes . . . . .	5
2.1	Cooperative communication system. . . . .	16
2.2	The relationship between a bandpass spectrum and its baseband equivalent. . . . .	20
2.3	Implementation the equivalent complex baseband system. . . . .	21
2.4	Relationship between mutual information and entropy. . . . .	24
2.5	The model of PNC technique. . . . .	27
2.6	PNC system structure. . . . .	28
2.7	QPSK mapping. . . . .	29
2.8	Rayleigh flat-fading channel. . . . .	31
2.9	The constellation point at the relay without noise. . . . .	33
2.10	The constellation point of the relay mapping to produce $\tilde{\mathbf{s}}_R$ . . . . .	34
2.11	BER performance for PNC system . . . . .	41
2.12	The throughput measurement for PNC and single user systems. . . . .	42
3.1	Encoder structures for non-systematic and recursive systematic with octal generators. . . . .	46
3.2	An example to illustrate the convolutional code with its state and trellis diagrams. . . . .	47
3.3	Structure of BICM-ID System. . . . .	51
3.4	Simulated performance of BICM-ID code for various numbers of decoder iterations. . . . .	53
3.5	The structure of a turbo encoder. . . . .	54
3.6	Turbo decoder schematic. . . . .	55
3.7	Simulated performance of turbo code for various numbers of decoder iterations. . . . .	55

3.8	Block diagram of RA encoder. . . . .	58
3.9	Tanner graph for H in equation (3.20). . . . .	58
3.10	Tanner graph for RA code in equation (3.25). . . . .	59
3.11	Simulated performance of LDPC code for various numbers of decoder iterations. . . . .	61
3.12	PNC Systems Employing BICM-ID Code. . . . .	63
3.13	PNC System Employing Turbo code. . . . .	64
3.14	PNC Systems Employing LDPC Code. . . . .	65
3.15	The performance of systems with code length 576 and code rate 1/2 on the AWGN channel. . . . .	67
3.16	The performance of systems with code length 2304 and code rate 1/2 on the AWGN channel. . . . .	67
3.17	The performance of systems with code length 64800 and code rate 1/2 on the AWGN channel. . . . .	68
3.18	The performance of systems with code length 576 and code rate 2/3 on the AWGN channel. . . . .	68
3.19	The performance of systems with code length 2304 and code rate 2/3 on the AWGN channel. . . . .	69
3.20	The performance of systems with code length 64800 and code rate 2/3 on the AWGN channel. . . . .	69
3.21	The performance of systems with code length 576 and code rate 3/4 on the AWGN channel. . . . .	70
3.22	The performance of systems with code length 2304 and code rate 3/4 on the AWGN channel. . . . .	70
3.23	The performance of systems with code length 64800 and code rate 3/4 on the AWGN channel. . . . .	71
3.24	The performance of systems with code length 576 and code rate 1/2 on the Rayleigh flat-fading channel. . . . .	71
3.25	The performance of systems with code length 2304 and code rate 1/2 on the Rayleigh flat-fading channel. . . . .	72
3.26	The performance of systems with code length 64800 and code rate 1/2 on the Rayleigh flat-fading channel. . . . .	72
3.27	The performance of systems with code length 576 and code rate 2/3 on the Rayleigh flat-fading channel. . . . .	73

3.28	The performance of systems with code length 2304 and code rate 2/3 on the Rayleigh flat-fading channel. . . . .	73
3.29	The performance of systems with code length 64800 and code rate 2/3 on the Rayleigh flat-fading channel. . . . .	74
3.30	The performance of systems with code length 576 and code rate 3/4 on the Rayleigh flat-fading channel. . . . .	74
3.31	The performance of systems with code length 2304 and code rate 3/4 on the Rayleigh flat-fading channel. . . . .	75
3.32	The performance of systems with code length 64800 and code rate 3/4 on the Rayleigh flat-fading channel. . . . .	75
4.1	The relation between the mutual information and variance of LLRs. . . . .	83
4.2	The demapper setup for PNC system employing BICM-ID. . . . .	85
4.3	BICM-ID demapper transfer characteristics function of QPSK mapping at different $\Xi$ in dB values for PNC system. . . . .	86
4.4	The decoder setup for PNC system employing BICM-ID to generate the transfer characteristics function. . . . .	87
4.5	BICM-ID decoder transfer characteristics function of code rate 1/2, code length 2304 bits and different constraint length for PNC system. . . . .	88
4.6	The system setup for PNC system employing LDPC code to generate the transfer characteristics function. . . . .	89
4.7	VND operation for PNC system employing LDPC code. . . . .	90
4.8	CND operation for PNC system employing LDPC code. . . . .	91
4.9	The system setup for PNC system employing turbo code to generate the transfer characteristics function. . . . .	92
4.10	DEC-1 operation for PNC system employing turbo code. . . . .	94
4.11	DEC-2 operation for PNC system employing turbo code. . . . .	95
4.12	EXIT chart with transfer characteristics function for a set of $\Xi$ values in dB and $R_c=1/2$ for PNC system employing turbo code. . . . .	96
4.13	BER curves for coded E2E PNC system of different code rate and code length 2304 bits. . . . .	97
4.14	EXIT chart for a set of $\Xi$ value in dB and different rate for E2E PNC system employing BICM-ID code. . . . .	99

4.15 ExIT chart for single user (SU) system employing BICM-ID code of code rate 1/2. . . . .	100
4.16 ExIT chart for single user (SU) system employing LDPC code of code rate 1/2. . . . .	101
4.17 ExIT chart for a set of $\Xi$ value in dB and different rate for E2E PNC system employing LDPC code. . . . .	102
4.18 ExIT chart for a set of $\Xi$ value in dB and different rate for E2E PNC system employing turbo code. . . . .	104
4.19 ExIT chart for single user (SU) system employing turbo code of code rate 1/2. . . . .	105
5.1 Angle modulation wave, (a) Large-amplitude low-frequency, (b) Large-amplitude high-frequency, (c) Small-amplitude low-frequency. . . . .	110
5.2 Sinusoidal message spectrum. . . . .	111
5.3 The structure of HT. . . . .	114
5.4 The system model for CE-PNC technique. . . . .	115
5.5 The structure for the coded PNC transmitter. . . . .	116
5.6 LPF design implementation. . . . .	118
5.7 Power spectral density of the input/output LPF. . . . .	119
5.8 The structure of the CE-PNC relay. . . . .	119
5.9 The structure of CE-PNC receiver. . . . .	120
5.10 BPF implementation. . . . .	122
5.11 The input/output of signal to/from the bandpass filter. . . . .	123
5.12 Analytic signal corresponding to original real signal. . . . .	124
5.13 Utilize HT to form a complex analytic signal. . . . .	126
5.14 Determination of the amplitude envelope and phase of the analytic signal. . . . .	127
5.15 The spectral behaviour of an FM signal with different values of $\Delta_f$ . . . . .	131
5.16 The spectral behaviour of a PM signal with different values of $\Delta_p$ . . . . .	132
5.17 The performance of uncoded PNC system with different deviations. . . . .	133
5.18 The structure of Opt-PNC system. . . . .	134
5.19 The performance for FM-PNC and PM-PNC employing LDPC code on AWGN channel with different $\Delta$ values. . . . .	135

---

5.20	The performance for FM-PNC and PM-PNC employing BICM-ID code on AWGN channel with different $\Delta$ values. . . . .	136
5.21	The performance for FM-PNC and PM-PNC employing turbo code on AWGN channel with different $\Delta$ values. . . . .	137
5.22	The performance for FM-PNC and PM-PNC employing LDPC code over Rayleigh flat-fading channel with different $\Delta$ values. . . . .	138
5.23	The performance for FM-PNC and PM-PNC employing BICM-ID code over Rayleigh flat-fading channel with different $\Delta$ values. . . . .	140
5.24	The performance for FM-PNC and PM-PNC employing turbo code over Rayleigh flat-fading channel with different $\Delta$ values. . . . .	141
5.25	The performance for PNC and CE-PNC employing LDPC code on AWGN channel. . . . .	142
5.26	The performance for PNC and CE-PNC employing BICM-ID code on AWGN channel. . . . .	143
5.27	The performance for PNC and CE-PNC employing turbo code on AWGN channel. . . . .	144
5.28	The performance for PNC and CE-PNC employing LDPC code over Rayleigh flat-fading channel. . . . .	144
5.29	The performance for PNC and CE-PNC employing BICM-ID code over Rayleigh flat-fading channel. . . . .	145
5.30	The performance for PNC and CE-PNC employing turbo code over Rayleigh flat-fading channel. . . . .	145
A.1	The constellation point at the relay. . . . .	153

# List of Tables

2.1	QPSK mapping. . . . .	28
2.2	The form of symbols received at the relay. . . . .	32
2.3	PNC mapping for the fist bit in the symbols received at the relay. . .	33
3.1	Summary of system performance for code rate $1/2$ on the AWGN channel. . . . .	76
3.2	Summary of system performance for code rate $2/3$ on the AWGN channel. . . . .	76
3.3	Summary of system performance for code rate $3/4$ on the AWGN channel. . . . .	76
3.4	Summary of system performance for code rate $1/2$ on the Rayleigh flat-fading channel. . . . .	77
3.5	Summary of system performance for code rate $2/3$ on the Rayleigh flat-fading channel. . . . .	77
3.6	Summary of system performance for code rate $3/4$ on the Rayleigh flat-fading channel. . . . .	77
4.1	The summarize of decoder parameters. . . . .	87
4.2	A brief description for the BICM-ID with E2E PNC system convergence. . . . .	98
4.3	A brief description for the LDPC code with E2E PNC system convergence. . . . .	103
4.4	A brief description for the turbo code with E2E PNC system convergence. . . . .	105
5.1	Lowpass filter design specification. . . . .	117
5.2	Bandpass filter design specification. . . . .	122
5.3	Summary of system performance for E2E coded Opt-PNC and PM-PNC systems on AWGN channel. . . . .	134

5.4 Summary of system performance for E2E coded Opt-PNC and FM-PNC systems over Rayleigh flat-fading channel. . . . . 139

5.5 Summary of system performance for E2E coded PM-PNC system over Rayleigh flat-fading channel. . . . . 139

# Nomenclature

## Acronyms

ACI	Adjacent Channel Interference
ACS	Add Compare Select
AM	Amplitude Modulation
ANC	Analog Network Coding
APP	A Posteriori Probability
ASK	Amplitude Shift Keying
AWGN	Additive White Gaussian Noise
BCJR	Bahl-Cocke-Jelinek-Raviv
BER	Bit Error Rate
BICM	Bit Interleaved Coded Modulation
BICM-ID	BICM with Iterative Decoding
BP	Belief Propagation
BPSK	Binary Phase Shift Keying
CE-PNC	Constant Envelope PNC
CND	Check Node Decoder
CDMA	Code Division Multiple Access
DNC	Digital Network Coding
DSB-AM	Double Side-Band AM

DSP	Digital Signal Processing
DVB-S2	Digital Video Broadcasting-Satellite-second generation
E2E	End-to-End
ECC	Error Correcting Code
EM	Electromagnetic
ExIT	Extrinsic Information Transfer
FDMA	Frequency Division Multiple Access
FEC	Forward Error Correction
FED	Free Euclidean Distance
FIR	Finite Impulse Response
FM	Frequency Modulation
FSK	Frequency Shift Keying
GF(2)	Galois field of two elements
IF	Intermediate-carrier Frequency
IRA	Irregular Repeat Accumulate
ISI	Inter-Symbol Interference
$L \times L$	Link-by-Link
LDPC	Low-Density Parity-Check
LLR	Logarithm Likelihood Ratio
LNC	Link-layer Network Coding
Log-MAP	MAP in logarithm domain
MAP	Maximum a Posteriori
MARC	Multiple Access Relay Channel
MI	Mutual Information

MLC	Multilevel Codes
MPA	Message Passing Algorithm
MUI	Multi User Interference
NP-hard	Non-deterministic Polynomial-time hard
NSC	Non-Systematic Convolutional
OFDM	Orthogonal Frequency-Division Multiplexing
Opt-PNC	Optimum-PNC
PDF	Probability Density Function
PM	Phase Modulation
PNC	Physical Layer Network Coding
PSD	Power Spectral Density
PSK	Phase Shift Keying
QAM	Quadrature Amplitude Modulation
QPSK	Quadrature Phase Shift Keying
RA	Repeat Accumulate
RF	Radio Frequency
RSC	Recursive Systematic Convolutional
SISO	Soft-Input Soft-Output
SNR	Signal to Noise Ratio
SSB	Single Side-Band
SU	Single user
TCM	Trellis-Coded Modulation
TWRC	Two-Way Relay Channel
VND	Variable Node Decoder
XOR	Exclusive-OR

# List of Symbols

$\mathcal{A}$	The envelope of signal
$\mathcal{A}_I$	Real part of $\mathcal{A}$
$\mathcal{A}_Q$	Imaginary part of $\mathcal{A}$
$\mathcal{A}_r$	The envelope of signal $\mathbf{r}$
$a$	Parameter
$\alpha$	Branch metric associated with the previous transition
$\bar{\alpha}$	natural logarithm of $\alpha$
$b$	Parameter
$\mathbf{b}$	Transmitted bits vector
$\hat{\mathbf{b}}$	Estimated bits vector
$\tilde{\mathbf{b}}_R$	Transmitted bits vector at relay
$b_t$	Bits associated with the state transition
$B$	Bandwidth requirement
$B_n$	Noise Bandwidth
$B_T$	Bandwidth of transmitted signal
$\beta$	Branch metric associated with the next transition
$\bar{\beta}$	natural logarithm of $\beta$
$c_t$	Encoder output associated with the state transition
$C$	Capacity
$\Psi$	Noisy signal received in term of constant envelope
$d_c$	CND degree
$d_v$	VND degree
$D_{1,2}$	Optimal decision
$D_R$	Euclidean distance
$\delta_L$	Mean value of LLR
$\Delta$	The peak deviation

$\Delta_f$	$\Delta$ for frequency
$\Delta_p$	$\Delta$ for phase
$\Delta t$	interval time
$E$	Total energy
$E(\cdot)$	The variance of the channel output
$E_s$	Symbol energy
$f_c$	Carrier frequency
$f_D$	Doppler frequency
$f_i$	Instantaneous frequency
$f_{IF}$	The frequency of intermediate carrier
$f_{i,FM}$	$f_i$ for FM signal
$f_s$	Sampling frequency
$f_u$	The frequency of modulating signal
$f_{\Delta t}$	The average frequency over an interval
$\mathbf{F}(\cdot)$	Correction function
$\mathcal{F}$	Fourier transform operation
$F$	Cauchy principal value
$\phi$	The phase
$\Phi$	Constant envelope signal
$G$	Low-density generator matrix
$\gamma$	Branch metric associated with the current transition
$\bar{\gamma}$	natural logarithm of $\gamma$
$\Gamma$	Transmitted constant envelope signal from relay
$F$	The Cauchy principal value
$h$	The complex gain of the channel
$\mathbf{h}$	The channel coefficient vector
$h_I$	Real part of $h$
$h_m$	Channel magnitude
$h_Q$	Imaginary part of $h$
$H$	The entropy
$\mathbf{H}$	Parity check matrix
$\mathcal{H}$	Hilbert transform operation
$\eta$	Mean value

$i$	Parameter
$I$	Real components
$I(\cdot)$	Mutual information
$I_A$	Mutual information between the <i>a priori</i> LLRs values and the bits
$I_E$	Mutual information between the extrinsic LLRs value and the bits
$I_r$	In-phase wave for $\mathbf{r}$
$I_R$	Real signal observed at the relay
$\mathcal{J}(\cdot)$	Imaginary part of an expression
$\lambda(\cdot)$	Fraction of edge that is connected to variable-nodes
$j$	Parameter
$j^2 = -1$	Imaginary unit
$J$	Function to describe the relationship between $I$ and variance of LLR
$\xi$	The amount of information provides about transmitted symbols
$\Xi$	Instantaneous SNR
$K$	Length of information bits
$K_c$	Constraint length
$L$	Set of LLR received symbols
$L_a$	LLR <i>a priori</i> information
$L_e$	LLR extrinsic information
$\Lambda$	The log-likelihood function
$M$	Constellation size
$\mu$	Function for both channel-coding and modulation
$N_0$	Power spectral density (Watt/Hz)
$N$	Total number of observed
$p(\cdot)$	Probability distribution
$P_{(\cdot)}^{(\cdot)}$	Sum product algorithm
$P_a$	Average power
$P_n$	Noise power
$P_s$	Symbol power
$Pr(\cdot)$	Probability of an expression
$\pi$	The ratio of a circle's circumference to its diameter
$q$	The number of users
$Q$	Quadrature component

$Q_r$	Quadrature wave for $\mathbf{r}$
$Q_R$	Imaginary signal observed at the relay
$r(t)$	Received signal
$\mathbf{r}$	Channel output vector
$r_I$	Real part of $\mathbf{r}$
$r_Q$	Imaginary part of $\mathbf{r}$
$r_t$	Function of channel output with the state transition
$R$	Set of received symbols
$R_s$	Symbol rate
$\Re(\cdot)$	Real part of an expression
$\rho(\cdot)$	Fraction of edge that is connected to check-nodes
$\mathbf{s}$	Transmitted symbols vector
$s$	Transmitted symbol
$\mathbf{s}$	A state sequence
$S$	Set of transmitted symbols
$\tilde{\mathbf{s}}_R$	Transmitted symbols vector at relay
$\mathbf{s}_t$	Initial state
$\mathbf{s}_{t-1}$	previous state
$\mathbf{s}_{t+1}$	Next state
$\sigma$	Noise variance
$t$	A period of time
$T$	Length of the time
$\mathbb{T}_I$	To represent $I_E$ by $I_A$
$T_s$	Sampling time
$\tau$	Time varying path delay
$\tau_0$	Channel delay
$u$	The sinusoidal signal in time domain
$u_I$	In-phase component of $u$
$u_Q$	Quadrature component of $u$
$U$	Fourier spectrum of $u$
$U(f)$	Carrier $u$ in the frequency domain
$\theta$	Phase of the carrier
$\Theta_w$	Phase of the noise

$\tilde{v}$	HT output for $v$ input
$V(f)$	The Fourier transform of $v(t)$
$V_a(f)$	The continuous-time analytic signal in the frequency domain
$v_u$	Speed of user
$v_l$	Speed of light
$\omega_c$	Angular frequency
$\Omega$	Observed constant envelope signal at receiver
$\mathbf{w}$	Noise vector
$\check{w}$	Real noise
$\check{w}_I$	Real part of $\check{w}$
$\check{w}_Q$	Imaginary part of $\check{w}$
$\mathbf{y}$	Observation symbols vector
$Y$	Analytic signal at the receiver
$v$	Parameter, constant
$\Upsilon_{(.)}$	Equivalent part in frequency domain
$\mathbf{z}$	Observation bits vector
$\zeta$	modulation index
$\zeta_f$	$\zeta$ for frequency
$\zeta_p$	$\zeta$ for phase
$\angle$	Angle of signal
$(.)^{-1}$	Inverse operation
$(.)^*$	Conjugate operation
$(.)^T$	Transpose operation

# Chapter 1

---

---

## Introduction

---

---

## 1.1 Background

Over the last century, great progress has been made in wireless communications technology. Portable communication devices now enable communications from and to virtually anywhere in the world. To improve performance, coverage, and efficiency, digital signalling techniques are utilized by modern wireless communication systems, and due to the characteristics of digital signalling, it is possible to use error control coding. Nowadays, a new class of codes, termed iterative decoders, has brought signalling power efficiencies close to the theoretically possible limits. The features of iterative decoders include exchanging information between two components, but different iterative decoding algorithms also provide a solution to a more general class of problems.

This chapter begins by presenting a brief overview of the history of wireless communication systems implemented by a novel strategy, which practically speaking is an operation known as physical layer network coding (PNC). PNC is increasingly considered a high-throughput technique for communication in a wireless network over a two-way relay channel (TWRC). Moreover, PNC is a technique that allows two users to exchange their messages in less time via an intermediate relay. This takes place at a relay node and exploits the interference caused by noisy incoming signals by performing special demapping/mapping and then by broadcasting again to the users.

## 1.2 Challenges and Motivation

Wireless network design can be classified as an NP-hard (Non-deterministic Polynomial-time hard in computational complexity theory) type problem due to the high and unexpected complication growth both in time and space. In order to design an efficient system that fulfils the fundamental requirements of communication through a wireless network, it is necessary to understand the challenges and problems that limit the performance of this particular system. Moreover, assessing these problems and analyzing them via a unique mathematical formulation allows to simultaneously tackle the problem to ensure maximum delivery of system performance. The work in this thesis attempts to address some of the issues in the context of the physical layer of a TWRC communication model. Therefore, the communication network can

be considered as being two nodes connected by links. The information is sent as one packet at a time from the source to the destination via intermediate node acting as relay. As a relatively new paradigm in networking techniques, PNC takes advantage of the additive nature of electromagnetic waves, and embraces interferences by performing coding operations to combine the otherwise convoluted messages. In such a way, both the communication time and the bandwidth are utilized more efficiently, which in turn boosts the network throughput.

Channel coding may be applied on PNC technique by using link-by-link ( $L \times L$ ) scheme or end-to-end (E2E) scheme. The difference between  $L \times L$  and E2E coding methods lies in how the relay processes the received signal. The relay makes use of the correlations between successive symbols, in the  $L \times L$  manner, to recover the desired symbols. In the E2E manner, errors may accumulate when the data is transferred from the source to the destination, because the relay does not correct the errors, and the channel coded scheme is transparent to the network system. With this background in mind, a crucial aspect of implementing PNC is the formulation of a simple relay receiver, and the selection of iterative decoding method formats that work well with the end-to-end system. The purpose of this study is to identify the general problem that is addressed by a relaying network and to seek a new design/application of a relaying scheme in the area of wireless communication scenario. The development of practical iterative detection algorithms will have much broader application throughout the field of communications. The central idea of this study is to design a combinatorial system between a constant envelope scheme and an end-to-end coded PNC system. The potential benefits of considering a new end-to-end coded PNC system is guaranteed code properties, information reliability, and a new principle of implementation, which includes a reduction the loss of transmitted data around zero point in the constellation and an increase in the efficiency of the coding system.

## 1.3 Literature Review

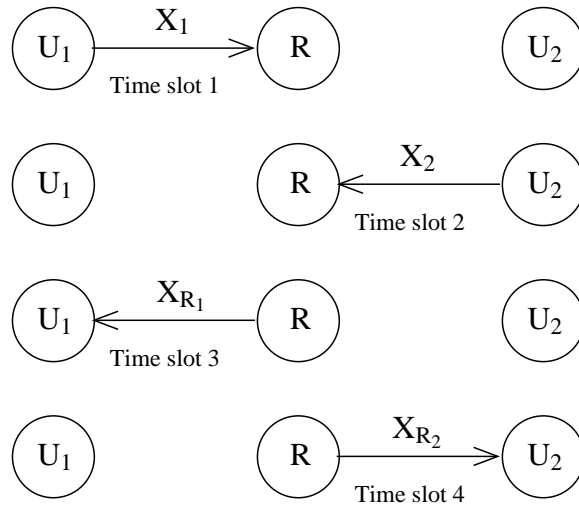
### 1.3.1 Overview

In a traditional transmission scheme and in the two-way relay channel (TWRC), the exchange of information between a pair of source terminals,  $U_1$  and  $U_2$ , without

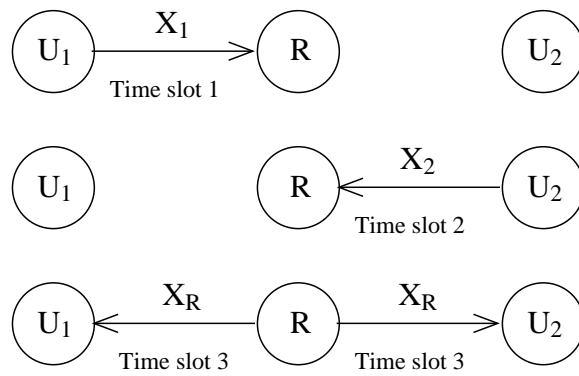
a direct link requires four time slots through an intermediate relay, R [1]. With each of the first two time slots, one of the terminals transmits information to the relay, while with each of the last two time slots, the relay transmits information to each of the terminals, as shown in Figure 1.1(a). By using the technique of network coding [2], the number of time slots can be reduced. This is illustrated by a link-layer network coding (LNC) system, in which the third and fourth time slots are combined into one time slot by having the relay add modulo-2 to the informations that it receives from the two terminals, as shown in Figure 1.1(b). Hence, the interference signal of the two users and the effect of the channel becomes part of the arithmetic operation in network coding. Therefore, the relay sends the sum of the two informations during the third time slot and each terminal is able to recover the information from the other terminal by adding/subtracting modulo-2 for its own message from the received information. However, in physical layer network coding (PNC) the transmission scheduling scheme for the first two time slots are combined by having the two terminals transmit their informations at the same time [3]. Therefore, the main idea of PNC is to find an apparatus similar to that of network coding but at the lower layer that deals with electromagnetic (EM) wave reception and modulation. This can be achieved through a suitable demapping and mapping process at the relay node, where the EM signals can be mapped to digital bit streams of a Galois field of two elements ( $GF(2)$ ). Thus, the relay receives a combination of both modulated packets during the first time slot, which it then broadcasts after appropriate processing to the two terminals during the second time slot, as shown in Figure 1.1(c). Consequently, depending on how the information is encoded, the exchange of information can occur in four, three, or two orthogonal time slots, as depicted in Figure 1.1.

### 1.3.2 Classification

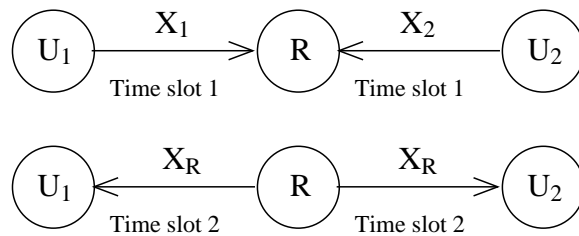
A prospective technique in the wireless two-way relay communications is PNC, which exploits interference to improve the throughput. By the two transmission phases, the uplink phase and the downlink phase, both end users transmit to the relay simultaneously and the relay directly transforms the received waves to the network coding form without individually detecting them. Then, in the downlink phase, the relay broadcasts the network coded signal to both end users. Specifically, PNC



(a) Traditional



(b) LNC



(c) PNC

Figure 1.1: Transmission Schemes

has proven to have the ability to approach the capacity of the TWRC in high SNR regions [4] as well as the throughput upper bound of wireless networks [5]. Recently, the researchers in [4] and [6], have shown that PNC can achieve within half a bit of the capacity of a single-input single-output Gaussian TWRC and it is asymptotically optimal at high signal to noise ratios (SNRs). PNC may be implemented using two different schemes. The relay may simply amplify and forward the received signal sum directly, without performing demodulation and decoding. This PNC scheme is referred to as analogue network coding (ANC) [7]. Another scheme is for the relay detects the received signal sum to clean up the noise by performing demodulation and decoding in an effort to estimate the network codeword. This PNC scheme is sometime called digital network coding (DNC). Multiple access techniques such as spatial reuse, frequency division multiple access (FDMA) [8], and code division multiple access (CDMA) [9] allow multiple simultaneous transmissions. However, these techniques are avoided because of the interference in space, frequencies, and code respectively, as they only divide channel capacity between multiple users. In contrast, PNC expands the capacity of the network.

### 1.3.3 Relay Network

In order for two terminals to exchange information, they need to reside within each other's transmission range. This type of communication is considered to be line-of-sight [10]. However, the line-of-sight condition is not always available, so a message from a source to a destination can be delivered in a multi-slot fashion. The source node chooses an in-between node to forward its message. This intermediate node serves as a relay between the two sources. In such a slot-by-slot fashion, energy, for example, can potentially be conserved. Such a communication chain can be simplified to a three-node model, the source, the destination and the relay. In Figure 1.1, the system consists of two terminals denoted by  $U_1$  and  $U_2$ , respectively. There is a relay  $R$  in between to assist the message exchange. Recently, one promising strategy is to deploy nodes in the region between a transmitter and its intended receiver. These intermediate nodes can improve communication for this transmitter-receiver pair by receiving a transmitted message, processing it and relaying the processed output to the receiver. This transmission strategy can be especially beneficial when the transmitter-receiver pair are either separated by a large distance or when a large

obstruction blocks the path between them. Several relays technique may be available to assist a particular transmitter-receiver pair. The relay channel was introduced by [11] and investigated extensively by [12] to provide a number of relaying strategies, in which of these strategies the communication link between the source and the relay is physically better than the source and destination link. The available transmission channel between each pair can be seen as a link connecting the two.

### 1.3.4 Error Detection and Correction

Error detection and correction technique is adopted for more reliable communication systems. Jointly design coding and modulation to enhance the performance of digital transmission schemes was proposed by Massey in 1974 to introduce the field of coded modulation scheme [13]. Powerful coded modulation schemes was began to optimize the performance include trellis-coded modulation (TCM) [14], multilevel codes (MLC) [15] [16] and bit-interleaved coded modulation (BICM) [17] [18]. An interesting scheme is BICM, which is used in most recent wireless standards due to its performance, flexibility, and simplicity. BICM encoder consists of the serial concatenation of a channel code, interleaver and mapper. At the receiver, the signal is consecutively demapped, deinterleaved and decoded.

Turbo codes were first introduced by Berrou et al [19] and these performed close to the Shannon limit with a comparatively simple encoder structure and a novel iterative decoding algorithm. The turbo decoder consists of the component decoders that exchange soft extrinsic information in an iterative fashion. The turbo principle of serial or parallel concatenated components can be applied at the receiver of a communication system [20]. Consequently, the breakthrough towards capacity approaching channel codes was the idea of iterative decoding of concatenated codes and the idea of iterative decoding has been shown to be valid in a more general sense. Soon after the appearance of turbo codes, low-density parity-check (LDPC) codes constructed from sparse parity-check matrices were introduced by Gallager in the 1960s [21], but were essentially forgotten for three decades after that. LDPC codes were rediscovered by Mackay et al [22], who found that LDPC codes form a compelling alternative for approaching Shannon limits. Nowadays, turbo and LDPC codes are considered to be capacity-approaching channel codes when employing iterative decoders. After turbo codes were introduced in 1993, another iterative

coding scheme presented in 1997 is bit interleaved coded modulation with iterative decoding (BICM-ID) [23] [24], which has a lower complexity than turbo codes but performs well on AWGN and Rayleigh fading channels. The performance of BICM receiver can be greatly improved through iterative information exchange between the demapper and the decoder according to the turbo principle.

### 1.3.5 Iterative Decoding

soon after the introduction of turbo codes, it was recognized that the iterative decoding scheme was suitable for many communication environment. Therefore, modern communication receivers typically consist of a linear sequence of signal processing components, each optimized to perform a single task. However, in a traditional system receiver, the contact between components involves the passing of bits to the system output. The bits may be introduced by hard decision process. Therefore, hard decisions are made, information is lost and becomes unavailable to the end component. Additionally, the sequence of components at the beginning of the system processing do not benefit from information derived by sequences further in the end component. The contact between steps can be greatly improved by using the same strategy used to decode turbo codes. In [25] the term of turbo processing was invented to describe the general strategy of iterative feedback, this strategy can be used for decoding or detection. With turbo processing, each component is implemented with a soft input soft output (SISO) algorithm. The term of soft decision values, typically in the form of log-likelihood ratios (LLR), can be passed to the end component and refined by subsequent steps. The soft output value of the final step is then fed back to the first step and a second iteration of processing is initiated. Several iterations of turbo processing can be executed. Consequently, a new technique of turbo processing can be used to combine channel decoding with: symbol detection [25], multiuser detection [26], source decoding [27], or equalization [28].

### 1.3.6 Joint PNC and Error Correction Coding

The scheme of error correction coding to be selected based on the characteristics of the communication channel achieves good error control performance. Hence, this scheme in a PNC system can either be done  $L \times L$  or E2E. With the former technique, the channel encoding and decoding is performed in the end nodes as well as the

relay node [29], whereas the E2E technique performs the channel coding only at the end nodes, and not at the relay node [30]. The channel-decoding network-coding process involves both channel decoding and network coding operations to transform the received signal at the relay. Specifically, it re-designs the belief propagation decoding algorithm at the relay. There are several publications in the literature that investigate the combination of LDPC codes and PNC for a multiple-access channel [31] [32] and two-way wireless relay channels [33]. Similarly, research on combining turbo codes and PNC has also taken place [34]. Very recently, BICM was employed with multi-level PNC for a two-way wireless relay network [35].

### 1.3.7 PNC and ExIT Chart Analysis

There are two major approaches to analyzing the performance of the iterative process. The first approach is to calculate bounds on the bit error rate of the system, which is extensively applied to the analysis of turbo codes [36]. However, it is unable to characterize the convergence behaviour of the system, for example at the onset of the turbo cliff in turbo code, so this requires a different analysis tool. The second approach is to analyze the convergence behaviour of the iterative process with the intent of determining signal to noise ratio regions where iteration gain can be obtained, such as the density evolution and extrinsic information transfer chart approaches [37]. A semi-analytical technique called an extrinsic information transfer (ExIT) chart was introduced by [38]. The substantial advantages of this technique are to evaluate the convergence properties and trace the evolution of different algorithms at the receiver through multiple iterations. The convergence behaviour of the proposed detectors over unknown the received signal is evaluated with the help of the ExIT chart. The convergence property of interference signals of a PNC system is not only related to its parameter but also related to its architecture and the type of channel coding used. Therefore, ExIT chart employs mutual information measurement to quantify the quality of the extrinsic information exchanged between the constituent components in an iterative process. It is comprised of two curves for two components in the system. Each curve plots the mutual information of the extrinsic LLRs versus the mutual information of the *a priori* LLRs of one component in the system, which it uses to measure the quality of the input and the output of the component. For the PNC system, the mutual information exchange

between the output of the PNC and channel decoders can give further information about user interference signals and has the ability to select correct parameters. The impact of the parameters includes different lengths of code memory, the data size then the code length, and the number of iterations needed to achieve convergence between the measured components.

### 1.3.8 PNC and the Modulation Technique

In a communication system, the fundamental reason for modulation is to enable efficient use of the available frequency spectrum on a particular medium. The modulation in the communication of a wireless network is a potential process by which information is conveyed of an electromagnetic wave. All the different modulation techniques can be classified under the composite modulation, which includes bandpass-modulation and the baseband-modulation, or analogue modulation, which includes amplitude-modulation and angle-modulation. Therefore, the modulation method for digital or analogue is described by the characteristics of the information. The parameters of digital modulation take on a discrete set of values, each of which represents a symbols, consisting of one or more bits. However, the parameters of analogue modulation consist of amplitude, frequency or phase and can be taken on a continuous scale of values which must carefully follow all of the inflections of the signal to be transmitted. There have been many attempts to employ the principle of analogue signal in terms of frequency modulation with an orthogonal frequency-division multiplexing (OFDM) system, [39] [40]. Soon after, the authors in [41] used an FM-radio channel for transmission of OFDM digital data, while others used analyzed an FM signal in an OFDM system [42] [43]. Sorenson et al. [44] first presented frequency shift keying with PNC, which was followed by Valenti et al. [45], who looked at FSK receiver design at the relay. Ferret et al. [46] extended the work in [45] with different assumptions for utilizing FSK with the detector of the two-way relay channel. However, the OFDM waveform has high amplitude fluctuations, a drawback known as the peak-to-average power ratio (PAPR) problem. Since Oct. 2003 the researcher team, S. C. Thompson, John G. Proakis, and James R. Zeidler, in University of California San Diego were introduced the constant envelope combined with OFDM to solve the PAPR problem [47]. This teamwork introduces a new approach of constant envelope OFDM and focuses on binary OFDM phase modu-

lation, which is a special case of OFDM angle modulation. Then they continues in this technique until they were recently published a paper about low-complexity receivers for constant envelope [48]. They study the performance of the new receiver when error correction coding is employed. They shows that the receiver provide excellent performance but also significantly outperform the conventional arctangent based receiver for coded Constant Envelope OFDM performance.

## 1.4 Research Contribution and Publications

This section outlines the main contributions of this thesis. Also, this section serves to identify the published parts of this thesis with the associated citations listed in the following section.

Chapter 2 provides background and no new results are presented. However, the PNC of interest here is the coded E2E PNC network. This technique has rarely been implemented by researchers due to the noise at the relay also being forwarded to the destinations. In larger networks especially, errors can also be left uncorrected and dealt with using the end-to-end network error correction framework proposed in [49]. Therefore, we must calculate, in our research, for the level of error correction needed to recover from the errors introduced at the relay.

Chapter 3 considers the system of PNC using end-to-end iterative decoding algorithms. The original contribution of this chapter is to evaluate the system performance with a different coding scheme. The implementation of the end-to-end PNC system with three different techniques for iterative decoding are investigated and compared with different block sizes and code rates in terms of BER performance, and comparisons are made between the different coding schemes. Chapter 3 represents the first publication, in which results are compared for LDPC, BICM-ID, and turbo codes combined with end-to-end PNC.

Chapter 4 follows on from Chapter 3 to consider EXIT chart analyses in order to investigate the achievable iterative decoding convergence when coded end-to-end PNC is employed. The original contribution of this chapter is the presentation of the proposed EXIT charts for studying the end-to-end PNC scheme with BICM-ID, LDPC and turbo codes. Chapter 4 was presented as a conference paper and subsequently journal paper under preparation.

In Chapter 5 the original contribution is the innovation of employing the constant

envelope technique to construct new coded end-to-end PNC. This new PNC system is presented, and compares well with the angle modulation choice and the iterative decoding performance. Chapter 5 is based on the journal paper under preparation.

### 1.4.1 Related publications

- **Alaa A. S. Al-Rubaie**, C. C. Tsimenidis, M. Johnston, B. Sharif, "Comparison of a physical-layer network coding system with iterative coding schemes," Wireless and Mobile Networking Conference (WMNC), 2013 6th Joint IFIP , pp.1-4, 23-25 April 2013
- **Alaa A. S. Al-Rubaie**, C. C. Tsimenidis, M. Johnston, B. Sharif, "Performance and ExIT chart analysis of BICM-ID for physical layer network coding," Electronics, Circuits, and Systems (ICECS), 2013 IEEE 20th International Conference, pp.205-208, 8-11 December 2013
- **Alaa A. S. Al-Rubaie**, C. C. Tsimenidis, M. Johnston, B. Sharif, "Convergence Behaviour of Joint Iterative Decoders and Physical Layer Network Coding," (under preparation to submit to Journal of the Institution of Engineering and Technology (IET))
- **Alaa A. S. Al-Rubaie**, C. C. Tsimenidis, M. Johnston, B. Sharif, "Physical Layer Network Coding and Constant Envelope Technique in Combination Method," (under preparation to submit to International Conference on Communications (ICC))
- **Alaa A. S. Al-Rubaie**, C. C. Tsimenidis, M. Johnston, B. Sharif, "Constant Envelope Physical Layer Network Coding Angle Modulation," (under preparation to submit to Vehicular Technology, IEEE Transactions.)

## 1.5 Organization of the Thesis

The rest of the thesis is organized as follows:

Chapter 2 describes the two way communication technique and the principle of PNC technique. The chapter also presents the effects of the bandpass wireless communication on the signal and system form. Furthermore, this chapter demonstrates the measure of informations, entropy and mutual information. The modulation

and channel model are introduced in the implementation of the system. Finally, a comprehensive literature review for system model is presented.

Chapter 3 introduces the main error correction coding and iterative decoding techniques in single user and PNC systems. Three conventional techniques for iterative schemes in the PNC systems are compared: low-density parity-check (LDPC) codes, bit interleaved coded modulation with iterative decoding (BICM-ID) code, and turbo codes, when the relay role is as simple as possible. Moreover, the section presents the parameters for selecting the different algorithms with a PNC system that can reduce the error effectively at the relay and simultaneously maintain the BER performance are studied.

Chapter 4 presents efficient techniques to analyse the PNC system performance by using an ExIT chart. The analysis of iterative decoding through extrinsic information transfer is given for PNC system and compared with a single-user system. Furthermore, the chapter presents the effect of a single parameter in terms of mutual information through the systems. Finally, a prediction of systems behaviour is obtained by studying system trajectory and obtaining the convergence of the systems.

Chapter 5 presents efficient techniques to improve the BER performance degradation due to the demapping and mapping characteristics process of the relay utilized in PNC-based systems, and performing a constant envelope modulation at the relay. Extensive simulation results have demonstrated that minimizing the effect provides significant BER reduction in comparison to traditional PNC techniques, which are optimised to reduce the BER. Moreover, measuring the performance of the proposed techniques constant envelope PNC (CE-PNC) is more effective than traditional PNC, as the LLRs transmitted do not lose through the system steps.

Finally, conclusions are summarised in Chapter 6 and the thesis ends with suggestions of future work.

## Chapter 2

---

---

# Theoretical Background and System Model

---

---

## 2.1 Introduction

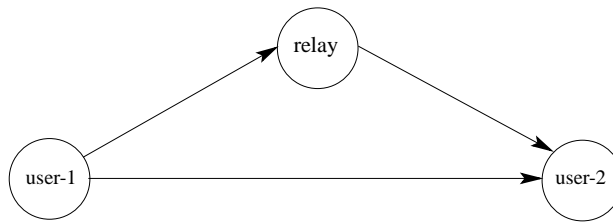
This chapter introduces the general framework and specific techniques that will be used throughout the thesis. For an assessment on the system performance, this chapter focuses on different techniques commonly used in the communication network. The chapter begins with an introduction to the two way communication technique, and is then followed by the bandpass signal and system representation. In addition, the chapter provides an overview of information theory and describes the principle of mutual information. Emphasis is placed on the description of the system model of the physical layer network coding (PNC) architecture. A mathematical representation of the relay demapping and mapping process are also given.

## 2.2 Two Way Communication Systems

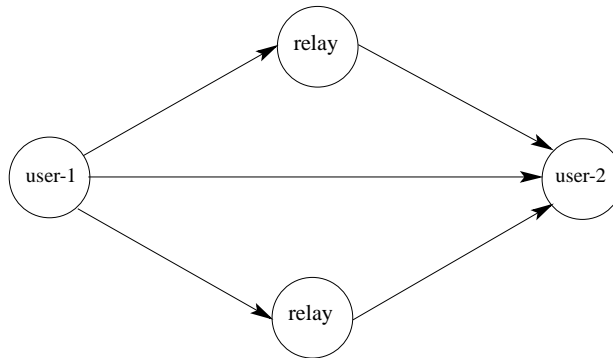
A relay network is a wide category of network topology commonly employed in wireless networks, where a pair of source terminals are interconnected by means of some nodes. In such a network the source and the destination cannot communicate to each other directly due to the distance is greater than the transmission range of sources, hence the need for intermediate node/nodes. This type of network holds several advantages such as; the information can travel long distances, even if the source and the destination are far apart. It also reliable data transmission between nodes. In some cases, such as with the employment of network coding techniques, the roles of the source and the destination are embodied by the same nodes, and the message flow goes in both directions. For this reason, the source and the destination are known as terminals and the link is a two-way communication channel in these scenarios. This channel was first studied by [50] and considered a basic two-way communication model consisting of two terminals and investigated effective bi-directional communication. Based on the availability of the links, the system has popular variants such as cooperative systems and two-way relay networks.

### 2.2.1 Cooperative Communication Systems

In this communication scenario, the source and the destination are distinguished as they do not transmit at the same time. Consider user-1 is the source and user-2 is the destination. Links user-1 with relay and user-1 with user-2 are both avail-



(a) Single relay



(b) Multi relay

Figure 2.1: Cooperative communication system.

able. Figure 2.1 depicts a simplified cooperative communication model. The basic idea of cooperative communication is that the source and the relay assist each other in sending messages to the destination collaboratively. This means; the message originated from the source is repeated in some form by the relay, and reaches the destination besides the original copy. Multiple copies introduce a type of diversity known as cooperative diversity, which contributes to the greater reliability of the system [51]. The message from the source to the destination, in multi-hop communications scenario, is relayed via another node. Therefore, this relaying scheme is essential in order to overcome the path loss incurred over long distances. Moreover, multi-hop techniques are utilized in cellular systems and wireless local area network (LAN) systems to provide power savings, extended coverage and a higher quality of service.

### 2.2.2 Two Way Relay Channels

For the two-way relay channel (TWRC), the link user-1 with user-2 is assumed to be unavailable. Thus, the transmission takes place solely relying on the relay's as-

sistance. Depending on the scheduling between the two terminals, the relay receives one message from either source at a time. After the relay receives a message or a combination of two messages, perturbed by the noise, there are several strategies that have been introduced such as decode-and-forward, compress-and-forward, and amplify-and-forward, for processing before the next stage. Later on, some pioneer work by [1] applied these strategies to the TWRC, where this topic has recently attracted significant attention. In the TWRC, two terminals simultaneously transmit their messages to each other and the messages interfere with each other.

### 2.2.3 Relaying Schemes

The relay node applies either, a very simple mathematical operation, or modifies the received signal and then forwards the new version of the signal to its destination. In this section, we discuss some of the particular relay mode for relaying network, which were first introduced by Cover and Gamel [12] as:

#### 2.2.3.1 Decode and Forward

The relay performs decoding operations on the received signals. Though it is possible to do exhaustive search among all the constellations to decode the individual symbols from either terminal, a more efficient way is to obtain the combination of the signals. Decode-and-forward attempts to process and eliminate the noise and fading corruption of the 1<sup>st</sup> time slot. The relay then re-encodes the signal and the new symbol is forwarded to the terminals in the 2<sup>nd</sup> time slot. This processing of the signal at the relay is also known as making a hard decision, as the information sent by the relay does not include any additional information about the reliability of the source-relay link. However, when uncoded modulation is used this protocol is also known as detect-and-forward as the processing of the relay is detection of the signal.

#### 2.2.3.2 Amplify and Forward

In this protocol, the relay does not attempt to decode the individual symbols or a combination of the symbols that were transmitted from the terminals. Since the energy dissipation as the electromagnetic waves travel from the source to their destinations, the power of the received signal is smaller than the terminal's transmission

power. The relay can be a transceiver of either the same capabilities, or different. In either case, the relay can scale the received signals to its own transmission power, practically amplifying them. Note that, during this process, since the noise is not isolated from the original signals, it is also amplified, and therefore the efficiency of energy use is suboptimal.

### 2.2.3.3 Estimate and Forward

This protocol is also known as compress-and-forward. At the relay, a transformation is applied to the received signal, which provides an estimate of the source signal. This estimate is also known as soft information, and it is forwarded to the destination. The relay estimates the information from the received signal by using the minimum mean squared error (MMSE) estimate, which is the conditional expectation of the source sent symbol given the received signal at the relay.

### 2.2.4 Physical Layer Network Coding

The communication system over a TWRC allowing an intermediate node to mix incoming message from multiple links. Network coding is a technique that allows the throughput of a network to be increased by applying encoding at the relay [2]. The concept of network coding has been applied to wireless relay networks to turn the broadcast property into a capacity-boosting advantage for wireless networks to increase network throughput significantly. Hence, in this case a receiver attempts to reconstruct the exclusive-or (XOR) of the incoming messages from two user nodes. This leads to the production of physical layer network coding (PNC) [3] which yields an even greater throughput gain because the simultaneous transmission of summed signals from relay nodes reduces the number of required time slots to exchange messages. Furthermore, the receiver of the PNC technique in the context of the TWRC can reconstruct the XOR of the two concurrently transmitted messages directly from the channel output. In the PNC system, the users' messages are transmitted to the relay during the up-link phase. After the process of the PNC special demapping and then mapping at the relay, the interference signal of the two users is broadcast to the destination node in the down link phase. The exchange of information between the two users occurs simultaneously via an intermediate relay in TWRC, which can potentially double the throughput of a conventional one-way

relay channel.

## 2.3 Bandpass Signals and Systems Representation

The communication systems always work with a baseband signal, such as coding/decoding, modulation/demodulation, synchronization, etc., even for wireless communication and then the baseband signal is converted to the bandpass signal at the desired carrier frequency. Similarly, at the receiver the first step is to down-convert the signal to the baseband before further processing. Let us begin with the sinusoidal signals for both continuous-time (waveforms) and discrete-time (sequences) which will become important building blocks for more general signals. Also, the representation using sinusoidal signals will lead to a very powerful set of ideas for representing signals and for analyzing an important class of systems. The sinusoidal signal  $u(t)$  can be mathematically expressed by its envelope and angle as

$$u(t) = \mathcal{A}(t) \cos(2\pi f_c t + \theta(t)) \quad (2.1)$$

where  $\mathcal{A}(t)$  is the carrier-envelope,  $f_c$  is the carrier-frequency,  $\theta(t)$  is the phase of the carrier, and  $t$  is time. The carrier angle can be represented by  $\phi(t) = 2\pi f_c t + \theta(t)$ , and the term  $\omega_c = 2\pi f_c$  is known as the angular frequency. A sinusoidal carrier wave, thus, has two fundamental properties: amplitude  $\mathcal{A}(t)$  and angle  $\phi(t)$ , either of these parameters can be varied with time  $t$  to transmit information.

### 2.3.1 Baseband Equivalent of Bandpass Signals

The information in a real-valued bandpass signal is contained in a corresponding complex-valued baseband signal. Therefore, this baseband signal represents the complex envelope of the bandpass signal. Consider  $U(f)$ , the Fourier spectrum of a real-valued signal  $u(t)$  over a band of frequencies  $B_T$ , centred around a carrier frequency  $f_c$ , then the essential information required to represent the signal is contained in the complex envelope of baseband signal. The relationship between the spectrum of real-valued bandpass signal and its complex envelope is illustrated in

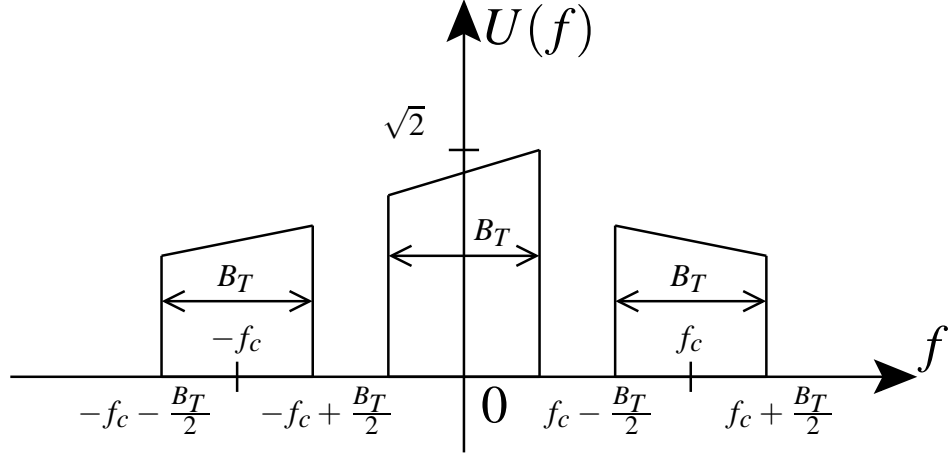


Figure 2.2: The relationship between a bandpass spectrum and its baseband equivalent.

Figure 2.2 and can be mathematically written as

$$U(f) = \frac{1}{2}U(f - f_c) + \frac{1}{2}U^*(f - f_c) \quad (2.2)$$

where  $U$  consists of magnitude and phase, then the complex conjugate  $U^*$  is composed of the magnitude  $U$  and changing the phase  $U$  sign. In rectangular notation, the complex conjugate is found by leaving the real part alone, and changing the sign (sgn) of the imaginary part. The complex signal can be mathematically represented by rectangular form,  $u(t) = u_I(t) + ju_Q(t)$ . Hence, the corresponding bandpass signal can be written in Trigonometric form as

$$u(t) = u_I(t) \cos(\omega_c t) + ju_Q(t) \sin(\omega_c t) \quad (2.3)$$

The utilization of the complex envelope permits sampling without the loss of any information and obtains a real bandpass signal at the lower rate of  $B_T$  complex samples per second.

### 2.3.2 Baseband Equivalent of Bandpass Systems

The implementation of the equivalent complex baseband system is depicted in Figure 2.3. The ability to transmit and receive bandpass signals over a physical communication channel is achieved by employing bandpass channels. Therefore, the bandpass system responds to a bandpass signal and then the received signal  $r(t)$

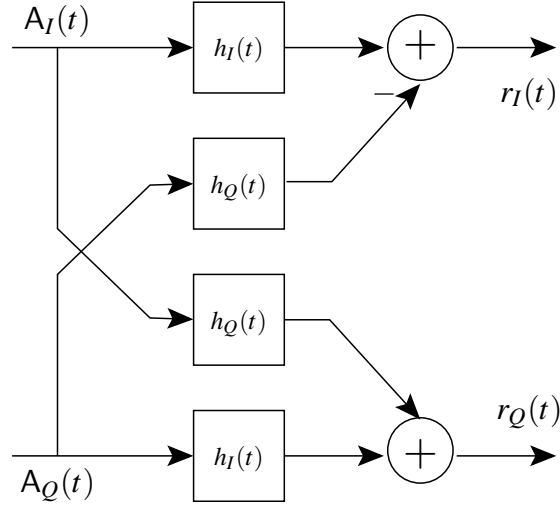


Figure 2.3: Implementation the equivalent complex baseband system.

can be written as

$$r(t) = \Re(h(t, \tau)\mathcal{A}(t - \tau)e^{j2\pi f_c(t-\tau)}) \quad (2.4a)$$

$$= (h_I(t) + jh_Q(t)) * (\mathcal{A}_I(t) + j\mathcal{A}_Q(t)) \quad (2.4b)$$

where  $h(t, \tau)$  is the complex gain of the channel,  $\tau$  is the delay, and the operator  $*$  denotes convolution. Hence, equation (2.4) can be written in terms of the in-phase and quadrature components as

$$r_I(t) = h_I(t) * \mathcal{A}_I(t) - h_Q(t) * \mathcal{A}_Q(t) \quad (2.5)$$

$$r_Q(t) = h_I(t) * \mathcal{A}_Q(t) + h_Q(t) * \mathcal{A}_I(t) \quad (2.6)$$

The received signal is corrupted by additive Gaussian noise, which affects noise bandwidth  $B_n$  (Hz) and power spectral density (PSD) of  $N_0$  (W/Hz). In this case, the baseband equivalent noise signal  $w(t) = w_I(t) + jw_Q(t)$  will be circularly symmetrical complex Gaussian noise and variance as

$$\sigma^2 = \mathbb{E}(w(t)w^*(t)) \quad (2.7a)$$

$$= N_0 B_n \quad (2.7b)$$

where the operators  $\mathbb{E}(\cdot)$  and  $(\cdot)^*$  denote the expectation and conjugate, respectively. However, in circularly symmetric complex Gaussian noise, the real and imaginary parts are independent Gaussian random variables with zero mean and equal variance

$\mathbb{E}(w_I^2(t)) = \mathbb{E}(w_Q^2(t)) = \sigma^2/2$  with  $\mathbb{E}(w(t)w^*(t)) = 0$ . When these conditions are satisfied,  $w(t)$  will be complex Gaussian probability density function (pdf) and can be written as

$$p(w) = \frac{1}{\pi\sigma^2} \exp\left(-\frac{|w|^2}{\sigma^2}\right) \quad (2.8)$$

## 2.4 A Measure of Information

The mathematical theory of communication, information theory, was founded by Shannon [52]. Information theory gives fundamental limits on the optimum performance achievable in various communication problems such as data transmission over a noisy channel, compression of data, and the quantization of analog information sources, etc. In the process of communication, information theory uses the entropy as a statistical measure to determine the amount of information contained in a given amount of data. Furthermore, information theory uses the quantities of entropy and mutual information as a function of the probability distributions.

### 2.4.1 Entropy

The entropy represents the average uncertainty of a random process [53]. Consider  $S$  to be a random variable from the alphabet  $\mathcal{S}$  with realizations  $s$  and  $R$  to be a random variable from the alphabet  $\mathcal{R}$  with realizations  $r$ . The entropy of  $S$ ,  $H(S)$ , for a finite size alphabet  $\mathcal{S}$  can be defined as

$$H(S) = \sum_{s \in \mathcal{S}} Pr(s) \log_2 \frac{1}{Pr(s)} \quad (2.9a)$$

$$= - \sum_{s \in \mathcal{S}} Pr(s) \log_2 Pr(s) \quad (2.9b)$$

where  $Pr(\cdot)$  is a probability mass function. Note that; in equation (2.9), with the logarithm to the base 2, the entropy can be thought of as the number of bits which are on average necessary to represent a realization  $s$  of  $S$ , or as the amount of information contained in  $s$ . The entropy  $H(S)$  is maximized if all values of  $S$  are equally likely, so that

$$\max_{p(s)} H(S) = \log_2(|\mathcal{S}|) \quad (2.10)$$

The conditional entropy  $H(R|S)$  is the entropy of the random variable conditional on the knowledge of another random variable and can be written as

$$H(R|S) = \sum_{r \in \mathcal{R}} \sum_{s \in \mathcal{S}} Pr(r, s) \log_2 \frac{1}{Pr(r|s)} \quad (2.11)$$

where  $S$  and  $R$  are independent. Hence, the amount of information,  $H(R|S)$ , contained in the realization  $r$  equals to  $H(S)$  due to  $s$  not having any information about  $r$ . On the other hand, the conditional entropy  $H(R|S)$  is zero if  $R = S$ .

### 2.4.2 Mutual Information

Mutual information represents a measure of the dependence between two random variables [53]. The mutual information is related to the information transfer as

$$I(S; R) = H(S) - H(S|R) \quad (2.12)$$

The quantity  $H(S) - H(S|R)$  is the average information provided about  $S$  by observing  $R$ . Thus, the mutual information  $I(S; R)$  is the reduction in the uncertainty of  $S$  due to the knowledge of  $R$ . The relationship between the mutual information of  $I(S; R)$  and the entropy of  $H(S)$ ,  $H(R)$ ,  $H(S, R)$ ,  $H(S|R)$ ,  $H(R|S)$  is illustrated in Figure 2.4 of the Venn diagram and is expressed as

$$I(S; R) = H(R) - H(R|S) \quad (2.13)$$

$$= H(R) + H(S) - H(S, R) \quad (2.14)$$

$$= H(S) \quad (2.15)$$

$$= I(R; S) \quad (2.16)$$

By the property of symmetry in equation (2.13),  $S$  knows as much about  $R$  as  $R$  knows about  $S$ . Since  $H(S, R) = H(S) + H(R|S)$ , then the relation in equation (2.14) is obtained [53]. One can notice from equations (2.15) and (2.16) that the mutual information of a random variable with itself is the entropy of the random variable, hence, for this reason the entropy is some times referred to as self information. To illustrate the concept of mutual information (MI), consider that the two variables are denoted by transmitted symbols  $S$  with the realization  $s$  and the received symbols  $L$  in terms of log-likelihood ratio (LLR) with the realization

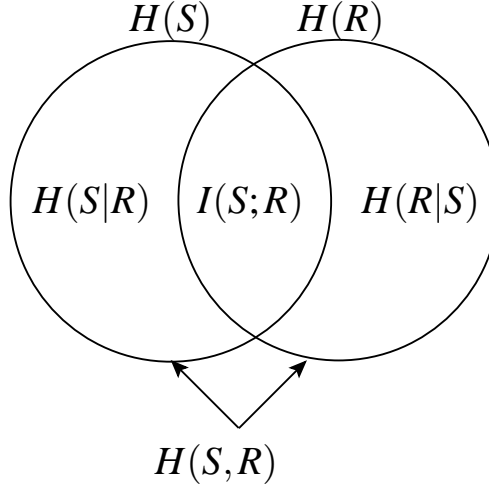


Figure 2.4: Relationship between mutual information and entropy.

$\xi$ . Again, if  $S$  and  $L$  are independent, the amount of information  $H(L|S)$  contained in the realization  $\xi$  is equal to  $H(L)$ , since  $s$  does not have any information about  $\xi$ . In this case, the mutual information,  $I$ , is zero and  $I(S;L)$  is defined as the amount of information  $\xi$  provides about  $s$ . Hence,  $I(S;L)$  is upper bounded by the minimum of  $H(S)$  and  $H(L)$  and the conditional entropy  $H(L|S)$  is zero if it holds that  $S = L$ . The mutual information between  $S$  and  $L$  can be defined for finite input and infinite output size as

$$I(S;L) = \sum \sum Pr(\xi|s) \log_2 \frac{Pr(\xi|s)}{Pr(\xi)Pr(s)} \quad (2.17)$$

#### 2.4.2.1 Mutual Information for Real-Values

The mutual information for input real value,  $S$ , of finite size and output soft information,  $L$ , of infinite size can be computed as

$$I(S;L) = \frac{1}{2} \sum_{s \in \pm 1} \int_{-\infty}^{+\infty} Pr(\xi|s) \log_2 \left( \frac{2Pr(\xi|s)}{Pr(\xi|s=+1) + Pr(\xi|s=-1)} \right) d\xi \quad (2.18)$$

However, a simple approach to evaluate the mutual information by exploit the symmetry and consistency properties of the pdf. The property of symmetry is valid for any linear code decoded by using *a posteriori* probability (APP) based decoders,

which can be written as [54]

$$Pr(\xi|s = +1) = Pr(-\xi|s = -1) \quad (2.19)$$

The property of consistency is satisfied with the accurate computation of the LLR output. Therefore, the consistency of the pdf is defined as [55]

$$Pr(\xi|s = +1) = Pr(-\xi|s = +1) \exp(\xi) \quad (2.20)$$

The equation results from the combination of equations (2.18), (2.19), and (2.20) to obtain

$$I(S; L) = 1 - \int_{-\infty}^{+\infty} Pr(\xi|s = +1) \log_2(1 + e^{-\xi}) d\xi \quad (2.21)$$

The equation (2.21) is closely approximated by using a time average as

$$I(S; L) \approx 1 - \frac{1}{N} \sum_{n=1}^N \log_2 \left( 1 + e^{-(s(n)L(n))} \right) \quad (2.22)$$

where  $N$  is the total number of observed  $L(n)$  of LLRs. Hence, the equation (2.22) can define the mutual information based on the decoder or demapper components.

### 2.4.2.2 Mutual Information for Complex-Values

Again, the mutual information for two random variables  $S$ ,  $L$  is defined in equation (2.17) and can be rewritten as

$$I(S; L) = \mathbb{E}_{s, \xi} \left( \log_2 \left( \frac{Pr(\xi|s)}{Pr(\xi)} \right) \right) \quad (2.23)$$

where  $\mathbb{E}$  denotes expectation over  $\{s, \xi\}$ ,  $Pr(\xi|s)$  is pdf of  $\xi|s$ , and  $Pr(\xi)$  is pdf of  $\xi$ . Consider  $s$  to be the transmitted complex-valued symbol by  $M$  signaling method and  $\xi$  the received decision variable, then the mutual information can be written as

$$I(S; L) = \frac{1}{M} \sum_{i=1}^M \mathbb{E}_{\xi|s_i} \left( \log_2 \left( \frac{Pr(\xi|s_i)}{Pr(\xi)} \right) \right) \quad (2.24)$$

The LLR,  $\Lambda$ , at modulation symbol level for a modulation with  $M$  states is defined as

$$\Lambda_{s_i}(\xi) = \ln \left( \frac{Pr(s_i|\xi)}{\sum_{j=1, j \neq i}^M Pr(s_j|\xi)} \right) \quad (2.25)$$

where the term  $Pr(s_i|\xi)$  means the probability that state  $s_i$  has been transmitted given that the received decision variable is  $\xi$  and  $\Lambda$  is the log-likelihood function. Assuming equal transmission probabilities for all modulation symbols, it can be easily proved that

$$\frac{Pr(\xi|s_i)}{Pr(\xi)} = \frac{M}{1 + e^{-\Lambda_{s_i}(\xi)}} \quad (2.26)$$

Hence, equation (2.24) becomes

$$I(S; L) = \frac{1}{M} \sum_{i=1}^M \mathbb{E}_{\xi|s} \left( \log_2 \left( \frac{M}{1 + e^{-\Lambda_{s_i}(\xi)}} \right) \right) \quad (2.27)$$

One can note that the LLRs are much larger than 1 and, therefore, the equation (2.27) tends to  $\log_2 M$ . Again, assuming equal transmission probabilities for all modulation symbols and AWGN channel, then equation (2.25) becomes

$$\Lambda_{s_i}(\xi) = \ln \left( \frac{e^{-d_{r_i}/\sigma^2}}{\sum_{j=1, j \neq i}^M e^{-d_{r_j}/\sigma^2}} \right) \quad (2.28)$$

where  $d_r$  is the distance from decision variable  $\xi$  to symbol  $s$  and  $\sigma^2$  is the noise variance.

## 2.5 System Model

A linear network for three nodes, user-1 and user-2 with a relay node in the middle, was considered for a PNC. The system model shown in Figure 2.5 gives an overview of all three nodes. The main concept of the PNC system is that user-1 and user-2 wish to exchange messages, but they are out of each other's transmission range and must use the relay. The relay operation in the network was performed for the TWRC. Therefore, the system consists of two phases or two time slots: uplink-phase, or 1<sup>st</sup> time slot, and downlink-phase, or 2<sup>nd</sup> time slot. In the first time slot, source nodes, user-1 and user-2, produce a sequence of information bits  $b_1$  and  $b_2$ , respectively. The two sources map the bits to a constellation diagram to generate  $S_1$  and  $S_2$  and then transmit simultaneously within the uplink phase. In the second time slot, or downlink phase, the relay receives the noisy signal,  $R$ , as  $R = S_1 + S_2 + W$ , where  $W$  is AWGN and then the relay maps  $R$  to produce the modulo-2 sum in another constellation diagram to produce  $Y$  as  $PNC : R \rightarrow Y$ , which is broadcast

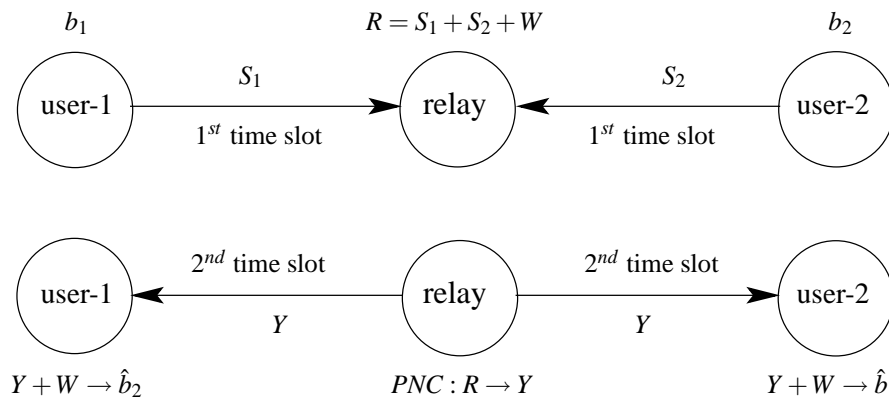


Figure 2.5: The model of PNC technique.

back to the destination nodes. At the destination, each user can then acquire their desired message from the summed signal  $Y$  received by performing an exclusive-OR operation and adding their own original messages to obtain their desired message  $Y + W \rightarrow \hat{b}_2$  for user-1 and  $Y + W \rightarrow \hat{b}_1$  for user-2.

### 2.5.1 Transmitter

In the wireless relaying network structure with binary data transmission, the transmitter sends only one of two possible signals during each bit interval  $T_b$ . The transmitted signal starts with the binary information bits  $\{\mathbf{b}_q(k)\}_{k=0}^{K-1} \in GF(2)$  of random binary data length  $K$  for each of the terminal nodes, where  $q \in \{1, 2\}$  is number of users as depicted in Figure 2.6. In a radio frequency (RF), the envelope and/or angle of the RF wave can be varied by using modulation techniques usually considered in digital baseband communications. A combined envelope and phase modulation with equally probable signal points on concentric rings was proposed in [56]. Based on this combination, wireless standards use standard signal constellations, including amplitude shift keying (ASK), phase shift keying (PSK) and a quadrature amplitude modulation (QAM) was first introduced by [57]. In digital transmission, the information bits are mapped to a suitable modulation scheme before performing baseband modulation. This is achieved by an array technique,  $M$ -ary, for PSK and QAM modulation schemes. Therefore,  $M$  can be defined as the constellation size of the utilized modulation scheme. The  $M$ -ary scheme groups the  $(\log_2 M)$  bits to each constellation point. For instance, the scheme with  $M=4$  is known as quadrature phase shift keying (QPSK), which maps two consecutive bits to a symbol taken from the QPSK alphabet. In this case, we have four symbols, each representing a

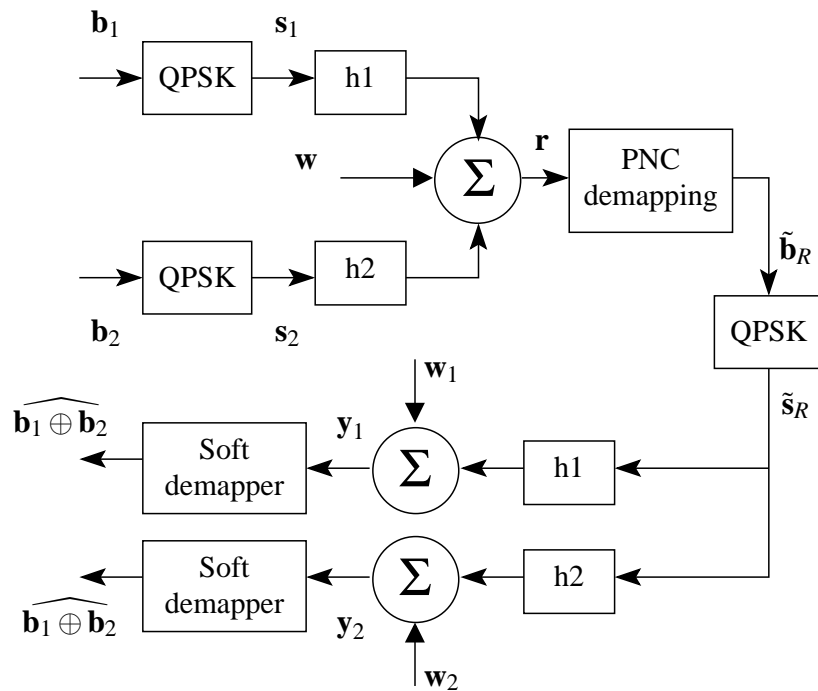


Figure 2.6: PNC system structure.

Table 2.1: QPSK mapping.

dibit (anti-gray map)	dibit (gray map)	phase
00	00	$\pi/4$
01	01	$3\pi/4$
10	11	$-3\pi/4$
11	10	$-\pi/4$

particular dibit value. The PSK modulation scheme offers only one degree of freedom as the amplitude of all the symbols is the same, whereas the QAM offers two degrees of freedom as the symbols exhibit different amplitude and phase distribution to achieve very efficient bandwidth. Consider the map listed in Table 2.1, to assign phase modulation to each of the four possible symbols. A constellation diagram shows the symbol locations in complex signal space, where the horizontal axis is the real or in-phase component and the vertical axis is the imaginary or quadrature component. The phase angle of a symbol is its angular displacement from the positive horizontal axis. The QPSK signal constellation resulting from the symbol map of Table 2.1 is shown in Figure 2.7. Consequently, the transmitters may send one of  $M$  possible signals during each signaling interval of duration  $T_s$ . Therefore, the message bits  $\mathbf{b}_q$  modulate a carrier signal using QPSK,  $M = 4$ , to produce the symbol sequence  $\{\mathbf{s}_q(n)\}_{n=0}^{N-1}$  of symbol length  $N$ . The bandwidth required for the

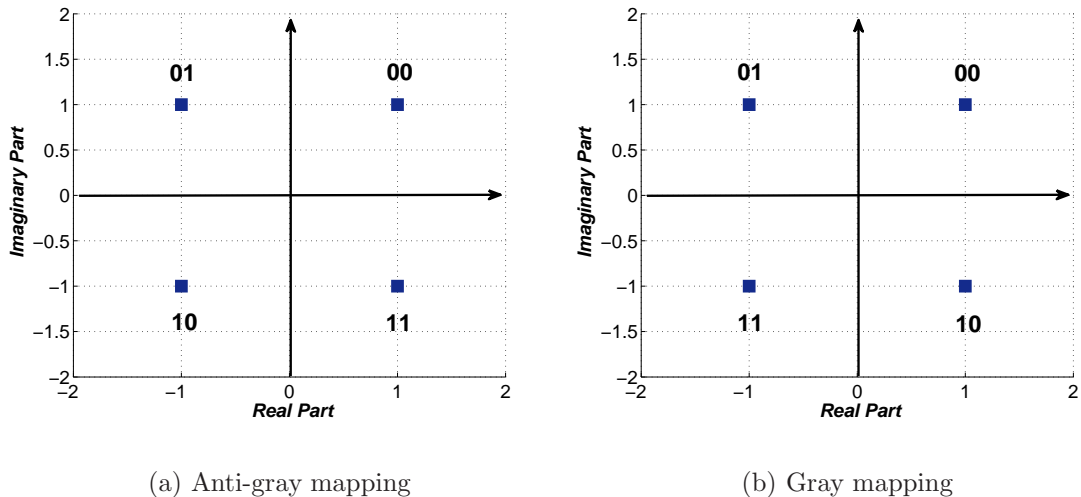


Figure 2.7: QPSK mapping.

QPSK signal is given by  $B = 1/T_s$  for bit rate  $\frac{\log_2 M}{T_s}$ . The  $s_q$  symbols are transmitted simultaneously by the two users over channels.

### 2.5.2 Channel Model and Characterization

In a wireless communications environment, the channel represents the medium between transmitter and receiver for the information transmission. As a result, signals suffer from multiple reflections while travelling from the transmitter to the receiver, so that the destination receives several replicas of the transmitted signal. The reflections are received with different amplitude and phase distortions, and the overall received signal is the combined sum of the reflections. Based on the relative phases of the reflections, the signals may add up constructively or destructively at the receiver. Consider the transmitter is moving with respect to the receiver, in this case, these destructive and constructive interferences will vary with time. The channel impulse response (CIR),  $h(t)$ , of a single path fading channel can be expressed as a time-varying linear filter with complex-baseband response given by [58]

$$h(t) = h_m(t)e^{j\phi(t)}\epsilon(\tau - \tau_0) \quad (2.29)$$

where  $h_m(t)e^{j\phi(t)}$  is a complex channel gain with amplitude  $h_m(t)$  and phase  $\phi(t)$  at time  $t$  and  $\tau_0$  is the channel delay. The phase  $\phi(t)$  is uniformly distributed in  $[0, 2\pi]$ , and the signal amplitude  $h_m(t)$  is a random variable with a Rayleigh

probability density function. The Rayleigh distribution is commonly used to describe the statistical time varying nature of the received envelope of a flat fading signal. In a flat fading channel,  $\epsilon(\tau - \tau_0)$  can be approximated as having no excess delay  $\tau_0=0$ , due to the reciprocal bandwidth of the transmitted signal is much larger than the multipath delay spread of the channel. It is well known that the envelope of the sum of two quadrature Gaussian noise signals obeys a Rayleigh distribution. The received baseband signal can be written as

$$r(t) = h(t)s(t) + w(t) \quad (2.30)$$

where  $w(t)$  is a zero-mean complex white Gaussian noise process and  $h(t)$  is a complex-valued process that describes the multiplicative distortion of the flat-fading channel. The Rayleigh distribution has a probability density function given by

$$p(r) = \begin{cases} \frac{r}{\sigma^2} e^{-\frac{r^2}{2\sigma^2}}, & \text{for } 0 \leq r \leq \infty \\ 0, & \text{for } r < 0 \end{cases} \quad (2.31)$$

In mobile radio channels, Rayleigh fading for the probability distribution model for the power spectral density of the fading process is accepted and even standardized. The parameters of implementing a Rayleigh flat-fading channel are related to the speed of the mobile user  $v_u$ , speed of light  $v_l$ , and the carrier frequency  $f_c$  to obtain the Doppler frequency  $f_D$  as

$$f_D = \frac{v_u f_c}{v_l} \quad (2.32)$$

Assume the value of  $f_c= 900\text{MHz}$ , the user moving at the speed of  $v_u= 80\text{Km/h}$ ,  $T_s= 1\text{ms}$ , and  $v_l = 3 \times 10^8 \text{ m/s}$ , then the Doppler frequency is  $f_D= 66.67\text{Hz}$ . Figure 2.8 shows a Rayleigh flat fading channel.

### 2.5.3 The Relay

As mentioned in Chapter 1, there are two approaches for the PNC technique, ANC and DNC. These approaches differ in how the relay processes the received signal. In the ANC approach, the relay does not try to perform demapping and then mapping. Instead, the relay may simply try to recover  $\mathbf{s}_1 \oplus \mathbf{s}_2$  in a symbol-by-symbol manner and pass the symbols along to the end nodes. Therefore, all the detection processing is performed at the destination. In the DNA approach, the relay makes use of the

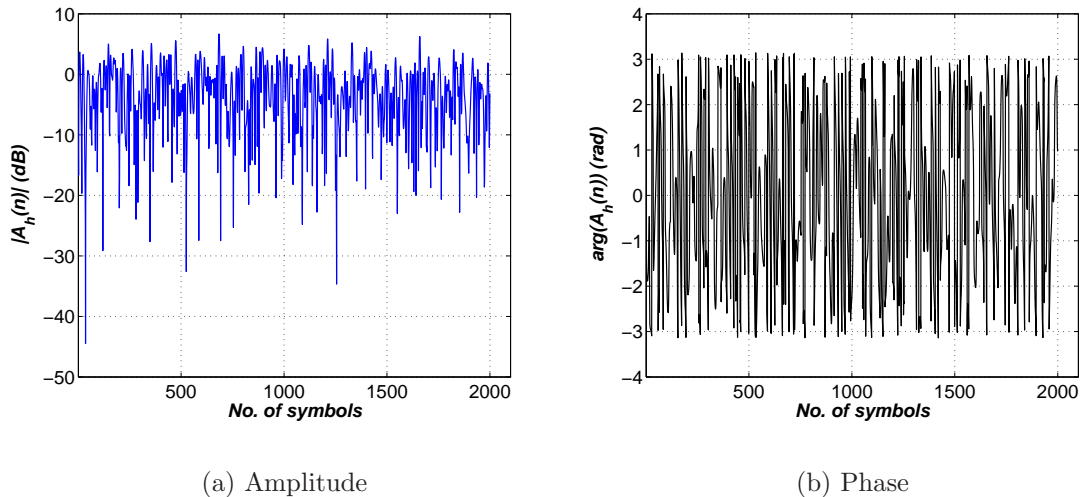


Figure 2.8: Rayleigh flat-fading channel.

correlations among successive symbols to recover the desired network-coded symbols, where the relay detects the received signal sum to clean up the noise and remodulates the signal and then broadcasts to the destinations. During a particular signalling interval, the received signal at the relay at time instant  $n$  can be represented as

$$\mathbf{r}|_{\text{AWGN}} = \sum_{i=1}^q \mathbf{s}_i + \mathbf{w} \quad (2.33)$$

$$\mathbf{r}|_{\text{Rayleigh}} = \sum_{i=1}^q h_i \mathbf{s}_i + \mathbf{w}_i \quad (2.34)$$

where  $\mathbf{w}$  is a complex additive white Gaussian noise process with zero-mean and variance  $\sigma^2 = N_0/2$ . For the PNC communication system, the channel implies that this should be for both time slots. However, the assessment requires the study of the proposed system in an ideal case, and to compare the results with the effect of the fading channel. At the relay, the most interesting process for the system is the PNC demapping to produce  $\tilde{\mathbf{b}}_R$  and then mapping to recover  $\tilde{\mathbf{s}}_R$ . To simplify this process, the noise is ignored in our simplified presentation for the time being. The relay combines the received signals during one symbol period as

$$\mathbf{r} = \mathbf{s}_1 + \mathbf{s}_2 \quad (2.35)$$

Due to the system using QPSK modulation in all the nodes and according to equation (2.35), the signal  $\mathbf{r}$  has corresponding bits mapping which can be summarized in

Table 2.2: The form of symbols received at the relay.

$\mathbf{r}$	$\mathbf{s}_1 \oplus \mathbf{s}_2$
00	00 $\oplus$ 00
	01 $\oplus$ 01
	10 $\oplus$ 10
	11 $\oplus$ 11
01	00 $\oplus$ 01
	01 $\oplus$ 00
	11 $\oplus$ 10
	10 $\oplus$ 11
10	00 $\oplus$ 10
	10 $\oplus$ 00
	11 $\oplus$ 01
	01 $\oplus$ 11
11	10 $\oplus$ 01
	01 $\oplus$ 10
	00 $\oplus$ 11
	11 $\oplus$ 00

Table 2.2, where  $\oplus$  denotes the pairwise application of symbol-by-symbol XOR over  $\mathbf{s}_1$  and  $\mathbf{s}_2$ . Figure 2.9 depicts the constellation point for the signal  $\mathbf{r}$  without noise. At the relay, the signal is received in a complex-valued form with the same phase and amplitude. This mean the symbol-level and carrier-phase are synchronized with power control applied. Thus, the real,  $\mathcal{R}$ , and the imaginary,  $\mathcal{J}$ , parts for the signal  $\mathbf{r}$  is combined as

$$\mathbf{r} \triangleq \mathcal{R}(\mathbf{r}) + \mathcal{J}(\mathbf{r}) \quad (2.36a)$$

$$\mathbf{r} = \mathcal{R}(\mathbf{s}_1 + \mathbf{s}_2) + \mathcal{J}(\mathbf{s}_1 + \mathbf{s}_2) \quad (2.36b)$$

In PNC, however, relay does not need the individual bits of the four unknowns bits in QPSK scheme. Instead, the relay only needs to derive the mapping form,  $\tilde{\mathbf{b}}_R$ , on the received symbols, which consists of two bits to produce the PNC mapping. There are three possible values 0, 2, and -2 at the relay in the PNC demapping under the condition of  $\mathcal{R}(\mathbf{r}) = 0$  when  $\mathcal{R}(\mathbf{s}_1) \neq \mathcal{R}(\mathbf{s}_2)$  and  $\mathcal{R}(\mathbf{r}) = -2$  or  $2$  when  $\mathcal{R}(\mathbf{s}_1) = \mathcal{R}(\mathbf{s}_2)$ . Consequently, the PNC mapping for  $\mathcal{R}(\mathbf{r}) = 0$  should be set to -1

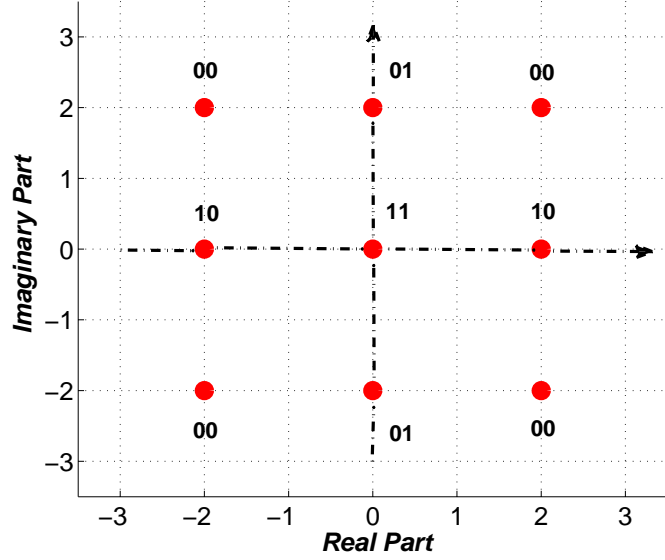


Figure 2.9: The constellation point at the relay without noise.

Table 2.3: PNC mapping for the first bit in the symbols received at the relay.

$s_1$	$s_2$	$\tilde{\mathbf{b}}_R$	$\tilde{\mathbf{s}}_R$
1	1	2	1
1	-1	0	-1
-1	1	0	-1
-1	-1	-2	1

when  $\mathcal{R}(s_1) \neq \mathcal{R}(s_2)$  and  $\mathcal{R}(r) = 1$  when  $\mathcal{R}(s_1) = \mathcal{R}(s_2)$ , which can be expressed as

$$\tilde{\mathbf{s}}_R = \begin{cases} -1, & \text{for } \tilde{\mathbf{b}}_R = 0 \\ 1, & \text{for } \tilde{\mathbf{b}}_R = -2 \text{ or } 2 \end{cases} \quad (2.37)$$

Table 2.3 shows the principle of PNC mapping for the first bit, in-phase, in the symbols  $s_1$  and  $s_2$ . The mapping for the second bit, quadrature, in the symbols  $s_1$  and  $s_2$  is similar. According to Table 2.3, the signal space is  $-2, 0, 2$  with corresponding probabilities of 25%, 50%, 25%, respectively. The relay maps the signal then forwards it back to the end nodes. Therefore, the probability of the received signal with the modulo-2 sum of the first transmitted bit from user-1 and user-2 is depicted in Figure 2.10. The demapping operates on a symbol-by-symbol basis, and therefore we may focus on a single signaling interval,  $\mathbf{b}$ . Since  $\mathbf{b}_1$  and  $\mathbf{b}_2$  are the bits transmitted by terminals, then let  $\tilde{\mathbf{b}}_R = \mathbf{b}_1 \oplus \mathbf{b}_2$  be the corresponding network

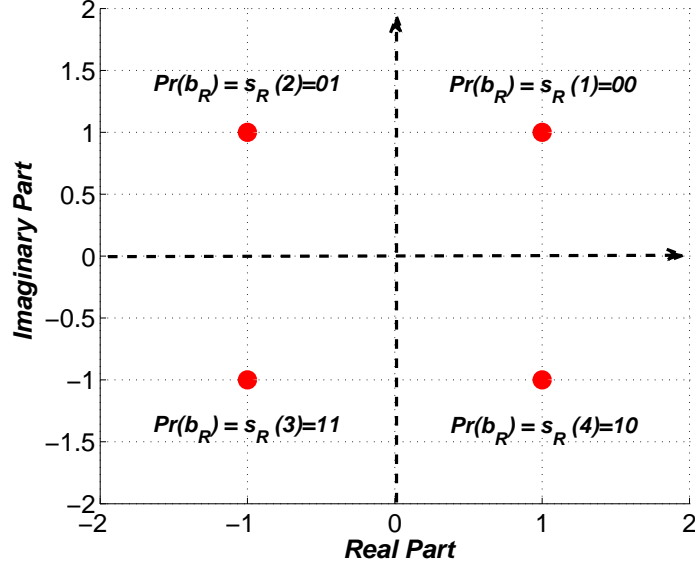


Figure 2.10: The constellation point of the relay mapping to produce  $\tilde{\mathbf{s}}_R$ .

coded bit. The relay demodulator computes the LLR as

$$\Lambda(\tilde{\mathbf{b}}_R) = \log \frac{Pr(\tilde{\mathbf{b}}_R = 1|\mathbf{r})}{Pr(\tilde{\mathbf{b}}_R = 0|\mathbf{r})} \quad (2.38a)$$

$$= \log \frac{Pr(\mathbf{b}_1 \oplus \mathbf{b}_2 = 1|\mathbf{r})}{Pr(\mathbf{b}_1 \oplus \mathbf{b}_2 = 0|\mathbf{r})} \quad (2.38b)$$

The term  $\mathbf{b}_1 \oplus \mathbf{b}_2 = 1$  is equivalent to the union of the terms  $\mathbf{b}_1 = 0, \mathbf{b}_2 = 1$  and  $\mathbf{b}_1 = 1, \mathbf{b}_2 = 0$ . Similarly, the term  $\mathbf{b}_1 \oplus \mathbf{b}_2 = 0$  is equivalent to the union of the terms  $\mathbf{b}_1 = 0, \mathbf{b}_2 = 0$  and  $\mathbf{b}_1 = 1, \mathbf{b}_2 = 1$ , which can be expressed as

$$\Lambda(\mathbf{b}_1 \oplus \mathbf{b}_2) = \log \frac{Pr(\{\mathbf{b}_1 = 0, \mathbf{b}_2 = 1\} \cup \{\mathbf{b}_1 = 1, \mathbf{b}_2 = 0\})}{Pr(\{\mathbf{b}_1 = 0, \mathbf{b}_2 = 0\} \cup \{\mathbf{b}_1 = 1, \mathbf{b}_2 = 1\})} \quad (2.39)$$

$$= \log \frac{Pr(\{\mathbf{b}_1 = 0, \mathbf{b}_2 = 1\}|\mathbf{r}) + Pr(\{\mathbf{b}_1 = 1, \mathbf{b}_2 = 0\}|\mathbf{r})}{Pr(\{\mathbf{b}_1 = 0, \mathbf{b}_2 = 0\}|\mathbf{r}) + Pr(\{\mathbf{b}_1 = 1, \mathbf{b}_2 = 1\}|\mathbf{r})} \quad (2.40)$$

where equation (2.40) follows from equation (2.39) because the terms are mutually exclusive. In the PNC demapping, it is not sensible to compute  $\Lambda(\mathbf{b}_1)$  and  $\Lambda(\mathbf{b}_2)$  separately. Instead, we can use equation (2.40) with the assumption that the four terms are equally likely along with Bayes' rule to obtain

$$\Lambda(\mathbf{b}_1 \oplus \mathbf{b}_2) = \log[p(\mathbf{r}|\{\mathbf{b}_1 = 0, \mathbf{b}_2 = 1\}) + p(\mathbf{r}|\{\mathbf{b}_1 = 1, \mathbf{b}_2 = 0\})] - \log[p(\mathbf{r}|\{\mathbf{b}_1 = 0, \mathbf{b}_2 = 0\}) + p(\mathbf{r}|\{\mathbf{b}_1 = 1, \mathbf{b}_2 = 1\})] \quad (2.41)$$

The LLR first summed bit can be calculated as

$$\Lambda_1(\mathbf{b}_1^{(q_1)} \oplus \mathbf{b}_1^{(q_2)}) = \ln \left( \frac{Pr(\mathbf{r}|\mathbf{b}_1^{(q_1)} \oplus \mathbf{b}_1^{(q_2)} = 0)}{Pr(\mathbf{r}|\mathbf{b}_1^{(q_1)} \oplus \mathbf{b}_1^{(q_2)} = 1)} \right), \quad (2.42)$$

Similarly, the conditional probabilities LLRs of the received symbol are given, such that the second message bits are

$$\Lambda_2(\mathbf{b}_2^{(q_1)} \oplus \mathbf{b}_2^{(q_2)}) = \ln \left( \frac{Pr(\mathbf{r}|\mathbf{b}_2^{(q_1)} \oplus \mathbf{b}_2^{(q_2)} = 0)}{Pr(\mathbf{r}|\mathbf{b}_2^{(q_1)} \oplus \mathbf{b}_2^{(q_2)} = 1)} \right). \quad (2.43)$$

where  $\Lambda_1(\cdot)$  and  $\Lambda_2(\cdot)$  are the LLRs reliability bits. The complete equation derivation of determining the LLRs XOR-ed bits when both users employ QPSK is presented in the Appendix A. The computation of each  $p(\mathbf{r}|\{\mathbf{b}_1, \mathbf{b}_2\})$  by the PNC relay given various levels of channel state information is the subject of the remainder of this Section.

### 2.5.3.1 Consideration of Noise

Our throughput analysis has been based on time slot counting, assuming whatever is sent will be received correctly. In the consideration of noise over AWGN channel, the equation (2.36) becomes

$$\mathbf{r} = \mathcal{R}(\mathbf{s}_1 + \mathbf{s}_2 + \mathbf{w}) + \mathcal{J}(\mathbf{s}_1 + \mathbf{s}_2 + \mathbf{w}) \quad (2.44)$$

where the noise  $\mathbf{w}$  is typically modelled as a complex Gaussian random variable. The optimal decision rule was adopted by [3] when applying the maximum posterior probability criterion [58] for the received signal  $\mathbf{r}$ . Here  $\mathcal{R}(\mathbf{r}) = -2$  when less than

$$D_1 = -1 - \frac{N_0}{4} \ln(1 + \sqrt{1 - e^{-8/N_0}}) \quad (2.45)$$

and  $\mathcal{R}(\mathbf{r}) = +2$  when greater than

$$D_2 = 1 + \frac{N_0}{4} \ln(1 + \sqrt{1 - e^{-8/N_0}}) \quad (2.46)$$

Otherwise, it is set to 0. This is similar to the case for the  $\mathcal{J}(\mathbf{r})$  to obtain the -2, 0, 2 in QPSK signal. However, a simple strategy for transmitting noisy modulo-2 sum of the bits to the relay over the real part of the channel in the E2E approach is

considered as follow. For ease of analysis, consider that the total power per channel use is  $P = 2$ , which means that we can allocate one unit of power to the real part and one unit to the imaginary part. Each user maps its bit to a channel input symbol using binary phase-shift keying (BPSK) as

$$\mathbf{s}_q = \begin{cases} 1, & \text{for } \mathbf{b}_q = 1 \\ -1, & \text{for } \mathbf{b}_q = 0 \end{cases} \quad (2.47)$$

Hence, if the modulo-2 sum of the bits,  $\tilde{\mathbf{b}}_R = \mathbf{b}_1 \oplus \mathbf{b}_2$  is 1, then the sum of the transmitted signals  $\mathbf{s}_1 + \mathbf{s}_2 = 0$ . Similarly, if  $\tilde{\mathbf{b}}_R = \mathbf{b}_1 \oplus \mathbf{b}_2$  is 0, then  $\mathbf{s}_1 + \mathbf{s}_2$  is either 2 or -2, depending on the original bits. The maximum *a posteriori* (MAP) rule to minimize the probability can be used to estimate  $\tilde{\mathbf{b}}_R$  as [59]

$$\tilde{\mathbf{b}}_R = \arg \max_{i=0,1} p(r|\mathbf{b}_1 \oplus \mathbf{b}_2 = i) Pr(\mathbf{b}_1 \oplus \mathbf{b}_2 = i) \quad (2.48)$$

where  $p(r|\mathbf{b}_1 \oplus \mathbf{b}_2 = i)$  is the conditional probability distribution of the channel output given the modulo-2 sum and  $i = 0$  or 1. Since the noise is Gaussian, the probability density function for  $p(r|\mathbf{b}_1 \oplus \mathbf{b}_2 = i)$  can be expressed as [60]

$$p(r|\mathbf{b}_1 \oplus \mathbf{b}_2 = i) = \begin{cases} \frac{1}{\sqrt{2\pi\sigma^2}} e^{-r^2/2\sigma^2}, & \text{for } \mathbf{b}_1 \oplus \mathbf{b}_2 = \tilde{\mathbf{b}}_R = 1 \\ \frac{1}{2\sqrt{2\pi\sigma^2}} (e^{-(r-2)^2/2\sigma^2} + e^{-(r+2)^2/2\sigma^2}), & \text{for } \mathbf{b}_1 \oplus \mathbf{b}_2 = \tilde{\mathbf{b}}_R = 0 \end{cases} \quad (2.49)$$

The conditional probability density functions (pdf) of the received signal,  $\mathbf{r} = r_1, r_2, \dots, r_n$ , can be defined as [58]

$$p(\mathbf{r}|\mathbf{s}) = \prod_{i=1}^N p(r_i|s_i) \quad (2.50a)$$

$$= \frac{1}{(\pi N_0)^{N/2}} \exp\left(-\frac{1}{N_0} \sum_{i=1}^N (r_i - s_i)^2\right) \quad (2.50b)$$

Hence, using the conditional distribution of  $\mathbf{r}$  with  $\Lambda(s) = p(\mathbf{r}|s)$  then yields

$$\Lambda(s) = -\frac{1}{N_0} \sum_{i=1}^N (r_i - s_i)^2 \quad (2.51a)$$

$$= \|\mathbf{r} - \mathbf{s}\|^2 \quad (2.51b)$$

where the term  $\|\cdot\|^2$  is normalized. One can note that for  $p(r|\mathbf{b}_1 \oplus \mathbf{b}_2) = 0$ ,  $\mathbf{r}$  follows a Gaussian mixture distribution since  $\mathbf{s}_1 + \mathbf{s}_2$  can be either  $+2$  or  $-2$  with equal probability. The same scheme can be applied to the imaginary part. Some calculation reveals that the MAP rule is just a threshold on the magnitude of the received signal as

$$\tilde{\mathbf{b}}_R = \begin{cases} 1, & |\mathbf{r}| \leq 1 + (\sigma^2 \ln 2)/2 \\ 0, & \text{otherwise} \end{cases} \quad (2.52)$$

Applying this method to every bit allows the relay to obtain a corrupted version of the modulo-2 sum of the bit strings,  $\tilde{\mathbf{b}}_R$ .

### 2.5.3.2 Consideration of Rayleigh flat-Fading Channels

The discussion thus far assumes that the channels are symmetric. In general, user-1 and user-2 may undergo fading. Therefore, the signal over the RF bandwidth of concern in the uplink-phase can be described as

$$\mathbf{r} = h_1 \mathbf{s}_1 + h_2 \mathbf{s}_2 + \mathbf{w} \quad (2.53)$$

where  $h_q$  is the complex channel coefficient and  $\mathbf{w}$  is the background noise sequence at the relay, which is assumed to be an independent and identically distributed (i.i.d.) sequence of circularly symmetric complex Gaussian random variables with zero mean and variance  $\sigma^2$ . The relay therefore sees the noisy sum of the transmitted signals and we can consider the real and imaginary parts of the channel separately. The real part of the signal observed at the relay is

$$I_R = \Re(\mathbf{r}) \quad (2.54a)$$

$$= \Re(h_1 \mathbf{s}_1 + h_2 \mathbf{s}_2 + \mathbf{w}) \quad (2.54b)$$

where  $h_1$  and  $h_2$  are the complex number of the channel gain for the uplink channel from user  $q$  to relay. Similarly, for imaginary part of the signal observed at the relay is

$$Q_R = \Im(\mathbf{r}) \quad (2.55a)$$

$$= \Im(h_1 \mathbf{s}_1 + h_2 \mathbf{s}_2 + \mathbf{w}) \quad (2.55b)$$

Let  $\eta$  be the mean of the received signal  $\mathbf{r}$  to produce  $\eta[\mathbf{b}_1, \mathbf{b}_2]$  for the given values of  $\mathbf{b}_1$  and  $\mathbf{b}_2$ . Therefore, there is a one-to-one correspondence between  $\{\mathbf{b}_1, \mathbf{b}_2\}$  and the mean vector  $\eta[\mathbf{b}_1, \mathbf{b}_2]$  since the terminals transmit different  $\eta[0, 1]$  and  $\eta[1, 0]$  when  $\mathbf{b}_1 \neq \mathbf{b}_2$  as

$$\eta[0, 1] = [\mathbf{h}_1 \ \mathbf{h}_2]^T \quad (2.56a)$$

$$\eta[1, 0] = [\mathbf{h}_2 \ \mathbf{h}_1]^T \quad (2.56b)$$

Similarly, when  $\mathbf{b}_1 = \mathbf{b}_2$  there are two terminals that transmit different  $\eta[0, 0]$  and  $\eta[1, 1]$  as

$$\eta[0, 0] = [(\mathbf{h}_1 + \mathbf{h}_2) \ 0]^T \quad (2.57a)$$

$$\eta[1, 1] = [0 \ (\mathbf{h}_1 + \mathbf{h}_2)]^T \quad (2.57b)$$

Hence, it is equivalent to write  $p(r|\{\mathbf{b}_1, \mathbf{b}_2\})$  as  $p(r|\eta[\mathbf{b}_1, \mathbf{b}_2])$  where

$$p(r|\eta[\mathbf{b}_1, \mathbf{b}_2]) = \left(\frac{1}{\pi N_0}\right)^2 \exp\left(-\frac{1}{N_0} \|r - \eta[\mathbf{b}_1, \mathbf{b}_2]\|^2\right) \quad (2.58)$$

The demodulator computes,  $\Lambda$ , as in equation (2.38). The flat-fading channel from users,  $q$ , to relay is characterized by the complex channel coefficients vector,  $\mathbf{h}_q$ , then the  $\Lambda(s)$  can be calculated from equation (2.51b) as

$$\Lambda(s) = \|\mathbf{r} - \mathbf{h}s\|^2 \quad (2.59)$$

However, the common approach for the demapping and then mapping of synchronization algorithms embodies the application of the maximum likelihood (ML) criterion. The strategy uses the conditional probability density functions of the received signal in equation (2.50) and then uses the conditional distribution of  $\mathbf{r}$  with  $\Lambda(s) = p(\mathbf{r}|s)$  as in equation (2.51). Thus, the  $\Lambda(s)$  depends only on the distance between the received vector  $\mathbf{r}$  and the constellation point  $s$ . In the maximum likelihood receiver the signal constellation closest to  $\mathbf{r}$  is determined as the constellation point  $s$  satisfying

$$\arg \min -\frac{1}{N_0} \sum_{i=1}^N (r_i - s_i)^2 = \arg \min -\frac{1}{N_0} \|r - s\|^2 \quad (2.60)$$

where  $s$  is determined from the decision region that contains  $r$ . This is equivalent to the computation of the minimum Euclidean distance,  $D_R$ , as

$$D_R(\hat{\mathbf{b}}, \mathbf{b}) = \min_{n=1,2,3,4} |\hat{\mathbf{b}} - \mathbf{b}_n| \quad (2.61)$$

where  $\mathbf{b}$  is the set the four possible transmitted QPSK symbols. The hard decision method takes the estimate and quantizes  $\mathbf{r}$  to one of the four possible points, as illustrated in Figure 2.10, on the basis of the following decision rule

$$\hat{\mathbf{b}}_1 > 0 \cap \hat{\mathbf{b}}_2 > 0 \rightarrow +1 + j \quad (2.62)$$

$$\hat{\mathbf{b}}_1 < 0 \cap \hat{\mathbf{b}}_2 > 0 \rightarrow -1 + j \quad (2.63)$$

$$\hat{\mathbf{b}}_1 > 0 \cap \hat{\mathbf{b}}_2 < 0 \rightarrow +1 - j \quad (2.64)$$

$$\hat{\mathbf{b}}_1 < 0 \cap \hat{\mathbf{b}}_2 < 0 \rightarrow -1 - j \quad (2.65)$$

Thus, the hard decision method computes the set of four possible distance and selects the symbol corresponding to the smallest distance metrics.

### 2.5.4 The Receiver

The receiver components are soft-in-soft-out (SISO) decoders or demapper to compute the LLRs of the soft information. The data detection algorithm mainly consists of a soft demapper which provides the bit metric to the detector. In the second time slot, the receiver receives the modulo-2 sum symbols as

$$\mathbf{y}_q = h_q \tilde{\mathbf{s}}_R + \mathbf{w}_q \quad (2.66)$$

In order to perform detection effectively, the coherent detection computes each channel gain and can invert it. Therefore, user-1 and user-2 can multiply the symbol  $\mathbf{y}_1$  by  $h_1^*/|h_1|^2$  and the symbol  $\mathbf{y}_2$  by  $h_2^*/|h_2|^2$ , respectively. Then the soft output demodulator is implemented as a SOMAP algorithm, which is described in its most generic form in [61]. The SOMAP algorithm works on a symbol-by-symbol basis to compute the likelihoods of each of the code bits associated with each received symbol. The process to obtain the LLRs bits to represent the modulo-2 sum of the

first and second estimated transmitted bits  $\widehat{\mathbf{b}_1 \oplus \mathbf{b}_2}$  for user-1 as

$$\widehat{\mathbf{b}_1 \oplus \mathbf{b}_2} = \mathbf{b}_1 \oplus \widehat{\mathbf{b}_1 \oplus \mathbf{b}_2} \quad (2.67a)$$

$$= \widehat{\mathbf{b}_2} \quad (2.67b)$$

Similarly, for user-2

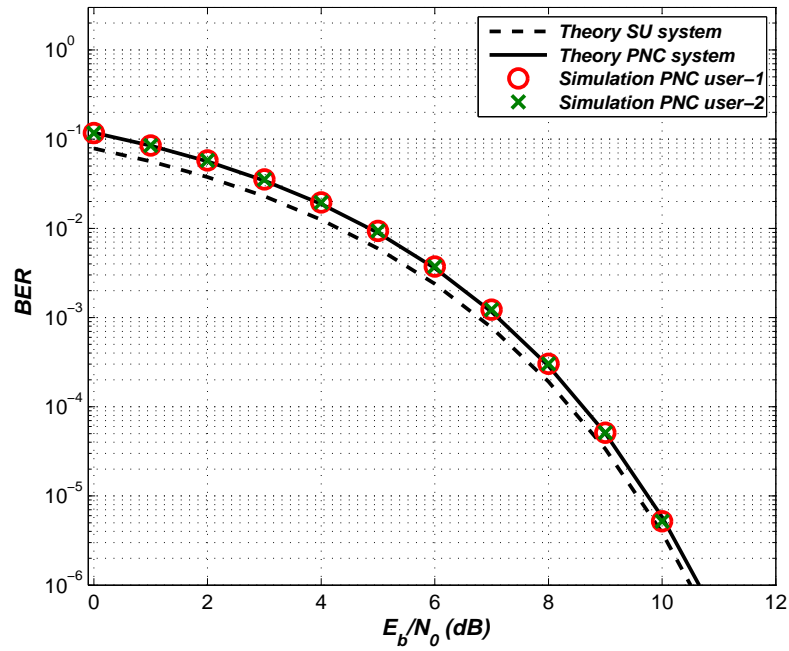
$$\widehat{\mathbf{b}_1 \oplus \mathbf{b}_2} = \mathbf{b}_2 \oplus \widehat{\mathbf{b}_1 \oplus \mathbf{b}_2} \quad (2.68a)$$

$$= \widehat{\mathbf{b}_1} \quad (2.68b)$$

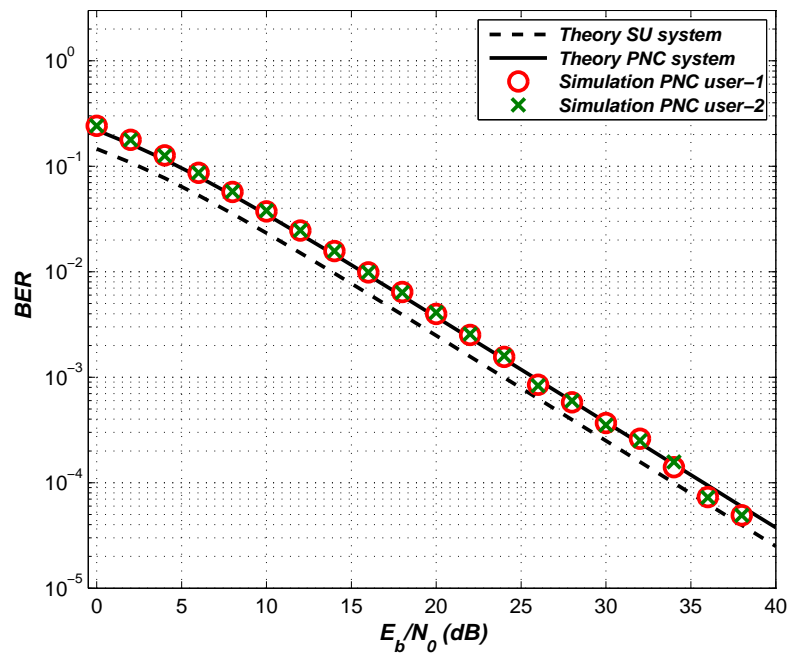
Coupling this strategy from relay to receiver with an E2E error correcting code allows the users to successfully exchange messages using just two time slots.

### 2.5.5 Simulation Results

In the study of the PNC system, the additive white Gaussian noise (AWGN) channel is the usual starting point for understanding and evaluating the basic performance relationships of the system. A distortion less channel has been assumed and AWGN with zero mean value independent of the signal. The uncoded PNC system is shown along with the simulated bit error rate (BER) performance over AWGN and Rayleigh flat-fading channels, as depicted in Figure 2.11. The BER performance of the classical QPSK point-to-point link and PNC on AWGN channel is plotted in Figure 2.11(a). Similar situation with the uncoded PNC over Rayleigh flat-fading channel for both phases, as shown in Figure 2.11(b). The classical QPSK point-to-point link is comparable to that of the E2E BER between users 1 and 2 of PNC, and is actually slightly better than that of PNC. The QPSK point-to-point link consists of four such one-hop links, hence for all the one-hop links the BER is similar. For comparison the BER of the XOR PNC system, which is also plotted in Figure 2.11(a), emphasizes that for PNC, the target signal at the receiver is the XOR signal. Thus, the BER is the BER of the decoded XOR of user's bits, not the BER of the individual bits from the two ends. Therefore, the E2E BER of PNC is approximately the same as in QPSK point-to-point link. However, the PNC uses two time slots and the QPSK point-to-point link uses four time slots. Thus, at equal BER, the throughput of PNC is twice that of QPSK point-to-point link, as shown in Figure 2.12.



(a) AWGN channel



(b) Rayleigh flat-fading channel

Figure 2.11: BER performance for PNC system

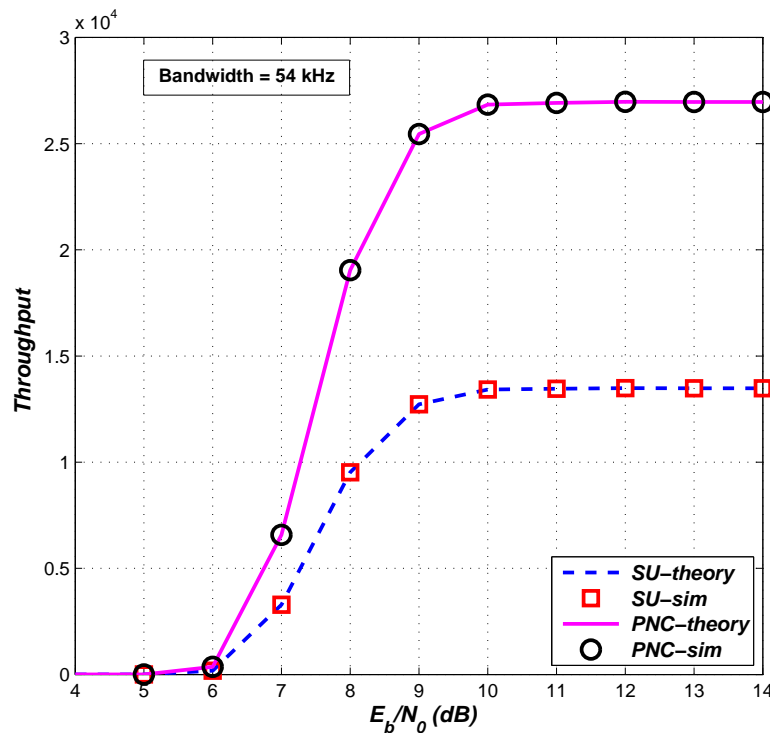


Figure 2.12: The throughput measurement for PNC and single user systems.

## 2.6 Chapter Summary

This chapter presents an overview of fundamental concepts which will be used throughout the remainder of the thesis. In order to introduce terminology, a review of two-way communication systems, bandpass signals and systems representation, information theory, and the system model were presented. A brief description of cooperative communication system, two way relay channel, and relaying scheme were discussed. The relationship between the two way relay channel and the physical-layer network coding was emphasized. Two representations for bandpass signal and system were discussed. It was shown how the mutual information could be calculated for real and complex mapping and the relation with the entropy. Once a foundation of the transmitter and channel model concepts were presented, a relay of PNC system was introduced. It was shown how AWGN and Rayleigh fading channels could be apply on the PNC system of two phases. A brief performance analysis of a PNC system was presented.

## Chapter 3

---

---

# Error Control Coding and Iterative Decoding Schemes Combined with E2E PNC

---

---

## 3.1 Introduction

Channel coding or forward error correction (FEC) is a technique used to correct errors for data transmission over noisy communication channels. Shannon's noisy channel coding theorem shows that if long random codes are used, reliable communication can take place provided the rate of transmission is less than the channel capacity [52]. However, truly random codes are impractical, as the codes should possess some structure in order to have computationally tractable encoding and decoding algorithms. Therefore, the code design and decoding for a group of error correction codes is achieved for reliable communication by employing algebraic methods in the form of convolution or block coding [62]. The key idea is that the sender encodes their message by adding redundant bits by using an error-correcting code (ECC). The mathematician Hamming pioneered this field in the 1940s and invented the first error-correcting code in 1950 with the Hamming codes [63].

The contribution of this chapter is a comparison of E2E PNC systems combined with different iterative coding schemes, namely low density parity check (LDPC), bit interleaved coded modulation with iterative decoding (BICM-ID) and turbo codes. The aim of this chapter is to evaluate the system performance with the different coding schemes. The software implementation of the E2E PNC system with three different techniques for iterative decoding are investigated and compared with different block sizes and code rates in terms of BER performance and comparisons are made between the different coding schemes.

## 3.2 Convolutional Codes

Convolutional codes were first introduced by Elias [64] as an alternative to block codes. Rather than segmenting data into distinct blocks as in block codes, the convolutional encoder adds redundancy to a continuous stream of input data by using a linear shift registers. Each set of encoder output bits is a linear combination of the current set of encoder input bits and the bits stored in the shift registers. The total number of bits that each output depends on is known as the constraint length  $K_c$ . The rate of the convolutional encoder  $R_c$  is the number of data bits taken in by the encoder in one coding interval divided by the number of output code bits during the same interval. Convolutional codes are similar to cyclic codes in the sense

that the encoder can be implemented using a linear shift register network. However, convolutional codes differ from cyclic codes in two fundamental ways; convolutional codes remove the requirement of a fixed block size and can be multi-input multi-output. Convolutional codes are now widely used in wireless communications and are highly structured, allowing simple implementation and good performance, but they are still some way from reaching the capacity limit predicted by Shannon. Viterbi [65] proposed a maximum likelihood decoding scheme that was relatively easy to implement for codes with moderate memory order. This scheme, called Viterbi decoding, led to the application of convolutional codes to deep-space and satellite communication in the early 1970s. There are also soft-input soft-output algorithms, like SOVA (Soft Output Viterbi Algorithm) or the Bahl-Cocke-Jelinek-Raviv (BCJR) algorithm, which provide not only a decision but also measurement of reliability.

### 3.2.1 Convolutional Encoder Structure

Like any error-correcting code, a convolutional code works by adding redundant bits to the input message and then corrects these errors at the receiver using this redundancy. The encoder input bits  $\mathbf{b}$  are first split into streams to produce output-streams and then the output is multiplexed to form the codeword  $\mathbf{c}$  as depicted in Figure 3.1. The output codeword  $\mathbf{c}$  is assembled from output streams by convolving the input stream with a generator sequence. Moreover, the structure of the encoder can be systematic or non-systematic. Systematic codes are those where the message is a part of the output sequence, and these are almost always recursive. Conversely, non-recursive codes are almost always non-systematic. Figures 3.1(a) and 3.1(b) shows the non-systematic convolutional (NSC) code and recursive systematic convolutional (RSC) codes, respectively.

### 3.2.2 Representation of Convolutional Code

The convolutional encoder can be viewed in many different ways. From one perspective, they can be considered as a number of input and output finite impulse response (FIR) filters with operations performed over the Galois field of two elements ( $GF(2)$ ). Alternatively, they can be represented by state diagrams, graphs, and trellises. The state of a convolutional encoder is determined by the contents

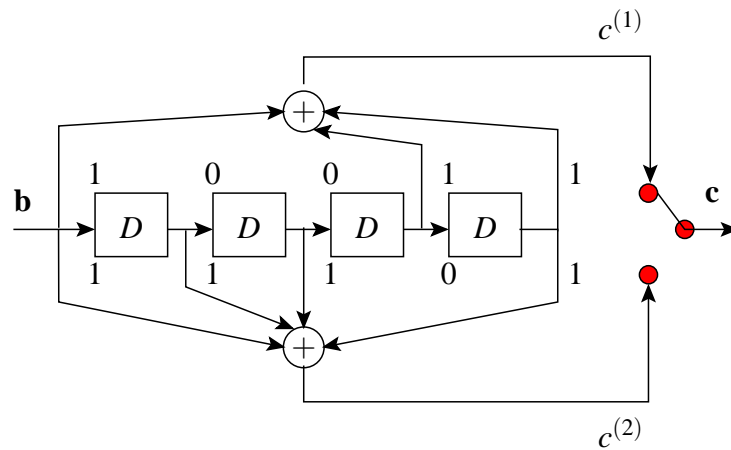
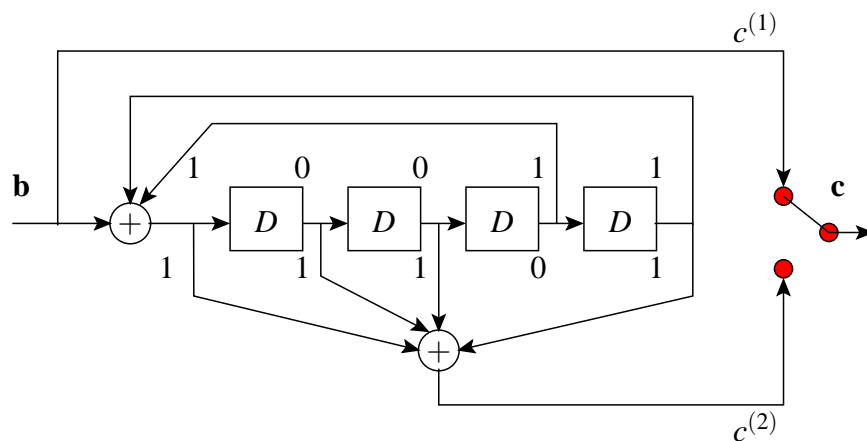
(a) NSC with  $(23, 35)_8$ (b) RSC with  $(1, \frac{23}{35})_8$ 

Figure 3.1: Encoder structures for non-systematic and recursive systematic with octal generators.

of its shift registers. For a rate convolutional encoder with memory  $m_c$ , there are  $2^{m_c}$  possible internal states. Once the encoder receives a new input bit, it can only make a transition to one of two other states depending on whether the input bit is a 0 or a 1. When the encoder makes a transition from one state to another, a particular sequence of bits is the output. The nodes in a trellis diagram correspond to a particular state and a discrete time step. The nodes depends on the state and the time index. Branches connect nodes at time  $t$  to nodes at time  $t + 1$ . The trellis diagram method shows how each possible input to the encoder influences both the output and the state transitions of the encoder. For convolutional codes, every code word is associated with a unique path through the trellis. This path is called a state

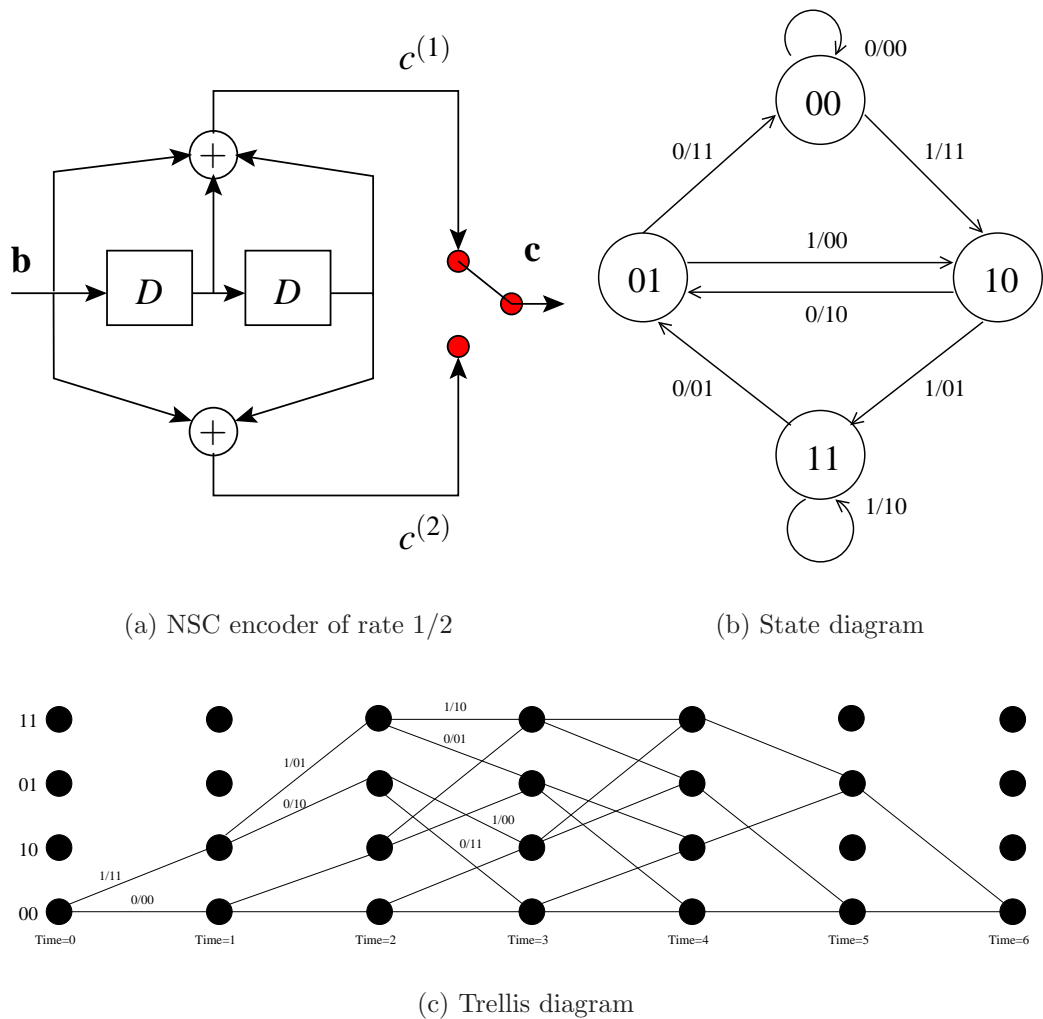


Figure 3.2: An example to illustrate the convolutional code with its state and trellis diagrams.

sequence and denoted as  $\mathbf{s} = (s_0, s_1, \dots)$ . For simplicity, an example of an NSC convolutional encoder represented by its state and trellis diagram is shown in Figure 3.2. The encode and its corresponding state diagram are shown in Figure 3.2(a) and 3.2(b). Multiple trellis diagram stages for this code are shown in Figure 3.2(c).

### 3.2.3 BCJR Decoding Algorithm

The symbol-by-symbol maximum *a posteriori* (MAP) algorithm was first presented in 1974 by Bahl et al [66] to decode both block and convolutional codes. The goal of the BCJR algorithm is to calculate the *a posteriori* probability (APP) of each state transition, information bit, and/or code symbol produced by a Markov process, given the noisy observation  $r$ . The BCJR algorithm first finds the probability  $Pr(\mathbf{s}_t \rightarrow$

$\mathbf{s}_{t+1}|r)$  of each valid state transition given the noisy channel output  $r$ , where  $\mathbf{s}_t$  is the initial state and  $\mathbf{s}_{t+1}$  is the next state. The conditional probability can be defined as

$$Pr(\mathbf{s}_t \rightarrow \mathbf{s}_{t+1}|r) = \frac{Pr(\mathbf{s}_t \rightarrow \mathbf{s}_{t+1}, r)}{Pr(r)} \quad (3.1)$$

The properties of the Markov process can be used to partition the numerator as

$$Pr(\mathbf{s}_t \rightarrow \mathbf{s}_{t+1}, r) = \alpha(\mathbf{s}_t)\gamma(\mathbf{s}_t \rightarrow \mathbf{s}_{t+1})\beta(\mathbf{s}_{t+1}) \quad (3.2)$$

where

$$\alpha(\mathbf{s}_t) = Pr(\mathbf{s}_t, (r_0, \dots, r_{t-1})) \quad (3.3)$$

$$\gamma(\mathbf{s}_t \rightarrow \mathbf{s}_{t+1}) = Pr(\mathbf{s}_{t+1}, r_t|\mathbf{s}_t) \quad (3.4)$$

$$\beta(\mathbf{s}_{t+1}) = Pr((r_{t+1}, \dots, r_{N-1})|\mathbf{s}_{t+1}) \quad (3.5)$$

The term  $\gamma(\mathbf{s}_t \rightarrow \mathbf{s}_{t+1})$  is the branch metric associated with the transition  $\mathbf{s}_t \rightarrow \mathbf{s}_{t+1}$  which can be expressed as

$$\gamma(\mathbf{s}_t \rightarrow \mathbf{s}_{t+1}) = Pr(\mathbf{s}_{t+1}|\mathbf{s}_t)Pr(r_t|\mathbf{s}_t \rightarrow \mathbf{s}_{t+1}) \quad (3.6a)$$

$$= Pr(b_t)Pr(r_t|c_t) \quad (3.6b)$$

where  $c_t$  is the encoder output associated with the state transition  $\mathbf{s}_t \rightarrow \mathbf{s}_{t+1}$ . In equation (3.6), the term  $Pr(b_t)$  is the *a priori* probabilities. The term  $Pr(r_t|c_t)$  is a function of the modulation and channel model. Note that if the states  $\mathbf{s}_t$  and  $\mathbf{s}_{t+1}$  are not connected in the trellis diagram, then the probability in equation (3.6) is zero. The probability  $\alpha(\mathbf{s}_t)$  can be found according to the forward recursion as

$$\alpha(\mathbf{s}_t) = \sum \alpha(\mathbf{s}_{t-1})\gamma(\mathbf{s}_{t-1} \rightarrow \mathbf{s}_t) \quad (3.7)$$

where  $\mathbf{s}_{t-1}$  is the previous state connected to state  $\mathbf{s}_t$ . Likewise,  $\beta(\mathbf{s}_t)$  can be found according to the backward recursion as

$$\beta(\mathbf{s}_t) = \sum \beta(\mathbf{s}_{t+1})\gamma(\mathbf{s}_t \rightarrow \mathbf{s}_{t+1}) \quad (3.8)$$

Once the *a posteriori* probability of each state transition  $Pr(\mathbf{s}_t \rightarrow \mathbf{s}_{t+1}|r)$  is found, the message bit probabilities can be found according to

$$Pr(b = 1|r) = \sum_{\mathbf{S}_1} Pr(\mathbf{s}_t \rightarrow \mathbf{s}_{t+1}|r) \quad (3.9a)$$

$$= \sum_{\mathbf{S}_1} \alpha(\mathbf{s}_t) \gamma(\mathbf{s}_t \rightarrow \mathbf{s}_{t+1}) \beta(\mathbf{s}_{t+1}) \quad (3.9b)$$

and

$$Pr(b = 0|r) = \sum_{\mathbf{S}_0} Pr(\mathbf{s}_t \rightarrow \mathbf{s}_{t+1}|r) \quad (3.10a)$$

$$= \sum_{\mathbf{S}_0} \alpha(\mathbf{s}_t) \gamma(\mathbf{s}_t \rightarrow \mathbf{s}_{t+1}) \beta(\mathbf{s}_{t+1}) \quad (3.10b)$$

where  $\mathbf{S}_1 = \{\mathbf{s}_t \rightarrow \mathbf{s}_{t+1} : b = 1\}$  and  $\mathbf{S}_0 = \{\mathbf{s}_t \rightarrow \mathbf{s}_{t+1} : b = 0\}$  are the set of all state transitions associated with a message bit of 1 and 0, respectively. The BCJR algorithm calculates the APPs of the information bits,  $Pr(b = 1|r)$  and  $Pr(b = 0|r)$ , which are represented as *a posteriori* LLRs,  $\Lambda$ , of the form

$$\Lambda = \frac{Pr(b = 1|r)}{Pr(b = 0|r)} \quad (3.11)$$

### 3.2.4 BCJR Algorithm in Logarithm Domain

The main benefit of executing the BCJR algorithm in the logarithm domain is that multiplication becomes addition. To illustrate how addition is performed in the logarithm domain, consider the Jacobian logarithm as

$$\ln(e^a + e^b) = \max(a, b) + \ln(1 + \exp(-|b - a|)) \quad (3.12a)$$

$$= \max(a, b) + \mathbf{F}(|b - a|) \quad (3.12b)$$

This shows that addition, when performed in the log-domain, becomes a maximization operation followed by a correction function  $\mathbf{F}(\cdot)$ . Moreover, it is noted that when  $b$  and  $a$  are different, the correction function is close to zero. Thus, a reasonable approximation to equation (3.12) is

$$\ln(e^a + e^b) \approx \max(a, b) \quad (3.13)$$

There are two classes of MAP algorithms that work in the log domain, log-MAP and max-log-MAP [67], both algorithms perform multiplication in the log-domain as additions. The difference between the two algorithms rests in how they compute addition in the log-domain. For the log-MAP algorithm, consider  $\bar{\gamma}(\mathbf{s}_t \rightarrow \mathbf{s}_{t+1})$  denotes the natural logarithm of  $\gamma(\mathbf{s}_t \rightarrow \mathbf{s}_{t+1})$  as

$$\bar{\gamma}(\mathbf{s}_t \rightarrow \mathbf{s}_{t+1}) = \ln(\gamma(\mathbf{s}_t \rightarrow \mathbf{s}_{t+1})) \quad (3.14a)$$

$$= \ln(Pr(b_t)) + \ln(Pr(r_t|c_t)) \quad (3.14b)$$

Now, consider  $\bar{\alpha}(\mathbf{s}_t)$  to be the logarithm of  $\alpha(\mathbf{s}_t)$  as

$$\bar{\alpha}(\mathbf{s}_t) = \ln(\alpha(\mathbf{s}_t)) \quad (3.15a)$$

$$= \ln\left(\sum \exp(\bar{\alpha}(\mathbf{s}_{t-1}) + \bar{\gamma}(\mathbf{s}_{t-1} \rightarrow \mathbf{s}_t))\right) \quad (3.15b)$$

Likewise, consider  $\bar{\beta}(\mathbf{s}_t)$  to denote the logarithm of  $\beta(\mathbf{s}_t)$  as

$$\bar{\beta}(\mathbf{s}_t) = \ln(\beta(\mathbf{s}_t)) \quad (3.16a)$$

$$= \ln\left(\sum \exp(\bar{\beta}(\mathbf{s}_{t+1}) + \bar{\gamma}(\mathbf{s}_t \rightarrow \mathbf{s}_{t+1}))\right) \quad (3.16b)$$

Consequently, the LLR can be found as

$$\Lambda_t = \ln\left(\sum_{\mathbf{S}_1} \exp(\bar{\alpha}(\mathbf{s}_t) + \bar{\gamma}(\mathbf{s}_t \rightarrow \mathbf{s}_{t+1}) + \bar{\beta}(\mathbf{s}_{t+1}))\right) - \ln\left(\sum_{\mathbf{S}_0} \exp(\bar{\alpha}(\mathbf{s}_t) + \bar{\gamma}(\mathbf{s}_t \rightarrow \mathbf{s}_{t+1}) + \bar{\beta}(\mathbf{s}_{t+1}))\right) \quad (3.17)$$

### 3.3 Bit-Interleaved Coded Modulation with Iterative Decoding

Bit-interleaved Coded Modulation (BICM) was proposed by Zehavi [17] with the aim of increasing the diversity order of Ungerboeck's trellis-coded modulation (TCM) scheme [14]. TCM is a coding scheme which has improved performance by constellation expansion and the combination of coding and modulation without sacrificing data rate or requiring extra bandwidth. Therefore, the method of employing multi-level/phase signal modulating and coding with the process of mapping is considered

### 3.3 Bit-Interleaved Coded Modulation with Iterative Decoding

the first step to finding an effective scheme for mapping the coded bits into a signal constellation. Practically, improvement in the performance for a robust communication system should be either over the AWGN or a fading channel. However, with a fading channel the errors occur in bursts relating to the period of the channel in deep fade. For this reason, most of the error correction codes are designed to correct random errors but not those of long bursts. Instead, to improve the system performance with a fading channel the implementation of combined coding and interleaving has been adopted. Hence, the coding and interleaving translate error bursts to received codewords with random error patterns, which can be corrected by the decoder. As a consequence, the coding and interleaving can be considered as a form of diversity, and the performance can be characterized by the diversity order, which is ideally a function of the minimum Hamming distance of the code. The diversity order of a code was defined by [68] in terms of the number of trellis stages encountered or, equivalently, defined by [18] in terms of the minimum Hamming distance of the code. However, the diversity order of a TCM code uses a symbol-based interleaver to reduce the number of different symbols between the erroneous path. BICM using Iterative Decoding (BICM-ID) was proposed by Li [23] and Ritcey [69] for further improving the free Euclidean distance (FED) of Zehavis BICM scheme. This FED improvement can be achieved with the aid of combining the set partitioning technique for constellation labelling, as in TCM, and by performing soft-decision feedback from the output of the decoder to the input of demodulator, which leads to exchange soft decision information between them. Therefore, upon each iteration the channel decoder improves the reliability of the soft information passed to the demodulator. BICM-ID involves an iterative demapping and decoding scheme using soft decision feedback, which is depicted in Figure 3.3.

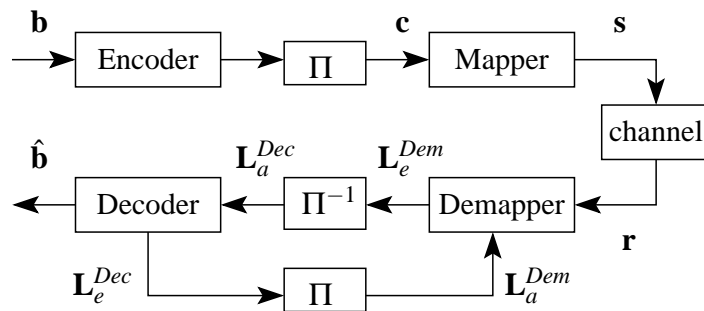


Figure 3.3: Structure of BICM-ID System.

### 3.3.1 BICM Encoder Structure

The structure of the encoder is the serial concatenation of the convolutional encoder, bit interleaver, and memoryless modulator, as shown in Figure 3.3. The mapper can be considered as a code due to it introducing dependencies between the  $M$ -bits associated to one symbol. The binary random message  $\mathbf{b}$  of length  $k$  information bits is convolutionally encoded to produce a codeword  $\mathbf{c}$  of length  $k/R_c$ . Then, the code bit sequence is permuted by bit-level interleaver of length  $k/R_c$ .

### 3.3.2 Iterative Demapper and Decoder Structure

The concept of the system depends on the demapper taking soft values from the channel output and producing extrinsic information, which is passed through a bit interleaver to become the *a priori* input. The decoder's extrinsic information of the coded bits is fed back to the demapper as *a priori* knowledge, to reduce the BER in further iterative decoding steps. The iterative receiver works as described in Figure 3.3, where the demapper processes the received complex symbols  $r$  from the channel output. Therefore, the extrinsic LLRs,  $L_e^{Dem}$  proceed to the decoder as *a priori* information  $L_a^{Dec}$ . Then, the extrinsic information LLRs,  $L_e^{Dec}$ , are fed back from the decoder to the demapper as *a priori* information  $L_a^{Dem}$  to improve the reliability of the demapper's decisions. To illustrate the behaviour of BICM iterative decoding, consider the single user system employing BICM-ID code of NSC encoder output 2304 codeword with a feedforward generator  $[23]_8$  and feedback generator  $[35]_8$ ,  $R_c=0.5$ ,  $K_c=5$ , and interleaver length  $\Pi=2304$ . The simulation was performed using the maximum a posteriori algorithm in logarithm domain (log-MAP) decoding of 6 iterations. Figure 3.4 shows the bit error performance of this code for various numbers of decoder iterations.

## 3.4 Turbo Code

Two RSC encoders are concatenated in parallel with an interleaver to obtain a turbo code [19]. The most significant feature of turbo codes is the iterative decoding process. The two decoders of a turbo code correspond to the two encoders. An iterative decoding process is performed between the two concatenated decoders by feeding the decoded results back to each other's input to converge in the best performance.

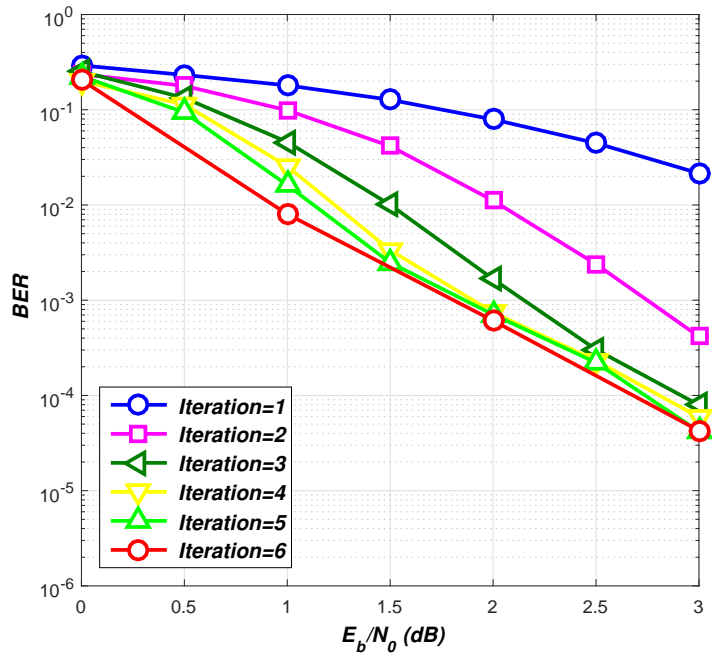


Figure 3.4: Simulated performance of BICM-ID code for various numbers of decoder iterations.

The advantages of the turbo code are its efficiency and the near Shannon capacity performance.

### 3.4.1 Turbo Encoder Structure

The turbo encoder structure is a parallel concatenation of two RSC encoders separated by an interleaver, as shown in Figure 3.5. The operation of the two RSC codes introduces two codewords. A binary message bit  $b$  is encoded by the first encoder (Encoder-1), then a codeword is generated  $c^{(1)}$ . Furthermore, the original message block  $b$  is interleaved to produce the scrambled information sequence, which is used as the message bits input for the second encoder (Encoder-2) to generate a second codeword  $c^{(2)}$ . Consequently, the codeword contains the original message bits and parity bits. Also, the work of the interleaver is to create randomness in the codeword and remove interdependences between the inputs of the two encoders. Subsequently, the information bits  $b$ ,  $c^{(1)}$ , and  $c^{(2)}$  are punctured to increase the code rate, multiplexed, and converted from a parallel to serial sequence (P/S). A simple way of puncturing is to send only one parity bit for each systematic bit, i.e. when  $x$  is even, the puncturer and parallel-to-serial (P/S) converter outputs a vector  $[b c^{(1)}]$ , and when  $x$  is odd, the output is a vector  $[b c^{(2)}]$ . When all the available bits are

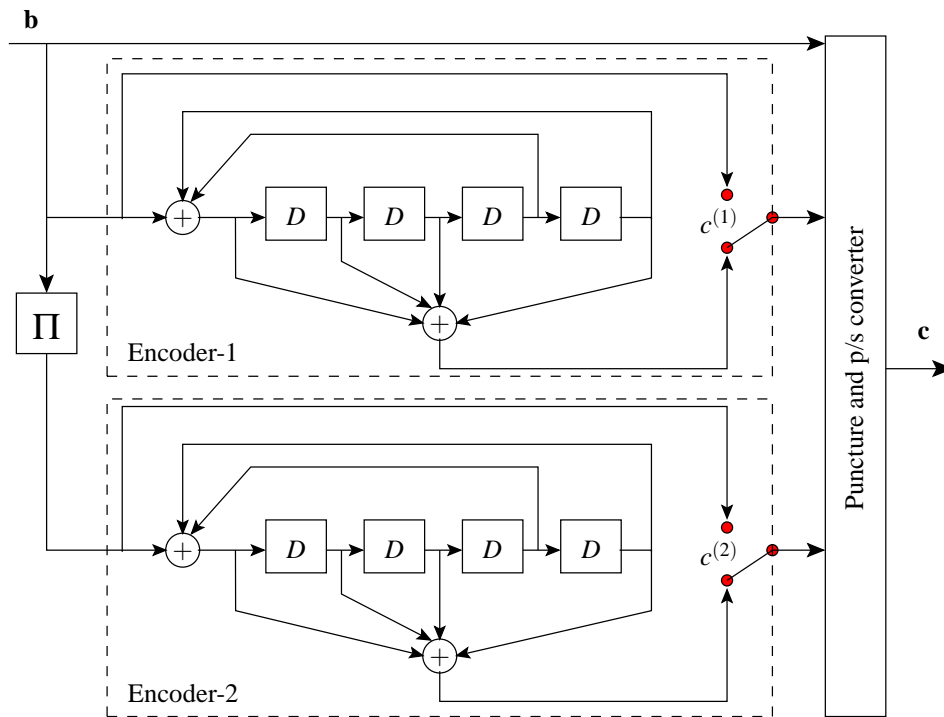


Figure 3.5: The structure of a turbo encoder.

sent out to the channel, the overall rate of the turbo encoder becomes  $R_c = 1/3$ . Therefore, the puncturing increases the overall code rate to  $R_c = 1/2$ .

### 3.4.2 Turbo Decoder Structure

The two component decoders are linked by interleavers and deinterleavers as shown in Figure 3.6. Each decoder takes three inputs: the systematically encoded channel output LLRs, the parity LLRs transmitted from the associated component encoder and the *a priori* information from the other component decoder. They also provide soft outputs of the decoded bits. This means that as well as providing the decoded output bit sequence, the component decoders must also give the associated probabilities for each bit that has been correctly decoded. The soft outputs are typically represented in terms of LLRs. To illustrate the behaviour of turbo iterative decoding, consider the single user system employing turbo code of a pair RSC encoders with generators  $[1, \frac{23}{35}]_8$  to produce 2304 codeword,  $R_c=0.5$ ,  $K_c=5$ , and interleaver length  $\Pi=2304$ . The simulation was performed using the log-MAP decoding of 4 iterations. Figure 3.7 shows the bit error performance of this code for various numbers of decoder iterations.

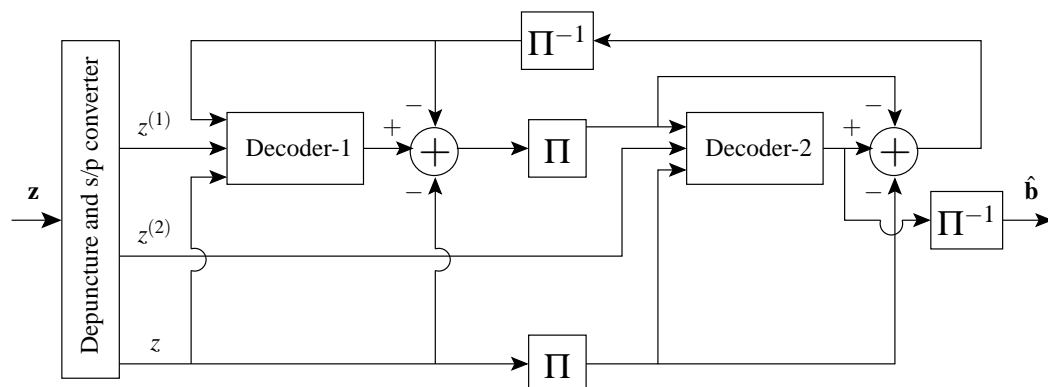


Figure 3.6: Turbo decoder schematic.

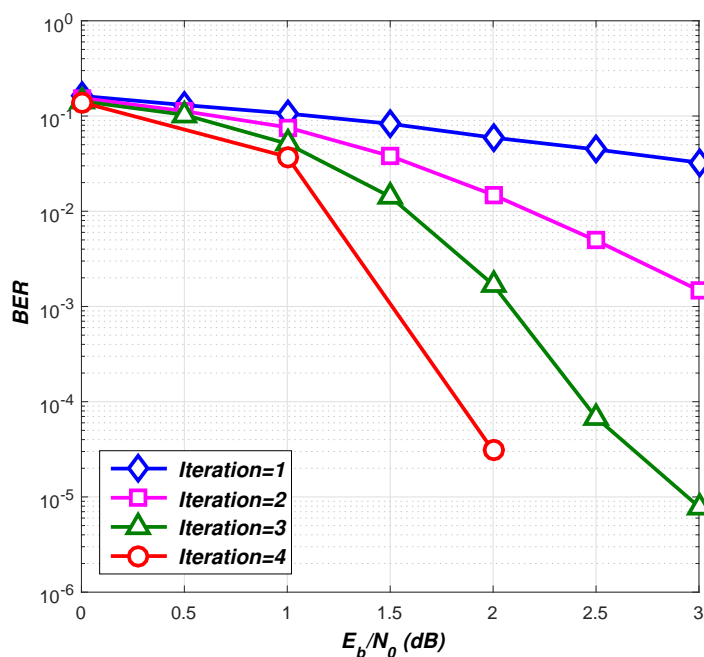


Figure 3.7: Simulated performance of turbo code for various numbers of decoder iterations.

### 3.5 Low-Density Parity-Check Code

LDPC codes are described by the variable node degree  $d_v$  and the check node degree  $d_c$ , giving the number of ones per column and row in the parity check matrix  $H$ , respectively. The LDPC code is a long linear binary block code whose  $H$  is sparse. An LDPC code can be represented in terms of a bipartite graph called a Tanner graph. The variable nodes correspond to coded bits of the codeword and the check nodes correspond to the set of parity-check equations satisfied by the coded bits of the codeword. The degree of a variable node is the number of check equations that it participates in. Similarly, the degree of a check node is the number of variable nodes which take part in that particular check. If all variable and check

node degrees are fixed, then it is a regular LDPC code. If the degrees are different, then it is irregular [70]. The irregularity is typically specified using two polynomials variable, node-degree,  $\lambda(\cdot)$ , and check-degree,  $\rho(\cdot)$ , defined as

$$\lambda(s) \triangleq \sum_{i=1}^{d_v} \lambda_i s^{i-1} \tag{3.18}$$

$$\rho(s) \triangleq \sum_{i=1}^{d_c} \rho_i s^{i-1} \tag{3.19}$$

where  $\lambda_i$  and  $\rho_i$  represent the fractions of edges that are connected to variable-nodes and check-nodes of degree  $i$ , respectively.

### 3.5.1 Tanner Graph

A Tanner graph is a graphical representation of a linear block code corresponding to the parity check matrix  $H$  of the code. A Tanner graph is a bipartite graph containing two sets of nodes. The first set consists of variable (bit) nodes which represent the bits of a codeword. The second set consists of check nodes, representing the parity constraints. A variable node is connected to a check node if it participates in the corresponding parity check equation. Each check node specifies a set of symbols whose sum must be zero. A Tanner graph can contain multiple cycles, which are paths made up of vertices and edges that begin and end at the same vertex. The number of edges in cycle is its length and the minimum length cycle is known as the girth. Consider the example of a regular parity-check matrix

$$H = \begin{bmatrix} 1 & 1 & 0 & 1 & 0 & 0 \\ 0 & 1 & 1 & 0 & 1 & 0 \\ 1 & 0 & 0 & 0 & 1 & 1 \\ 0 & 0 & 1 & 1 & 0 & 1 \end{bmatrix} \tag{3.20}$$

### 3.5.2 Quasi-cyclic codes

A quasi-cyclic code has the property that if any codeword is shifted  $c$  places then this results in another codeword. If  $c = 1$  then the code is a cyclic code. In general, a quasi-cyclic codes has a parity-check matrix comprising binary circulant matrices,

$b_1, b_2, \dots$ , with dimensions  $v \times v$ , defined as

$$H = [b_1, b_2, \dots] \quad (3.21)$$

A systematic generator matrix for a quasi-cyclic code can be formed if one of these circulant matrices is invertible and has the form

$$G = \begin{bmatrix} & (b_x^{-1} b_1)^T \\ I_{v(x-1)} & (b_x^{-1} b_2)^T \\ & \vdots \\ & (b_x^{-1} b_{x-1})^T \end{bmatrix} \quad (3.22)$$

### 3.5.3 Repeat-accumulate codes

A repeat-accumulate (RA) code is an LDPC code with characteristics of both LDPC codes and serial turbo codes, which was proposed by [71]. The encoder for an RA code repeats the user bits, permutes, them and are then sent through an accumulator. Therefore, an RA code is regular if its parity-check matrix has a fixed Hamming weight in each row of  $H_1$  and a fixed Hamming weight in each column of  $H_1$ . An RA code  $H$  has two parts as

$$H = [H_1 \ H_2] \quad (3.23)$$

where  $H_2$  is matrix with the form as

$$H_2 = \begin{bmatrix} 1 & 0 & 0 & & 0 & 0 & 0 \\ 1 & 1 & 0 & \dots & 0 & 0 & 0 \\ 0 & 1 & 1 & & 0 & 0 & 0 \\ & \vdots & \ddots & & \vdots & & \\ 0 & 0 & 0 & & 1 & 0 & 0 \\ 0 & 0 & 0 & \dots & 1 & 1 & 0 \\ 0 & 0 & 0 & & 0 & 1 & 1 \end{bmatrix} \quad (3.24)$$

The RA codes can repeat some bits more than others yielding irregular an repeat-accumulator (IRA) code, which have an irregular column weight distribution in  $H_1$ , with  $H_2$  the same as for a regular code. The IRA encoder comprises a low-density generator matrix  $G$ , a permuter  $\Pi$ , and an accumulator, as depicted in Figure 3.8. The Tanner graph representation of the parity-check matrix in equation (3.20) is

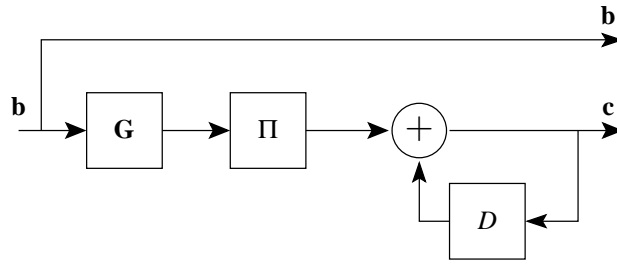
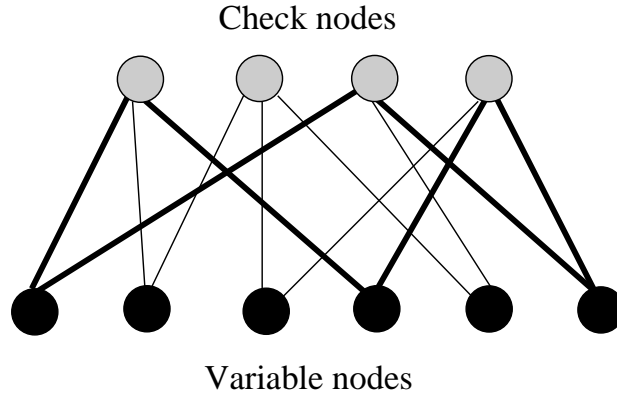


Figure 3.8: Block diagram of RA encoder.


 Figure 3.9: Tanner graph for  $H$  in equation (3.20).

depicted in Figure 3.9, with a 6-cycle is shown in bold. Now, consider the parity-check matrix in equation (3.25) for a repeat-accumulate code. The Tanner graph representation is illustrated in Figure 3.10.

$$H = \begin{bmatrix}
 1 & 0 & 0 & 1 & 0 & 0 & 0 & 0 & 0 & 0 & 0 & 0 \\
 1 & 0 & 0 & 1 & 1 & 0 & 0 & 0 & 0 & 0 & 0 & 0 \\
 0 & 1 & 0 & 0 & 1 & 1 & 0 & 0 & 0 & 0 & 0 & 0 \\
 0 & 0 & 1 & 0 & 0 & 1 & 1 & 0 & 0 & 0 & 0 & 0 \\
 0 & 0 & 1 & 0 & 0 & 0 & 1 & 1 & 0 & 0 & 0 & 0 \\
 0 & 1 & 0 & 0 & 0 & 0 & 0 & 1 & 1 & 0 & 0 & 0 \\
 1 & 0 & 0 & 0 & 0 & 0 & 0 & 0 & 1 & 1 & 0 & 0 \\
 0 & 1 & 0 & 0 & 0 & 0 & 0 & 0 & 0 & 1 & 1 & 0 \\
 0 & 0 & 1 & 0 & 0 & 0 & 0 & 0 & 0 & 0 & 1 & 1
 \end{bmatrix} \tag{3.25}$$

### 3.5.4 The Sum-Product Algorithm

The most common class of decoding algorithm to decode LDPC codes is the message-passing algorithm (MPA), where messages are passed along the edges in the Tanner

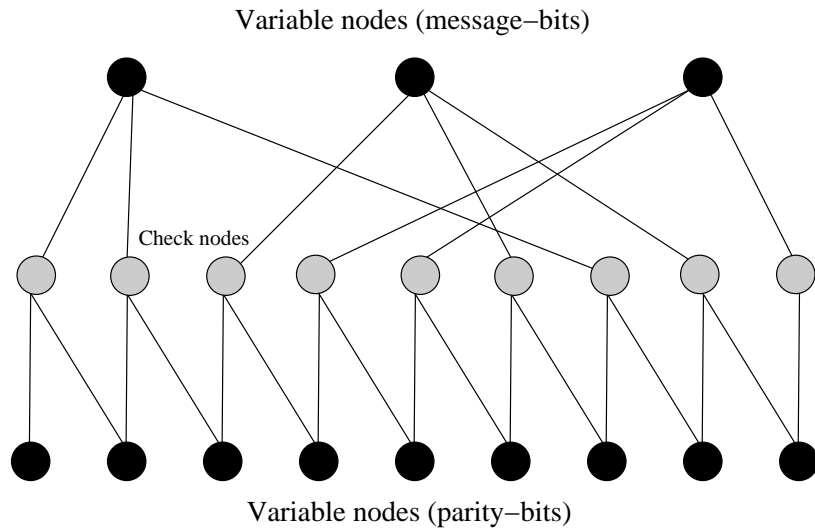


Figure 3.10: Tanner graph for RA code in equation (3.25).

graph, which comprises a variable node decoder (VND) and a check node decoder (CND). Each variable/check node in the Tanner graph is processed independently of the other variable/check nodes, since it only has access to information from the edges connect to this node. The MPA iteratively computes the distributions of variables as the messages are passed back and forth between variable and check nodes in an iterative manner until the algorithm converges to a final result. The messages are represented as probabilities indicating the level of reliability of the value of the coded bits. However, for convenience it is more common to replace these probabilities with log-likelihood ratios (LLRs), which simplifies the MPA by only using sum and product operations, hence it is known as the Sum-Product algorithm. The input values to the sum-product algorithm are the initial LLRs of the received bits, known as *a priori* LLRs since they are already known before decoding begins. The output values are called the *a posteriori* LLRs since they are conditional on the *a priori* LLRs. At the decoder, the received signal  $r$  from the channel output is used to decode the symbol  $s$  that was sent. Since, a memoryless channel is described by its input and output symbols. Therefore, the conditional probability distribution,  $p(\cdot)$ , for each channel input and output pair can be described as

$$p(r|s) = \prod_{i=0}^{N-1} p(r_i|s_i) \quad (3.26)$$

In the sum product algorithm, the extrinsic message probability,  $P_{j,i}^{ext}$ , from check node to variable node is

$$P_{j,i}^{ext} = \frac{1}{2} + \frac{1}{2} \prod_{i \in B_j, i \neq i} 1 - 2P_{j,i}^{int} \quad (3.27)$$

where  $P_{j,i}^{int}$  is the current estimate, available to check  $j$ , of the probability that bit  $i$  is a one. The LLR of  $P_{j,i}^{ext}$  is

$$L_{j,i}^E = \log\left(\frac{1 - P_{j,i}^{ext}}{P_{j,i}^{ext}}\right) \quad (3.28)$$

Substituting equation (3.27) in equation (3.28) gives

$$L_{j,i}^E = \log\left(\frac{\frac{1}{2} + \frac{1}{2} \prod_{i \in B_j, i \neq i} 1 - 2P_{j,i}^{int}}{\frac{1}{2} - \frac{1}{2} \prod_{i \in B_j, i \neq i} 1 - 2P_{j,i}^{int}}\right) \quad (3.29)$$

Using the relationship,  $1 - 2p = \tanh\left(\frac{1}{2} \log\left(\frac{1-p}{p}\right)\right)$ , gives

$$L_{j,i}^E = \log\left(\frac{1 + \prod_{i \in B_j, i \neq i} \tanh(L_{j,i}^A/2)}{1 - \prod_{i \in B_j, i \neq i} \tanh(L_{j,i}^A/2)}\right) \quad (3.30)$$

where  $L_{j,i}^A = \log\left(\frac{1 - P_{j,i}^{int}}{P_{j,i}^{int}}\right)$ . Alternatively, equation (3.30) can be written as

$$L_{j,i}^E = 2 \tanh^{-1}\left(\prod_{i \in B_j, i \neq i} \tanh(L_{j,i}^A/2)\right) \quad (3.31)$$

The LLR of the  $i$ -th bit is the sum of these extrinsic LLRs as

$$L_i^A = r_i + \sum_{j \in A_i} L_{j,i}^E \quad (3.32)$$

The message from the  $i$ -th bit node to the  $j$ -th check node is the sum in equation (3.32), but without the component  $L_{j,i}^E$  which was just received from the  $j$ -th check node as

$$L_{j,i}^A = \sum_{j \in A_i, j \neq j} L_{j,i}^E + r_i \quad (3.33)$$

To illustrate the behaviour of LDPC iterative decoding, consider the single user system employing LDPC code of encoder output 2304 codeword and  $R_c=0.5$ . The

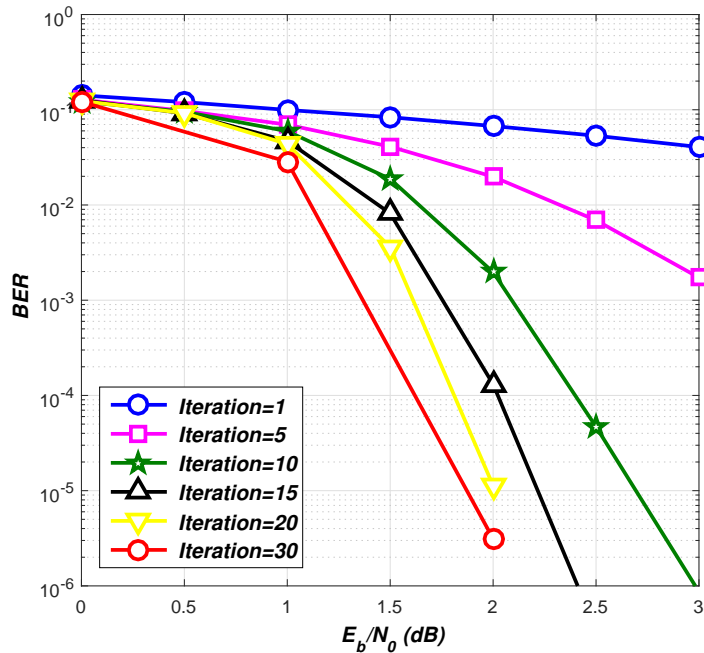


Figure 3.11: Simulated performance of LDPC code for various numbers of decoder iterations.

simulation was performed using the MPA algorithm of 30 iterations. Figure 3.11 shows the bit error performance of this code for various numbers of decoder iterations.

### 3.6 Channel Coding with Physical Layer Network Coding

Many communication systems make use of channel coding for the information reliability by protect the message being transmitted. An issue of interest is therefore how the PNC system with TWRC can employ channel coding. As mentioned in Chapter 1, there are two approaches for PNC system to employ channel coding:  $L \times L$  [30] and E2E [29]. Again, for both possibilities, the two terminal nodes are encoded their signal before sending them out. However, the difference between  $L \times L$  and E2E coding methods lies in how the relay processes the received signal. In the  $L \times L$  case, the relay performs detection of the network-coded bits, essentially cleaning up the noise at the relay. It then remodulates the signal and broadcasts to the terminals. The benefit of  $L \times L$  is that the noise received at the relay is not retransmitted and the terminal receivers are simplified, but the disadvantage is that a more complex

receiver is required at the relay. In the E2E case, the relay forwards the received signal sum directly and all of the processing is performed at the terminals. While the benefit of E2E is a simple relay implementation, the disadvantage is that the noise at the relay is also forwarded to the terminals and the processing requirements at the terminals can be burdensome. At the higher layer where channel coding and decoding are performed, the end nodes simply treat the PNC system as a bit pipe with a particular bit error rate and then the system is considered as a traditional point-to-point channel. Our approach to make the relay simple as possible with coded E2E PNC. Note that both terminal nodes, use the same channel code scheme and code rate value.

### 3.6.1 BICM-ID with PNC

BICM is the serial concatenation of a code, interleaver and mapper. Zehavi proposed this scheme in [17] and a thorough investigation was done by Caire, Taricco and Biglieri in [18]. Li and Ritcey [23] [72] and ten Brink, Speidel and Yan [24] proposed the receiver with iterative demapping and decoding depicted in Figure 3.3. For the PNC system, the iterative receiver works as described in Figure 3.12. After non-systematic convolutional encoding and random bit-interleaving, the binary signal is mapped onto the I- and Q-channels applying anti-Gray mapping. The complex noisy symbols  $\mathbf{r}$  are received at the relay to get PNC the demapping process to achieve the bits to introduce the combination of the users' message.

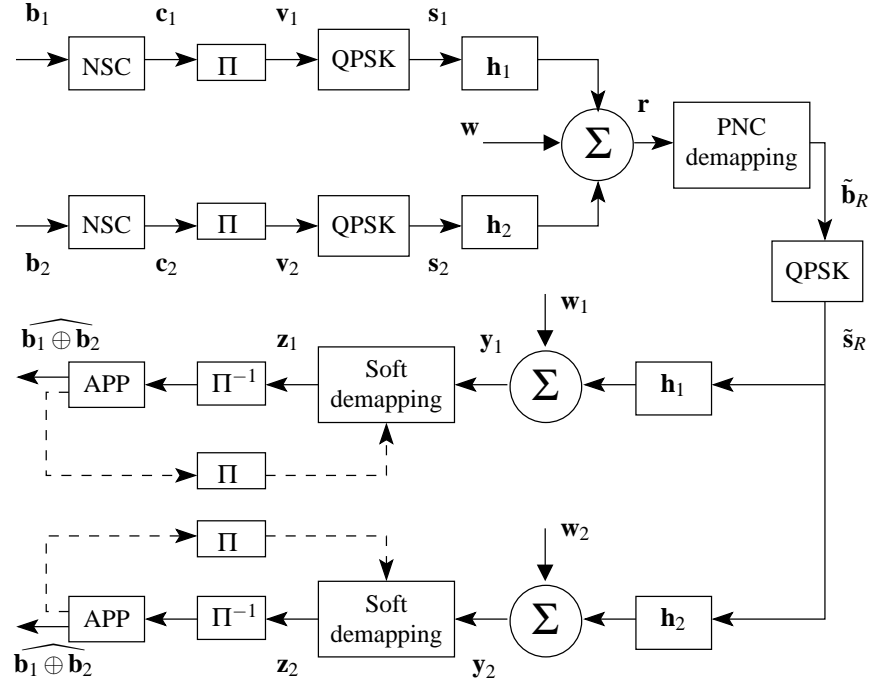


Figure 3.12: PNC Systems Employing BICM-ID Code.

### 3.6.2 Turbo Codes with PNC

The structure of the turbo decoder consists of two SISO component decoders corresponding to the two encoder arrangements. The block diagram of turbo code with a PNC system is given in Figure 3.13. In contrast to the single user system, which has almost no-relay, PNC with demapping of two-way relay takes place at the relay. The two steps of time slot to transfer information gives the SISO components inaccurate LLRs value about the transmitted symbols due to the errors that occur within the first time slot and mapped after demapped by the PNC technique, and then broadcast to the destination. Therefore, the SISO modules of the PNC system affect the performance and complexity of the SISO module of the no-relay system.

### 3.6.3 LDPC codes with PNC

A PNC system employing an LDPC code has been implemented at the source and destination as depicted in Figure 3.14. The message of user-1 and user-2 are encoded by a single link LDPC encoder, with same code rate  $R_c$  for both users. The relay generates the network bit vector  $\tilde{\mathbf{b}}_R$  from noisy of a special PNC demapping process, which are then broadcast after the mapping by QPSK to the sequence of symbols  $\tilde{\mathbf{s}}_R$ . At the destination, there is a SISO belief propagation (BP) decoder.

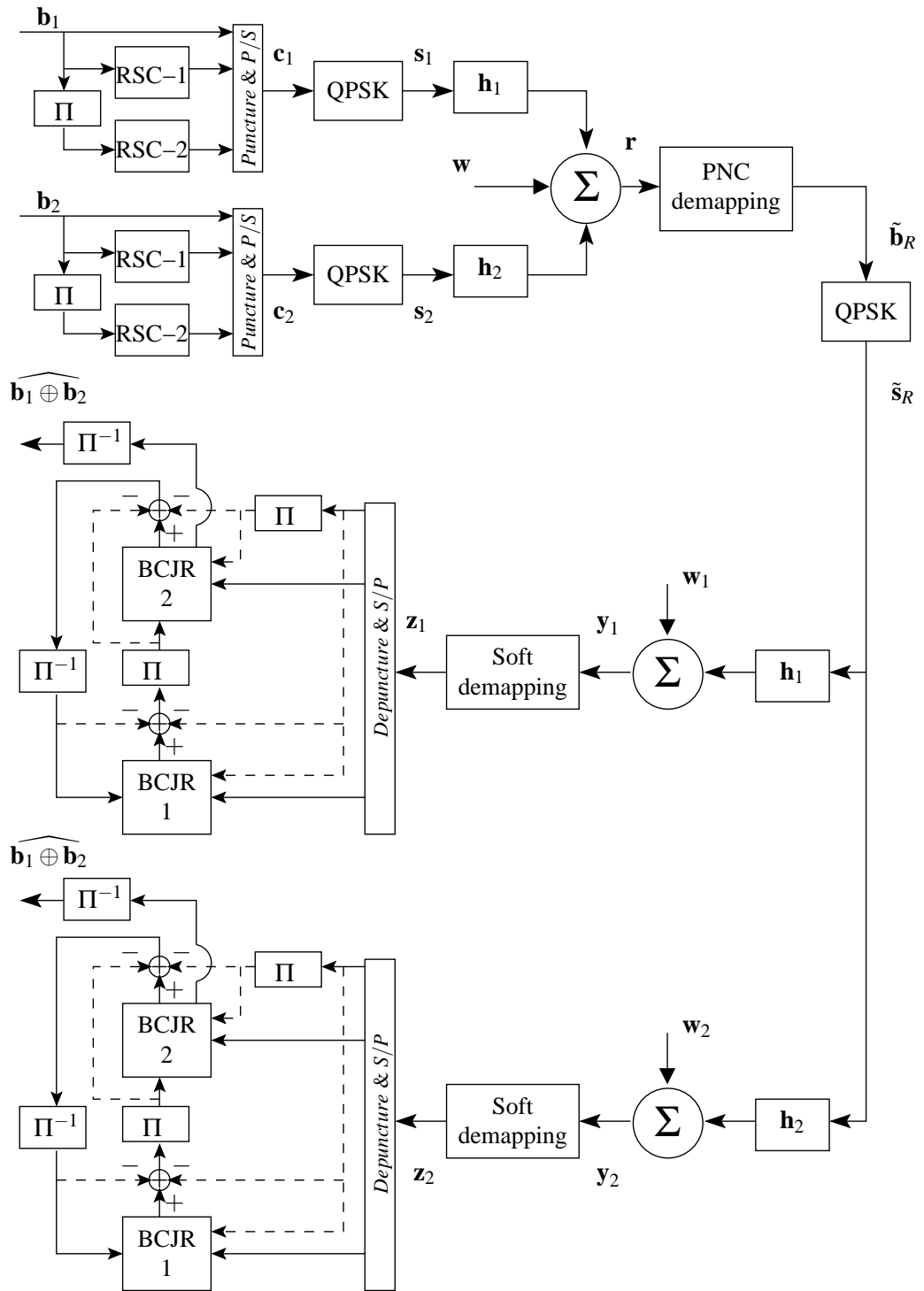


Figure 3.13: PNC System Employing Turbo code.

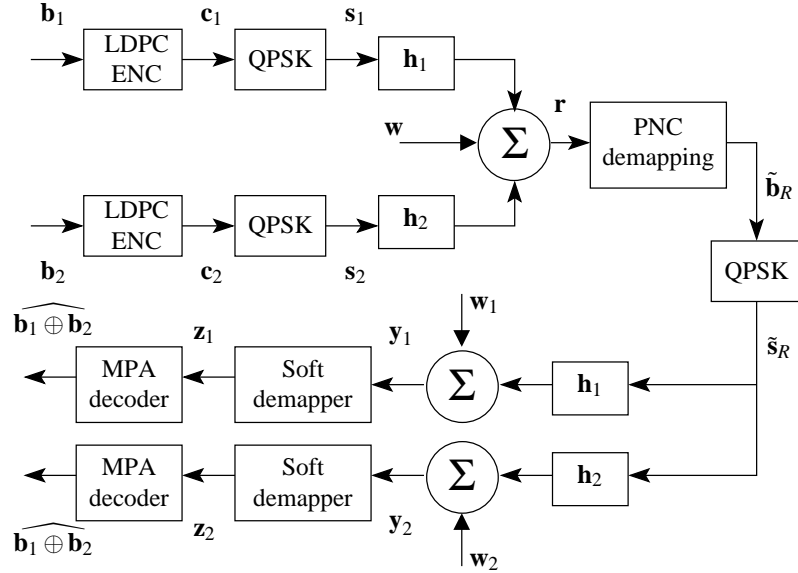


Figure 3.14: PNC Systems Employing LDPC Code.

### 3.7 Simulation Results and Discussions

In this section, BICM-ID, turbo and LDPC code of different lengths and code rates are evaluated with PNC on the AWGN and Rayleigh fading channels. The BICM-ID code is composed of a  $K_c=5$  NSC encoder with a feedback generator  $[35]_8$  and feedforward generator  $[23]_8$ . The interleaver size is fixed with the length of the encoder output. The turbo code is composed of a pair of  $K_c=5$  RSC encoders with generators  $[1, \frac{23}{35}]_8$ . The encoded bits are Gray mapped to a QPSK constellation, except BICM-ID where anti-Gray mapping is used. The proposed coded systems were simulated on an AWGN and Rayleigh flat-fading channels for code rates  $1/2$ ,  $2/3$ , and  $3/4$  with different code lengths of 576, 2304, and 64800 bits. In all plots, the coded PNC performance is compared with a single user (SU) system. The BER results for code rate  $1/2$  and code length 576 bits with different iterative decoders is given in Figure 3.15 on the AWGN channel. For the same code rate but different code length of 2304, Figure 3.16 shows the performance of the PNC system with different decoding schemes and Figure 3.17 shows the BER results for code length of 64800 bits. Table 3.1 summarizes the performance of the systems for a code rate  $1/2$  on the AWGN channel. The results for the same channel and same code lengths but for rate  $2/3$  are depicted in Figures 3.18, 3.19, and 3.20, with a summary in Table 3.2. The last results on the AWGN channel are shown in Figures 3.21, 3.22, and 3.23 for a code rate  $3/4$  and code length 576, 2304, and 64800 bits, respectively. Table 3.3 summarizes these results.

All three coding schemes are shown to perform well on a single user AWGN channel, with the LDPC code and turbo code performing very similarly. However, on the TWRC, it was observed that the turbo code and BICM-ID code both outperformed the LDPC codes. The results show that turbo codes and BICM-ID codes with trellis-based decoding algorithms are more suited to PNC networks than LDPC codes on the AWGN channel. Further results for rate  $2/3$  shows that puncturing the turbo code causes it to perform worse than BICM-ID and LDPC codes combined with PNC.

The BER performance of the coded PNC systems was evaluated over the Rayleigh flat-fading channel. The BER results for the code rate  $1/2$  are shown in Figures 3.24, 3.25, and 3.26 with code lengths 576, 2304, 64800 bits, respectively. The results summary for rate  $1/2$  over the Rayleigh channel are given in Table 3.4. Also, Figures 3.27, 3.28, and 3.29 show the BER performance of rate  $2/3$  coded PNC systems with different code lengths 576, 2304, and 64800 bits, respectively. Table 3.5 summarizes the performance of the systems. Finally, the results for the rate  $3/4$  over the Rayleigh channel are presented in Figures 3.30, 3.31, and 3.32 for code lengths 576, 2304, and 64800 bits, respectively. The performance is summarized in Table 3.6.

In the single user system, the BER results indicate that the performance of the system with BICM-ID is slightly worse than the systems with LDPC and turbo codes. The BER performance of the LDPC code after 30-iterations, and turbo code after 4-iterations outperformed BICM-ID after 6-iterations, with PNC iterative decoder systems.

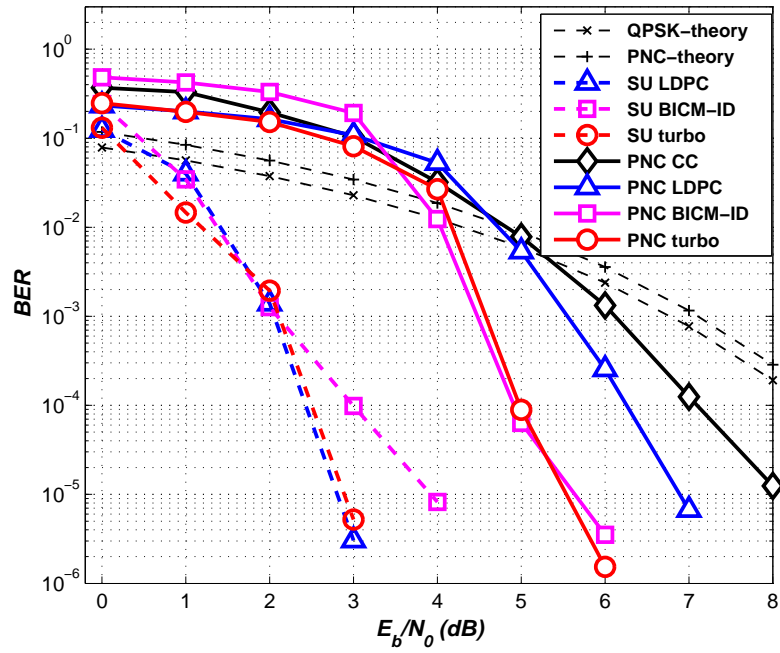


Figure 3.15: The performance of systems with code length 576 and code rate 1/2 on the AWGN channel.

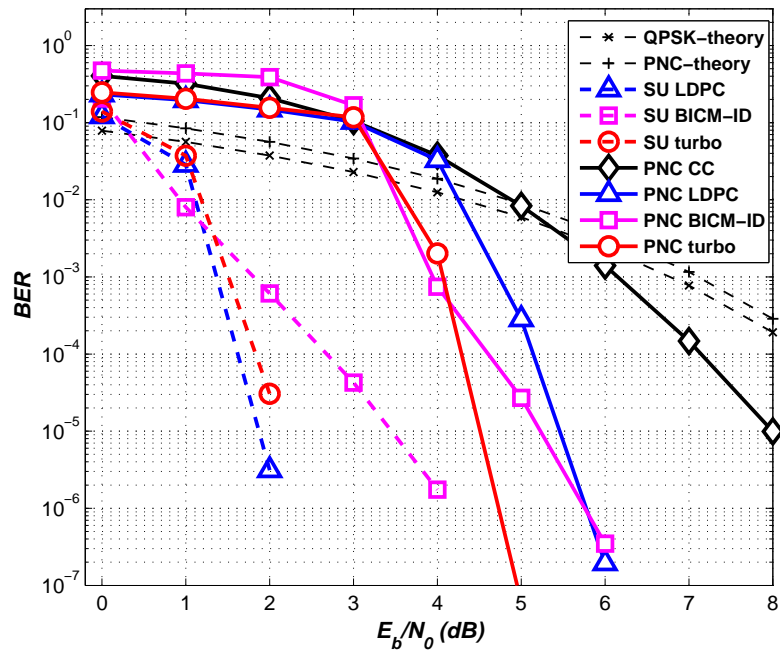


Figure 3.16: The performance of systems with code length 2304 and code rate 1/2 on the AWGN channel.

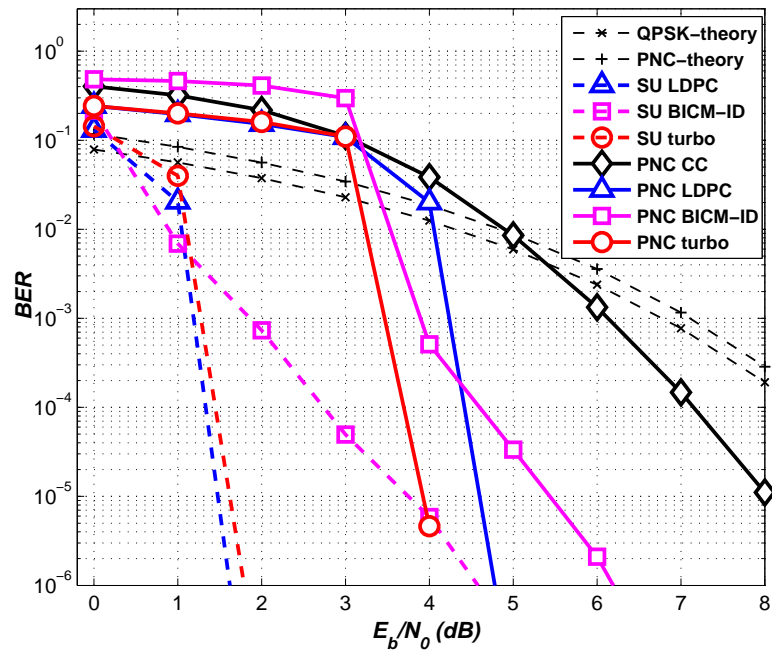


Figure 3.17: The performance of systems with code length 64800 and code rate 1/2 on the AWGN channel.

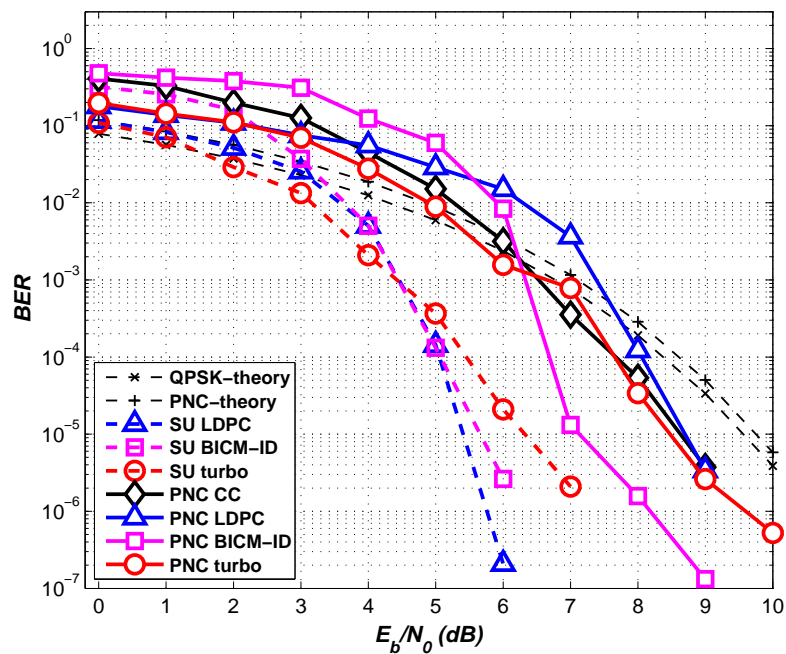


Figure 3.18: The performance of systems with code length 576 and code rate 2/3 on the AWGN channel.

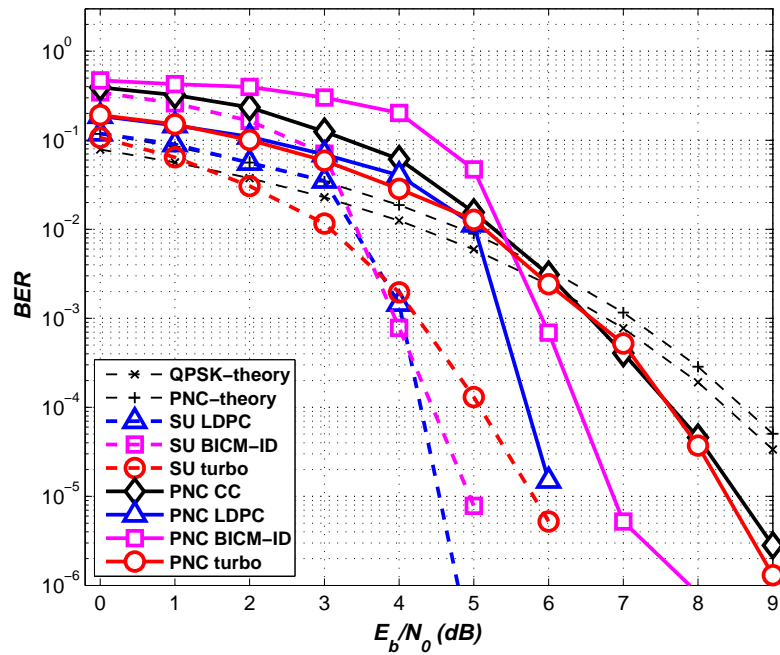


Figure 3.19: The performance of systems with code length 2304 and code rate 2/3 on the AWGN channel.

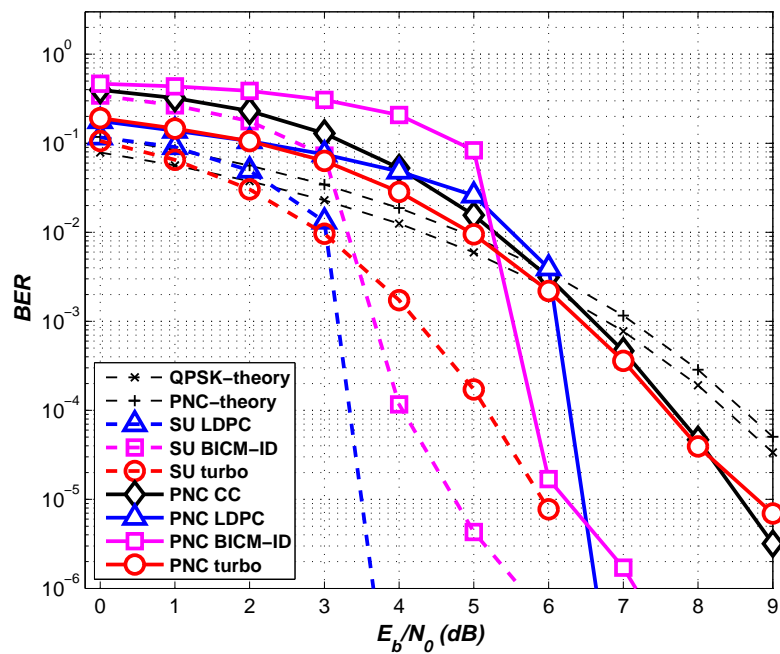


Figure 3.20: The performance of systems with code length 64800 and code rate 2/3 on the AWGN channel.

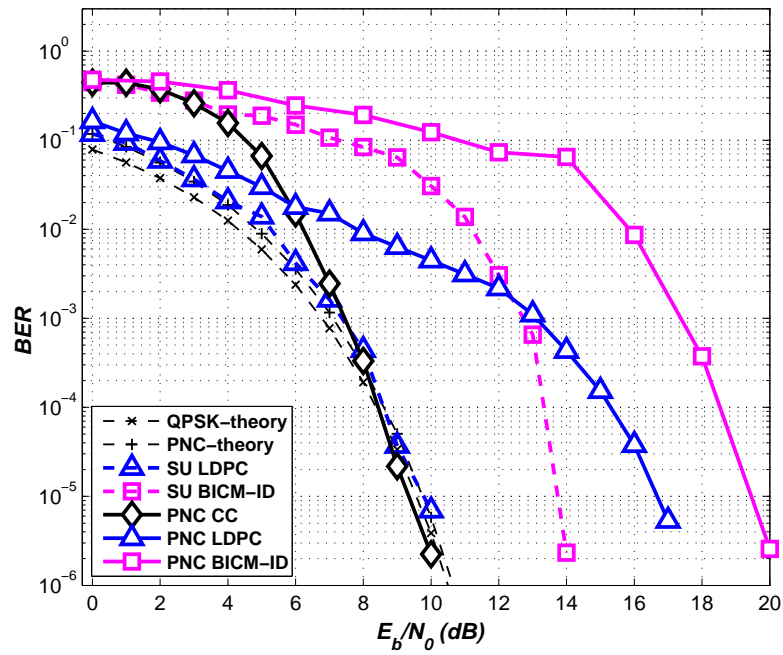


Figure 3.21: The performance of systems with code length 576 and code rate 3/4 on the AWGN channel.

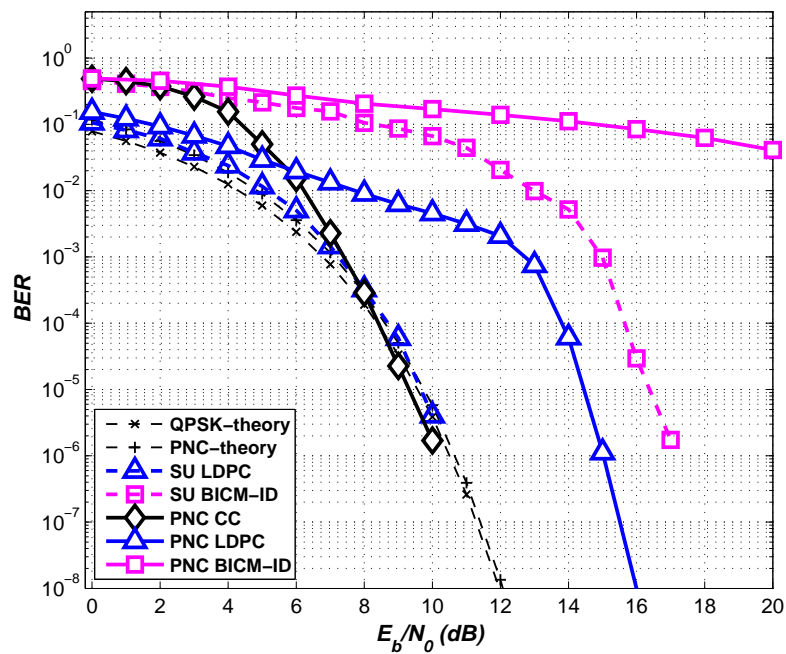


Figure 3.22: The performance of systems with code length 2304 and code rate 3/4 on the AWGN channel.

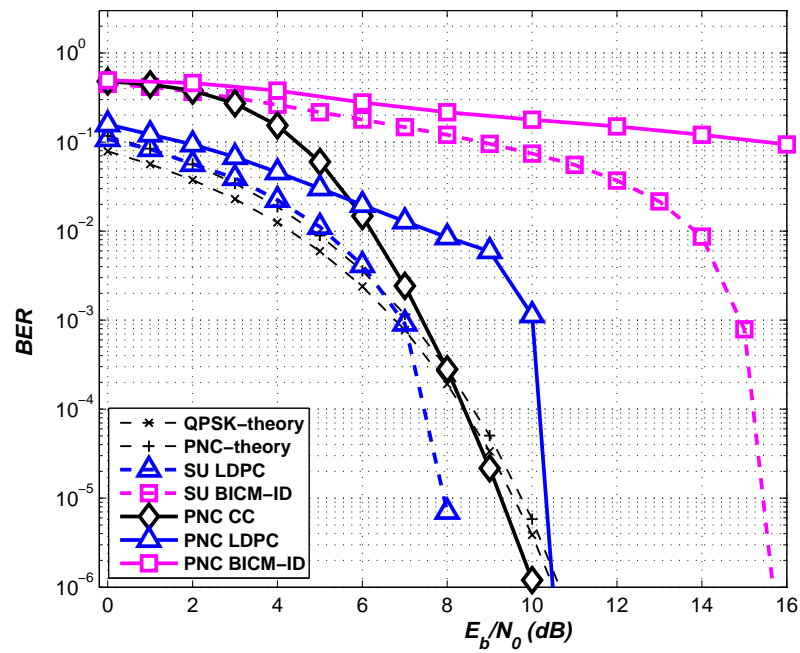


Figure 3.23: The performance of systems with code length 64800 and code rate 3/4 on the AWGN channel.

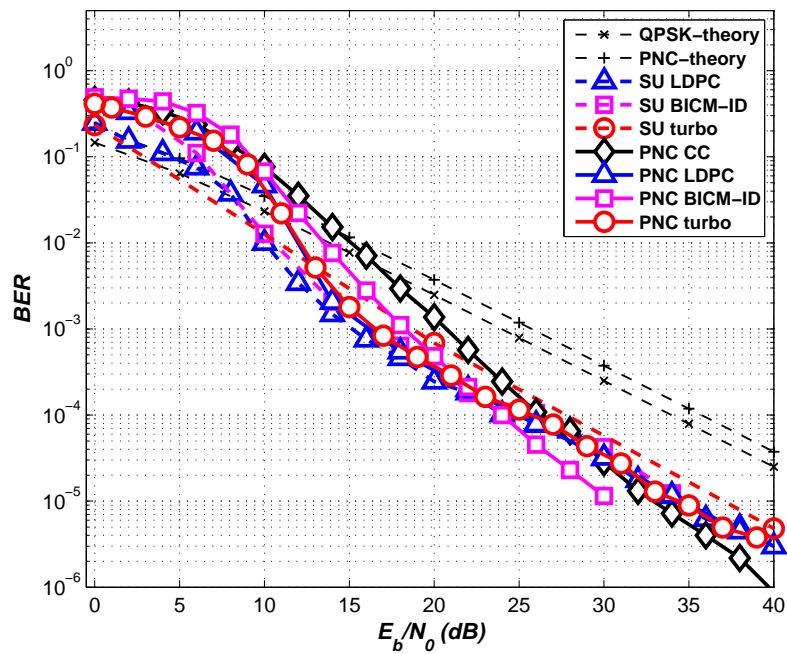


Figure 3.24: The performance of systems with code length 576 and code rate 1/2 on the Rayleigh flat-fading channel.

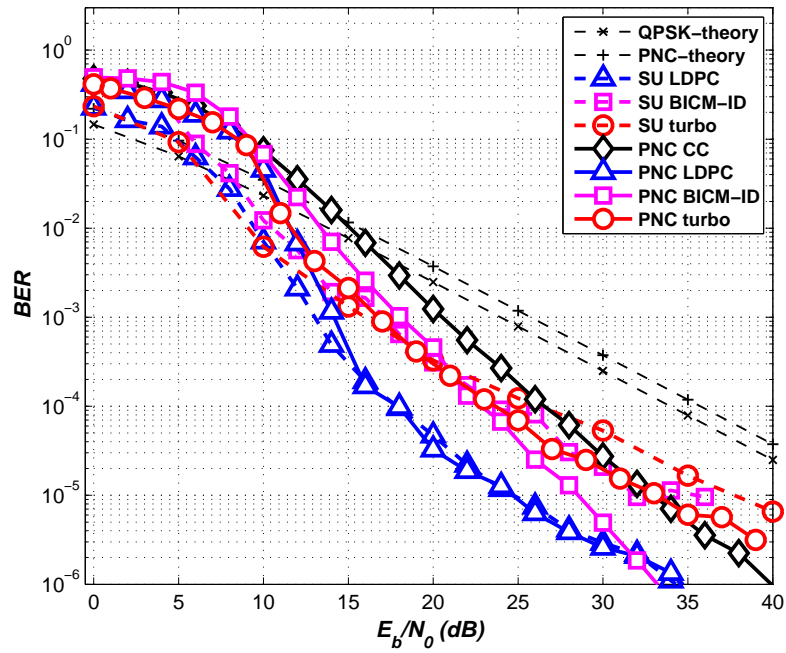


Figure 3.25: The performance of systems with code length 2304 and code rate 1/2 on the Rayleigh flat-fading channel.

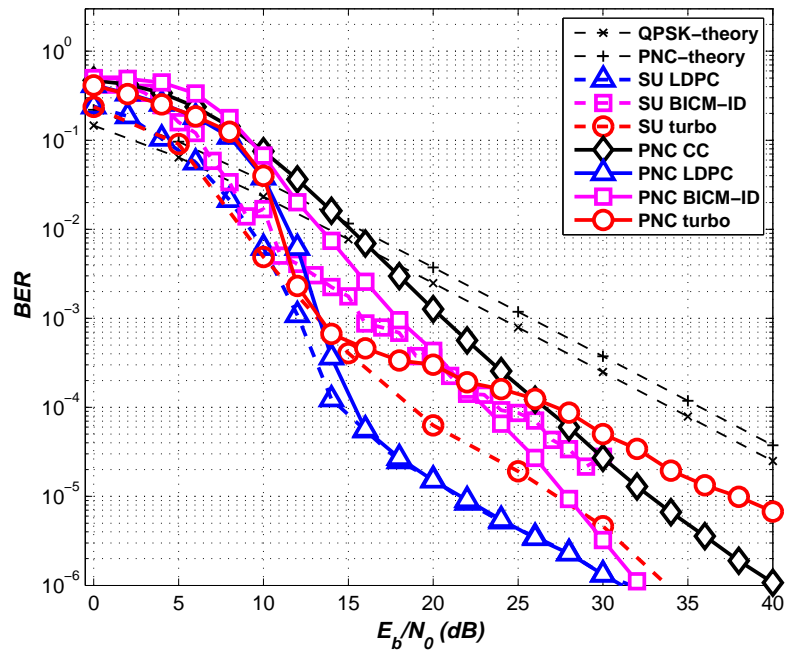


Figure 3.26: The performance of systems with code length 64800 and code rate 1/2 on the Rayleigh flat-fading channel.

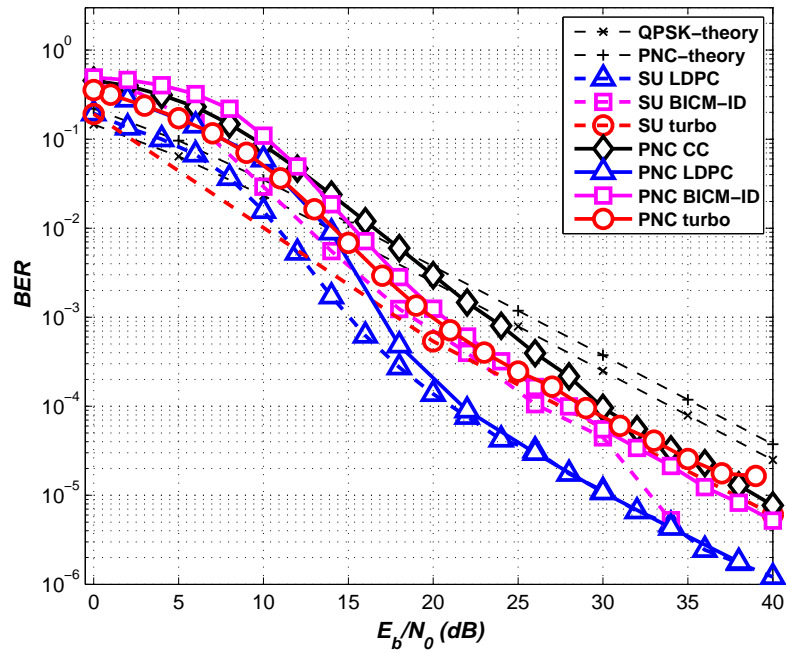


Figure 3.27: The performance of systems with code length 576 and code rate 2/3 on the Rayleigh flat-fading channel.

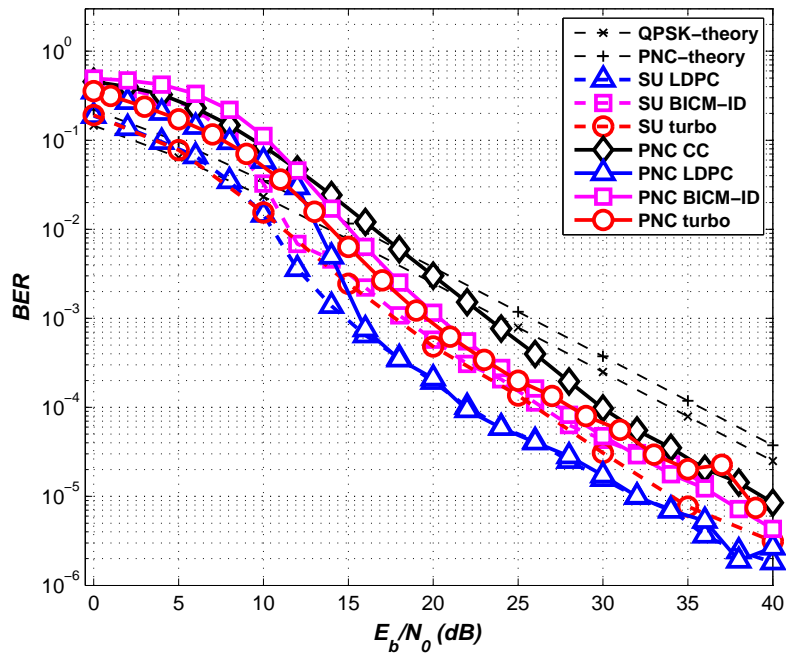


Figure 3.28: The performance of systems with code length 2304 and code rate 2/3 on the Rayleigh flat-fading channel.

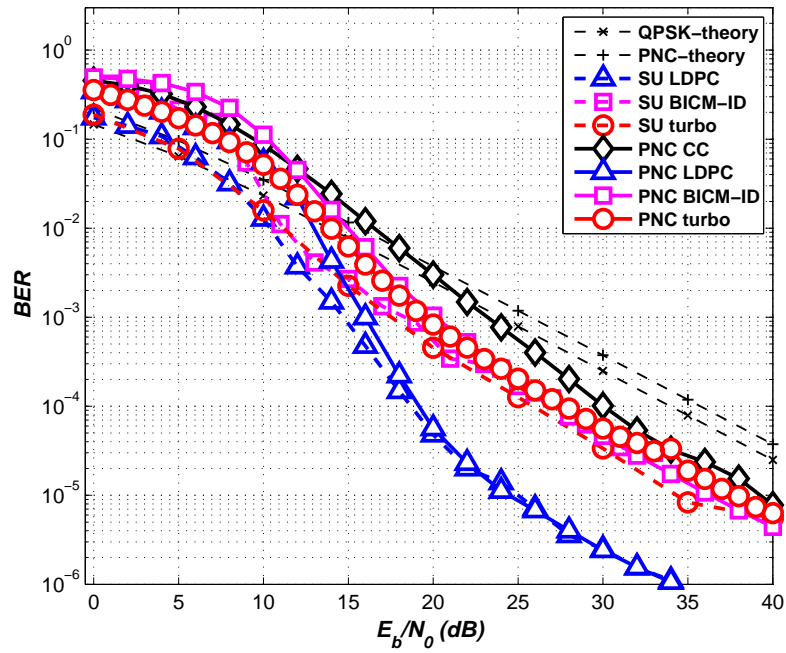


Figure 3.29: The performance of systems with code length 64800 and code rate 2/3 on the Rayleigh flat-fading channel.

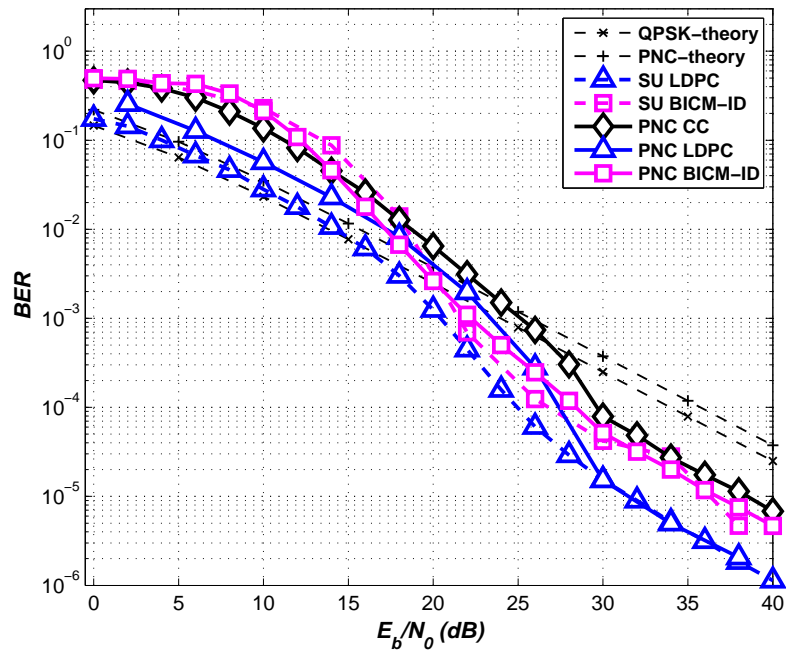


Figure 3.30: The performance of systems with code length 576 and code rate 3/4 on the Rayleigh flat-fading channel.

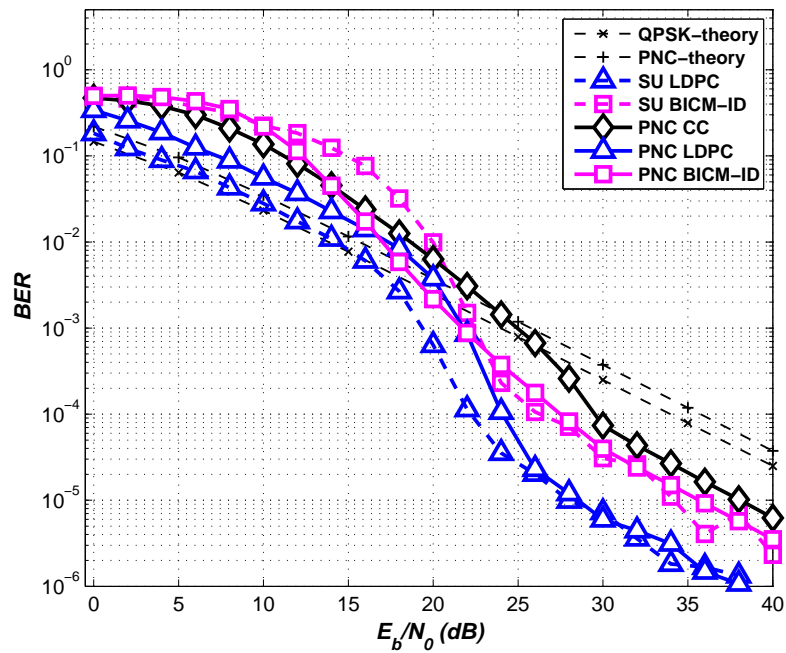


Figure 3.31: The performance of systems with code length 2304 and code rate 3/4 on the Rayleigh flat-fading channel.

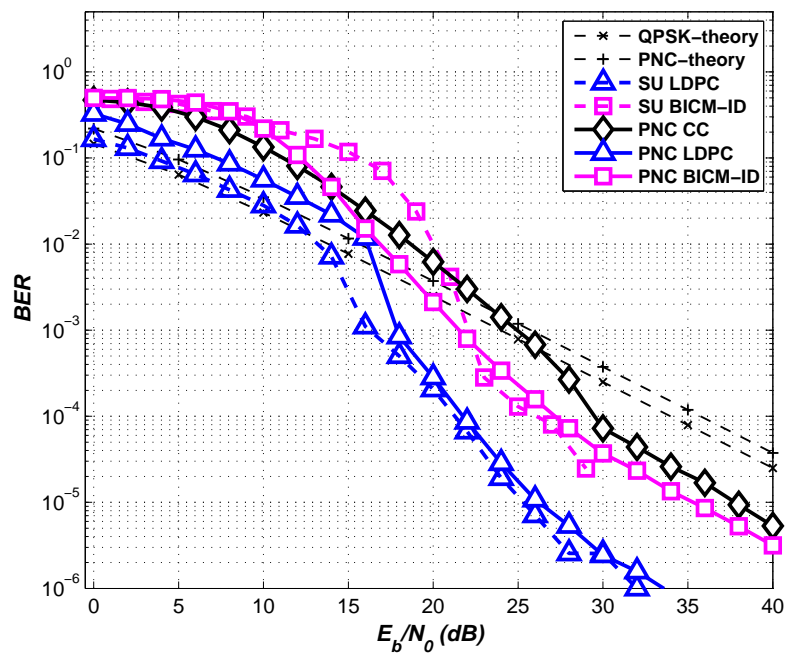


Figure 3.32: The performance of systems with code length 64800 and code rate 3/4 on the Rayleigh flat-fading channel.

Table 3.1: Summary of system performance for code rate 1/2 on the AWGN channel.

Code length	BER	Conv. code $(\frac{E_b}{N_0})$ , dB PNC	LDPC code $(\frac{E_b}{N_0})$ , dB		BICM-ID code $(\frac{E_b}{N_0})$ , dB		Turbo code $(\frac{E_b}{N_0})$ , dB	
			SU	PNC	SU	PNC	SU	PNC
576	$10^{-2}$	4.9	1.4	5	1.4	4.1	1	4.3
2304	$10^{-2}$	4.9	1.2	4.3	0.8	3.5	1.1	3.5
64800	$10^{-2}$	4.9	1	4	0.8	3.5	1.1	3.2
576	$10^{-3}$	6.2	2.1	5.5	2.1	4.5	2.1	4.5
2304	$10^{-3}$	6.2	1.4	4.8	1.7	3.9	1.5	4.1
64800	$10^{-3}$	6.2	1.2	4.3	1.7	3.9	1.3	3.4
576	$10^{-5}$	8	2.8	6.8	4	5.6	2.2	5.5
2304	$10^{-5}$	8	1.8	5.4	3.4	5.3	2.2	4.5
64800	$10^{-5}$	8	1.5	4.5	3.8	5.5	1.6	3.8

Table 3.2: Summary of system performance for code rate 2/3 on the AWGN channel.

Code length	BER	Conv. code $(\frac{E_b}{N_0})$ , dB PNC	LDPC code $(\frac{E_b}{N_0})$ , dB		BICM-ID code $(\frac{E_b}{N_0})$ , dB		Turbo code $(\frac{E_b}{N_0})$ , dB	
			SU	PNC	SU	PNC	SU	PNC
576	$10^{-2}$	5.3	3.5	6.4	3.6	6	3	5
2304	$10^{-2}$	5.3	3.3	5	3.4	5.4	3	5.2
64800	$10^{-2}$	5.3	3	5.5	3.3	5.3	3	5
576	$10^{-3}$	6.5	4.4	7.4	4.4	6.4	4.5	6.7
2304	$10^{-3}$	6.5	4	5.4	4	5.8	4.3	6.7
64800	$10^{-3}$	6.5	3.2	6.2	3.6	5.5	4.3	6.4
576	$10^{-5}$	8.5	5.4	8	5.6	7	6.3	8.5
2304	$10^{-5}$	8.5	4.5	6	4.4	6.8	5.3	8.4
64800	$10^{-5}$	8.5	3.5	6.5	4.7	6.3	5.8	8.7

Table 3.3: Summary of system performance for code rate 3/4 on the AWGN channel.

Code length	BER	Conv. code $(\frac{E_b}{N_0})$ , dB PNC	LDPC code $(\frac{E_b}{N_0})$ , dB		BICM-ID code $(\frac{E_b}{N_0})$ , dB	
			SU	PNC	SU	PNC
576	$10^{-2}$	6.3	5.4	8	11.2	15.8
2304	$10^{-2}$	6.3	6.3	8	13	-
64800	$10^{-2}$	6.3	5.3	7.7	14	-
576	$10^{-3}$	7.5	7.4	13	13	17.2
2304	$10^{-3}$	7.5	7.5	12.8	15	-
64800	$10^{-3}$	7.5	7	10	15	-
576	$10^{-5}$	9.3	9.7	16.8	13.8	19.2
2304	$10^{-5}$	9.3	9.3	14.5	16.5	-
64800	$10^{-5}$	9.3	7.8	10.4	15.5	-

Table 3.4: Summary of system performance for code rate 1/2 on the Rayleigh flat-fading channel.

Code length	BER	Conv. code ( $\frac{E_b}{N_0}$ ), dB PNC	LDPC code ( $\frac{E_b}{N_0}$ ), dB		BICM-ID code ( $\frac{E_b}{N_0}$ ), dB		Turbo code ( $\frac{E_b}{N_0}$ ), dB	
			SU	PNC	SU	PNC	SU	PNC
576	$10^{-2}$	15.5	10	12	10.5	13.5	11	12
2304	$10^{-2}$	15.5	9.5	11.5	10.5	13.5	9.4	11.5
64800	$10^{-2}$	15.5	9.5	11.5	10.5	13.5	9	11
576	$10^{-4}$	26	24	25	24	24.5	27	25
2304	$10^{-4}$	26	16	16	24	24	26	24
64800	$10^{-4}$	26	14	15.5	23.5	23	17.5	27

Table 3.5: Summary of system performance for code rate 2/3 on the Rayleigh flat-fading channel.

Code length	BER	Conv. code ( $\frac{E_b}{N_0}$ ), dB PNC	LDPC code ( $\frac{E_b}{N_0}$ ), dB		BICM-ID code ( $\frac{E_b}{N_0}$ ), dB		Turbo code ( $\frac{E_b}{N_0}$ ), dB	
			SU	PNC	SU	PNC	SU	PNC
576	$10^{-2}$	16.5	11	14	12.5	15.5	10	14
2304	$10^{-2}$	16.5	10.5	13	11.5	15	11.5	14
64800	$10^{-2}$	16.5	10.5	13	11.5	15	11.3	14
576	$10^{-4}$	30	21	22	26	28	26	28
2304	$10^{-4}$	30	22.5	23	26	27.5	26	28
64800	$10^{-4}$	30	17.5	18.5	26	27	26	27.5

Table 3.6: Summary of system performance for code rate 3/4 on the Rayleigh flat-fading channel.

Code length	BER	Conv. code ( $\frac{E_b}{N_0}$ ), dB PNC	LDPC code ( $\frac{E_b}{N_0}$ ), dB		BICM-ID code ( $\frac{E_b}{N_0}$ ), dB	
			SU	PNC	SU	PNC
576	$10^{-2}$	19	14	17.5	18	18
2304	$10^{-2}$	19	14.5	18	20	18
64800	$10^{-2}$	19	13	16.5	20	18
576	$10^{-4}$	29	25	27.5	26	28.5
2304	$10^{-4}$	29	22	24	26	27.5
64800	$10^{-4}$	29	21	22	26	27

### 3.8 Chapter Summary

This chapter began with an overview of the encoder and decoder for LDPC, BICM-ID, and turbo codes. The coded PNC systems were formally introduced and a discussion of how certain code parameters affect performance was presented. There

are several parameters that influence the performance of channel codes. One of the most important factors for turbo and BICM-ID codes are the size of the interleaver. However, the design of the interleaver is a factor, but only at high signal to noise ratios (SNRs) [73]. At low SNR, turbo and BICM-ID codes perform well with almost any interleaver provided that the two RSC turbo encoders receive inputs that are sufficiently uncorrelated. At higher SNR, performance is dominated by the low weight code words, which are significantly influenced by the interleaver design. In particular, the E2E performance of an LDPC code, turbo code and BICM-ID code of the same code length and code rate was evaluated on a TWRC with PNC employed at the relay. This included the impact of iterative decoding algorithms, code rate, type of channel (AWGN and Rayleigh flat-fading), and code length was compared through simulation with non-iterative code. All three coding schemes are shown to perform well on a single user AWGN channel, with the LDPC code and turbo code performing very similarly. However, on the TWRC it was observed that the turbo code and BICM-ID code both outperformed the LDPC codes. This is a surprising results and highlight a weakness in the message-passing decoding algorithm of the LDPC codes. LDPC code appears to be less robust when the initial conditional LLRs are incorrect due to errors propagating from the relay and being transmitted to the destination causing LDPC code degrader to initialize incorrectly. Now this is a problem because LDPC degrader is very sensitive to the LLR initializing, if slightly wrong we have a sever degradation performance. When as the turbo and BICM-ID codes are much robust because initialized differently. Therefore, LLR does not matter if not quit correct because these two codes less effected by the error propagation in the relay. As with other class of codes, the performance of turbo codes degrades as code rate increases. If puncturing is used to increase the code rate, then the manner of puncturing is also a performance and puncturing factors may need to be considered. The joint optimization of interleaver and puncturing matrix is perhaps the most important aspect of turbo code design [74]. Another important parameter is the choice of decoding algorithm. Most decoding algorithms are iterative, and therefore the number of iterations has an impact on the performance. Also the manner of the code that the two constituent encoders are terminated affects performance. This part of our work is to our knowledge the first publication comparing results for LDPC, BICM-ID, and turbo codes combined with E2E PNC [75].

## Chapter 4

---

---

# ExIT Chart Analysis of Iterative Decoding Schemes with E2E PNC

---

---

## 4.1 Introduction

Extrinsic information transfer (ExIT) charts, first proposed by S. T. Brink [76], have become an essential part of iterative error correction code design and have also been used as a complementary design tool for traditional bit error rate simulations. One significant method, based on bitwise mutual information, was implemented as a tool for studying the convergence behaviour of iterative decoding schemes. This yielded new visualization rules for improving the choice of constituent codes by an iterative process. Characterizing decoders via average mutual information was originally introduced for the constituent decoders in an iterative decoding algorithm. Moreover, the characteristics of a constituent decoder describe the processing of mutual information of the *a priori* information input and the extrinsic information output.

In this chapter, ExIT chart analyses are performed in order to investigate the achievable iterative decoding convergence when coded E2E PNC is employed. The importance of the ExIT chart technique is that it can predict the system's performance without simulating the transmitter and receiver, thus gaining an insight into the convergence of the iterative process. Moreover, the use of the ExIT chart on different iterative decoding schemes combined with E2E PNC has not been reported before. The difficulty at the relay part of the E2E PNC system is the demapping of interference to coded bits from the source resulting in a loss of reliable information that is not available to the destination nodes. This means that when applying channel coding the signal at the destination contains inaccurate information in terms of log-likelihood ratios (LLRs) due to the errors from the uplink-phase. The attainable performance of different coding schemes having different code rates, different decoding algorithms and block sizes is studied, when communicating over AWGN channels and using QPSK modulation. More specifically, the proposed ExIT charts are then invoked for studying the E2E PNC scheme with bit-interleaved coded modulation using iterative decoding (BICM-ID), low-density parity-check (LDPC) and turbo codes.

## 4.2 Extrinsic Information Transfer Charts

ExIT charts [38] constitute a useful tool in the design of iterative schemes, since the characteristics of the constituent components can be visualised based on their exchange of mutual information. ExIT charts have been used for analysing both concatenated binary coding schemes [76] and non-binary coding schemes [77]. The ExIT chart technique relies on the Gaussian approximation, but provides some intuition regarding the dynamics and convergence properties of an iteratively decoded code. The formulation of a turbo-cliff after a certain number of iterations enables us to predict a low bit error rate (BER) for the ratio between the energy per information bit ( $E_b$ ) and the variance of the two-dimensional noise ( $N_0$ ),  $E_b/N_0$ , in excess of the turbo-cliff. The ExIT characteristics of the constituent decoders describes the processing of mutual information, which measures the dependence between two variables, associated with *a priori* information inputs to mutual information associated with the extrinsic information outputs.

### 4.2.1 The Gaussian Approximation

The conditional distribution for two variables is a probability distribution that gives the probability at any particular range or discrete set of values specified for those remaining variables [78]. In order to analyze the system components separately, the need arises to obtain the probability density function (pdf) for *a priori* LLR values. In this case, a simple and accurate approximation of the pdf is the single parameter Gaussian model. The principle of Gaussian approximation is to approximate the message pdf by Gaussian densities, which are defined by the mean and variance. Moreover, Gaussian approximation employs a consistency assumption, which allows the evolution of the message in order to determine approximate decoding thresholds. The channel message satisfies the consistency condition, as mentioned in Chapter 2, and the assumption is that other messages satisfy it at least approximately. Consider the channel inputs  $s \in \{+1, 1\}$  and channel outputs  $r = s + w$ , where  $w \sim W(0, \sigma^2)$  is white Gaussian noise. A generic conditional LLR,  $L(r|s)$ , from the channel is

given by

$$L(r|s) = \ln\left(\frac{Pr(r|s = +1)}{Pr(r|s = -1)}\right) \quad (4.1a)$$

$$= \frac{2r}{\sigma^2} \quad (4.1b)$$

which is clearly conditionally Gaussian, so we need only determine its mean and variance as

$$E(L(r|s)) = \frac{2E(r)}{\sigma^2} = \frac{2}{\sigma^2} \quad (4.2)$$

$$\text{var}(L(r|s)) = \frac{4\text{var}(r)}{\sigma^4} = \frac{4}{\sigma^2} \quad (4.3)$$

where the assumption that only  $s = +1$  is sent,  $r \sim W(+1, \sigma^2)$ , so that the relation between mean value and variance can be described as

$$\text{var}(L(r|s)) = 2E(L(r|s)) \quad (4.4a)$$

$$\frac{1}{\sqrt{2\pi}\sigma} e^{-\frac{1}{2\sigma^2}(\xi - \delta_L)^2} = \frac{1}{\sqrt{2\pi}\sigma} e^{-\frac{1}{2\sigma^2}(-\xi - \delta_L)^2} e^\xi \quad (4.4b)$$

$$\sigma^2 = 2\delta_L \quad (4.4c)$$

where  $\delta_L$  is a mean value for LLR.

### 4.2.2 Mutual Information

Recall from Chapter 2 that the mutual information,  $I$ , between two random variables,  $S$  and  $L$ , gives the amount of uncertainty in  $S$  that is removed by knowing  $L$ . In our case,  $S$  is the transmitted sequence and  $L$  is the decoded sequence in term of LLR. Therefore, the mutual information is related to the entropy and conditional entropy as follows

$$I(S; L) = H(S) - H(S|L) \quad (4.5a)$$

$$= H(L) - H(L|S) \quad (4.5b)$$

where  $H(\cdot)$  denotes the entropy. In the case where  $S$  and  $L$  are independent, then the mutual information is zero. The relationship between mutual information and the variance of LLRs can be formally described by the  $J$  function introduced in [76]

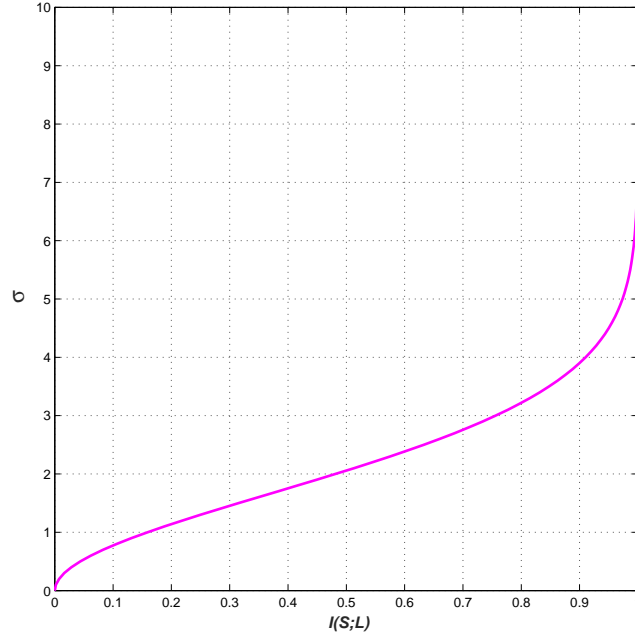


Figure 4.1: The relation between the mutual information and variance of LLRs.

using the Gaussian approximation and a good analytical approximation is derived in [79] as

$$J(\sigma) = I(\sigma_L = \sigma) \quad (4.6a)$$

$$= (1 - 2^{-v_1 \sigma^{2v_2}})^{v_3} \quad (4.6b)$$

where  $v_1 = 0.3073$ ,  $v_2 = 0.8935$ , and  $v_3 = 1.1064$ . This transformation can be calculated through numerical integration of the change of mutual information with the variance, as illustrated in Figure 4.1, where the value of  $I(S; L)$  is represented by the *a priori* information. The iterative process described by the output of one component is the input of the other. Therefore, the trajectory of the iteration system is evaluated by the progress of the data components in terms of mutual information, and both characteristic functions can be plotted in a single figure. Using the mutual information gives the most accurate prediction due to the assumption of a Gaussian distribution being dependent only on the input pdf and not on the output [80].

## 4.3 ExIT Charts Construction and Properties

The basic ingredients in the construction of the ExIT chart are the extrinsic information curves formed for the constituent decoder. The ExIT chart technique involves the calculation of the mutual information of the extrinsic information and the message bits, in addition to the mutual information of the *a priori* knowledge with respect to the message bits. Furthermore, links have been made between ExIT charts and the corresponding BER curves. The convergence behaviour of the iterative receiver is based on an unknown received signal and evaluated with the help of an ExIT chart. The vertical and horizontal axes of the ExIT chart represents the input and output information of the decoder components. Since the output metric for one decoder is the input metric for its companion decoder, one can plot both transfer curves on the same axes, but with the abscissa and ordinate reversed for one decoder. Therefore, a large number of iterations is needed when the tunnel between transfer curves narrows. However, the convergence property of the multi user interference (MUI) signal is not only related to its architecture but also to the parameters and the type of channel coding used. Unlike the BER results, the performance investigation is dependent on the mutual information between the transmitter and receiver to achieve convergence.

### 4.3.1 ExIT Charts for BICM-ID Code with PNC

BICM-ID constitutes a serially concatenated arrangement, where the inner and outer codes are constituted by the demapper and SISO decoder, respectively. We model the *a priori* LLRs  $L_a$  by an independent Gaussian random variable in conjunction with the information  $s$  as

$$r = \delta_L \cdot s + w \quad (4.7)$$

where  $\delta_L = \sigma^2/2$  and  $\sigma^2$  is the variance of the noise with a mean of zero and  $s \in \{+1, 1\}$ . The pdf of the *a priori* LLRs can be expressed as

$$p(r|s) = \frac{1}{\sqrt{2\pi\sigma}} e^{-|r-s|^2/2\sigma^2} \quad (4.8)$$

For the PNC system employing BICM-ID, a system based on BICM-ID consists of two components, namely a demapper (Dem) and decoder (Dec) to perform the iterative process. The two receiver components of the BICM-ID scheme iteratively

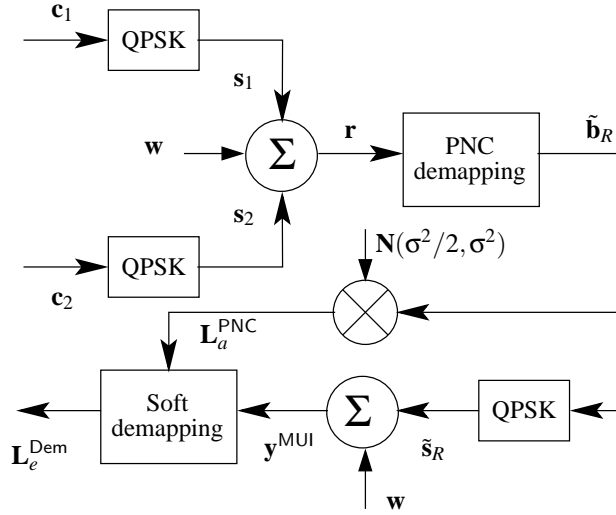


Figure 4.2: The demapper setup for PNC system employing BICM-ID.

exchange information between the inner, Dem, and outer codes, Dec, to improve the performance. Since the decoder for each constituent code is a SISO module and the conditional pdf of the input LLRs to the SISO module is not known, the iterative process in a BICM-ID system is simulated separately for the receiver components [81]. First we investigate the transfer characteristic of the inner demapper, the mutual information between the transmitted sequence  $s$  and the *a priori* LLR  $L_a^{Dem}$  is denoted as  $I_A^{Dem} = I(S; L_a^{Dem})$ , where  $0 \leq I_A^{Dem} \leq 1$  as given in equation (2.27). In the demapper system setup, as depicted in Figure 4.2, the users' symbols are summed after QPSK mapping and sent through the AWGN channel. The demapper transfer characteristic  $I_{E,MUI}$  is the transfer function  $\mathbb{T}_I(\cdot)$  of the *a priori* mutual information  $I_A$  and  $E_b/N_0$  value of the AWGN channel, which can be written as

$$I_{E,MUI} = \mathbb{T}_I(I_{A, Dem}, E_b/N_0) \quad (4.9)$$

where  $I_{A, Dem}(\sigma)$  can be obtained for real values by equation (2.21) and for complex values by equation (2.27). The output sequence from PNC demapping is multiplied by the independent samples taken from a Gaussian distribution with mean value  $\sigma^2/2$  and variance  $\sigma^2$  to form the LLRs input to the soft demapping as *a priori* information,  $L_a^{PNC}$ . Consequently, the  $L_a^{PNC}$  and the channel information  $y^{MUI}$  are the inputs to the soft demapper. When both natural and Gray mappings are utilized in the transfer function of the demapper, the demapper is affected by the channel information due to its dependence on the SNR,  $\Xi$ . Therefore, the demapper transfer characteristics almost approach non-convex shapes depending on the SNR values.

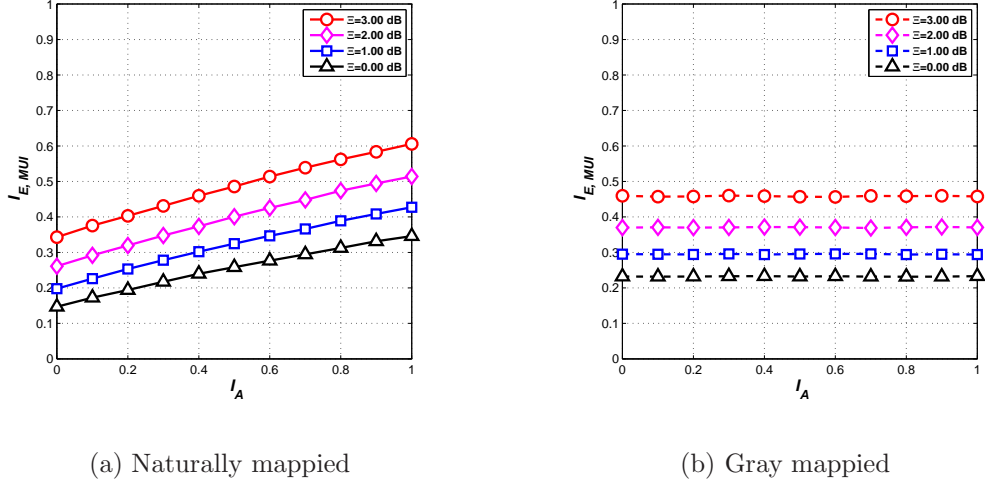


Figure 4.3: BICM-ID demapper transfer characteristics function of QPSK mapping at different  $\Xi$  in dB values for PNC system.

Figure 4.3 shows the EXIT chart function when the channel is AWGN and the SNRs values are 0, 1, 2, 3 dB for natural and Gray mapping. Observe that the transfer characteristic for natural mapping, as shown in Figure 4.3(a), has a steep slope, yielding the strong potential for performance improvement in the PNC with BICM-ID system. Moreover, a decrease/increase in the value of SNR will shift the EXIT curve down/up. Whereas the demapper transfer characteristics are almost straight lines with Gray mapping, as shown in Figure 4.3(b), and the mutual information  $I_{E, \text{MUI}}$  remains constant even when *a priori* information knowledge increases.

The decoder setup of the BICM-ID system with PNC starts with a block of independent message bits  $b_k$  from each user and is encoded by a non-recursive systematic code (NSC) encoder to obtain  $c_u$ . The modulo-2 sum of the users coded bits  $\mathbf{c}$  is multiplied by the random independent samples. Therefore, the LLRs are modelled as random independent Gaussian distributed variables with a mean value of  $\sigma^2/2$  and a variance of  $\sigma^2$  to form the decoder input  $L_a^{\text{ENCs}}$  [79]. The decoder employs the maximum *a posteriori* algorithm in the Log domain (Log-MAP) to provide information about the message bits, which can be utilized to estimate the source bits  $\widehat{b_1 \oplus b_2}$ . Figure 4.4 shows the decoder setup to generate the EXIT function. The decoder input is *a priori* information coming from the decoders  $L_a^{\text{ENCs}}$  in terms of LLRs, where the outputs are the extrinsic information of coded bits  $L_e^{\text{Dec}}$ , which are in turn fed back for the next iteration, and  $\widehat{b_1 \oplus b_2}$ . Several parameters have been considered to simulate the BICM-ID system, as illustrated in Table 4.1,

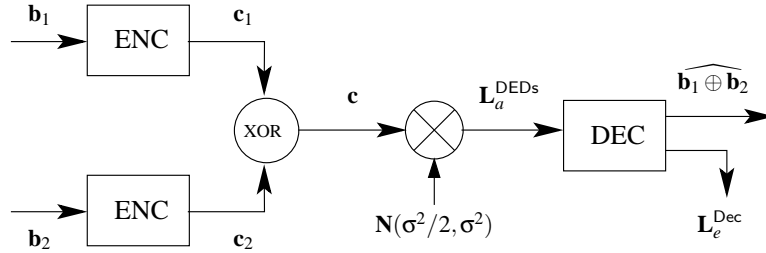


Figure 4.4: The decoder setup for PNC system employing BICM-ID to generate the transfer characteristics function.

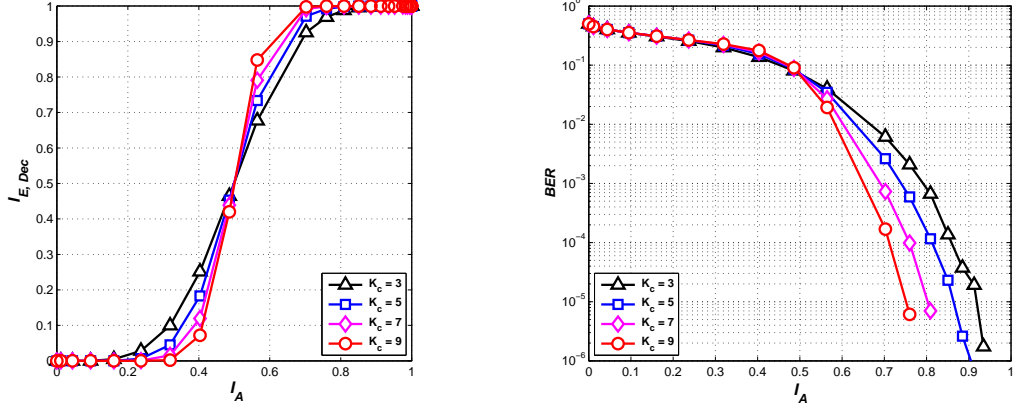
Table 4.1: The summarize of decoder parameters.

Constraint length	Generator polynomials	Code rate
3	[5 7]	0.5
5	[23 35]	0.5
7	[133 171]	0.5
9	[561 753]	0.5

which summarizes the parameters for simulation. Figure 4.5(a) shows the transfer characteristics for convolutional codes of rate 0.5 with constraint length 3,5,7 and 9. Moreover, the decoder curve shows the relationship between the *a priori* information and predict the BER for the system by using the EXIT function, as depicted in Figure 4.5(b). It can be observed that the stronger code of constraint length 9 has a steeper EXIT function than the weaker code of constraint length 3, and therefore needs lower mutual information at the input to produce high quality LLRs at the output and lower BER. In fact, the performance of the receiver is given by the trajectory between two transfer functions, exchanging information of the extrinsic LLR output from soft demapper  $L_e^{\text{Dem}}$ , and the extrinsic LLR output from decoder  $L_e^{\text{Dec}}$ , in each iteration.

### 4.3.2 EXIT Charts for LDPC Code with PNC

The idea behind EXIT charts for LDPC codes begins with the fact that the variable-node decoder (VND) and check-node decoder (CND) work cooperatively and iteratively to make bit decisions, with the metric of interest generally improving with each half-iteration. The system setup used for generating the extrinsic information transfer function for a PNC system employing an LDPC code is depicted in Figure 4.6. A transfer curve plotting the input metric versus the output metric can be obtained both for the VND and for the CND, where the transfer curve for the



(a) Constraint length as a function

(b) BER as a function

Figure 4.5: BICM-ID decoder transfer characteristics function of code rate 1/2, code length 2304 bits and different constraint length for PNC system.

VND depends on the channel  $E_b/N_0$ . Such a chart aids in the prediction of the decoding threshold of the ensemble of codes characterized by given VND degree,  $d_v$ , and CND degree,  $d_c$ , distributions. The decoding threshold is the  $E_b/N_0$  at which the VND transfer curve touches the CND curve, precluding convergence of the two decoders. Therefore, the convergence evaluation is achieved by transferring the mutual information between VND and CND. The notation of  $I_A$  is the average mutual information between the *a priori* LLRs values and the bits on the graph edges of the decoder. Whereas,  $I_E$  is the average mutual information between the extrinsic LLRs value and the bits on the graph edges. The extrinsic information,  $L_e^{VND}$ , and the processing characteristic of the VND describe the processing of mutual information, becoming *a priori* information for the CND,  $L_a^{VND}$ . Similarly, the extrinsic information from the CND,  $L_e^{CND}$ , becomes *a priori* information for the VND,  $L_a^{CND}$  [82]. The extrinsic information of the LDPC decoder components for the binary message are represented as a binary symmetric channel with a certain crossover probability [83]. Consequently, the mutual information is plotted at the output of each block as a function of the mutual information at the input, i.e. drawing the corresponding EXIT chart, it is possible to predict the convergence characteristics of the considered system.

Since the LDPC code's iterative components are between VND and CND, then the decoding process can be described as a recursive computation of the mutual information between them. The decoding operation of the VND, as illustrated

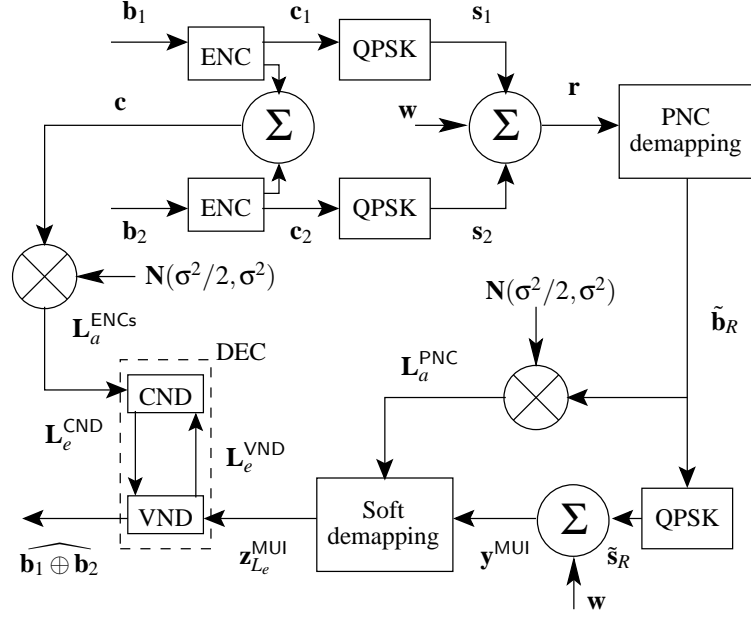
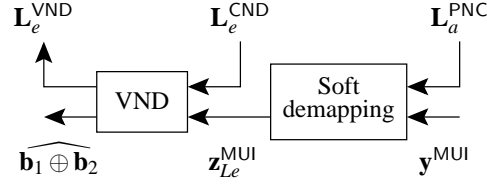


Figure 4.6: The system setup for PNC system employing LDPC code to generate the transfer characteristics function.

in Figure 4.7, is equivalent to computing extrinsic LLRs for a repetition code of length equal to  $d_v + 1$ , where the decoder has one code bit of channel information and *a priori* information about the other coded bits. Therefore, the EXIT chart method is used to determine whether the decoding of an LDPC code converges by characterizing the LDPC decoder's operation. The distribution of messages from VND to CND are symmetric Gaussian random variables, since the inputs of the *i.i.d* AWGN samples are added to the VND [84]. We adopt the consistent-Gaussian assumption for the VND *a priori* inputs and its output, as shown in Figure 4.7(a). Under this assumption, the inputs of the VND are the received channel impaired symbols  $z_{L_e}^{\text{MUI}}$  and the extrinsic information from CND,  $L_e^{\text{CND}}$ . One can note that the combining of the *a priori* information,  $L_a^{\text{PNC}}$ , and the multi user interference (MUI),  $y^{\text{MUI}}$ , signal received from the channel to produce the extrinsic information in terms of LLRs entering the VND,  $z_{L_e}^{\text{MUI}}$  [85]. The EXIT function for the VND is computed as [82]

$$I_{E,VND}(I_A, d_c, \Xi) = J \left( \sqrt{(d_v - 1)[J^{-1}(I_A)]^2 + E(z^2)} \right) \quad (4.10)$$

where  $E(z^2)$  is the variance of the channel output information  $z$ . To express  $I_{E,VND}$  as a function of  $I_{A,VND}$ , we first exploit the consistent-Gaussian assumption for the



(a) Input/output VND component

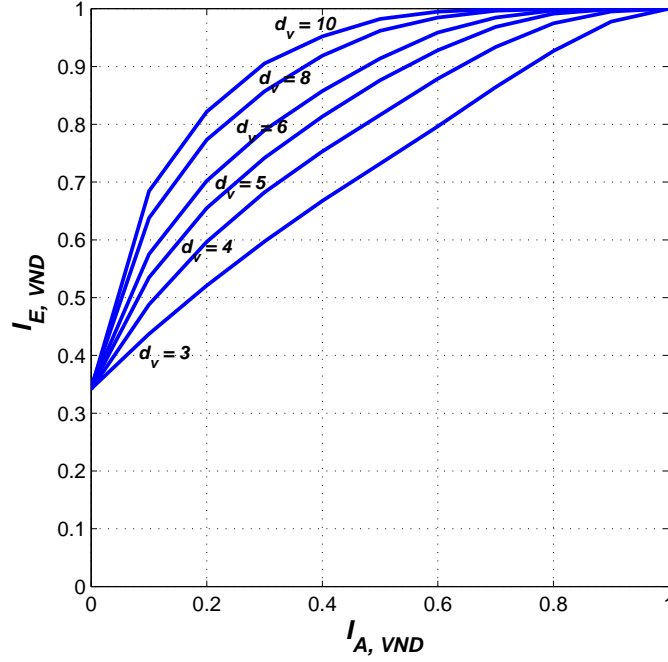

 (b) VND EXIT curves at  $\Xi=3$  dB and  $R_c=1/2$ 

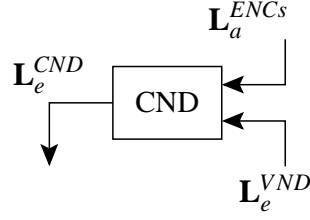
Figure 4.7: VND operation for PNC system employing LDPC code.

inputs as

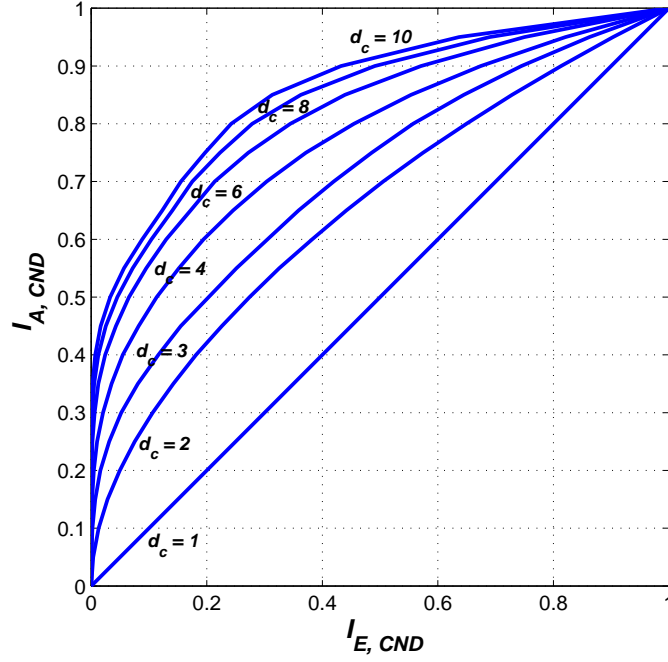
$$I_{A, VND} = J(\sigma_L) \quad (4.11)$$

The distribution of messages from CND to VND is modelled by a symmetric Gaussian distribution, and thus the VND detector will give approximated values depending on the parameters of  $I_{E, VND}(I_A, d_c, \Xi)$  in equation (4.10). Figure 4.7(b) shows several variable node curves depending on various VND degrees  $d_v = 3, 4, 5, 6, 8, 10$  when  $\text{SNR} = 3$  dB. The information updated at the VND by the information coming from the CND  $L_e^{\text{CND}}$  with the MUI information in terms of LLRs  $z_{L_e}^{\text{MUI}}$  comes from the soft demapper to obtain the extrinsic information of the VND to go to CND as extrinsic information  $L_e^{\text{VND}}$  and estimate the transmitted bits  $\widehat{b_1 \oplus b_2}$ .

Similarly, the decoding operation of the CND, as shown in Figure 4.8, is equiv-



(a) Input/output CND



(b) CND EXIT Curves

Figure 4.8: CND operation for PNC system employing LDPC code.

alent to computing the extrinsic LLRs for a single parity check code of  $d_c$ , where the decoder has *a priori* information about all coded bits. The inputs of the CND decoder are the *a priori* information  $L_a^{ENCs}$  and the extrinsic information from the VND decoder  $L_e^{VND}$ , both in term of LLRs, as depicted in Figure 4.8(a). The EXIT function for the CND can be expressed as [82]

$$I_{E,CND}(I_A, d_c) = 1 - J\left(\sqrt{(d_c - 1)[J^{-1}(1 - I_A)]^2}\right) \quad (4.12)$$

where  $J^{-1}(\cdot)$  is the inverse function of  $J(\cdot)$ . As can be observed from Figure 4.8(b), several check node curves are dependent on the degree of  $d_c$  and all curves start from the origin.

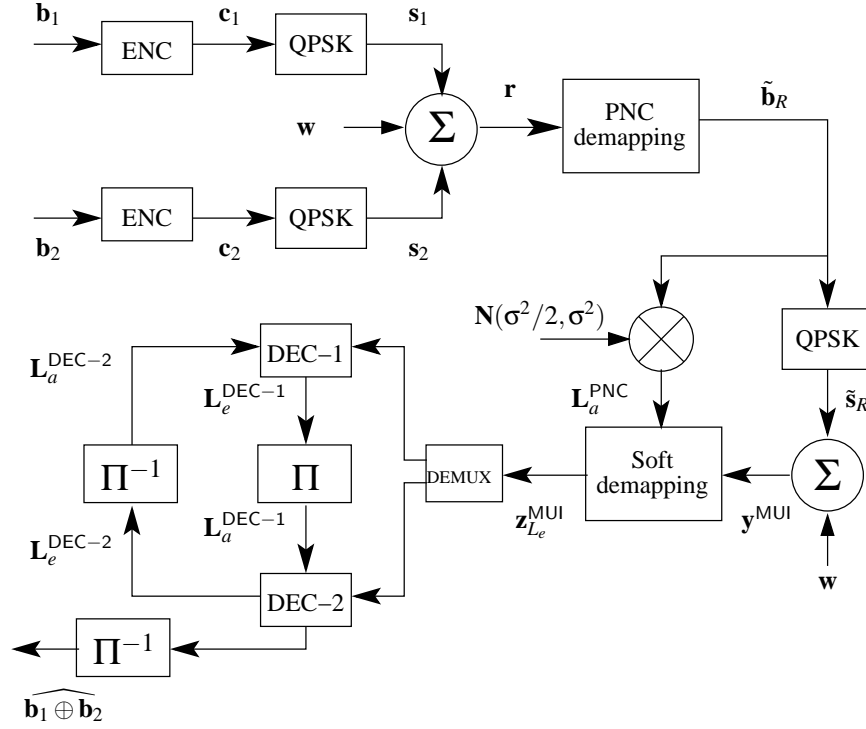


Figure 4.9: The system setup for PNC system employing turbo code to generate the transfer characteristics function.

### 4.3.3 EXIT Charts for Turbo Code with PNC

The EXIT chart technique for turbo codes is very similar to that for LDPC codes. For LDPC codes, there is one extrinsic information transfer curve for the CND and one for the VND. The CNDs are not connected to the channel, so only the VND transfer curve is affected by changes in  $E_b/N_0$ . For turbo codes, there is one extrinsic information transfer curve for each constituent encoder and both encoders are directly connected to the channel, so the transfer curves for both depend on  $E_b/N_0$ . For a PNC system employing a turbo code, the setup of the decoders is represented in Figure 4.9. The iterative process in the turbo decoder is between two SISO components, namely decoder-1 (DEC-1) and decoder-2 (DEC-2). Therefore, the EXIT function of DEC-1 and DEC-2 can be expressed as

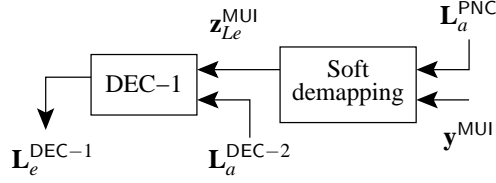
$$\begin{aligned} I_{E,DEC-1} &= \mathbb{T}_I(I_{A,DEC-2}) \\ I_{E,DEC-2} &= \mathbb{T}_I(I_{A,DEC-1}) \end{aligned} \quad (4.13)$$

where the term  $I_{A,DEC-2}$  is the mutual information between  $I_A$  and a *a priori* information of DEC-2 output, and the term  $I_{A,DEC-1}$  is the mutual information between  $I_A$  and a *a priori* information of DEC-1 output. The inputs of DEC-1 and DEC-2

are similar, therefore, we use  $\mathbb{T}_I(\cdot)$  to represent  $I_{E,\text{DEC-1}}$  by  $I_{A,\text{DEC-2}}$  and, similarly, to represent  $I_{E,\text{DEC-2}}$  by  $I_{A,\text{DEC-1}}$ . Consequently, the mutual information  $I_{E,\text{DEC}}$  is given by equation (2.18) and because  $I_{A,\text{DEC}}$  is monotonic in  $\sigma$ , there is a one-to-one correspondence between  $I_{A,\text{DEC}}$  and  $\sigma$  given by equation (2.21), which can be written as

$$I_{A,\text{DEC}} = 1 - \int_{-\infty}^{+\infty} \frac{1}{\sqrt{2\pi}\sigma} e^{-\frac{(\xi-\sigma^2/2)^2}{2\sigma^2}} \log_2(1 + e^{-\xi}) d\xi \quad (4.14)$$

Both the constituent decoder receives information from channel impaired symbols  $z_{L_e}^{\text{MUI}}$ , and extrinsic information that was received from a counterpart decoder, used as *a priori* information. The ExIT function for the mutual information of the constituent DEC-1 versus DEC-2 is modelled by the *a priori* information. For each iterations, both decoders are swapped and interchange their roles. This involves the extrinsic output of DEC-1 becoming the *a priori* input of DEC-2, where the *a priori* input value is subtracted from the *a posteriori* probability of the soft extrinsic output, which avoids propagation of already known information. Therefore, the performance of separate decoders allows for the investigation and optimization of each constituent code. For DEC-1, as depicted in Figure 4.10, the output extrinsic information,  $L_e^{\text{DEC-1}}$ , is sent to the counterpart DEC-2 which uses it as *a priori* information,  $L_a^{\text{DEC-1}}$ , as shown in Figure 4.10(a). The ExIT function for the constituent DEC-1 is shown in Figure 4.10(b). For DEC-2, as illustrated in Figure 4.11, the output extrinsic information,  $L_e^{\text{DEC-2}}$ , is sent to the counterpart DEC-1 which uses it as *a priori* information,  $L_a^{\text{DEC-2}}$ , and estimates the output bits,  $\widehat{b_1 \oplus b_2}$ , as shown in Figure 4.11(a). The ExIT chart function for the constituent DEC-2 is shown in Figure 4.11(b). The ExIT chart function of two concatenated codes, as shown in Figure 4.12, is due to the symmetry. This means the inner decoder is identical to that of the outer decoder. Therefore, the curve of the ExIT chart is displayed with swapped axes, in that the horizontal axis is the mutual information of the extrinsic output and the vertical axis is the mutual information of the *a priori* input. The iterative decoding process of the turbo code makes the output of one decoder the input of the other decoder in the next iteration, and so the second curve swaps axes, as depicted in Figure 4.12(a) and Figure 4.12(b).



(a) Input/output DEC-1 component

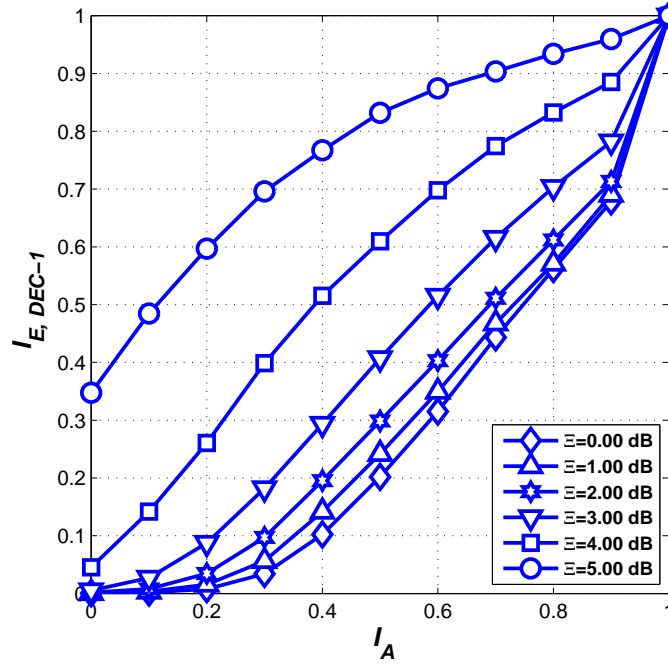
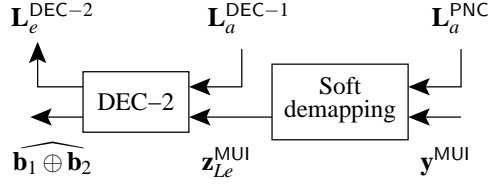

 (b) DEC-1 ExIT Curves for  $R_c=1/2$  and different value of  $\Xi$  in dB

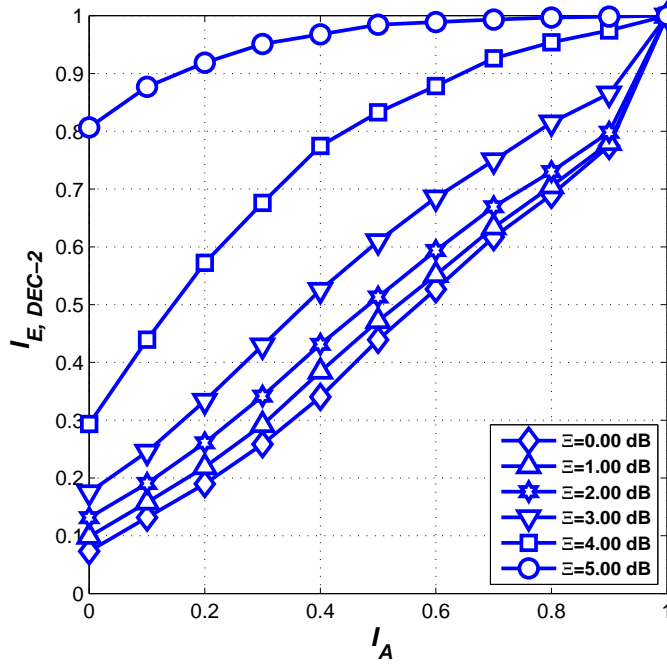
Figure 4.10: DEC-1 operation for PNC system employing turbo code.

## 4.4 Iterative Decoder Behaviour with E2E PNC

Unlike previous results in Chapter 3, the investigation of the E2E PNC system with iterative decoders are now dependent on the mutual information between the transmitter and receiver. The convergence behaviour of the proposed detectors of a two-way relay network from the unknown received signal is evaluated with the help of an ExIT chart. A PNC system employing different algorithms for iterative error correction code with a coding rate of  $1/2$  and  $2/3$  was adopted. The key idea of the PNC system is to implement the recomposition of the interference signal of the two users and broadcast it to the destinations. The 2304 coded bits size are mapped on a QPSK constellation, resulting in number of symbols 1152. All simulation results are carried out on the simulated AWGN channel. The parameters considered as



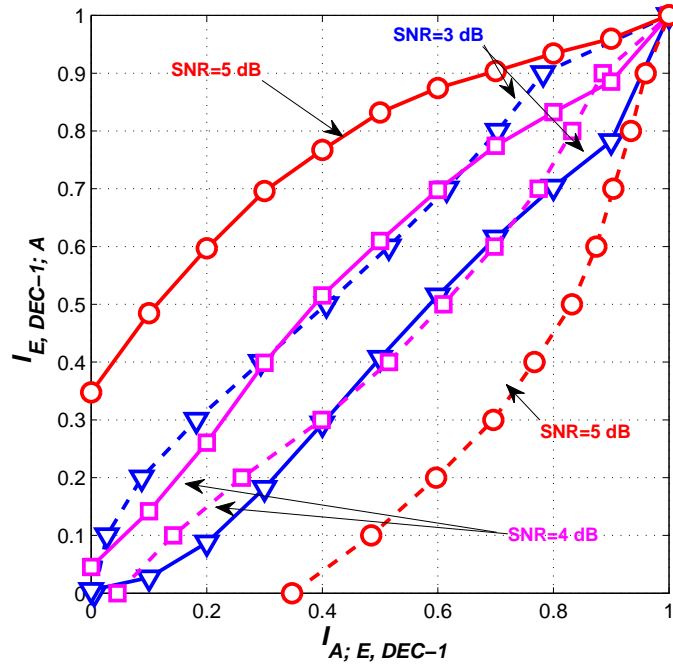
(a) Input/output DEC-2 component



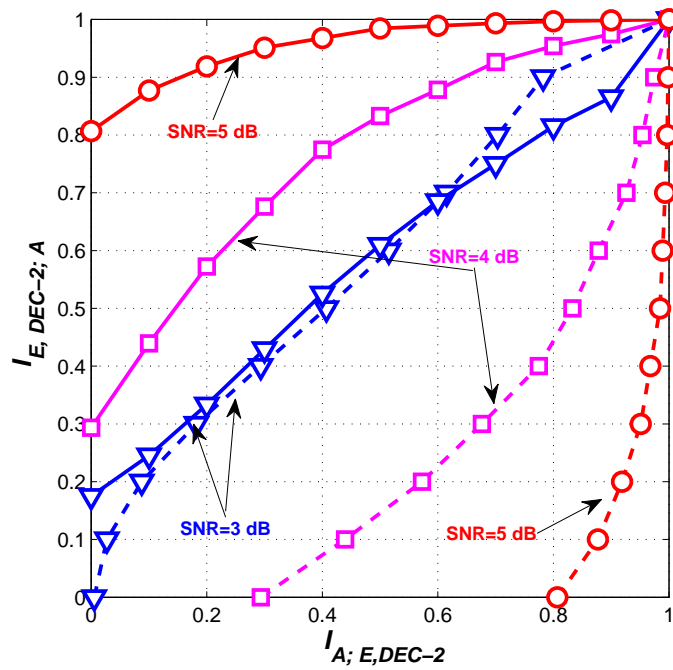
(b) DEC-2 ExIT Curves for  $R_c=1/2$  and different value of  $\Xi$  in dB

Figure 4.11: DEC-2 operation for PNC system employing turbo code.

identical system configurations are kept for a fair comparison and in terms of mutual information. However, the convergence property of interference signals of a PNC system is not only related to its architecture but also to the parameters and the type of channel coding used. The realization of a robust receiver that constantly decodes is difficult due to the errors occurring at the relay, since there is no decoding at the relay. Therefore any errors occurring at the relay from the uplink-phase are broadcast to both destination nodes. Hence, the initial LLRs at the input of each decoder will be incorrect, since it is assumed that the received signal was transmitted with no errors. The systems performance in term of bit error rate (BER) for code rate 1/2 and 2/3 are implemented in Figure 4.13(a) and Figure 4.13(b), respectively. The performance of the systems with code rate 1/2 tends that turbo code better



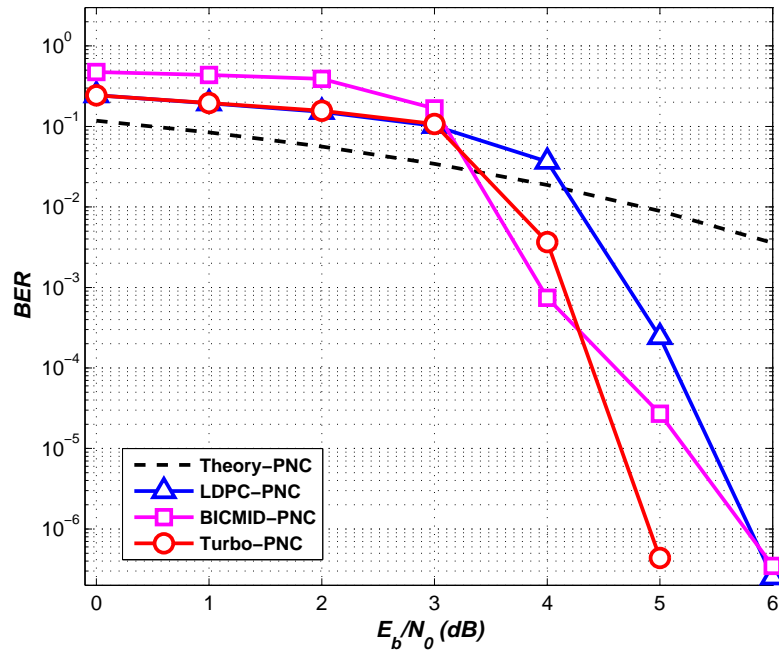
(a) DEC-1 component



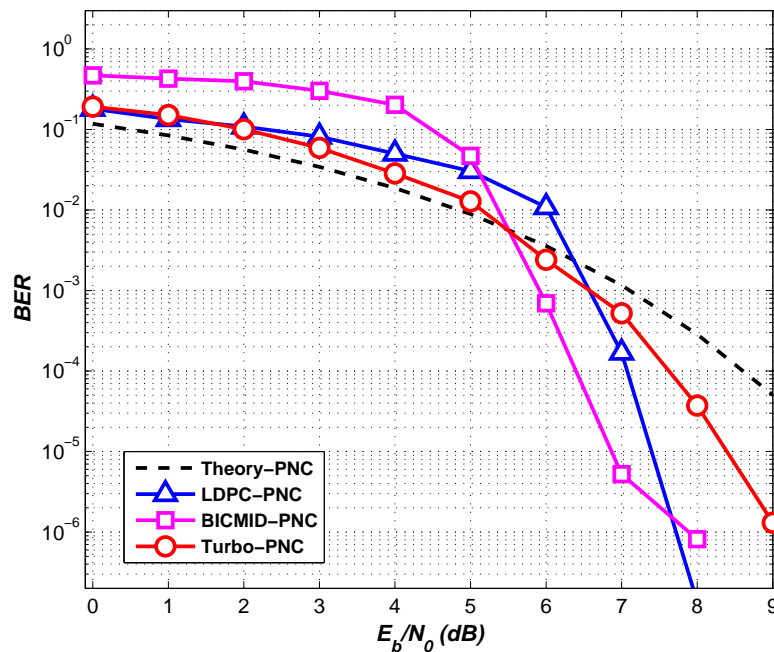
(b) DEC-2 component

Figure 4.12: EXIT chart with transfer characteristics function for a set of  $\Xi$  values in dB and  $R_c=1/2$  for PNC system employing turbo code.

performance than BICM-ID and LDPC code. However, the performance with code rate 2/3 tends to be improved for the BICM-ID and LDPC code than turbo code.



(a) BERs for code rate 1/2



(b) BERs for code rate 2/3

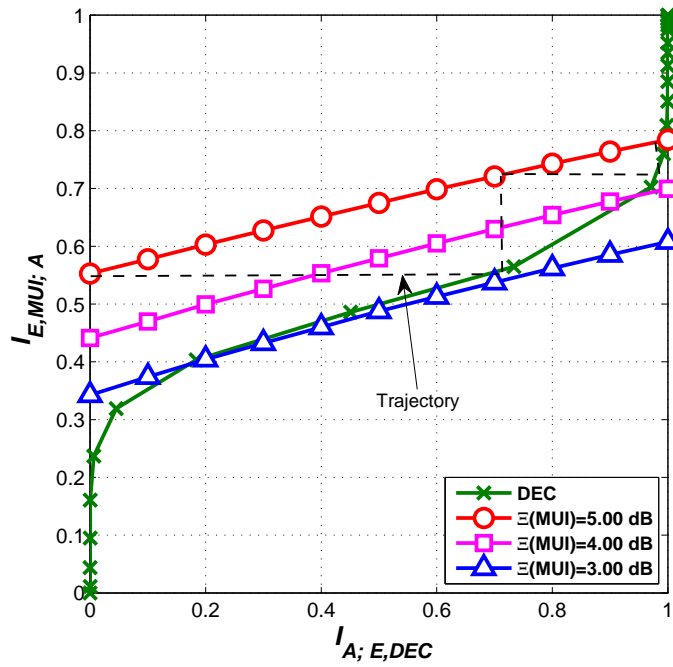
Figure 4.13: BER curves for coded E2E PNC system of different code rate and code length 2304 bits.

### 4.4.1 Analysis for BICM-ID Code with PNC

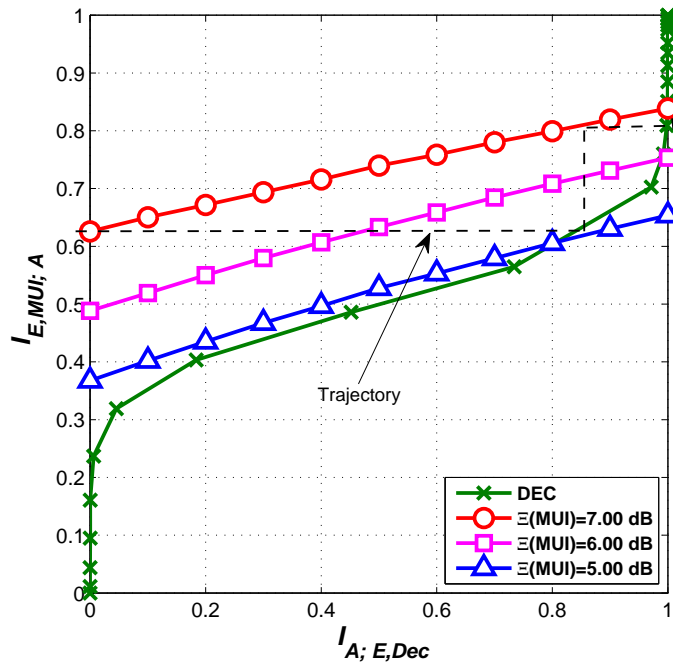
The stronger code of constraint length,  $K_c$ , equal 5 with generator polynomials [23 35]<sub>8</sub> was implemented to generate the coded bits, and the decoder uses the BCJR algorithm. A number of blocks are simulated for different values of  $\sigma^2$  in order to estimate the output mutual information for the decoder. The system trajectory can be predicted as the stair case between the two curves to obtain the trajectory of the proposed system. For the trajectory to propagate, the increase in SNR,  $\Xi$ , value must raise the transfer characteristic of the demapper high enough to open the tunnel. The system with rate 1/2 in Figure 4.14(a) shows that the tunnel closes at  $I_{A;E,Dec}=0.185$  and  $I_{E,MUI;A}=0.395$  for  $\Xi=3$  dB and at  $\Xi=4$  dB, the tunnel closes at  $I_{A;E,Dec}=0.93$  and  $I_{E,MUI;A}=0.68$ , implying that the receiver will not converge at 3 and 4 dB. Whereas, the tunnel opens at  $\Xi=5$  dB and the trajectory experiences a bottleneck at  $I_{E,MUI;A}=0.79$  and  $I_{A;E,Dec}=0.99$  implying that further increase in iterations at this particular value of SNR will not improve the performance of the system. In Figure 4.14(b), it can be seen that the system with rate 2/3 the tunnel opening closes at  $I_{A;E,Dec}=0.8$  and  $I_{E,MUI;A}=0.6$  for  $\Xi=5$  dB implying that the receiver will not converge. While the converge are occurs at  $\Xi=7$  dB for PNC system with 2/3 rate. For comparison purposes, the single user system is adopted as illustrated in Figure 4.15, with the tunnel open at 3 dB. Table 4.2 summarizes the numeric results for systems with BICM-ID code employing ExIT function, for different code rates and SNR values, to predict the system's behaviour.

Table 4.2: A brief description for the BICM-ID with E2E PNC system convergence.

System	Code rate	$I_{E,MUI;A}$ point	$I_{A;E,DEC}$ point	$\Xi$ (dB)	Convergence
single user	1/2	0.7	0.97	0	No
single user	1/2	open tunnel		3	Yes
PNC	1/2	0.39	0.18	3	No
		0.68	0.92	4	No
PNC	1/2	open tunnel		5	Yes
PNC	2/3	0.6	0.8	5	No
		0.75	0.96	6	No
PNC	2/3	open tunnel		7	Yes



(a) ExIT curves for code rate 1/2



(b) ExIT curves for code rate 2/3

Figure 4.14: ExIT chart for a set of  $\Xi$  value in dB and different rate for E2E PNC system employing BICM-ID code.

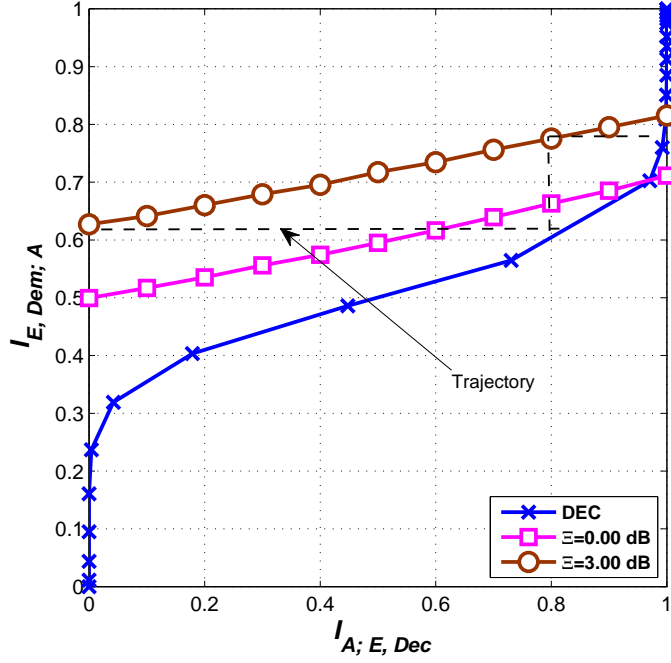


Figure 4.15: ExIT chart for single user (SU) system employing BICM-ID code of code rate 1/2.

#### 4.4.2 Analysis for LDPC Code with PNC

At the commencement of the iterative decoding process, single user and PNC systems were presented as the ExIT function for the systems employing LDPC codes, where the decoders utilized an MPA algorithm. Figure 4.17 presents the ExIT function for the PNC system with rate 1/2 and 2/3. The vertical and horizontal axes of the ExIT chart represent the input and output information of the decoder components. The result shows the trajectory obtained from the CND - VND iterative process, therefore, for convenience each component is simulated separately. The interaction of the two concatenated decodes, VND and CND, can be predicted on the ExIT chart. The complete ExIT chart of the LDPC code with the PNC based system is generated by simulation results, where the value set of the  $E_b/N_0$  is seen by the VND as a constant value and evaluates the output extrinsic information for various values of the input extrinsic information. The CND starts from the origin, where the feedback *a priori* information  $I_A = 0$ . Since the condition of the decoding trajectory start from point (0,0) with low probability and by reaching the point (1,1) has a high probability, that the ExIT chart has open tunnel. Therefore, the maximum likelihood decoding has been found at point (1,1) and the BER will be in the error floor region. Then, the output extrinsic information is fed to the VND

component  $I_E^{\text{CND}} = I_A^{\text{CND}}$ , yielding the LLRs described by  $I_E^{\text{VND}} = I_A^{\text{VND}}$ , which are then fed back to the CND and so on. *A priori* information comes from the joint soft demapped received symbols and VND, yielding the LLRs described by  $z_{L_e}^{\text{MUI}}$ . Then the extrinsic information output is fed back to the CND. Since the information input to the VND comes from the channel impaired sequence, the VND operation is affected by the change of SNR,  $\Xi$ , value. In the ExIT chart curves for PNC with code rate 1/2 at  $\Xi = 3$  dB, the VND start from higher point  $I_{E,\text{CND};A} = 0.34$  and cross the CND curve at point  $I_{A,E,\text{VND}} = 0.02$  and  $I_{A,E,\text{VND}} = 0.38$ , this means no convergence occurs at this SNR value as shown in Figure 4.17(a). Therefore, a large number of iterations is needed when the tunnel between transfer curves narrows. At  $\Xi = 5$  dB, the decoder converges. In contrast, for the similar system with rate 2/3 at  $\Xi$  value 6 dB the VND starts from  $I_{E,\text{CND};A} = 0.41$  and crosses with the CND curve at  $I_{A,E,\text{VND}} = 0.1$  and  $I_{A,E,\text{VND}} = 0.36$ , as shown in Figure 4.17(b). The system at a  $\Xi$  value of 7 dB, shows the decoder converges. The system employing LDPC codes for single user without a relay was considered as shown in Figure 4.16, the open tunnel at 2 dB corresponding to the BER system performance in Figure 3.16.

Table 4.3 shows a summary of the numerical results for the single user and PNC systems with LDPC codes, for different code rates and SNR,  $\Xi$ , values. Moreover,

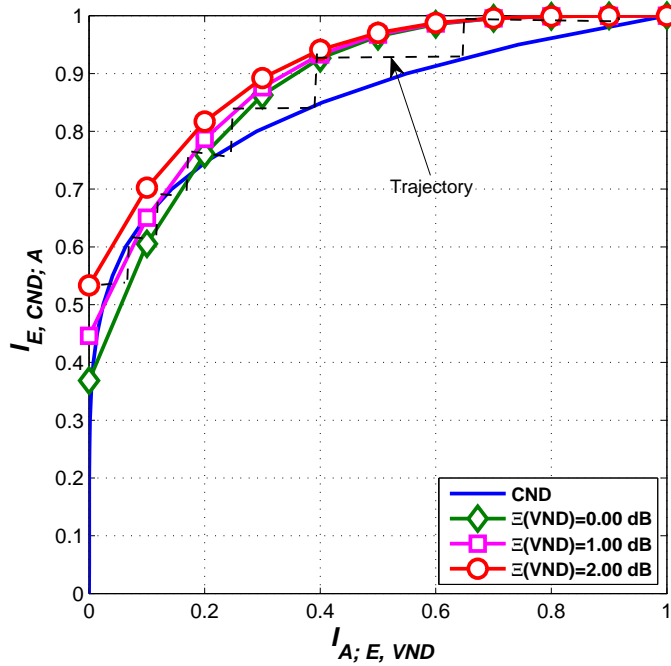
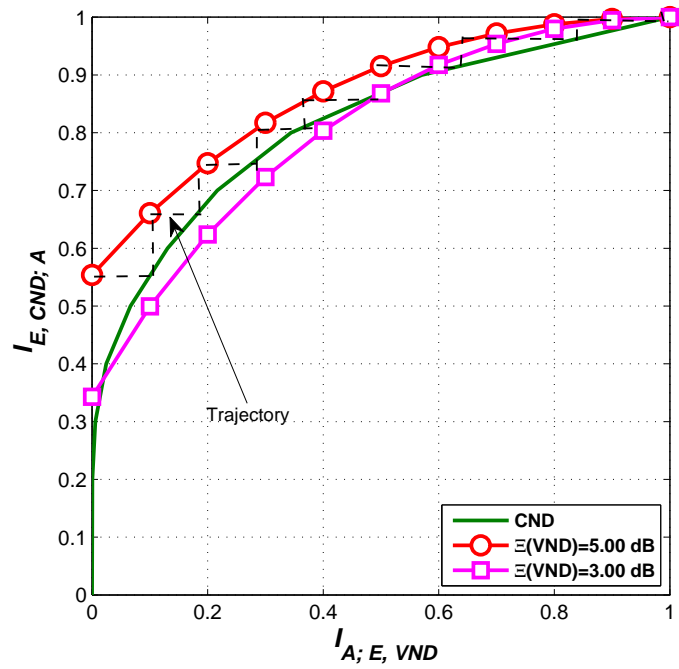
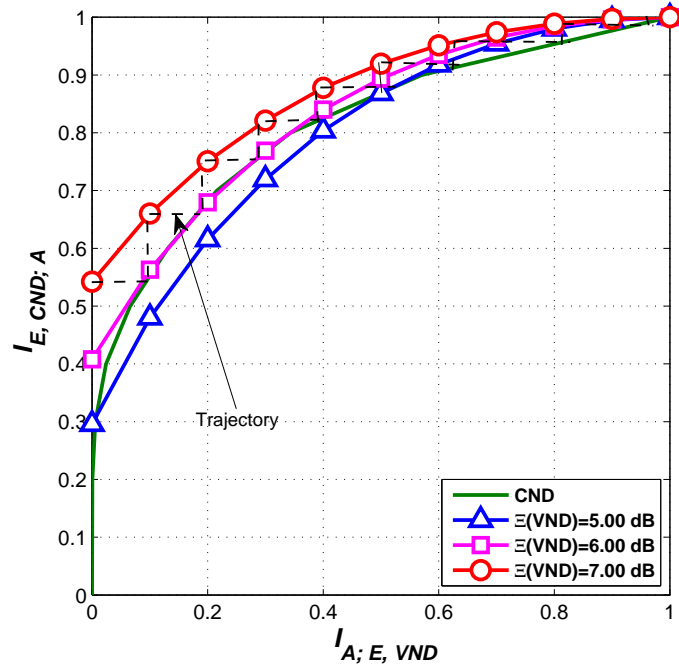


Figure 4.16: ExIT chart for single user (SU) system employing LDPC code of code rate 1/2.



(a) ExIT curves for code rate 1/2



(b) ExIT curves for code rate 2/3

Figure 4.17: ExIT chart for a set of  $\Xi$  value in dB and different rate for E2E PNC system employing LDPC code.

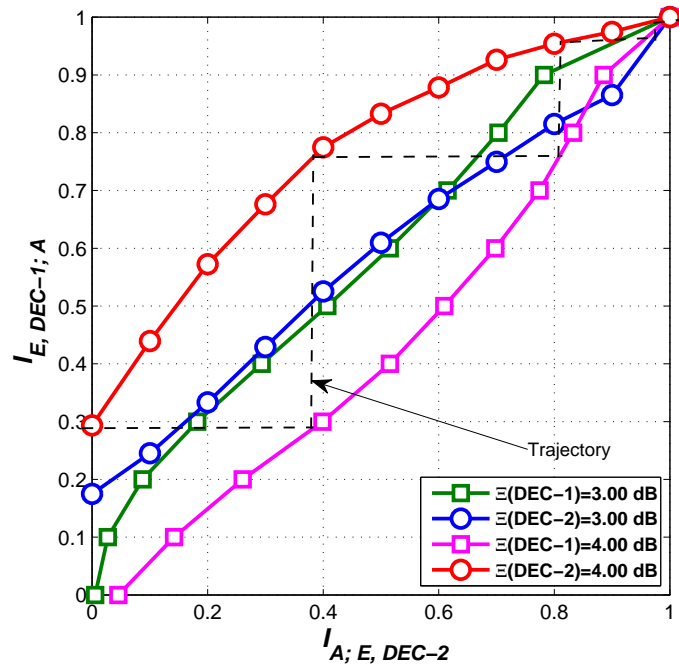
the table shows the points for both curves when there is no system convergence and when convergence occurs.

Table 4.3: A brief description for the LDPC code with E2E PNC system convergence.

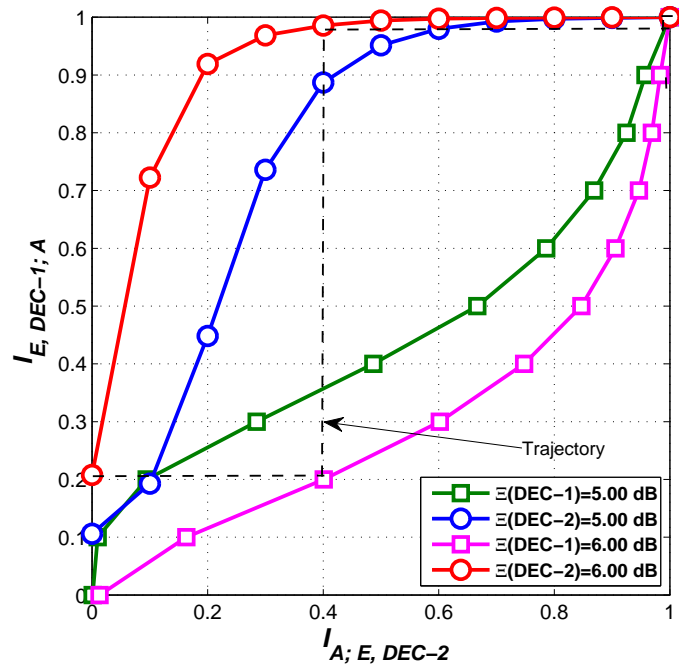
System	Code rate	$I_{E,CND;A}$ point	$I_{A;E,VND}$ point	$\Xi$ (dB)	Convergence
single user	1/2	0.37	0.002	0	No
		0.49	0.004	1	No
single user	1/2	open tunnel		2	Yes
PNC	1/2	0.36	0.005	3	No
PNC	1/2	open tunnel		5	Yes
PNC	2/3	0.3	0.001	5	No
		0.52	0.1	6	No
PNC	2/3	open tunnel		7	Yes

### 4.4.3 Analysis for Turbo Code with PNC

The performance is presented for a turbo decoder structure, DEC-1 and DEC-2, by putting the input of the decoder and the output of the other decoder in the same axis. The iterative turbo decoder for PNC system is considered in Figure 4.18 and the iterative turbo decoder for single user without a relay is shown for the rate 1/2 code in Figure 4.19. The ExIT function gives the average convergence behaviour of the investigated encoding and decoding trajectory starting from no *a priori* information coming from the other decoder. Therefore, the mutual information of the first decoder output can be obtained by the lower curve in ExIT chart and is provided as the input of the second decoder. It can be observed that in Figure 4.18(a) no convergence occurs due to the lack of information at the receiver for  $\Xi = 3$  dB. With the increase of SNR, the system is capable of recovering the information at the receiver after a few iterations at  $\Xi = 4$  dB. This is a significant result as the large number of iterations required for decoding is reduced and the system performance is enhanced. Similarly, the convergence occurs after three iterations at  $\Xi = 6$  dB with code rate 2/3, as depicted in Figure 4.18(b), in spite of the fact that no convergence occurs at 5 dB. Also, the convergence occurs for the single user system after three iterations at  $\Xi = 2$  dB. It can be seen that the SNR increase will impact on the system to increase/decrease the iterations. Table 4.4 summarizes the system with turbo codes, for different code rates and different SNR,  $\Xi$ , values, to predict the



(a) ExIT curves for code rate 1/2



(b) ExIT curves for code rate 2/3

Figure 4.18: ExIT chart for a set of  $\Xi$  value in dB and different rate for E2E PNC system employing turbo code.

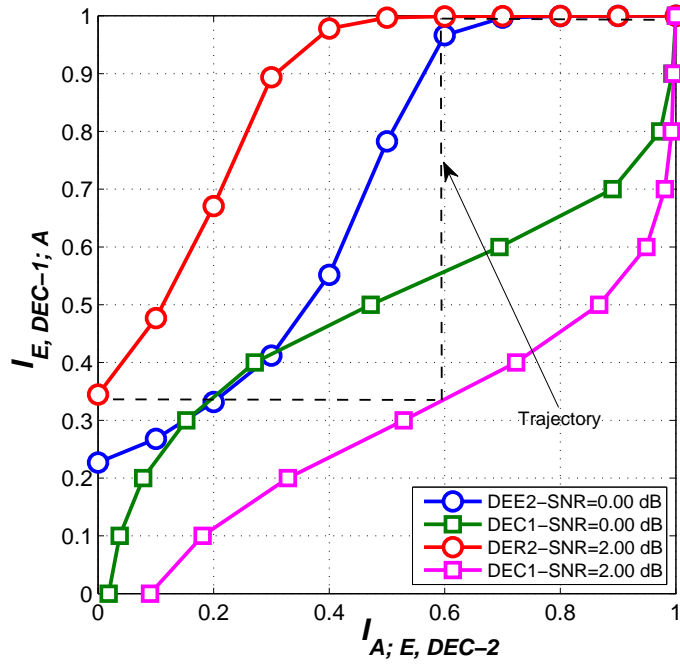


Figure 4.19: EXIT chart for single user (SU) system employing turbo code of code rate 1/2.

system's behaviour.

Table 4.4: A brief description for the turbo code with E2E PNC system convergence.

System	Code rate	$I_{E,DEC-1;A}$ point	$I_{A;E,DEC-2}$ point	$\bar{\Xi}$ (dB)	Convergence
single user	1/2	0.32	0.18	0	No
single user	1/2	open tunnel		2	Yes
PNC	1/2	0.68	0.6	3	No
PNC	1/2	open tunnel		4	Yes
PNC	2/3	0.18	0.15	5	No
PNC	2/3	open tunnel		6	Yes

## 4.5 Summary

In this chapter, the ExIT chart technique is considered for different iterative decoders employed by a PNC system. The simulation results are evaluated for the system with PNC-demapping at the relay based on two users using QPSK modulation. The ExIT chart was implemented as a tool to analyze the convergence properties of iterative receivers, which included LDPC, BICM-ID, and turbo codes over a AWGN channel. We reviewed the ExIT chart, the simulation setup and the construction, to analyse the major features of these architectures. The predicted results for the PNC system employing iterative BICM-ID codes were compared with LDPC and turbo codes, and were presented at the 2013 international conference on electronics, circuits and systems in Abu Dhabi, UAE [86]. ExIT chart analysis was adopted of the tree iterative decoding schemes when we observed the converges properties of all the tree decoder. The convergence behaviour of each architecture was analysed and used for comparing the effect of PNC and matches close in the simulated trajectory. The different receivers in the PNC system were investigated under various parameters and then compared under several SNRs. The presented results also show that PNC with a turbo code outperforms PNC with BICM-ID and LDPC codes. Therefore, the ExIT function result shows that receiver with a turbo decoder converges with fewer iterations. This result highlights a weakness in the MPA decoding of LDPC codes, which appears to be less robust when the initial conditional LLRs are incorrect due to errors propagating from the relay. Initial results would suggest that turbo codes and BICM-ID codes with trellis-based decoding algorithms are more suited to E2E PNC networks than LDPC codes. Again, this shows that the LDPC required more iteration to converge than the other two decoders. Therefore, the analysis that validate the first contribution of the simulation results and they connected in that way.

# Chapter 5

---

---

## Constant Envelope PNC Angle Modulation

---

---

## 5.1 Introduction

Recently, PNC is a popular technique for wireless scenario over TWRC. It takes place at a relay node when two users can exchange messages faster by performing demapping on the sequences received followed by mapping processes and then broadcasting to the users. However, PNC has two primary drawbacks. The first is a hard decision process at the relay to perform the demapping and mapping methods on the received signal. The second is that we observe the constellation diagram at the relay is comprised of points that are not equally likely and received symbols with magnitudes concentrated around zero occur with more frequency than received symbols with greater magnitudes. For these reasons, our novel technique keeps the envelope of the received symbols at the relay constant. Thus, the reliable information will transfer the LLRs from relay to destination without being further affected by the downlink phase. In this chapter, we propose the use of angle modulation, namely frequency and phase modulation, during the downlink phase of PNC system, where the amplitudes of the received symbols modulate the frequency or phase of a carrier signal. Moreover, the proposed system performance is evaluated for PNC with a TWRC, employing three types of iterative error-correcting codes implemented at the source and destination nodes (E2E): LDPC, BICM-ID, and turbo codes. Consequently, this chapter presents efficient techniques to improve the performance of the signals transmitted over TWRC employing E2E coded PNC over AWGN and Rayleigh flat-fading channel for evaluation and assessment of the improvements in the system's performance.

## 5.2 Angle Modulation

Frequency-modulation (FM) and phase-modulation (PM) are two important cases of angle modulated signalling. A significant feature of FM and PM is that they have constant amplitude nature, hence, they can withstand non-linear distortion and amplitude fading. Therefore, they can provide much better protection to the information against the channel noise. In this modulation scheme, the angle of a modulated sinusoidal carrier  $\phi(t)$  is assumed a function of the message signal, as shown in equation (2.1). Therefore, we can interpret the angle modulated signal,  $u(t)$ , as a rotating phasor of length  $\mathcal{A}$  and angle  $\phi(t)$ . When  $\phi(t)$  increases mono-

tonically with time, the average frequency over an interval from  $t$  to  $t + \Delta t$  can be described as [87]

$$f_{\Delta t}(t) = \frac{\phi(t + \Delta t) - \phi(t)}{2\pi\Delta t} \quad (5.1)$$

Accordingly, the instantaneous frequency  $f_i(t)$  of angle modulated signal can be defined as

$$f_i(t) = \lim_{\Delta t \rightarrow 0} f_{\Delta t}(t) \quad (5.2a)$$

$$= \frac{1}{2\pi} \frac{d\phi(t)}{dt} \quad (5.2b)$$

where  $\omega_c = d\phi(t)/dt$  is the angular velocity. Thus, the oscillation occurs whenever  $\phi(t)$  changes by  $2\pi$  radians. Regardless of the rate at which the amplitude changes, frequency or phase deviates in proportion to the instantaneous amplitude of the modulating signal. In angle modulation, the modulated property of the carrier is illustrated in Figure 5.1, which shows the frequency swing as the difference between the highest and the lowest output. Therefore, the relationship between the message envelope and the bandwidth of modulating signal is known frequency modulation index,  $\zeta_f$ , which can be expressed as

$$\zeta_f = \frac{\Delta_f}{f_{IF}} \quad (5.3)$$

where  $\Delta_f$  is the peak frequency deviation of the transmitter, which represents the maximum change of  $f_i(t)$  from  $f_c$ , and  $f_{IF}$  is the maximum bandwidth of the modulating signal. Phase modulation index,  $\zeta_p$ , is the peak phase deviation of the transmitter, which specifies how much change in the angle occurs for every unit of variation of message and can be written as

$$\zeta_p = \Delta_p \quad (5.4)$$

Estimating modulation index is important in recognition and demodulation of the waveform in term of angle modulation.

In radio communications, all forms of modulation produce sidebands, spaced at multiples of  $f_{IF}$  above and below the carrier frequency  $f_c$ . Therefore, the size and significance of these sidebands is very dependent on  $\zeta$ . A simple example is depicted in Figure 5.2, which illustrates the sinusoidal message spectrum. From the spectrum

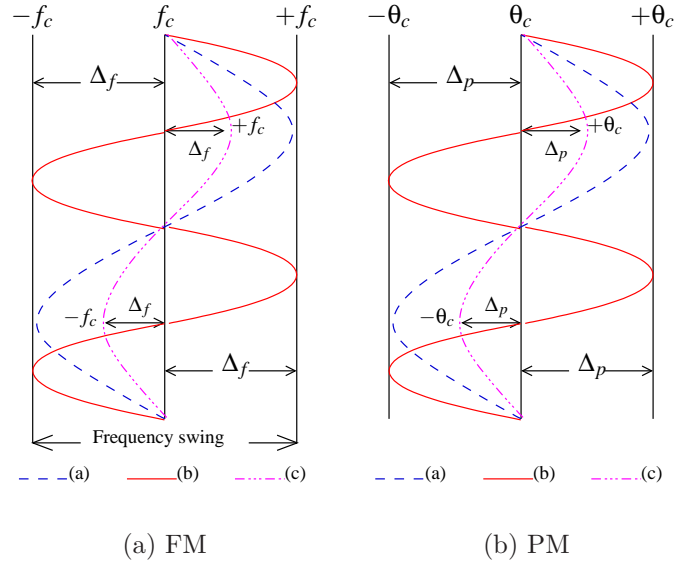


Figure 5.1: Angle modulation wave, (a) Large-amplitude low-frequency, (b) Large-amplitude high-frequency, (c) Small-amplitude low-frequency.

in Figure 5.2(a), it can be seen that there are only two significant sidebands for  $\zeta < 1$ , and thus the spectrum looks very similar to that for an amplitude modulation carrier. From the spectrum in Figure 5.2(b) and Figure 5.2(c), it can be seen that with  $\zeta = 1$  and  $\zeta = 3$  the number of significant sidebands has increased to four and eight, respectively. The practical bandwidth is given by the number of significant sidebands multiplied by the width of each sideband. Therefore, we can calculate the necessary bandwidth B using the approximation as

$$B = 2(\zeta + 1)f_{IF} \tag{5.5a}$$

$$= 2\left(\frac{\Delta}{f_{IF}} + 1\right)f_{IF} \tag{5.5b}$$

$$= 2(\Delta + f_{IF}) \tag{5.5c}$$

It can be noted that the ratio  $\zeta_f$  equates to the ratio  $\zeta_p$  and thus there is no specific limit to the degree of modulation index.

### 5.2.1 Frequency Modulation

FM is one angle modulation form realized by the carrier frequency,  $f_c$ , which is caused to vary in accordance with an amount proportional to some characteristics of the baseband modulating message signal. Therefore, to produce the FM signal at a rate proportional to the modulating signal frequency, the message information,

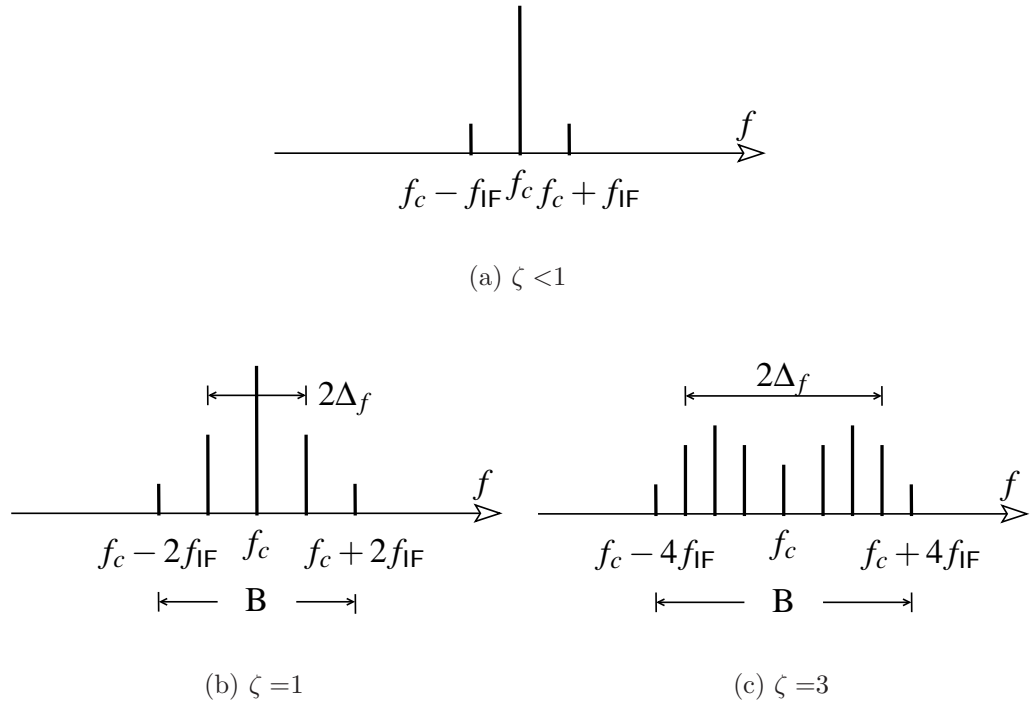


Figure 5.2: Sinusoidal message spectrum.

$r(t)$ , is proportional and changes linearly with the instantaneous frequency,  $f_i$ , to give

$$f_{i,\text{FM}}(t) = f_c + \Delta_f r(t) \quad (5.6)$$

Because of the modulating signal increase and decrease linearly with time, the  $f_i$  increases linearly over a half-cycle and decreases linearly over the remaining half-cycle of the modulating signal. Hence, the changes in the frequency of the carrier in response to the message signal leads to obtain the FM signal,  $\Gamma_{\text{FM}}(t)$ , which can be described in the time domain as

$$\Gamma_{\text{FM}}(t) = \mathcal{A} \cos\left(2\pi f_c t + 2\pi \Delta_f \int_0^t r(\tau) d\tau\right) \quad (5.7)$$

### 5.2.2 Phase Modulation

PM is another form of angle modulation that maps information onto changes in the phase of the carrier depending on the instantaneous level of the signal. According to this method, the carrier frequency switches back and forth every half-cycle of the signal and consequently the angle,  $\phi(t)$ , varies linearly with the message signal,

which can be described as

$$\phi_{\text{PM}}(t) = 2\pi f_c t + \Delta_p r(t) \quad (5.8)$$

where the  $\Delta_p$  is linearly proportional the signal  $r(t)$  depending on the instantaneous phase and then the PM signal  $\Gamma_{\text{PM}}(t)$  can be obtained directly related to the change in the instantaneous phase. Hence, PM signal,  $\Gamma_{\text{PM}}(t)$ , can be described in the time domain as

$$\Gamma_{\text{PM}}(t) = \mathcal{A} \cos\left(2\pi f_c t + \Delta_p r(t)\right) \quad (5.9)$$

### 5.3 Analytic Technique

An analytic technique is an important concept in continuous-time signal processing, and was introduced by [88]. This correspondence presents transform-based algorithm techniques to compute an analytic-like signal in the finite duration discrete-time case. Therefore, analysis of seismic data as an analytic signal, complex trace analysis, is a transform technique which retains local significance for complex wave analysis [89]. Furthermore, transformations of data from one form to another are common in signal analysis, and various techniques are used to extract significant information from time series. Therefore, the transformation of a carrier from the time domain to the frequency domain is the most common example of data rearrangement which provides insight and is useful in data analysis. The Fourier transform which accomplishes this allows us to look at average properties of a reasonably large portion of a trace. Also, complex trace analysis provides new insight, like Fourier transforms, and is useful in interpretation problems. Hence, a real-valued continuous-time signal has the property that its Fourier transform is a complex symmetric. It is well known that a signal  $v(t)$  is real if and only if

$$V(-f) = V^*(f) \quad (5.10)$$

where  $V(f)$  is the Fourier transform of  $v(t)$  and  $(\cdot)^*$  denotes the conjugate operation. A real signal is one that exhibits Hermitian symmetry between the positive-frequency and negative-frequency components, allowing the latter to be deduced from the

former. Furthermore, a signal  $v(t)$  is analytic if and only if

$$V(-f) = 0 \quad \text{for } f < 0 \quad (5.11)$$

where an analytic signal contains no negative frequencies. Hence, the negative-frequency components of a real signal can be eliminated from the signal representation without losing information. A mathematical method to determine wave attributes, including reflection strength and instantaneous frequency, is considered using the Hilbert transform.

### 5.3.1 Fourier Transform

In continuous-time linear system theory, the Fourier transform, FT, is primarily an analytical tool for representing signals and systems. In signal processing, it is more common to deal with digital signals that by definition are discrete. Consider  $v(t)$  a real-valued signal defined over the temporal interval  $-\infty < t < \infty$  with continuous-time FT as [90]

$$V(f) = \int_{-\infty}^{\infty} v(t) \exp(-j(2\pi ft)) dt \quad (5.12)$$

where  $V(f)$  defined over the frequency interval  $-\infty < f < \infty$ . The inverse FT is given by

$$v(t) = \int_{-\infty}^{\infty} V(f) \exp(j(2\pi ft)) df \quad (5.13)$$

where  $V(f)$  is a periodic sequence in frequency domain. In analogy with the transform pairs of the FT,  $v(t)$  and  $V(f)$  are a one-to-one discrete Fourier transform series pair.

### 5.3.2 Hilbert Transform

The Hilbert transform, HT, is a special form of the FT. HT expresses the relationship between the real and imaginary components of a discrete-time analytic signal, the structure of which is illustrated in Figure 5.3. Therefore, HT is considered a useful tool in the analysis. The HT definition is stated as [91]

$$\mathcal{H}(v(t)) = \frac{1}{\pi} \int_{-\infty}^{\infty} \frac{v(\tau) d\tau}{t - \tau} \quad (5.14)$$

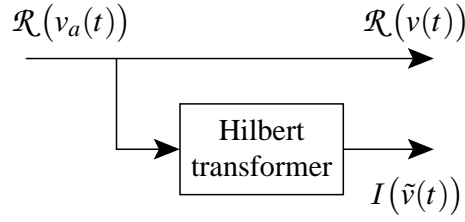


Figure 5.3: The structure of HT.

where  $\mathcal{H}(\cdot)$  mathematically denotes the Hilbert transform process and evaluates at the point  $t$ , the term  $F$  is the Cauchy principal value, and  $v(t)$  is the HT input. The inverse of the HT process,  $\mathcal{H}^{-1}(\cdot)$ , is defined as

$$\mathcal{H}^{-1}(v(t)) = -\left(\frac{1}{\pi}F \int_{-\infty}^{\infty} \frac{v(\tau)}{t - \tau} d\tau\right) \quad (5.15)$$

## 5.4 Joint Constant Envelope Technique and PNC

One issue affecting the performance of a TWRC employing PNC is the demapping of the received summed symbols at the relay to binary bits representing the XOR of the two users' message bits. By making a hard decision on the received symbols, we lose the reliable information of these bits when broadcasting the signal back to both users. Since the PNC system requires two phases to transfer the information through uplink-phase and downlink-phase. Alternatively, we could simply forward the received symbols to both users so that the soft values at the relay are available to the decoders at the destination nodes. Transmitting these small-value symbols can cause synchronization problems at the destination nodes. Therefore, it is preferable to broadcast a signal from the relay that has a constant envelope (CE) characteristic. This has led to the implementation of the modulation technique to keep some parameters constant and also contains the reliability information of the summed received symbols. In this case, the envelope of the carrier signal will be constant, thus ensuring no synchronization issues. At the destination nodes, a frequency or phase demodulator will recover the reliability information of the summed received symbols, which can then be used by the soft-input-soft-output (SISO) decoders.

### 5.4.1 CE-PNC System Model

The constant envelope PNC, CE-PNC, system model gives an overview of the concept at all three nodes, as shown in Fig. 5.4. In the first time slot, or uplink phase,

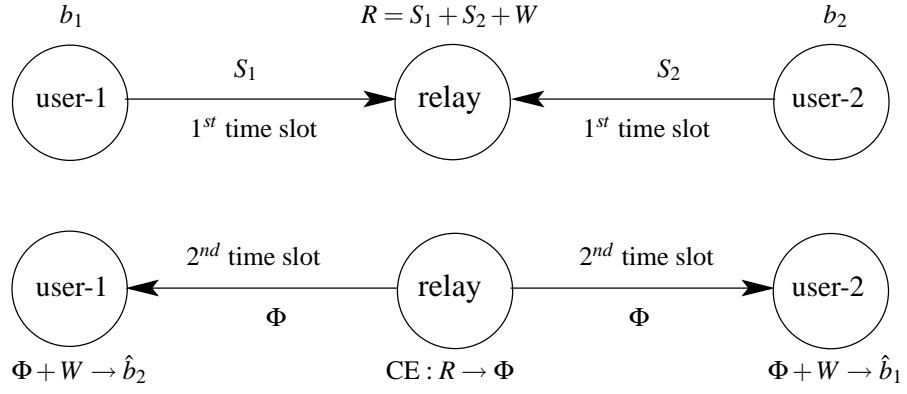


Figure 5.4: The system model for CE-PNC technique.

source nodes for user-1 and user-2 produce a sequence of information bits  $b_1$  and  $b_2$ , respectively. The two terminals encode and map the coded bits to a constellation diagram to generate  $S_1$  and  $S_2$ . The signals are transmitted simultaneously by the two users within the first time slot. The relay receives the noisy signal,  $R$ , as  $R = S_1 + S_2 + W$ , where  $W$  is AWGN. In the second time slot, or downlink phase, the received values  $R$  are then used to modulate the frequency or phase of a carrier signal  $\Phi$ , which is broadcast back to the destination nodes. This signal is then demodulated by a frequency of phase demodulator at the destination nodes to obtain the received values from the relay, which are then decoded to give the XOR sum of the two original messages  $\hat{b}_1$  and  $\hat{b}_2$ .

### 5.4.2 Transmitter and Signal Structures

The wireless relaying network structure for the transmitted signal, as illustrated in Figure 5.5, describes the processing at all three nodes. Accordingly, the system contains a generic transmitter, where the binary information bits  $\{\mathbf{b}_q(k)\}_{k=0}^{K-1} \in GF(2)$  of length  $K$  are encoded to produce  $K/R_c$  coded bits  $\mathbf{c}_q \in GF(2)$ , where  $q$  is the number of users and  $R_c \in (0, 1]$  is the coding rate. The coded bits sequence is permuted by a random interleaver of length  $K/R_c$  in the case of BICM-ID to give bit-interleaved codewords. The two nodes encode and modulate their message sequences using the same function  $\mu(\cdot)$ , which is common to both users. The  $M$ -ary signalling method is applied by grouping bits together and choosing the phase modulation accordingly. Consequently, the coded bits  $\mathbf{c}_q$  modulate a carrier signal using quadrature phase-shift keying (QPSK) to produce  $\mathbf{s}_q$  symbols sequence. Then, the symbols  $\mathbf{s}_q$  are simultaneously transmitted to the relay. All the links are assumed

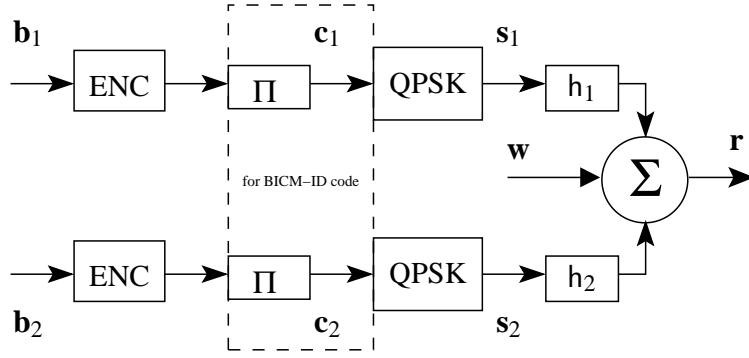


Figure 5.5: The structure for the coded PNC transmitter.

to have AWGN or a Rayleigh flat-fading channel and the fading coefficient between users and relay is denoted as  $h_1$  and  $h_2$ . Also, all the nodes have an AWGN variance of  $\sigma^2$ .

### 5.4.3 CE-PNC Relay Structure

The relay receives the noisy electromagnetic sum of interfered and faded signals,  $\mathbf{r}$ , as shown in equation (2.33) for AWGN channel and equation (2.34) for Rayleigh flat-fading channel. The standard analogue implementation of the orthogonal independent signals impresses baseband information onto an intermediate carrier by changing the carrier's phase in sympathy with the baseband signal. To achieve this, we must take these complex received values,  $\mathbf{r}$ , and use them to modulate the frequency or phase of a carrier signal to be broadcast to both destination nodes.

#### 5.4.3.1 Passband Quadrature Modulation Schemes

The simplest type of passband quadrature modulator consists of two orthogonal carriers at an intermediate frequency  $f_{IF}$ , followed by low-pass filters (LPF). In the literature, the complex signal can be mathematically represented by rectangular form and, therefore, the signal  $\mathbf{r}$  can be expressed in terms of its real,  $r_I = \mathcal{R}(\mathbf{r})$ , and imaginary,  $r_Q = \mathcal{J}(\mathbf{r})$ , parts, which each modulate two orthogonal carriers at an intermediate frequency (IF). One can note that a pair of two real-value signals  $r_I$  and  $r_Q$  carry the real,  $\mathcal{R}(\mathbf{r})$ , and imaginary,  $\mathcal{J}(\mathbf{r})$ , parts of the signal  $\mathbf{r}$ , respectively. Hence, the IF carriers carefully translate the signal  $\mathbf{r}$ , and follow all of the inflections to ride on the two orthogonal and independent magnitudes that describe signal  $\mathbf{r}$ 's behaviour. The standard analogue implementation of the orthogonal independent signals impresses baseband information onto an intermediate carrier, by changing

Table 5.1: Lowpass filter design specification.

Filter Type	Passband	Stopband Attenuation	Number of Coefficients
Equiripple Bandpass	0 kHz-10 kHz	>100 dB	41

the carrier's phase in sympathy with the baseband signal. The main reason for using an IF carrier is to improve the frequency response to the radio signal. The corresponding bandpass signal can be written as

$$[\mathcal{R}(I_r)](t) = r_I \times \cos(2\pi f_{IF}t) \tag{5.16}$$

$$[\mathcal{J}(Q_r)](t) = -r_Q \times \sin(2\pi f_{IF}t) \tag{5.17}$$

where the  $\cos(\cdot)$  and  $\sin(\cdot)$  components of IF wave have now acquired the value of the real signals  $r_I$  and  $r_Q$ , respectively, and  $\times$  is the multiple operation, as shown in Figure 5.8. The  $I_r$  and  $Q_r$  branches are equivalent to the real and imaginary parts of the complex  $\mathbf{r}$  signal. Then each branch of the independent components  $I_r(t)$  and  $Q_r(t)$  passes through LPF. The functional complement of LPF is to settle the waves by rolling off the gain at higher frequencies, where excessive phase shift may cause oscillations, by eliminating imaging caused from the up-sampling and avoiding aliasing produced in the down-sampling. The specification parameters for the design low-pass filter are summarized in Table 5.1. The filter was designed using the equiripple linear phase of the finite impulse response (FIR) method. Equiripple filters are ideally suited to the design of a filter with a given minimum stop-band attenuation or a given maximum passband ripple, for applications in which a specific tolerance must be met. Thus, the frequency characteristics of LPF setup configuration are illustrated in Figure 5.6. Consequently, the input and output of independent components (real and imaginary parts) are affected by LPF to eliminate the unwanted sidebands, as shown in Figure 5.7. The resulting waves from the LPF output, in-phase and quadrature, are collected to represent the passband signal as

$$r(t) = [\mathcal{R}(I_r)](t) + [\mathcal{J}(Q_r)](t) \tag{5.18}$$

$$= \mathcal{A}e^{j\phi(t)} \tag{5.19}$$

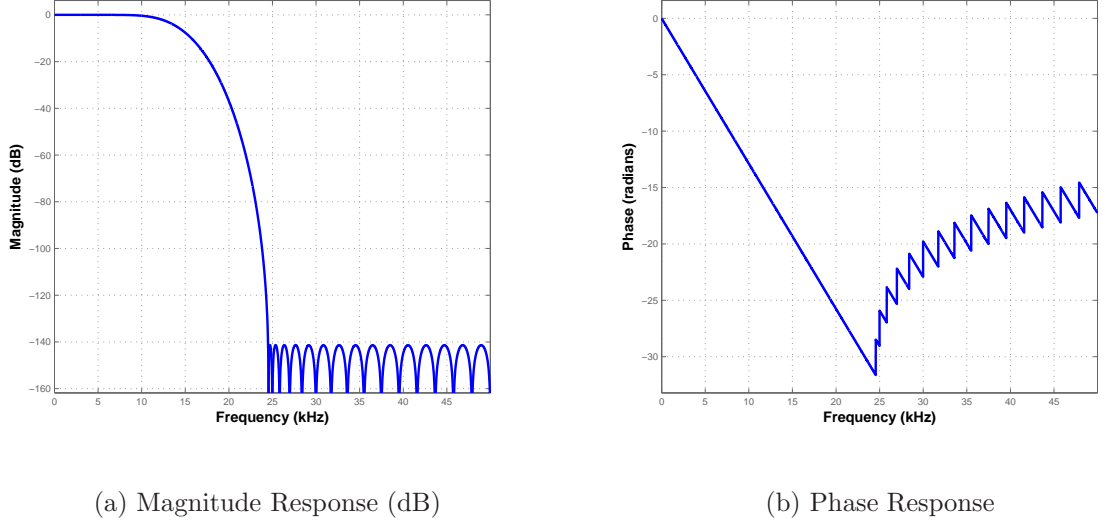


Figure 5.6: LPF design implementation.

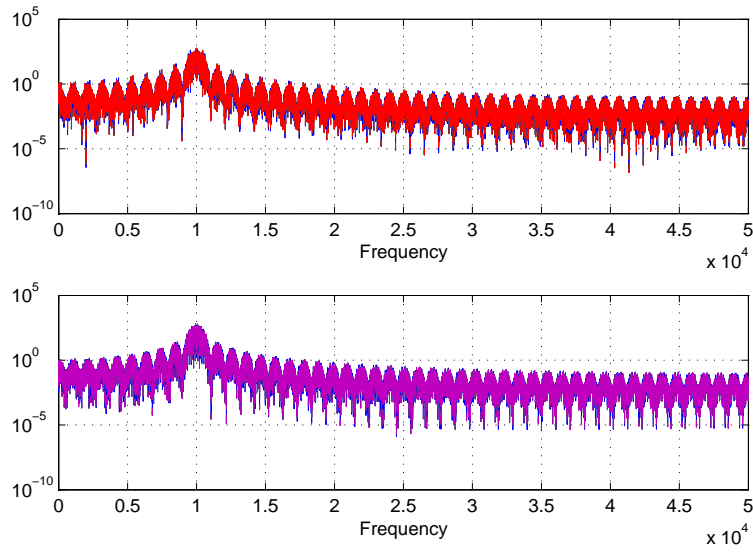
where  $\mathcal{A}$  is the signal envelope and  $\phi(t)$  is the information bearing phase signal. One can note that the complex signal  $\mathbf{r}$  carry by the real signal  $r(t)$ .

#### 5.4.3.2 Constant Envelope Scheme

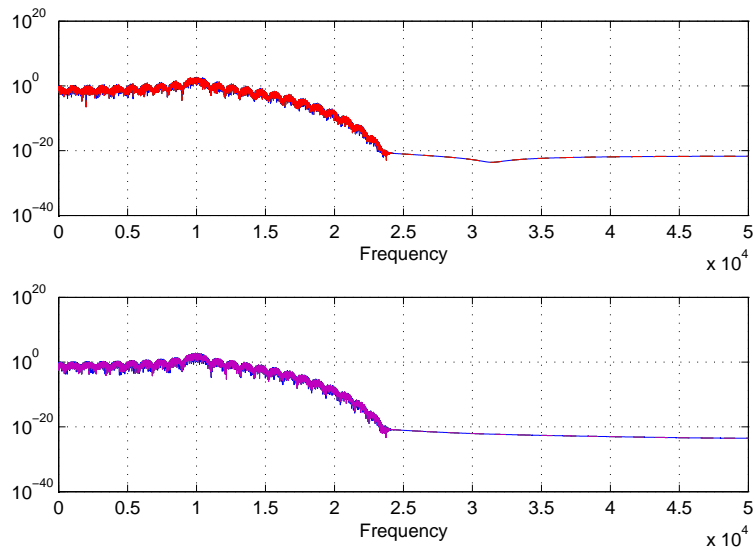
Constant envelope of angle modulation encompasses FM and PM, which refers to the process by which the phase angle of the carrier wave is varied according to the message signal, but the amplitude of the carrier is fixed. The IF wave,  $r(t)$ , will modulate the frequency of the FM carrier or phase of the PM carrier. The changes in the frequency of the carrier, in response to the  $r(t)$  result in the signal  $\Gamma_{\text{FM}}(t)$  as in equation (5.7). Also, the changes in the phase of the carrier, in response to the  $r(t)$  result in the signal  $\Gamma_{\text{PM}}(t)$  as in equation (5.9). The relay, therefore, broadcasts the signal in term of  $\Gamma_{\text{FM}}(t)$  or  $\Gamma_{\text{PM}}(t)$ .

#### 5.4.4 The Structure of CE-PNC Receiver and Signal Detection Techniques

The receiver in a radio communication system must down-convert the passband received signal down to baseband in order to recover the message. The demodulator receiver essentially consists of a angle demodulator followed by a conventional PNC demapper. The received signal, either in terms of  $\Gamma_{\text{FM}}(t)$  or  $\Gamma_{\text{PM}}(t)$ , has a carrier frequency  $f_c$  and transmission bandwidth. It should also be noted that the receiver applies the demodulating and decoding function  $\mu^{-1}(\cdot)$ . Figure 5.9 depicts the re-



(a) LPF input, (Upper) real part, (Lower) imaginary part



(b) LPF output, (Upper) real part, (Lower) imaginary part

Figure 5.7: Power spectral density of the input/output LPF.

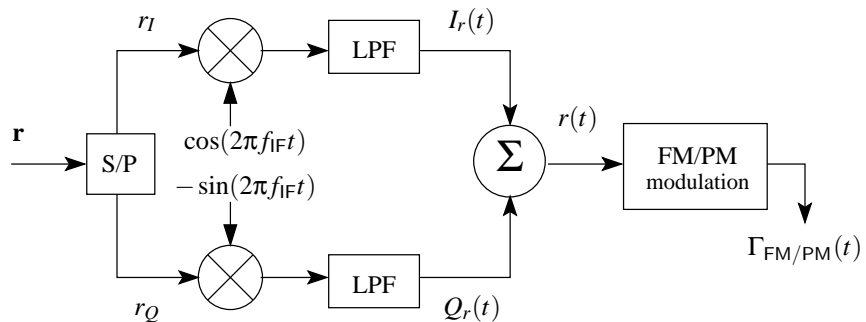


Figure 5.8: The structure of the CE-PNC relay.

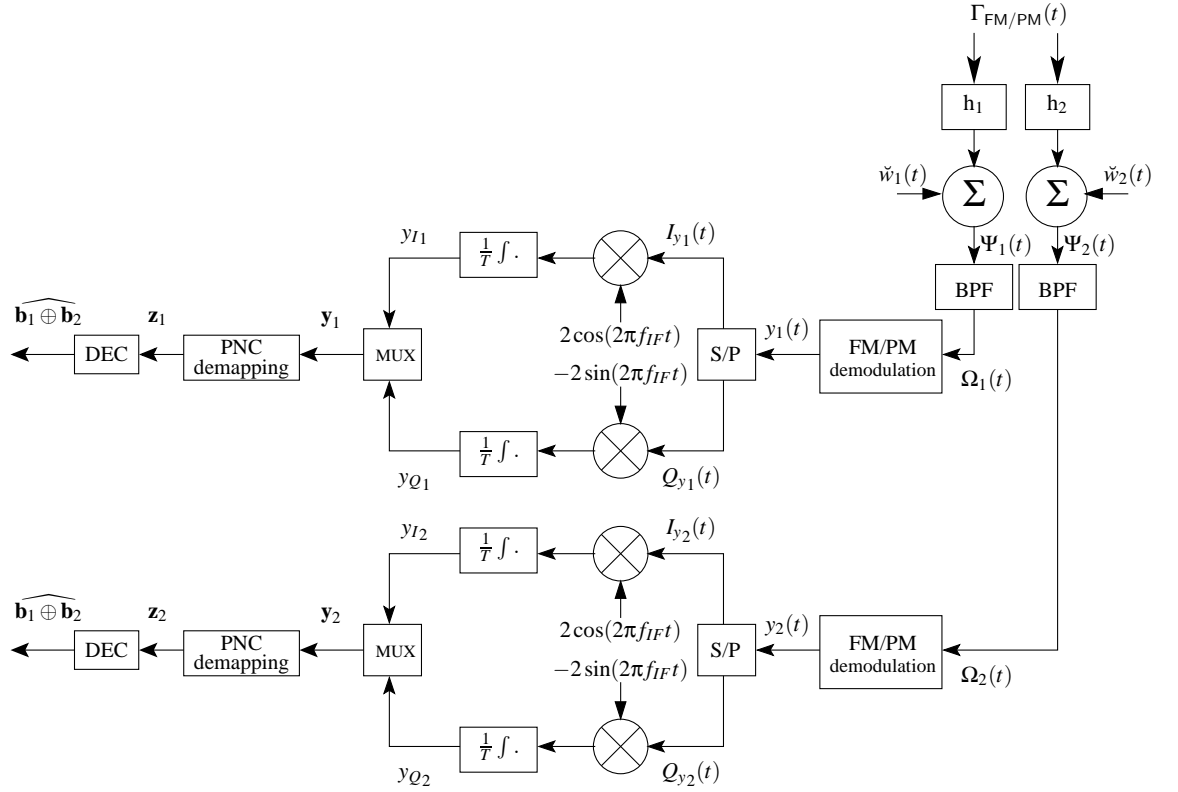


Figure 5.9: The structure of CE-PNC receiver.

ceiver structure for the CE-PNC system. The received signal  $\Gamma(t)$  is corrupted by the channel during downlink-phase, which can be described as

$$\Psi_{q,FM/PM}(t)|_{\text{AWGN}} = \Gamma_{q,FM/PM}(t) + \check{w}_q(t) \quad (5.20)$$

$$\Psi_{q,FM/PM}(t)|_{\text{Rayleigh}} = h_q(t)\Gamma_{q,FM/PM}(t) + \check{w}_q(t) \quad (5.21)$$

where  $\Psi_{q,FM/PM}(t)$  is the noisy signal received in term of frequency or phase modulation.

#### 5.4.4.1 Effect of Noise on Angle Modulation

In angle modulation, the message information is contained in frequency or phase of the signal. Therefore, the effect of noise on an FM or PM signal is determined by the extent to which it changes the frequency or phase of the modulated signal. The noise  $\check{w}(t)$  can be represented as a narrowband stochastic process as [87]

$$\check{w}(t) = \check{w}_I(t) \cos(2\pi f_c t) - \check{w}_Q(t) \sin(2\pi f_c t) \quad (5.22a)$$

$$= \mathcal{A}_{\check{w}} \cos(2\pi f_c t + \Theta_{\check{w}}(t)) \quad (5.22b)$$

where  $\check{w}_I(t)$  and  $\check{w}_Q(t)$  are the noise in terms of its in-phase and quadrature components, respectively, and have the power density spectrum as

$$\Phi_{\check{w}_I}(f) = \Phi_{\check{w}_Q}(f) = \begin{cases} N_0, & |f| \leq B_{BPF}/2 \\ 0, & |f| > B_{BPF}/2 \end{cases} \quad (5.23)$$

where  $B_{BPF}$  is the bandwidth of the bandpass filter. The envelope,  $\mathcal{A}_{\check{w}}$ , and the phase,  $\Theta_{\check{w}}$ , of the noise can be defined as

$$\mathcal{A}_{\check{w}} = \sqrt{\check{w}_I^2(t) + \check{w}_Q^2(t)} \quad (5.24)$$

$$\Theta_{\check{w}} = \tan^{-1} \frac{\check{w}_Q(t)}{\check{w}_I(t)} \quad (5.25)$$

One can note that the phase of  $\mathcal{A}_{\check{w}} \cos(2\pi f_c t + \Theta_{\check{w}}(t))$  in equation (5.22b) is  $\Theta_{\check{w}}$  and its instantaneous frequency is  $2\pi f_c + \dot{\Theta}_{\check{w}}(t)$ ; hence, in either case, FM or PM, the interference output is inversely proportional to the carrier amplitude. However, in the signal with angle modulation form, the message signal is transmitted by variations of the instantaneous frequency or phase of an unmodulated carrier wave, and its amplitude is constant. Accordingly, any variations of the carrier amplitude at the receiver input must result from noise or interference. Furthermore, the channel noise acts as interference and the white noise form has a constant power spectral density for the signal with angle modulation form [92]. Therefore, all components have the same amplitudes because of uniform power spectral density. Thus, the interference amplitude spectrum is constant for PM signal and increases linearly with  $2\pi f_c$  for FM signal. Moreover, in angle modulation, the message is in the phase of the modulated signal and, consequently, increasing the transmitter power does not increase the demodulated message power. Hence,  $\Psi_{FM}(t)$  and  $\Psi_{PM}(t)$  have the unique property that the RF bandwidth  $B$  is not only related to the bandwidth  $f_{IF}$  of the modulating signal, but also to the modulation index  $\zeta$  that can be chosen freely, as expressed in equation (5.5). This yields either a bandwidth-efficient narrowband FM or PM signal,  $\zeta < 1$ , or a wideband signal,  $\zeta > 1$ , that can occupy any required bandwidth compatible with the RF oscillator's tuning range. The trade-off is that narrowband FM, as opposed to wideband FM, requires more sophisticated demodulation and hence more complex circuits are required. Therefore, the bandwidth of the signal  $\Psi_{FM/PM}(t)$  is limited by a bandpass filter (BPF) to remove any

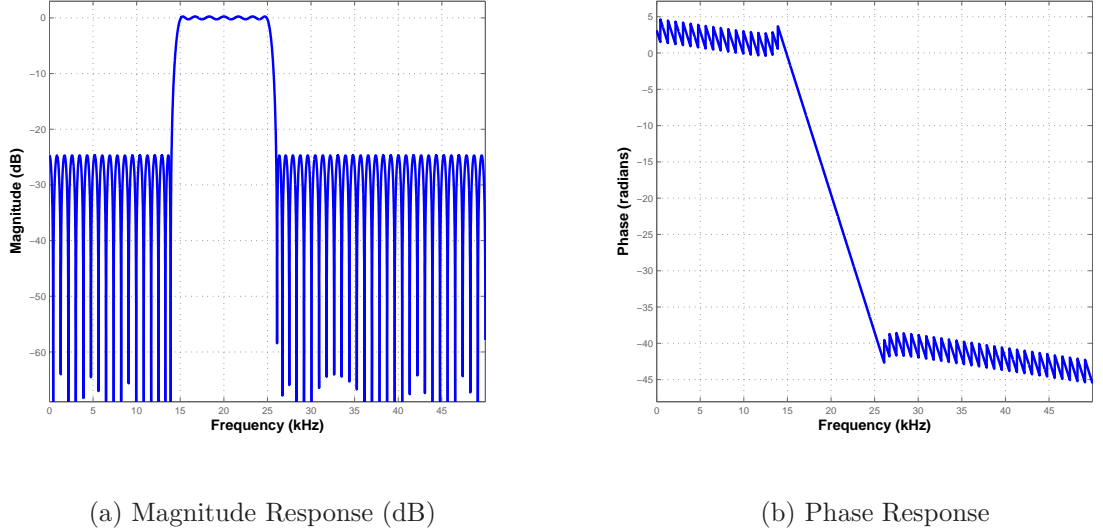


Figure 5.10: BPF implementation.

Table 5.2: Bandpass filter design specification.

Filter Type	Passband	Stopband Attenuation	Number of Coefficients
Equiripple Bandpass	9 kHz-15 kHz	30 dB	81

signals outside the bandwidth. The BPF has a midband frequency  $f_c$  and bandwidth  $f_c \pm B/2$ , and then passes the  $\Psi_{\text{FM/PM}}(t)$  signal essentially without distortion. Figure 5.10 illustrates the frequency characteristics of BPF. The filter was designed using the equiripple linear phase of the FIR method, and Table 5.2 summarizes the specifications employed in the design of the filter. The BPF passes a band of frequencies between a lower cut off frequency and an upper cut off frequency. The frequencies below lower cut off and above upper cut off are in the stop band. This will restrict the bandwidth usage in the system due to the FM and PM waves having unlimited bandwidth. Figure 5.11 shows the spectrum of input/output of signal to/from BPF. The signal  $\Psi_{\text{FM/PM}}(t)$  being fed through the BPF input, as illustrated in Figure 5.11(a). The Figure 5.11(b) depicts the BPF output in term of signal  $\Omega_{\text{FM/PM}}(t)$ . The output signal from the BPF is

$$\Omega_{q,\text{FM/PM}}(t) = \Psi_{q,\text{FM/PM}}(t) + \check{w}_q(t) \quad (5.26)$$

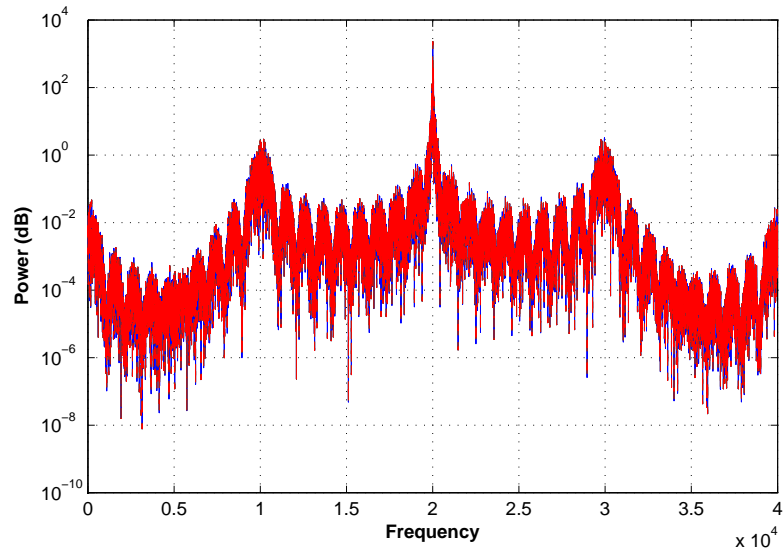
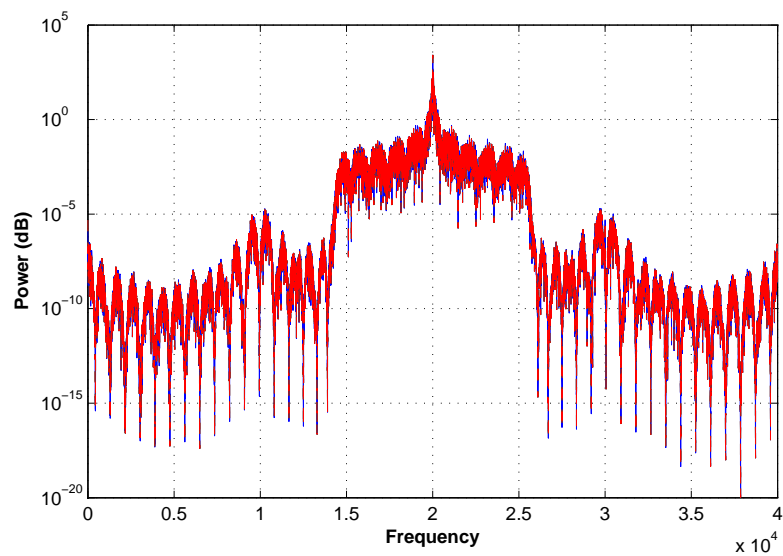
(a) The input of signal  $\Psi(t)$  to BPF(b) The output of signal  $\Omega(t)$  from BPF

Figure 5.11: The input/output of signal to/from the bandpass filter.

Hence, the detection process is employed on the output signal,  $\Omega_{\text{FM/PM}}(t)$ , from the BPF and proceeds by using a Hilbert transform-based demodulation, which is a convenient way of constructing the analytic signal with a judicious use of the Fourier transform.

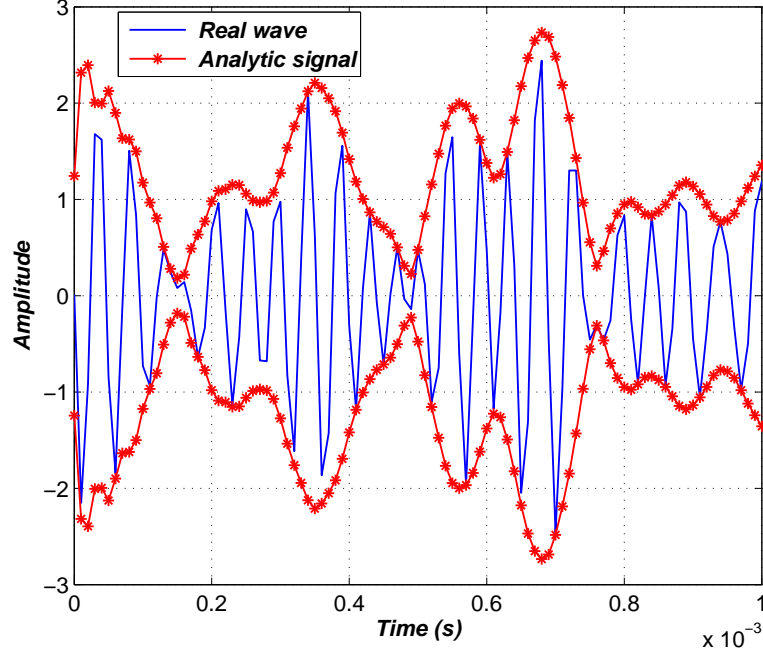


Figure 5.12: Analytic signal corresponding to original real signal.

#### 5.4.4.2 Hilbert Transform Based Demodulation

The signal  $\Omega_{\text{FM/PM}}(t)$  involves reconstruction by setting out and calculating the angle of the signal characterized by variation of time. However, data are usually presented in a time-domain and one needs to transform the data from time to frequency-domain before performing the spectrum analysis. Demodulation using an analytic signal is described by Randall [93], where the use of the analytic signal makes possible a simple computation of the instantaneous amplitude and phase values for each moment in time. We should state that the demodulation of the whole frequency band is a Hilbert transform-based demodulation since it is based upon calculating the analytic time signal of the whole input signal via the Hilbert transform. Figure 5.12 illustrates an analytic signal corresponding to an  $\Omega_{\text{FM/PM}}(t)$  real signal. The analytic signal is often and simply obtained via the Hilbert transform, which is defined in equation (5.14). The computation of each signal component, real and imaginary parts, by the CE-PNC receiver given various levels of signal state information, is the subject of the remainder of this section. It has been shown by [94] and [89] that the FT of the real component is a conjugate symmetric function and, hence, we can apply this on a given signal  $\Omega_{\text{FM/PM}}(t)$  in time domain as

$$\Omega_{I(\text{FM/PM})}(t) = \Omega_{\text{FM/PM}}(t) \quad (5.27)$$

Now, consider the real part of  $\Omega_{I_{(\text{FM/PM})}}(t)$  in time domain equivalent to the real part of  $\Upsilon_{I_{(\text{FM/PM})}}(f)$  in frequency domain. Therefore, the FT of the imaginary component can be defined in frequency domain as

$$\Upsilon_{Q_{(\text{FM/PM})}}(f) = (-j \operatorname{sgn} f) \Upsilon_{I_{(\text{FM/PM})}}(f) \quad (5.28)$$

where  $\Upsilon_{Q_{(\text{FM/PM})}}(f)$  is the imaginary part in frequency domain of  $\Omega_{I_{(\text{FM/PM})}}(t)$  and  $\operatorname{sgn} f$  defines as [95]

$$\operatorname{sgn} f \triangleq \begin{cases} +1, & \text{for } f > 0 \\ 0, & \text{for } f = 0 \\ -1, & \text{for } f < 0 \end{cases} \quad (5.29)$$

Consequently, the FT of  $\Omega_{I_{(\text{FM/PM})}}(t)$  and  $\Omega_{Q_{(\text{FM/PM})}}(t)$  are related according to equation (5.28), and then we can say that  $\Omega_{Q_{(\text{FM/PM})}}(t)$  is the HT of  $\Omega_{I_{(\text{FM/PM})}}(t)$  and written as

$$\Omega_{Q_{(\text{FM/PM})}}(t) = \mathcal{H}\left(\Omega_{I_{(\text{FM/PM})}}(t)\right) \quad (5.30)$$

Thus, given a real signal  $\Omega_{\text{FM/PM}}(t)$ , we can construct the complex signal as

$$Y(t) = \Omega_{\text{FM/PM}}(t) + j\mathcal{H}\left(\Omega_{\text{FM/PM}}(t)\right) \quad (5.31)$$

Hence, we can evaluate the HT of  $\Omega_{I_{(\text{FM/PM})}}(t)$  by FT as

$$\mathcal{H}\left(\Omega_{I_{(\text{FM/PM})}}(t)\right) = \mathcal{F}_{t \leftarrow f}^{-1} \left( (-j \operatorname{sgn} f) \mathcal{F}_{t \rightarrow f} \left( \Omega_{I_{(\text{FM/PM})}}(t) \right) \right) \quad (5.32)$$

where  $\mathcal{F}$  denotes the FT mathematically. In equation (5.32), take the FT  $\Upsilon_{I_{(\text{FM/PM})}}(f)$  of  $\Omega_{I_{(\text{FM/PM})}}(t)$ , and then multiply  $\Upsilon_{I_{(\text{FM/PM})}}(f)$  by  $(-j)$  for positive  $f$ ,  $(+j)$  for negative  $f$ , and by zero for  $f = 0$ . According to this procedure, HT introduces a phase lag of 90 degrees,  $-j = \exp(-j\pi/2)$ , producing a signal in quadrature to the input signal. Moreover, equation (5.28) indicates that the transfer function of a HT is  $-j \operatorname{sgn} f$ . Then the corresponding impulse response is

$$\mathcal{F}_{t \leftarrow f}^{-1}(-j \operatorname{sgn} f) = \frac{1}{\pi t} \quad (5.33)$$

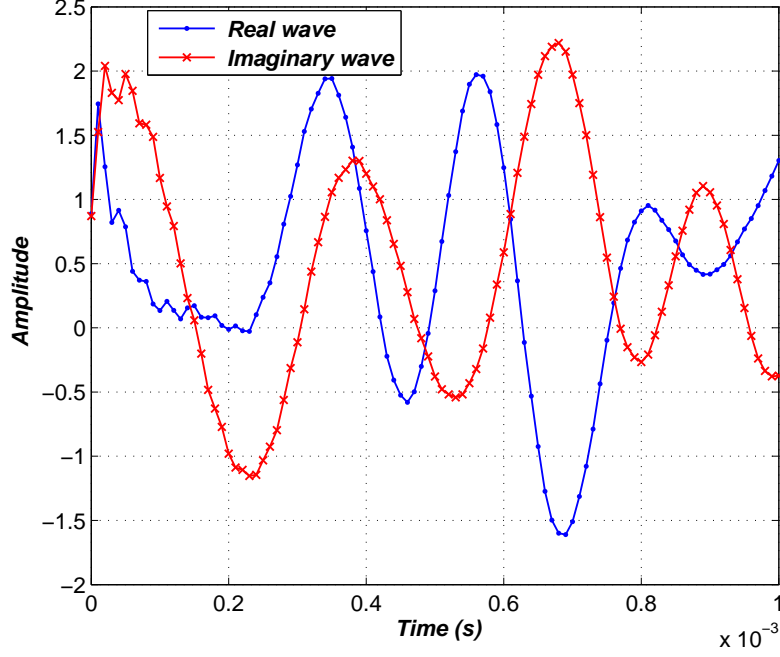


Figure 5.13: Utilize HT to form a complex analytic signal.

One can note that the imaginary part of the complex analytic sequence is a version of the original real sequence with a phase shift. The effect is well illustrated in Figure 5.13, which shows a pair of real signals from a real signal in Figure 5.12. From equation (5.31), we have obtained the complex analytic signal,  $Y(t)$ , corresponding to the real signal  $\Omega_{\text{FM/PM}}(t)$ . Therefore, the complex sequence  $Y(t)$  in equation (5.31) can be rewritten in polar form as

$$Y(t) = \mathcal{A}(t)e^{j\phi(t)} \quad (5.34)$$

This mean that one can calculate the reflection strength  $\mathcal{A}(t)$  as [96]

$$\widehat{\mathcal{A}}(t) = |Y(t)| \quad (5.35)$$

and instantaneous phase,  $\phi(t)$  as

$$\widehat{\phi}(t) = \angle Y(t) \quad (5.36a)$$

$$= \tan^{-1} \frac{\mathcal{I}(Y(t))}{\mathcal{R}(Y(t))} \quad (5.36b)$$

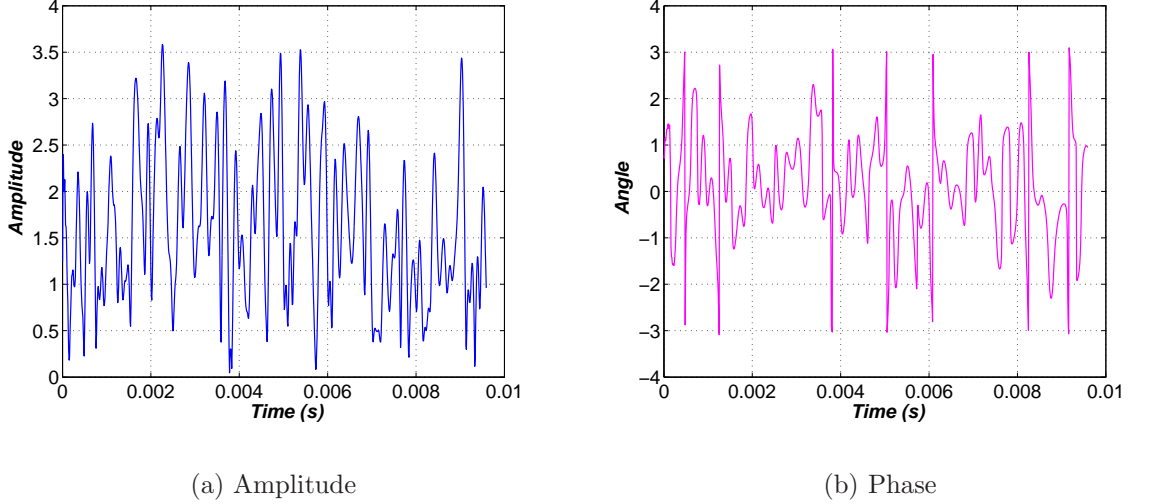


Figure 5.14: Determination of the amplitude envelope and phase of the analytic signal.

However, the rate of change of the time-dependent phase gives a time-dependent frequency  $\omega(t) = d\phi(t)/dt$  and, therefore, we can express it in convolutional form as

$$\omega(t) = \int_{-\infty}^{\infty} d(\tau)\phi(t - \tau)d\tau \quad (5.37)$$

where  $d\tau$  is the differentiation [97]. A difficulty with this is that the phase must be continuous, whereas the arctangent computation of equation (5.36) gives only the principle value. We then have to unwrap the phase by determining the location of  $2\pi$  phase jumps and correcting them. Figure 5.14 shows the envelope and phase of  $Y(t)$  signal. Consequently, writing  $y_q(t)$  in the form [58]

$$y_q(t) = I_{y_q}(t) \cos(2\pi f_{IF}t) - Q_{y_q}(t) \sin(2\pi f_{IF}t) \quad (5.38)$$

where  $I_{y_q}(t) = \mathcal{A} \cos[\phi(t)]$  and  $Q_{y_q}(t) = \mathcal{A} \sin[\phi(t)]$ .

#### 5.4.4.3 Passband Quadrature Demodulation Schemes

To reobtain the baseband signal, the passband quadrature demodulation is the process by which the IF carrier is removed. This involves implementing the down-convert method by multiplying the incoming signal  $y_q(t)$  again by two independent and orthogonal components of the IF carrier,  $2 \cos(2\pi f_{IF}t)$  and  $-2 \sin(2\pi f_{IF}t)$ , of the same carriers that specified the frequency and phase. The low pass waveform in

equation (5.38) can then be rewritten as

$$y_q(t) = [I_{y_q}(t) + \check{w}_I(t)] \cos(2\pi f_{IF}t) - [Q_{y_q}(t) + \check{w}_Q(t)] \sin(2\pi f_{IF}t) \quad (5.39)$$

The in-phase output branch of the down-converter is

$$y_I|_q(t) = y_q(t) \times 2 \cos(2\pi f_{IF}t) \quad (5.40a)$$

$$= I_{y_q}(t) + \check{w}_I(t) \quad (5.40b)$$

Similarly, the quadrature output branch of the down-converter is

$$y_Q|_q(t) = y_q(t) \times -2 \sin(2\pi f_{IF}t) \quad (5.41a)$$

$$= Q_{y_q}(t) + \check{w}_Q(t) \quad (5.41b)$$

where  $I_{y_q}(t)$  and  $Q_{y_q}(t)$  are the in-phase and quadrature components of incoming signal  $y_q(t)$ , respectively. The continuous-time receive signal is then sampled at the rate  $f_s = 1/T_s$  sample/sec to obtain the discrete-time signal. This process of reducing the sampling rate of the signal is usually done by reducing the data rate [99]. Hence, the two branches are combined to obtain

$$\mathbf{y}_q = y_I|_q + jy_Q|_q \quad (5.42)$$

The multiplexed signal  $\mathbf{y}_q$  is applied simultaneously to two separate coherent detectors.

#### 5.4.4.4 Decoding Process

At the two destination nodes, iterative decoders are employed comprising an iterative receiver structure. The conditional probability of the signal  $\mathbf{y}_q$  is presented as the users' information plus uplink noise. First, the demapper computes the LLR,  $\Lambda$ , to iterate between the decoder components for LDPC and turbo codes or between demapper and decoder for BICM-ID. Accordingly, in the downlink phase, the LLRs of every coded bit are calculated using the channel output,  $\mathbf{y}_q$ , and the feedback information. The detection technique is related to the coherent receiver when the amplitude and phase of the fading are known and, thus,  $p(y|s_1 \oplus s_2)$  is conditionally Gaussian, as shown in equation (2.38). The extrinsic information at the output of

the demapper is passed to a SISO decoder. However, the demapper and decoder are SISO components to compute the LLRs as the soft information. The details of the decoder will not be discussed here, as this has already been addressed extensively in Chapter 3. Therefore, the conditional LLRs for the first summed bit was given by equation (2.42). Similarly, the conditional LLRs for the second summed bit was given by equation (2.43). The final process decodes the LLRs bits to represent the modulo-2 sum of the first and second estimations bits,  $\widehat{b_1 \oplus b_2}$ .

## 5.5 Systems performance

The performance of any communication system is ultimately limited by the transmission bandwidth and the noise. However, the power depends on time as the signal is dependent and the average power consumption over the interval is given by dividing the total energy consumed by the length of the time interval. FM and PM waves are basically called the amplitude of the signal, and hence the power remains constant. This means that only the amount of power lies outside the frequency band for positive frequencies and similar for negative frequencies. The modulation index,  $\zeta$ , is the important parameter that controls the trade off between performance and the spectral properties (bandwidth) when embedded digital information into constant envelope waveform [100]. However, FM and PM bandwidth depends on the modulation index; when the modulation index changes the total power must redistribute itself over the resulting frequency components. Therefore, the efficiency of the FM and PM signals are generally high because of the power in the sidebands as a fraction of the total. The sideband structure is fairly complicated, but is generally improved by making the modulation index,  $\zeta$ , larger then making the bandwidth larger.

### 5.5.1 Simulation Setup

The source nodes each encode an information sequence to a codeword of length 2304 bits. The code chosen for BICM-ID and turbo codes have the constraint length  $K_c=5$ , and octal generators  $(23, 35)_8$  and  $(1, \frac{23}{35})_8$ , respectively. The decoding is achieved using the BCJR algorithm at the receiver. All the systems shared similar code rate  $R_c = 0.5$ . AWGN and Rayleigh flat-fading channels were considered.

Bandwidth of the signal is roughly proportional to the symbol rate  $1/T$  Hz, where  $T$  is the period of one symbol. A very common parameters (100 MHz carrier, 2.5 kHz FM and 5 kHz deviation) can be sat to bring people, electronics and communication together in Amateur Radio (harm radio). For simplicity, we are used a simple parameter values to illustrate our technique. At the relay, the baseband receiving signal  $\mathbf{r}$  of length 1152 symbols were up-converted using an IF wave of frequency  $f_{\text{IF}}$  10 kHz. The carrier frequency  $f_c$  was set to  $2f_{\text{IF}}$ , whereas the sampling frequency  $f_s$  was  $5f_c$  and the oversampling factor  $N_s$  was 86. Initial phase was set to  $\pi/4$ . The  $\Delta_f$  values were considered 0.5, 1, 1.5, 2, and 3 kHz. Also, the deviation coefficient  $\Delta_p$  was implemented for  $\pi/32$ ,  $\pi/16$ ,  $\pi/8$  as values.

### 5.5.2 Simulation Study

The system under consideration is E2E coded CE-PNC, where the modulation technique at the relay for FM and PM are denoted as FM-PNC and PM-PNC. As we mentioned before, it is important to note that the performance of FM-PNC differs between various values of  $\Delta_f$  and, thus, it changes the values of  $\zeta_f$  and B according to equation (5.5). The performance of the frequency modulation is depicted in Figure 5.15, which shows the different values of  $\Delta_f$  and describes the spectral behaviour of an FM signal. Similarly, for the PM-PNC, the values of  $\Delta_p$  affect the  $\zeta_p$  and B. The performance of the phase modulation is illustrated in Figure 5.16, which shows the different values of  $\Delta_p$  and describes the spectral behaviour of a PM signal. Thus, the system performance is influenced  $\Delta$  even in the uncoded system, as shown in Figures 5.17(a) for an uncoded FM-PNC system and 5.17(b) for an uncoded PM-PNC system. Unlike spectrum analyzer, there are no theoretical limits to the modulation index,  $\zeta$ , or the deviation,  $\Delta$ , of an FM or PM signal. The limits are a practical compromise between  $E_b/N_0$  and B. Therefore, the system needs accurate adjustments of FM and PM transmitters by measuring  $\Delta_f$  and  $\Delta_p$  in order to evaluate the performance of FM-PNC and PM-PNC. Hence, an optimum-PNC (Opt-PNC) system was adopted to draw the lower bound performance and then evaluate the proposed system. The structure of Opt-PNC system is depicted in Figure 5.18, in which the relay mode consists of an amplify-and-forward scheme. Thus, the relay directly forwards the received signal to the destination nodes to exchange user messages. To set  $\zeta$ , FM-PNC and PM-PNC, systems are compared with Opt-

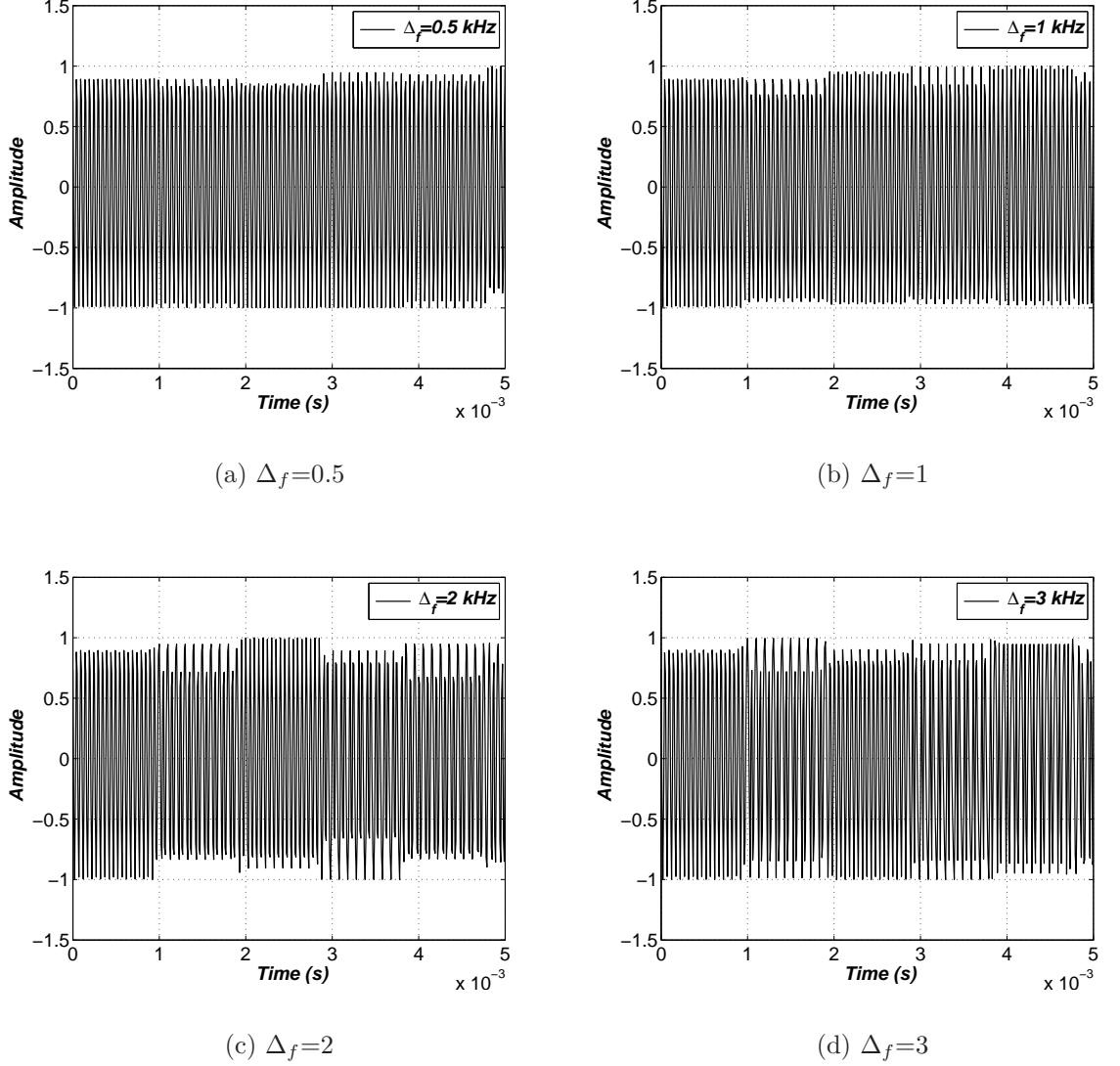


Figure 5.15: The spectral behaviour of an FM signal with different values of  $\Delta_f$ .

PNC for setting up the systems and chose the best deviation values for  $\Delta_f$  and  $\Delta_p$ . According to Carson's rule in equation (5.5) the bandwidth requirement changes are related to the deviation value for  $\Delta_f$  or  $\Delta_p$  and, hence, this in turn implies an increase/decrease in the noise. First, consider the E2E coded FM-PNC and then PM-PNC systems on AWGN channel. In Figure 5.19, the systems of FM-PNC and PM-PNC employing LDPC code are considered to set  $\Delta_f$  and  $\Delta_p$  values, respectively. Similarly, the systems FM-PNC and PM-PNC employ BICM-ID code and turbo code to set the deviation values, as shown in Figures 5.20 and 5.21 respectively. Each figure represents the performance in term of  $E_b/N_0$  in (dB), which indicate the energy per bit to noise power spectral density ratio, and BER performance obtained at the output of the decoders. Each system performs a number of iterations de-

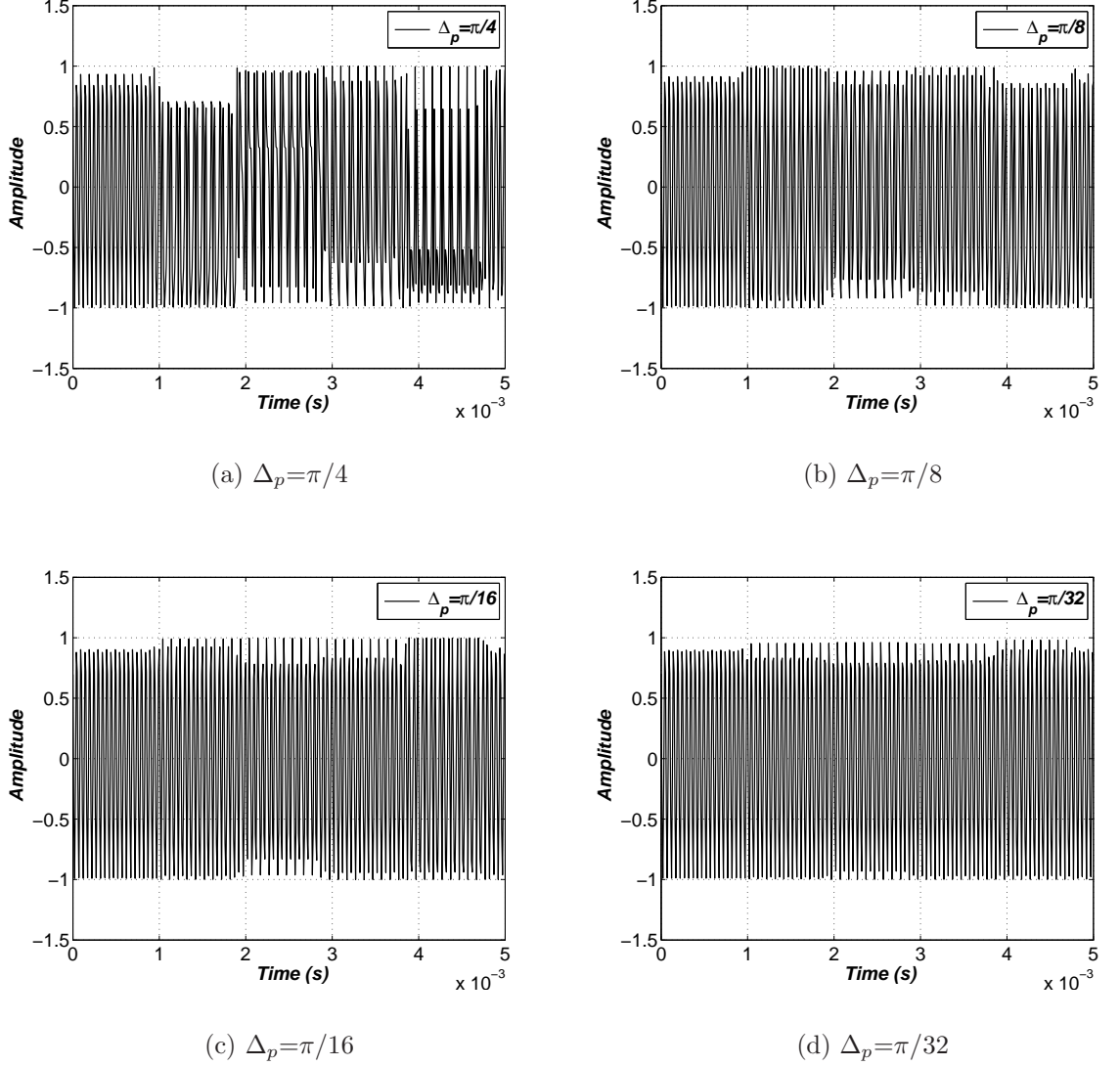
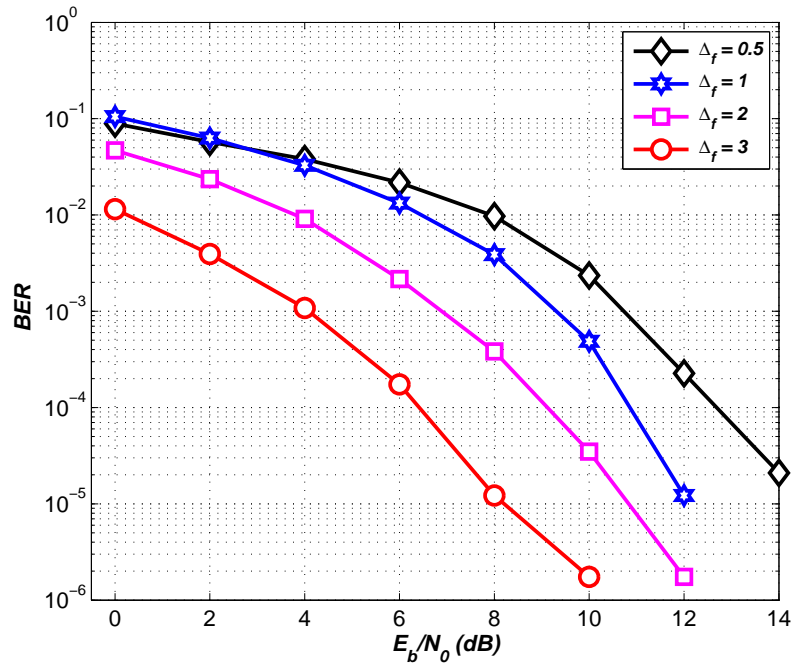
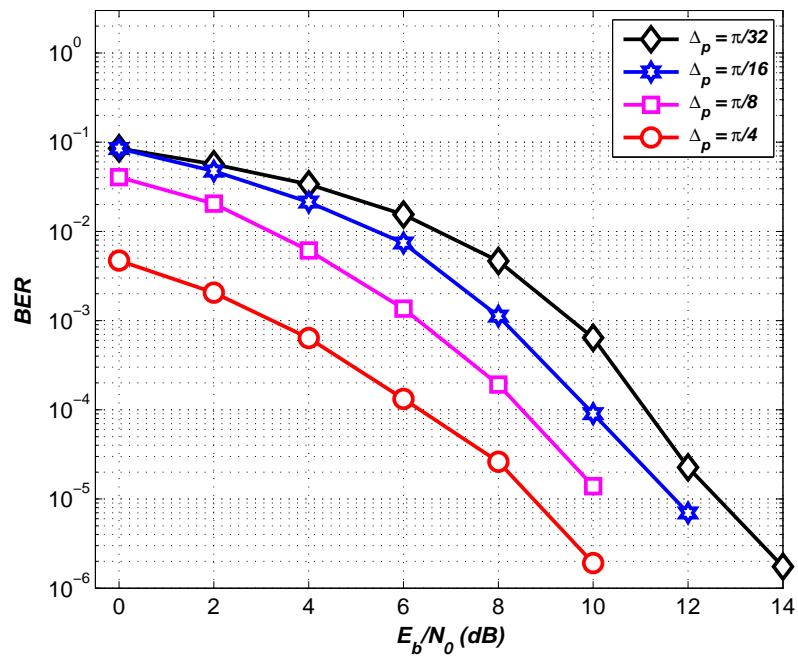


Figure 5.16: The spectral behaviour of a PM signal with different values of  $\Delta_p$ .

pending on the algorithms utilized by the decoder. At  $10^{-5}$  in Figures 5.19(a) for FM-PNC system, there is a performance gain of approximately 3.6 dB of  $\Delta_f=1$  kHz, and at the same level of BER about 2.4 dB and 0.8 dB of  $\Delta_f=0.5$  kHz and  $\Delta_f=1.5$  kHz, respectively. Again, at  $10^{-5}$  for FM-PNC employing BICM-ID code, there is a performance gain of 4 dB of  $\Delta_f=1$  kHz and there is a minor gain of about 2.6 dB of  $\Delta_f=0.5$  kHz and nearly 0.7 dB of  $\Delta_f=1.5$  kHz, as depicted in Figures 5.20(a). Even for FM-PNC employing turbo code, again at  $10^{-5}$ , the performance is within 3.4 dB of  $\Delta_f=1$  kHz and about 1.8 dB of  $\Delta_f=0.5$  kHz and approximately 0.7 dB of  $\Delta_f=1.5$  kHz, as shown in Figure 5.21(a). In Figures 5.19(b), 5.20(b), and 5.21(b), there is a performance gain for  $\Delta_p=\pi/16$  at  $10^{-5}$  of nearly 3.4 dB for LDPC with PM-PNC and for BICM-ID with PM-PNC, and for turbo with PM-PNC about 3



(a) FM-PNC



(b) PM-PNC

Figure 5.17: The performance of uncoded PNC system with different deviations.

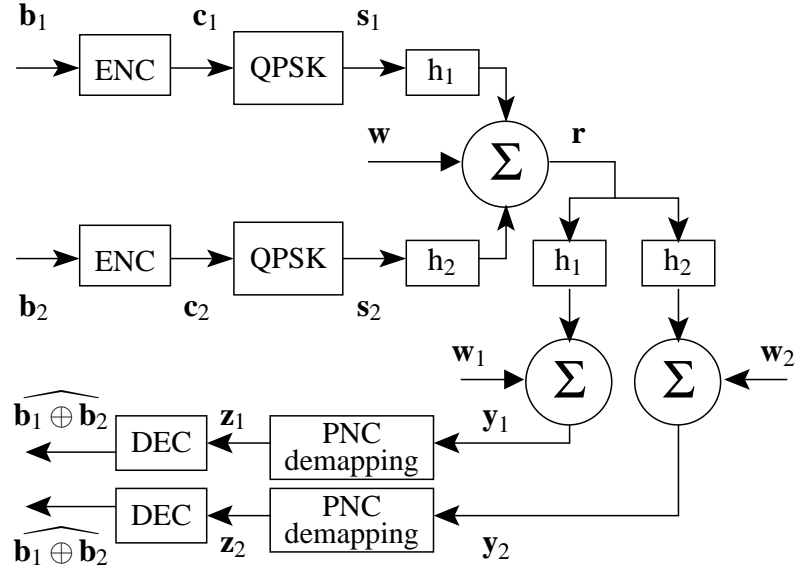
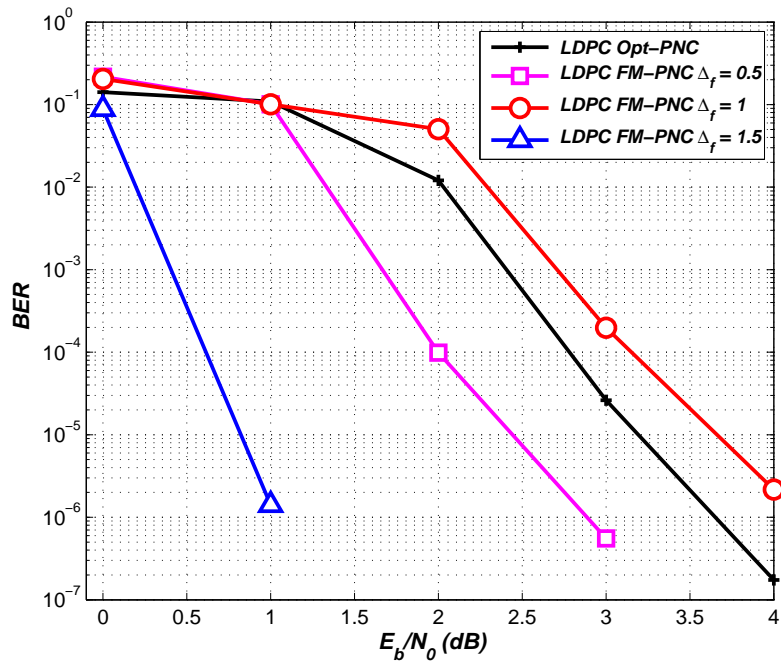


Figure 5.18: The structure of Opt-PNC system.

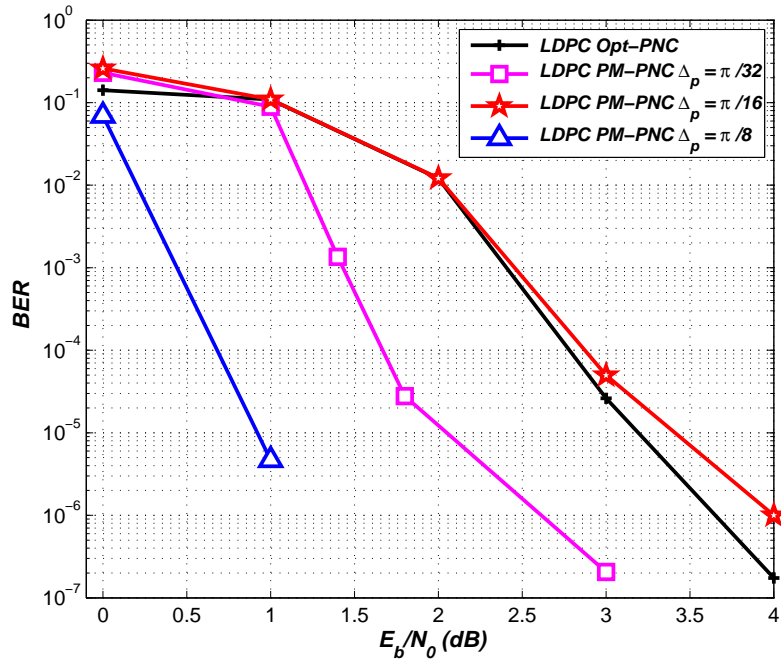
Table 5.3: Summary of system performance for E2E coded Opt-PNC and PM-PNC systems on AWGN channel.

At point of BER	$\Delta_p$	LDPC code		BICM-ID code		Turbo code	
		Opt $(\frac{E_b}{N_0})$ , dB	PM	Opt $(\frac{E_b}{N_0})$ , dB	PM	Opt $(\frac{E_b}{N_0})$ , dB	PM
$10^{-5}$	$\pi/32$	3.2	2.1	3.4	1.7	2.9	0.9
$10^{-5}$	$\pi/8$	3.2	0.9	3.4	1	2.9	0.7

dB. However, the curves lower the performance line of Opt-PNC are related to the  $\Delta_p=\pi/8$  and  $\Delta_p=\pi/4$ . The performance of PM-PNC employing channel coding can be summarized in Table 5.3. For AWGN channel, the results are encouraging when one considers  $\Delta_f=1$  kHz and  $\Delta_p=\pi/16$  for the better performance, this is due to the BER performance still being close to the BER performance of Opt-PNC system curve. Now, consider the coded E2E FM-PNC and PM-PNC systems over Rayleigh flat-fading channel. Figure 5.22 shows the systems of FM-PNC and PM-PNC employing LDPC code. Similarly, for the same channel, Figures 5.23 and 5.24 show the BICM-ID and turbo codes with a FM-PNC and PM-PNC system. Each system tries to obtain an appropriate value for  $\Delta_f$  and  $\Delta_p$ . A different view of the simulated data is shown in Figures 5.23(a), 5.22(a), and 5.24(a). For  $\Delta_f=2$  kHz, the BER of LDPC with FM-PNC reaches  $10^{-4}$  at about 8.9 dB, for turbo code with FM-PNC system it is about 8.8 dB, and for BICM-ID with FM-PNC system it reaches  $10^{-4}$  at approximately 15.5 dB. However, the BER performance at  $10^{-4}$  for  $\Delta_f=2$  kHz of Opt-PNC systems is about 8 dB, 8.2 dB, and 15 dB for LDPC,

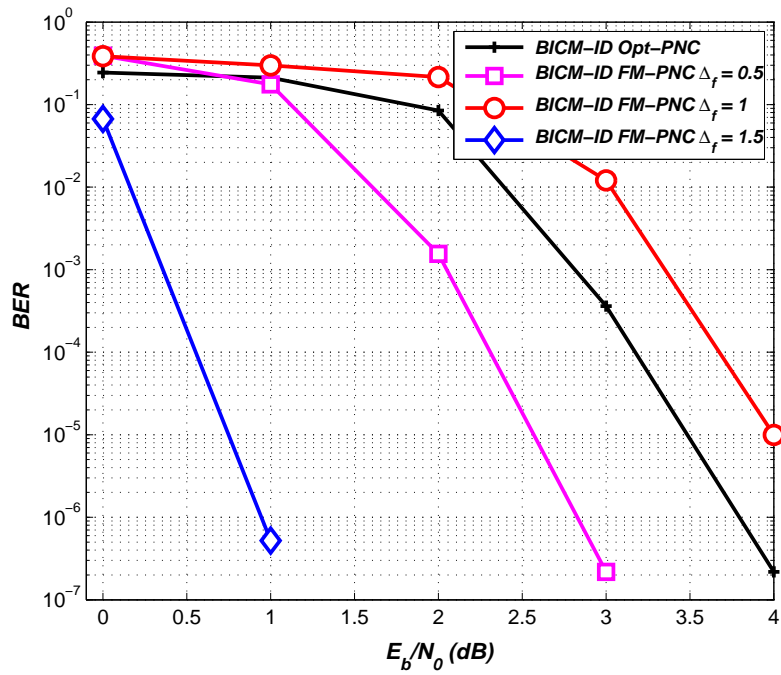


(a) FM-PNC system

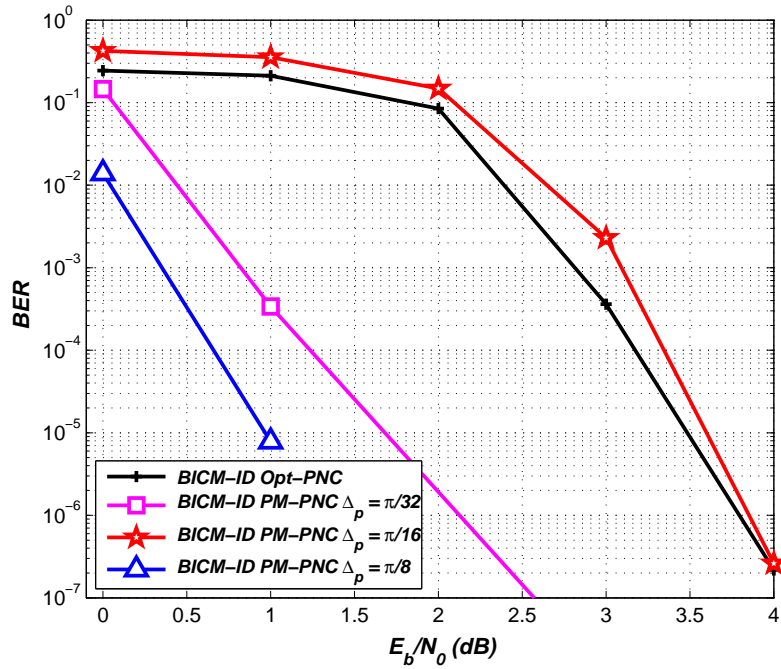


(b) PM-PNC system

Figure 5.19: The performance for FM-PNC and PM-PNC employing LDPC code on AWGN channel with different  $\Delta$  values.

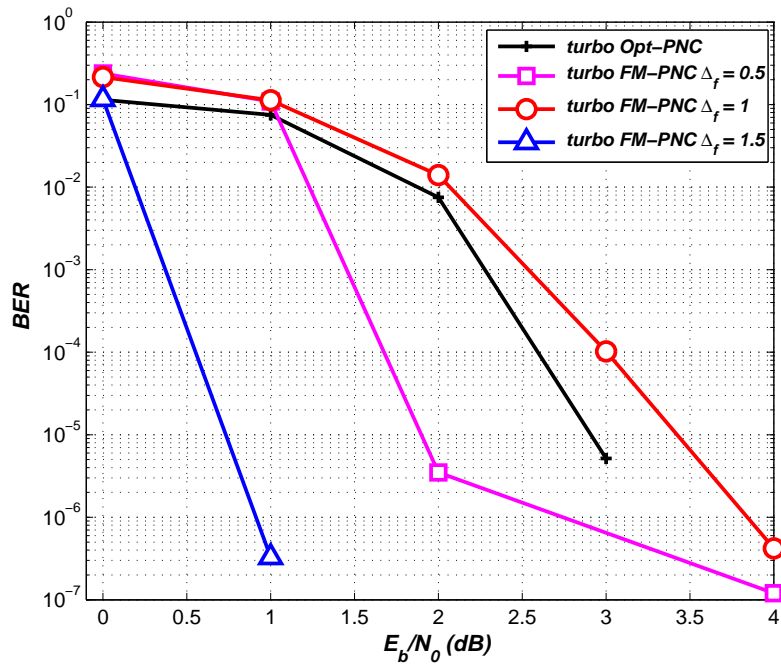


(a) FM-PNC system

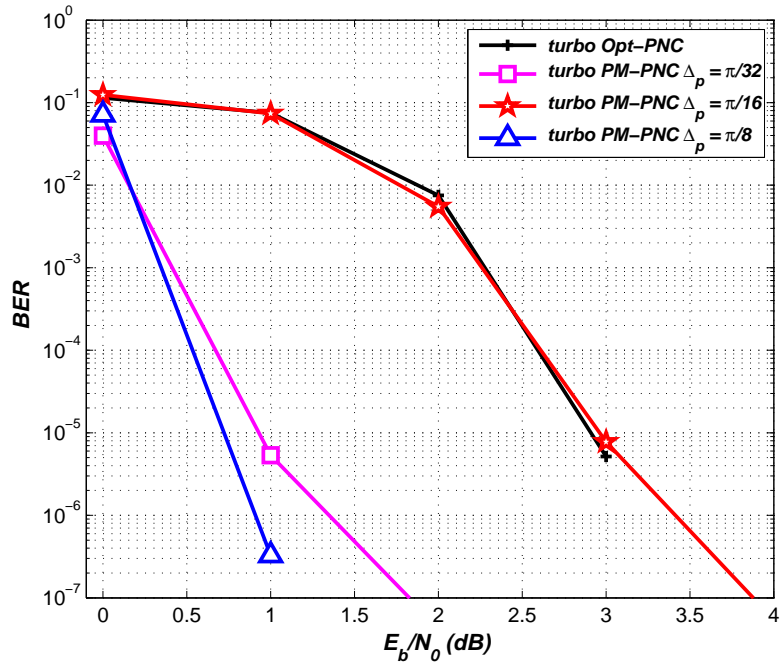


(b) PM-PNC system

Figure 5.20: The performance for FM-PNC and PM-PNC employing BICM-ID code on AWGN channel with different  $\Delta$  values.

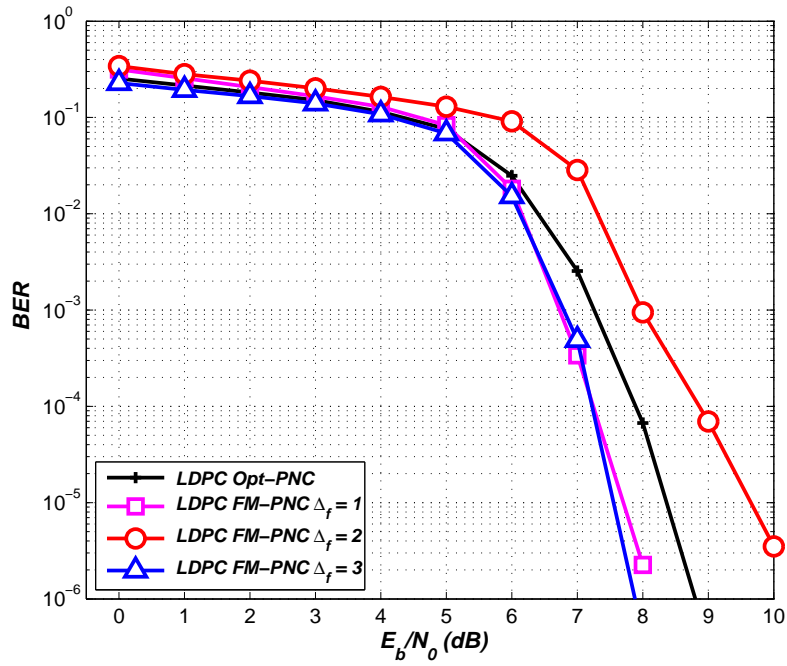


(a) FM-PNC system

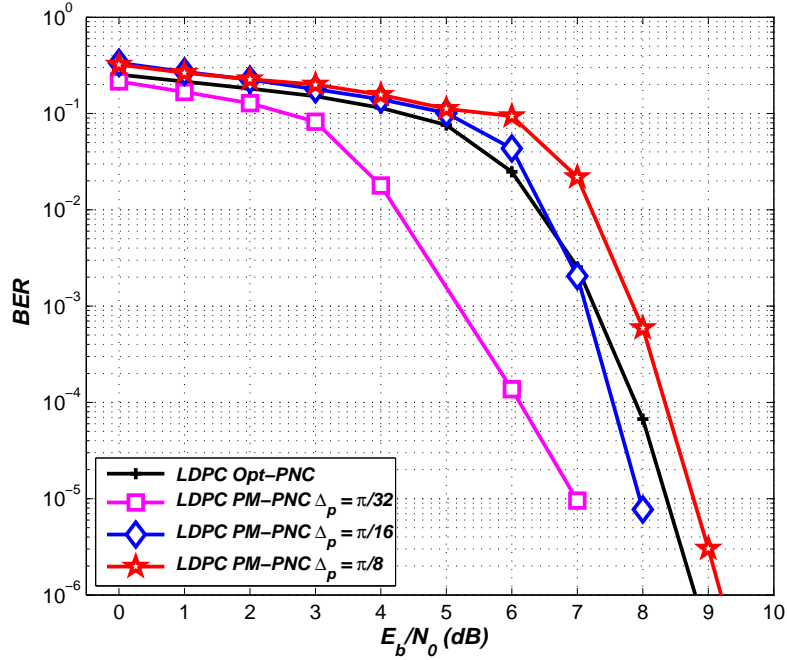


(b) PM-PNC system

Figure 5.21: The performance for FM-PNC and PM-PNC employing turbo code on AWGN channel with different  $\Delta$  values.



(a) FM-PNC system



(b) PM-PNC system

Figure 5.22: The performance for FM-PNC and PM-PNC employing LDPC code over Rayleigh flat-fading channel with different  $\Delta$  values.

Table 5.4: Summary of system performance for E2E coded Opt-PNC and FM-PNC systems over Rayleigh flat-fading channel.

At point of BER	$\Delta_f$	LDPC code		BICM-ID code		Turbo code	
		Opt	FM	Opt	FM	Opt	FM
		$(\frac{E_b}{N_0}), \text{ dB}$		$(\frac{E_b}{N_0}), \text{ dB}$		$(\frac{E_b}{N_0}), \text{ dB}$	
$10^{-4}$	1	8	7.5	15	14.6	8.2	6.8
$10^{-4}$	3	8	7.5	15	14.1	8.2	7.2

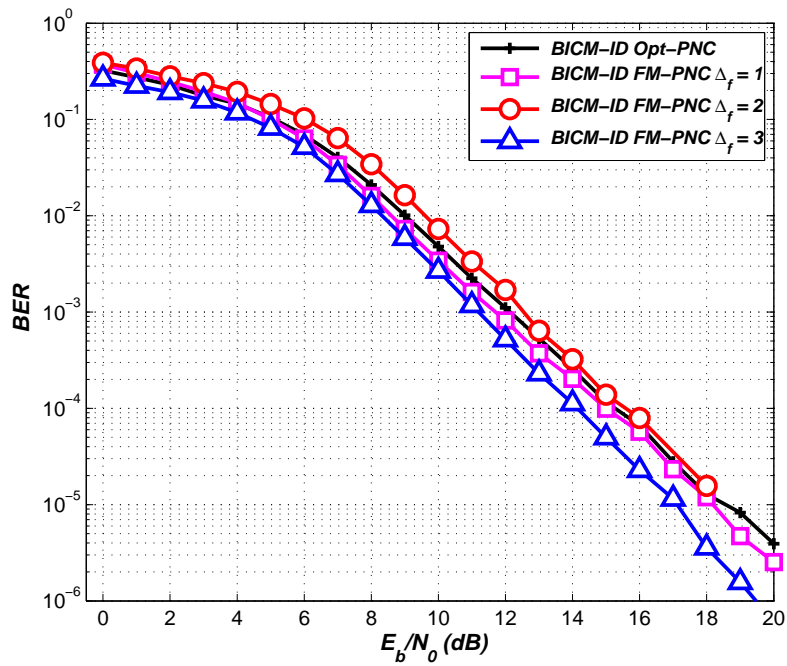
Table 5.5: Summary of system performance for E2E coded PM-PNC system over Rayleigh flat-fading channel.

At point of BER	$\Delta_p$	LDPC code		BICM-ID code		Turbo code	
		Opt	PM	Opt	PM	Opt	PM
		$(\frac{E_b}{N_0}), \text{ dB}$		$(\frac{E_b}{N_0}), \text{ dB}$		$(\frac{E_b}{N_0}), \text{ dB}$	
$10^{-5}$	$\pi/32$	8.4	7	18.4	15.5	8.5	7
$10^{-5}$	$\pi/16$	8.4	8	18.4	18.2	8.5	7.8

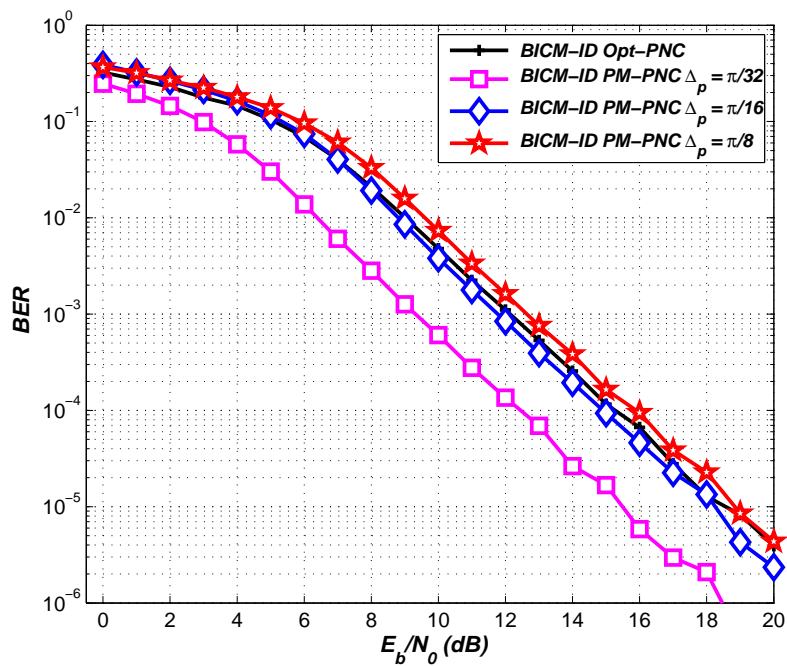
turbo, and BICM-ID, respectively. The curves lower than the performance line of Opt-PNC system are related to the  $\Delta_f=1$  kHz and  $\Delta_f=3$  kHz. The performance of Opt-PNC and FM-PNC systems employing channel coding are summarized in Table 5.4. Similarly, the systems of PM-PNC are again Rayleigh flat-fading channel. The value of  $\Delta_p=\pi/8$ , for LDPC with PM-PNC at  $10^{-5}$  BER is about 8.8 dB and nearly 8.6 dB for turbo with PM-PNC. This value is better than the one obtained for BICM-ID with PM-PNC about 18.5 dB. With the PM-PNC method, the performance also degrades with different values of  $\Delta_p$  in the system. Almost all of the performance benefit is obtained with  $\Delta_p=\pi/8$ , as shown in Figures 5.23(b), 5.22(b), and 5.24(b). It is interesting to note that the energy per bit to noise power spectral density ratio ( $E_b/N_o$ ) shows that the gap between the  $\Delta_p=\pi/32$  and  $\Delta_p=\pi/4$  curves of the systems gets wider. These results are summarized in Table 5.5.

### 5.5.3 Simulation Results

A method of performing a combined constant envelope and channel decoding for PNC system is proposed. This method uses SISO detection and channel decoding implemented by a modified version of the relay process and the system operates in an iterative manner. Simulations are repeatedly employed to analyze complex communication systems in order to evaluate their performance. The performance results of Opt-PNC, CE-PNC, and conventional PNC in terms of BER were evaluated using

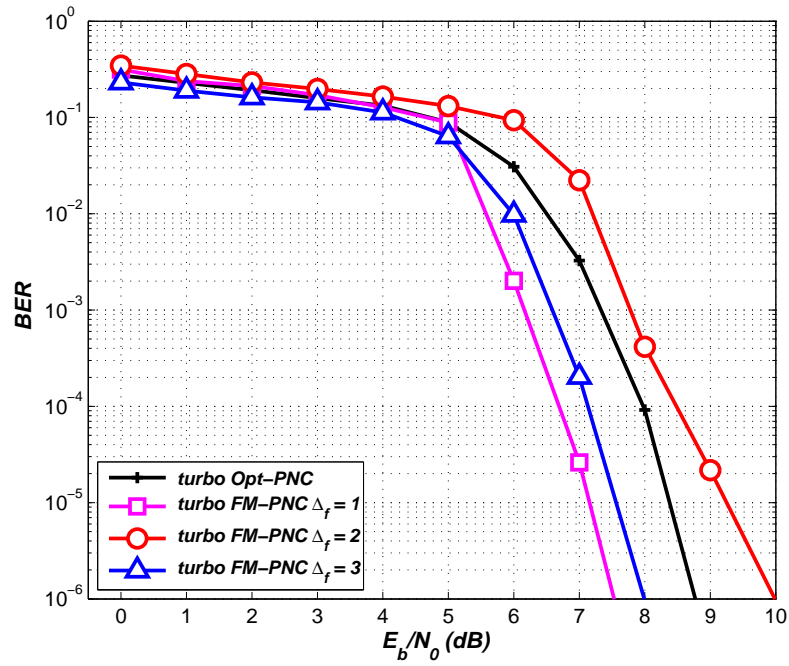


(a) FM-PNC system

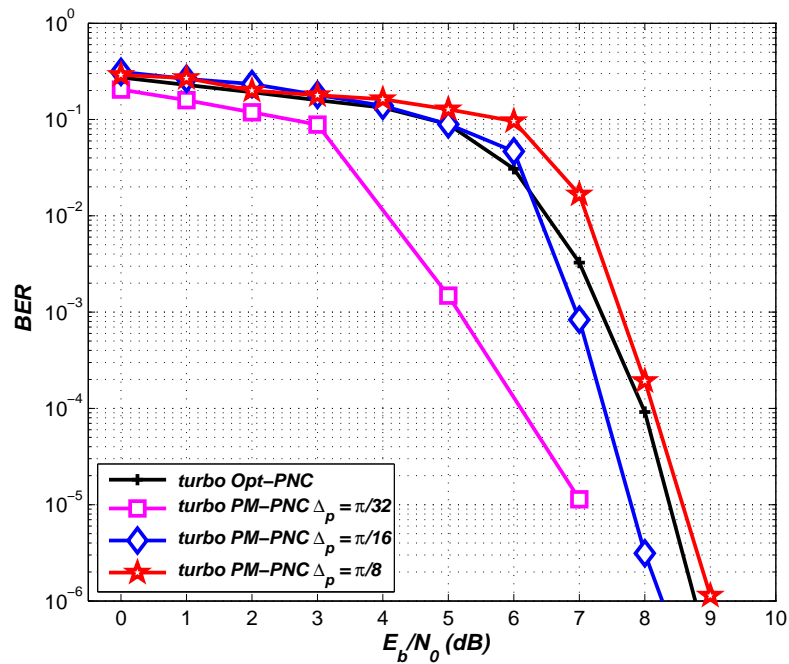


(b) PM-PNC system

Figure 5.23: The performance for FM-PNC and PM-PNC employing BICM-ID code over Rayleigh flat-fading channel with different  $\Delta$  values.



(a) FM-PNC system



(b) PM-PNC system

Figure 5.24: The performance for FM-PNC and PM-PNC employing turbo code over Rayleigh flat-fading channel with different  $\Delta$  values.

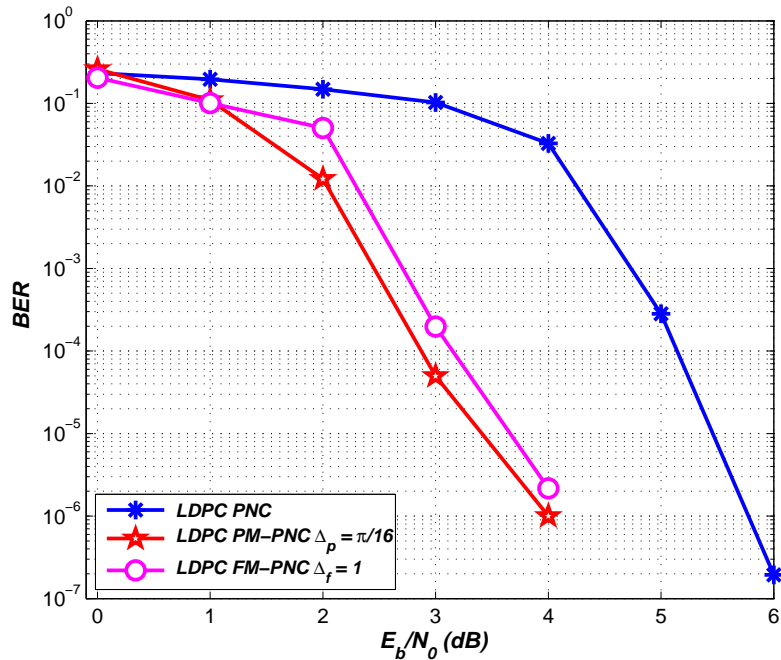


Figure 5.25: The performance for PNC and CE-PNC employing LDPC code on AWGN channel.

the transmitted signals through the AWGN and Rayleigh fading channels. For the AWGN channel, the simulation results for the systems employing LDPC code are shown in Figure 5.25. The upper curve of this plot shows the performance of the conventional PNC system for coded LDPC, which consists of a relay implementing a hard decision for the demapping/mapping process. The two solid curves in the lower of the plot show the performance of the proposed CE-PNC processing technique. For bit error rates between  $10^{-0}$  and  $10^{-1}$ , the performance of all the iterations of LDPC was very close. However, as the bit error rate drops, the performance of the FM-PNC moves slightly away from the PM-PNC bound. The performance of PM-PNC with LDPC code reaches  $10^{-5}$  BER at about 3.5 dB. At this BER level, FM-PNC is about 3.7 dB, while the PNC with LDPC code achieves this performance at 5.4 dB, both at thirty iterations. With a similar number of BICM-ID iterations at the same value of BER  $10^{-6}$ , as depicted in Figure 5.26, the PNC over AWGN gives the  $E_b/N_0$  nearly 5.8 dB and decreases for the FM-PNC and PM-PNC by about 4.5 dB and 3.9 dB, respectively. For the conventional system of PNC, the bit error performance was once again very poor. Again, we observed improved performance for the FM/PM for PNC with turbo code, although the absolute performance is comparable to the same system under a conventional PNC scenario. In the case of the turbo code, as shown in Figure 5.27, we observed that around  $10^{-6}$  BER, the

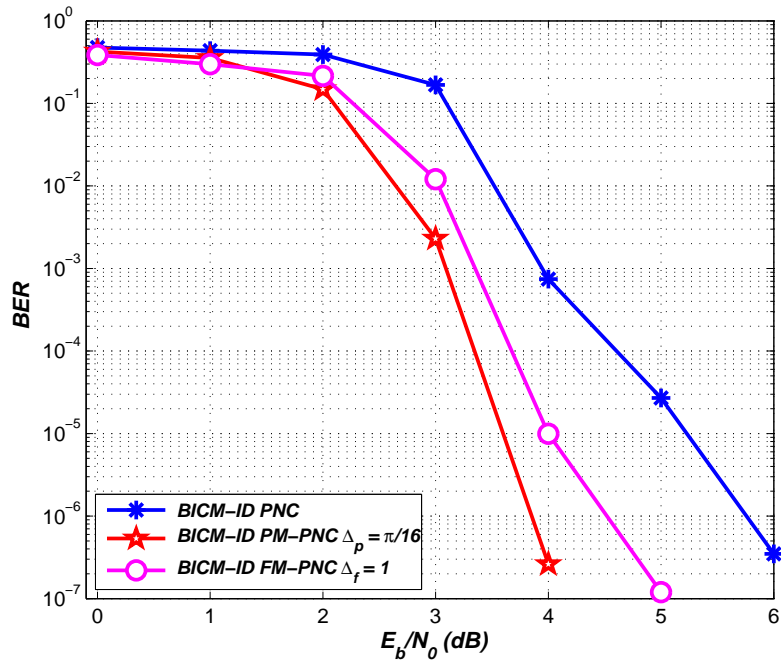


Figure 5.26: The performance for PNC and CE-PNC employing BICM-ID code on AWGN channel.

iterative decoder reached the best performance of around 3.4 dB of the PM-PNC and about 3.8 dB for the FM-PNC, and outperformed 4.7 dB the conventional PNC system case. The simulation results for the Rayleigh flat-fading channel are obtained for the comparison of the performance of the conventional PNC, FM-PNC, and PM-PNC systems employing LDPC, BICM-ID, and turbo codes. The number of schemes are varied in the process, while the parameter setup was held at similar values for all systems. However, the performance of the PNC with the constant envelope technique achieved the new value level of  $\Delta_f$  and  $\Delta_p$ . The observation shows that the PM-PNC and FM-PNC performances of  $10^{-4}$  BER at around 8.2 dB and 9 dB, respectively, were better than the PNC system for same BER level at about 18 dB; where all systems' results with LDPC code are given in Figure 5.28. In Figure 5.29, the BER is shown as a function of the level of system performance. Again, there were three systems and the channel was the Rayleigh flat-faded with BICM-ID coded. For the two schemes that directly use the FM/PM modulation at the relay, performance improved and outperformed the conventional PNC behaviour. Over the Rayleigh flat-fading channel, the same BICM-ID code achieved the  $10^{-3}$  BER of performance at around 12.5 dB for PM-PNC and FM-PNC, which is about 5.5 dB better than the PNC case for BICM-ID. This behaviour shows that the constant envelope operation not only increases the performance of the PNC

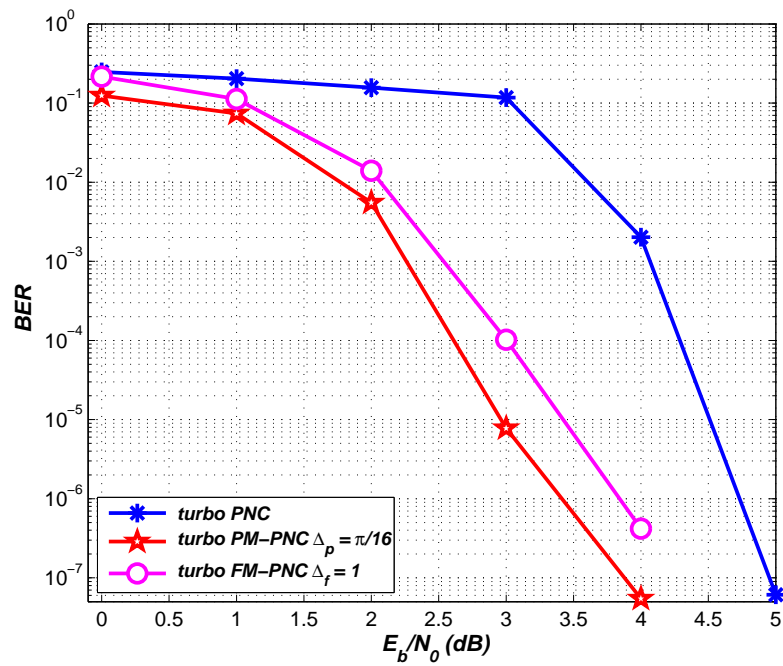


Figure 5.27: The performance for PNC and CE-PNC employing turbo code on AWGN channel.

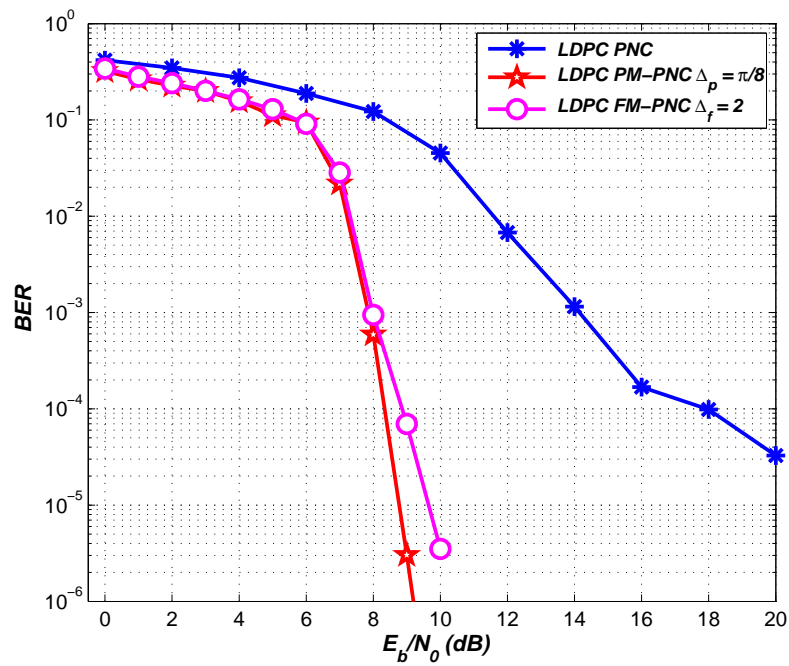


Figure 5.28: The performance for PNC and CE-PNC employing LDPC code over Rayleigh flat-fading channel.

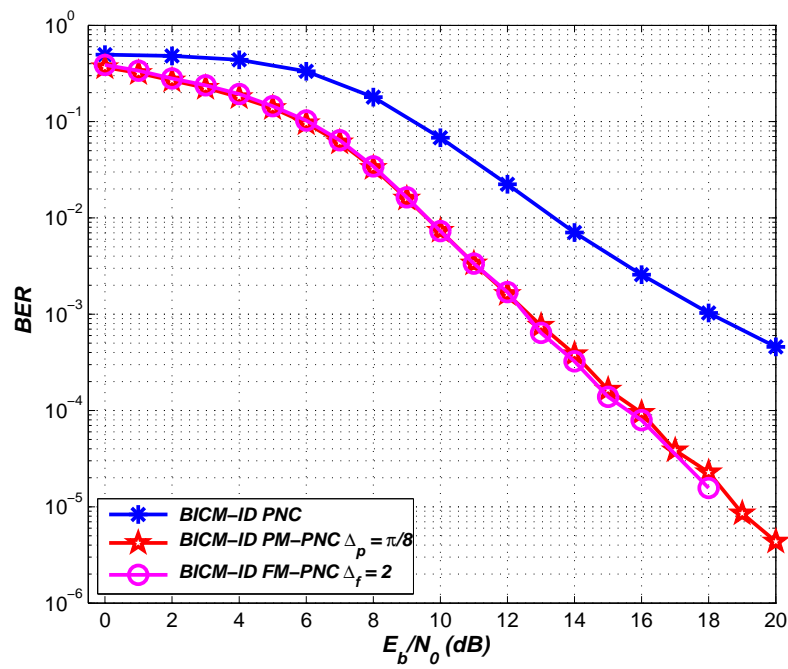


Figure 5.29: The performance for PNC and CE-PNC employing BICM-ID code over Rayleigh flat-fading channel.

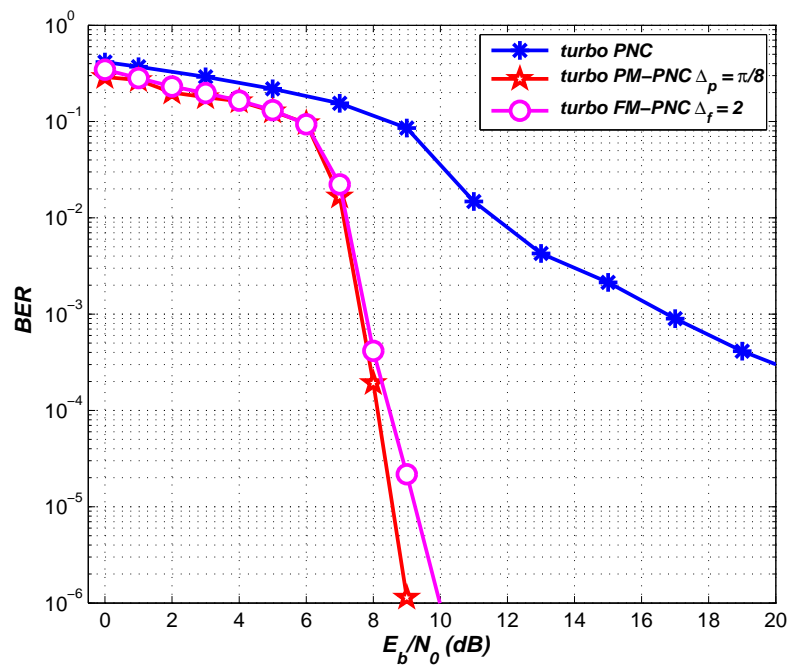


Figure 5.30: The performance for PNC and CE-PNC employing turbo code over Rayleigh flat-fading channel.

system by reducing the error propagation in the channel output, but also benefits from the *a priori* information generated in the decoder. Simulation results for the turbo code on the Rayleigh flat-fading channel for conventional PNC, FM-PNC, and PM-PNC systems are shown in Figure 5.30. There was a significant improvement in the proposed system of FM/PM with PNC compared to the conventional PNC system. No significant improvement was observed between FM and PM with PNC. For the BER  $10^{-3}$ , performance was about 7.8 dB of the PM-PNC system as well as FM with PNC system about 7.9 dB. However, in the BER range for the Rayleigh flat-fading channel, beyond  $10^{-3}$  the PNC system with turbo code was about 16.5 dB and around 8.6 dB worse than the PM-PNC and FM-PNC systems cases.

## 5.6 Chapter Summary

In a wireless network scenario, the structure of iterative channel coding schemes combined with PNC were presented in Chapter 3 is examined using traditional angle modulation when broadcasting from the relay. However, the received complex values at the relay can have many different values, but most of these values are centred around zero. Furthermore, directly forwarding these values to the destination nodes results in many transmitted symbols having values close to zero, which is undesirable since it can result in synchronization issues. In this Chapter, a strategy for combining the angle modulation technique with E2E channel coding for PNC systems was proposed. A signal transformation method for solving the hard decision problem at the relay is presented. Our method allows the complex received values at the relay to be transferred to the destination nodes while maintaining a constant envelope carrier signal. Simulation results were presented for the PNC system on the AWGN and Rayleigh flat-fading channels. It is shown that the modulation index controls the spectral containment and the system performance, where the angle signal variance is only a function of it. Moreover, the modulation index for CE-PNC can be chosen accordingly to balance the bandwidth and the performance. Since the modulation index controls the CE-PNC spectral containment, smaller modulation index can be used if a tighter bandwidth is required. In this case, we have a severe degradation in performance. The performance of FM-PNC and PM-PNC systems after a number of iterations was close to the proposed optimal-PNC system, where the received values are directly forwarded to the destination nodes. Both schemes

also perform significantly better than conventional coded PNC, where hard decisions are made on the received values at the relay. However, this work demonstrates a limitation of the angle demodulator receiver. For instance, the angle demodulator receiver was degraded for a large modulation index and low SNR due to the angle demodulator has difficulty demodulating the noisy samples. Nonlinearities in the relay transmitter also cause the generation of new frequencies in the transmitted signal. This intermodulation distortion causes interference known as adjacent channel interference (ACI). Another important parameter is the phase unwrapper, since phase unwrapping a noisy signal is a big problem and the process of unwrapper makes mistakes, therefore, the performance degrades slightly. We have shown that employing analogue modulation at the relay of a TWRC is a practical method to transfer the received values from the relay to the destination nodes. Both FM-PNC and PM-PNC schemes match the performance of the optimal PNC system, but the envelope of the carrier signal is fixed and we do not have the synchronization issues that would occur with the optimal PNC system.

## Chapter 6

---

---

### Concluding Remarks

---

---

---

## Conclusions

In this thesis, the combination of different iterative coding schemes with physical layer network coding has been investigated, evaluated and analysed on a two-way wireless relay channel. In particular, end-to-end PNC was considered where the relay does not perform any encoding or decoding of the demapped binary vector, which reduces the complexity of the system but results in a degradation of performance at the destination nodes due to uncorrected errors at the relay. This project addressed two issues associated with coded end-to-end PNC: the effect on the performance of turbo codes, LDPC codes and BICM-ID at the destination nodes and how the performance can be improved by investigating modulation schemes during the broadcast phase of PNC.

Essential background information was presented in Chapter 2, covering the construction, encoding and decoding of BICM-ID, turbo and LDPC codes. It also introduced fundamental concepts from information theory in order to explain an important tool for analysing the iterative behaviour of the different decoders, known as the ExIT chart. Here, the mutual information between the *a priori* information and extrinsic information of the component decoders/demappers is measured at each iteration and can be plotted to observe if the iterative decoder will converge at a particular signal-to-noise ratio.

Chapter 3 investigated the performance of BICM-ID turbo and LDPC codes of different block sizes and code rates combined with end-to-end PNC. Many simulation results were presented on TWRCs with AWGN and Rayleigh fading and comparisons were made between the three coding schemes. An unexpected result from this research was the poorer performance of the LDPC codes compared to BICM-ID and turbo codes. On a single-user system with no relay the LDPC codes and turbo codes both performed almost identically and outperformed BICM-ID. However, uncorrected errors from the relay caused all three iterative decoding algorithms to generate incorrect initial LLR values, but the sum-product decoder of the LDPC code was less robust to these incorrect LLR values and the performance was severely degraded at the destination nodes. Meanwhile the performance of BICM-ID and the turbo codes was only slightly degraded at the destination nodes.

Chapter 4 presented a thorough ExIT chart analysis of all three iterative decoders at the destination nodes when combined with end-to-end PNC. The set up to obtain

---

the ExIT chart for each coding scheme was explained and ExIT charts diagrams were given showing their convergence behaviour at different signal-to-noise ratios. The ExIT charts validated the simulation results obtained in Chapter 3, showing how at a particular SNR the tunnel formed by the mutual information curves for each component decoder/demapper was much wider for BICM-ID and turbo codes indicating that convergence occurs in few iteration steps. Conversely, the tunnel for the LDPC codes was much narrower showing how the sum-product decoder struggled to converge at the same SNR.

Chapter 5 addressed the issue of the degradation in performance of the coding schemes combined with PNC by proposing the employment of angle modulation for the broadcast phase. Making a hard decision on the interference at the relay causes all reliability information about that signal to be removed. Hence, when the binary sequence is broadcast to the destination nodes we only gain reliability information about the received signal at the destination nodes. The iterative decoders also assume that the received signal was transmitted error free but this is not true due to uncorrected errors at the relay. In this chapter, we take the received symbols at the relay and use them to modulate the frequency or phase of a carrier signal, i.e. frequency or phase modulation. This is a more preferred method over simply amplifying and forwarding the received symbols, where there will be a significant probability of transmitting values close to zero resulting in potential synchronisation problems. FM and PM both have constant envelopes and will not have this problem. Also, amplify-and-forward will not remove the noise added at the relay from the multiple access phase of PNC so the performance at the destination nodes will be much worse. Simulation results have shown that employing FM or PM reliably transfer the received values at the relay to the destination nodes, which aids the decoders by correctly initialising the received LLR values.

## Future Work

This thesis has investigated different iterative decoding and detection algorithms combined with PNC. There are still many area of investigation for PNC.

- Suggestion for extensions of this work might include other iterative coding schemes such as the construction of non-binary channel coding, where non-

---

binary codes can provide performance improvements over binary LDPC codes, and may also be better suited to some communications channels and systems.

- The EXIT chart was used to predict the performance of iterative decoding and one can envision extending this method in order to use BER estimation based EXIT chart. The original EXIT chart was successfully used to design the encoder of the turbo code. Therefore, a second area of future interest is the design of constituent encoders using an EXIT chart.
- The concepts regarding the implementation and improvement of angle modulation with PNC may be directly applied to optical or underwater communication systems.
- Emphasis should be placed on the technique of OFDM at the relay to mitigate multiuser interference and the results should be compared with a single carrier PNC system.
- While this thesis covered AWGN and Rayleigh flat-fading channels of the end-to-end PNC system, extending the work to a multipath channel is worth investigating, as the frequency selectivity will require an advanced equalization stage.
- Further work should consider multi-relaying and multiple-input-multiple-output (MIMO) systems.

# Appendix A

## Soft Demapping of 9-Point Constellation at the Relay with LLRs

At the relay, we have a 9-point constellation, as shown in Figure 2.9, and we wish to determine the individual log-likelihood ratios (LLRs) of the pair of demapped bits. For the QPSK mapping signal, assume that the first bit denotes as  $b_1^{(1)} \oplus b_1^{(2)}$  and second bit denotes as  $b_2^{(1)} \oplus b_2^{(2)}$ . Each constellation point can be demapped to a pair of bits representing the XOR of the users bits,  $b_1^{(1)} \oplus b_1^{(2)}$  and  $b_2^{(1)} \oplus b_2^{(2)}$ , as illustrated in Figure A.1. User 1 generates two bits,  $b_1^{(1)}$  and  $b_2^{(1)}$ , and user 2 generates two bits,  $b_1^{(2)}$  and  $b_2^{(2)}$ . Each user maps their pair of bits to a QPSK signal and at the relay we obtain the 9-point constellation. To determining the LLR of the first demapped bit, the conditional pdf that the first demapped bit is a 0,  $p(r|b_1^{(1)} \oplus b_1^{(2)} = 0)$ , is determined as

$$p(r|b_1^{(1)} \oplus b_1^{(2)} = 0) = e^{-\frac{[(r_I - \sqrt{2})^2 + (r_Q - \sqrt{2})^2]}{2\sigma^2}} + e^{-\frac{[(r_I + \sqrt{2})^2 + (r_Q - \sqrt{2})^2]}{2\sigma^2}} + e^{-\frac{[(r_I + \sqrt{2})^2 + (r_Q + \sqrt{2})^2]}{2\sigma^2}} + e^{-\frac{[(r_I - \sqrt{2})^2 + (r_Q + \sqrt{2})^2]}{2\sigma^2}} + 2e^{-\frac{[r_I^2 + (r_Q - \sqrt{2})^2]}{2\sigma^2}} + 2e^{-\frac{[r_I^2 + (r_Q + \sqrt{2})^2]}{2\sigma^2}}. \quad (\text{A.1})$$

where  $r_I$  and  $r_Q$  are the real and imaginary part of  $r$ . The equation (A.1) can be simplified to

$$p(r|b_1^{(1)} \oplus b_1^{(2)} = 0) = \left( e^{-\frac{(r_Q - \sqrt{2})^2}{2\sigma^2}} + e^{-\frac{(r_Q + \sqrt{2})^2}{2\sigma^2}} \right) \left( e^{-\frac{(r_I - \sqrt{2})^2}{2\sigma^2}} + e^{-\frac{(r_I + \sqrt{2})^2}{2\sigma^2}} + 2e^{-\frac{r_I^2}{2\sigma^2}} \right). \quad (\text{A.2})$$

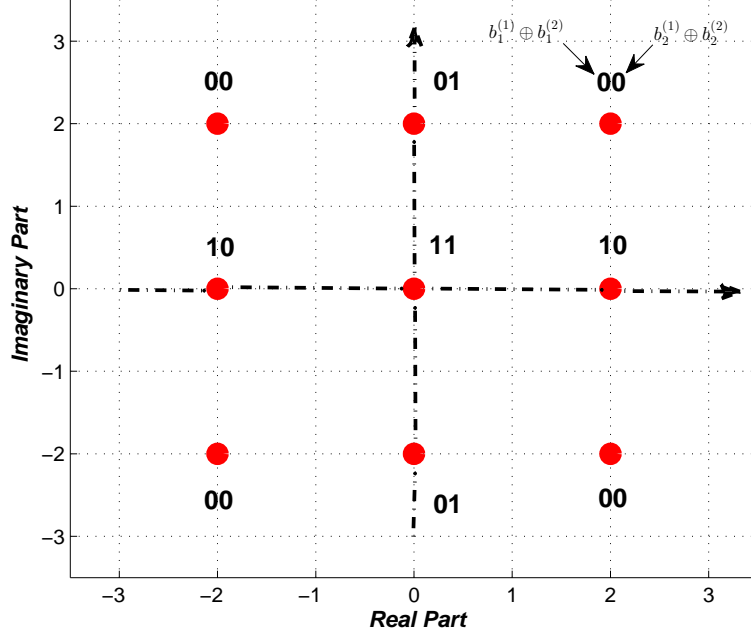


Figure A.1: The constellation point at the relay.

Similarly, the conditional pdf that the first demapped bit is a 1,  $p(r|b_1^{(1)} \oplus b_1^{(2)} = 1)$ , is determined as

$$p(r|b_1^{(1)} \oplus b_1^{(2)} = 1) = 4e^{-\frac{r_I^2 + r_Q^2}{2\sigma^2}} + 2e^{-\frac{[(r_I - \sqrt{2})^2 + r_Q^2]}{2\sigma^2}} + 2e^{-\frac{(r_I + \sqrt{2})^2 + r_Q^2}{2\sigma^2}}. \quad (\text{A.3})$$

This can be simplified to

$$p(r|b_1^{(1)} \oplus b_1^{(2)} = 1) = 2e^{-\frac{r_Q^2}{2\sigma^2}} \left( e^{-\frac{(r_I - \sqrt{2})^2}{2\sigma^2}} + e^{-\frac{(r_I + \sqrt{2})^2}{2\sigma^2}} + 2e^{-\frac{r_I^2}{2\sigma^2}} \right). \quad (\text{A.4})$$

Therefore, the LLR of the first demapped bit,  $\Lambda(rb_1^{(1)} \oplus b_1^{(2)})$ , is

$$\Lambda(r | b_1^{(1)} \oplus b_1^{(2)}) = \ln \left( \frac{p(r | b_1^{(1)} \oplus b_1^{(2)} = 0)}{p(r | b_1^{(1)} \oplus b_1^{(2)} = 1)} \right), \quad (\text{A.5a})$$

$$= \ln \left( \frac{\left( e^{-\frac{(r_Q - \sqrt{2})^2}{2\sigma^2}} + e^{-\frac{(r_Q + \sqrt{2})^2}{2\sigma^2}} \right) \left( e^{-\frac{(r_I - \sqrt{2})^2}{2\sigma^2}} + e^{-\frac{(r_I + \sqrt{2})^2}{2\sigma^2}} + 2e^{-\frac{r_I^2}{2\sigma^2}} \right)}{2e^{-\frac{r_Q^2}{2\sigma^2}} \left( e^{-\frac{(r_I - \sqrt{2})^2}{2\sigma^2}} + e^{-\frac{(r_I + \sqrt{2})^2}{2\sigma^2}} + 2e^{-\frac{r_I^2}{2\sigma^2}} \right)} \right), \quad (\text{A.5b})$$

$$= \ln \left( \frac{\left( e^{-\frac{(r_Q - \sqrt{2})^2}{2\sigma^2}} + e^{-\frac{(r_Q + \sqrt{2})^2}{2\sigma^2}} \right)}{2e^{-\frac{r_Q^2}{2\sigma^2}}} \right), \quad (\text{A.5c})$$

$$= \ln \left( \frac{e^{-\frac{r_Q^2}{2\sigma^2}} e^{\frac{\sqrt{2}r_Q}{\sigma^2}} e^{-\frac{1}{\sigma^2}} + e^{-\frac{r_Q^2}{2\sigma^2}} e^{\frac{\sqrt{2}r_Q}{\sigma^2}} e^{-\frac{1}{\sigma^2}}}{2e^{-\frac{r_Q^2}{2\sigma^2}}} \right), \quad (\text{A.5d})$$

$$= \ln \left( \frac{e^{\frac{\sqrt{2}r_Q}{\sigma^2}} + e^{\frac{\sqrt{2}r_Q}{\sigma^2}}}{2e^{-\frac{1}{\sigma^2}}} \right). \quad (\text{A.5e})$$

Finally, the LLR of the first demapped bit is

$$\Lambda(r | b_1^{(1)} \oplus b_1^{(2)}) = \ln \left( \cosh \left( \frac{\sqrt{2}r_Q}{\sigma^2} \right) \right) - \frac{1}{\sigma^2} \quad (\text{A.6})$$

To determining the LLR of the second demapped bit, we can also use the same method to determine the LLR as

$$p(r | b_2^{(1)} \oplus b_2^{(2)} = 0) = e^{-\frac{[(r_I - \sqrt{2})^2 + (r_Q - \sqrt{2})^2]}{2\sigma^2}} + e^{-\frac{[(r_I + \sqrt{2})^2 + (r_Q - \sqrt{2})^2]}{2\sigma^2}} + e^{-\frac{[(r_I + \sqrt{2})^2 + (r_Q + \sqrt{2})^2]}{2\sigma^2}} + e^{-\frac{[(r_I - \sqrt{2})^2 + (r_Q + \sqrt{2})^2]}{2\sigma^2}} + 2e^{-\frac{[(r_I - \sqrt{2})^2 + r_Q^2]}{2\sigma^2}} + 2e^{-\frac{[(r_I + \sqrt{2})^2 + r_Q^2]}{2\sigma^2}}. \quad (\text{A.7})$$

This can be simplified to

$$p(r | b_2^{(1)} \oplus b_2^{(2)} = 0) = \left( e^{-\frac{(r_I - \sqrt{2})^2}{2\sigma^2}} + e^{-\frac{(r_I + \sqrt{2})^2}{2\sigma^2}} \right) \left( e^{-\frac{(r_Q - \sqrt{2})^2}{2\sigma^2}} + e^{-\frac{(r_Q + \sqrt{2})^2}{2\sigma^2}} + 2e^{-\frac{r_Q^2}{2\sigma^2}} \right). \quad (\text{A.8})$$

Similarly, the conditional pdf that the second demapped bit is a 1,  $p(r | b_2^{(1)} \oplus b_2^{(2)} = 1)$ , is determined as

$$p(r | b_2^{(1)} \oplus b_2^{(2)} = 1) = 4e^{-\frac{r_I^2 + r_Q^2}{2\sigma^2}} + 2e^{-\frac{[r_I^2 + (r_Q - \sqrt{2})^2]}{2\sigma^2}} + 2e^{-\frac{r_I^2 + (r_Q + \sqrt{2})^2}{2\sigma^2}}, \quad (\text{A.9})$$

which can be simplified to

$$p(r|b_1^{(1)} \oplus b_1^{(2)} = 1) = 2e^{-\frac{r_I^2}{2\sigma^2}} \left( e^{-\frac{(r_Q - \sqrt{2})^2}{2\sigma^2}} + e^{-\frac{(r_Q + \sqrt{2})^2}{2\sigma^2}} + 2e^{-\frac{r_Q^2}{2\sigma^2}} \right). \quad (\text{A.10})$$

Therefore, the LLR of the second demapped bit,  $\Lambda(r|b_2^{(1)} \oplus b_2^{(2)})$ , is

$$\Lambda(r | b_2^{(1)} \oplus b_2^{(2)}) = \ln \left( \frac{p(r|b_2^{(1)} \oplus b_2^{(2)} = 0)}{p(r|b_2^{(1)} \oplus b_2^{(2)} = 1)} \right), \quad (\text{A.11a})$$

$$= \ln \left( \frac{\left( e^{-\frac{(r_I - \sqrt{2})^2}{2\sigma^2}} + e^{-\frac{(r_I + \sqrt{2})^2}{2\sigma^2}} \right) \left( e^{-\frac{(r_Q - \sqrt{2})^2}{2\sigma^2}} + e^{-\frac{(r_Q + \sqrt{2})^2}{2\sigma^2}} + 2e^{-\frac{r_Q^2}{2\sigma^2}} \right)}{2e^{-\frac{r_I^2}{2\sigma^2}} \left( e^{-\frac{(r_Q - \sqrt{2})^2}{2\sigma^2}} + e^{-\frac{(r_Q + \sqrt{2})^2}{2\sigma^2}} + 2e^{-\frac{r_Q^2}{2\sigma^2}} \right)} \right), \quad (\text{A.11b})$$

$$= \ln \left( \frac{\left( e^{-\frac{(r_I - \sqrt{2})^2}{2\sigma^2}} + e^{-\frac{(r_I + \sqrt{2})^2}{2\sigma^2}} \right)}{2e^{-\frac{r_I^2}{2\sigma^2}}} \right), \quad (\text{A.11c})$$

$$= \ln \left( \frac{e^{-\frac{r_I^2}{2\sigma^2}} e^{\frac{\sqrt{2}r_I}{\sigma^2}} e^{-\frac{1}{\sigma^2}} + e^{-\frac{r_I^2}{2\sigma^2}} e^{\frac{\sqrt{2}r_I}{\sigma^2}} e^{-\frac{1}{\sigma^2}}}{2e^{-\frac{r_I^2}{2\sigma^2}}} \right), \quad (\text{A.11d})$$

$$= \ln \left( \frac{e^{\frac{\sqrt{2}r_I}{\sigma^2}} + e^{\frac{\sqrt{2}r_I}{\sigma^2}}}{2e^{-\frac{1}{\sigma^2}}} \right). \quad (\text{A.11e})$$

Finally, the LLR of the second demapped bit is

$$\Lambda(r | b_2^{(1)} \oplus b_2^{(2)}) = \ln \left( \cosh \left( \frac{\sqrt{2}r_I}{\sigma^2} \right) \right) - \frac{1}{\sigma^2} \quad (\text{A.12})$$

# Appendix B

## The Signal Power and Symbol Energy

The average power consumption over the interval is given by dividing the total energy consumed by the length of the time interval as

$$P_a = \frac{E}{T} \quad (\text{B.1})$$

where

$$E = \int_{-\infty}^{\infty} P(t) dt \quad (\text{B.2a})$$

$$= \int_{-\infty}^{\infty} (|u(t)|)^2 dt \quad (\text{B.2b})$$

Since the signals represented in terms of power and the power depends on time as signal is dependant, therefore, the term  $P(t) = s^2(t)$  is called instantaneous power.

The average power can be expressed as

$$P_a = \frac{1}{T} \int_{-T/2}^{T/2} (|u(t)|)^2 dt \quad (\text{B.3})$$

The mathematically introduce the power from equation (2.1) as

$$P_a = \frac{1}{T} \int_{-T/2}^{T/2} A^2(t) \cos^2(2\pi f_c t + \theta(t)) dt \quad (\text{B.4})$$

---

where  $\cos^2(\varepsilon) = \frac{1}{2} + \frac{1}{2} \cos(2\varepsilon)$  then equation (B.4) becomes

$$P_a = \frac{1}{2T} \int_{-\infty}^{\infty} A^2(t) dt + \frac{1}{2T} \int_{-\infty}^{\infty} A^2(t) \cos(4\pi f_c t + 2\theta(t)) dt \quad (\text{B.5a})$$

$$= \frac{1}{2T} \int_{-\infty}^{\infty} A^2(t) dt + 0 \quad (\text{B.5b})$$

By evaluation of integral in equation (B.5b), we note that power is not a function of time [101]. Thus, the power is

$$P_a \approx \frac{A^2}{2T} T \quad (\text{B.6a})$$

$$= \frac{A^2}{2} \quad (\text{B.6b})$$

This is mean that at any point in the signal the power of the signal is simply equal to its amplitude squared. In the log domain, we can expressed  $E_s$  and  $N_0$  as

$$E_s = P_s - 10 \log(R_s) \quad (\text{B.7})$$

$$N_0 = P_n - 10 \log(B_n) \quad (\text{B.8})$$

where  $P_s$  and  $P_n$  are the symbol and noise power in dB, respectively, and  $B_n$  is the noise bandwidth. Therefore,

$$E_s/N_0 = P_s - 10 \log(R_s) - P_n + 10 \log(B_n) \quad (\text{B.9})$$

Evaluating BER vs  $E_s/N_0$  provides a means for comparing modulation types against each other in AWGN independent of the bandwidth used in each test. Using the definitions for  $E_s$  and  $N_0$  in equations (B.7) and (B.8), this can be done even for partial-response systems or other systems where matched filtering is not used and  $E_s/N_0$  may not equal SNR as

$$E_s/N_0 \text{ (dB)} = 10 \log\left(\frac{T}{2T_s}\right) + \Xi \text{ (dB)} \quad (\text{B.10a})$$

$$= 10 \log\left(\frac{N_s}{2}\right) + \Xi \text{ (dB)} \quad (\text{B.10b})$$

$$= 10 \log\left(\frac{f_s}{2B}\right) + \Xi \text{ (dB)} \quad (\text{B.10c})$$

---

where the two quotients of  $E_s/N_0$  and  $E_b/N_0$  are related to each other according to the following

$$E_s/N_0 = (E_b/N_0) \log_2 M \quad (\text{B.11})$$

where  $M$  is the number of points in the modulated constellation. When FEC is used, the code rate  $R_c$  of the FEC needs to be taken into account so that  $E_b$ , the user information bit energy, is accurately accounted for. The bit energy,  $E_b$ , can be computed from  $P_s$  as

$$E_b = P_s - 10 \log_{10}(R_b) \quad (\text{B.12a})$$

$$= E_s - 10 \log_{10}(m) - 10 \log_{10}(R) \quad (\text{B.12b})$$

where  $R_b$  and  $R$  are the bit rate and the overall FEC code rate, respectively, and  $m = \log_2 M$ . Then equation (B.10) becomes

$$E_b/N_0 \text{ (dB)} = 10 \log_{10}\left(\frac{f_s}{2B}\right) - 10 \log_{10}(m) + \Xi \text{ (dB)} \quad (\text{B.13a})$$

$$= 10 \log_{10}\left(\frac{f_s}{2B}\right) - 10 \log_{10}(m) + 10 \log_{10}(\Xi) \quad (\text{B.13b})$$

$$= 10 \log_{10}\left(\frac{f_s}{2B}\right) + 10 \log_{10}(\Xi) \quad (\text{B.13c})$$

where the term  $10 \log_{10}(m)$  equal 0 for QPSK. However, the logarithm of a product is the sum of the logarithms of the factors  $\log(\varepsilon\kappa) = \log(\varepsilon) + \log(\kappa)$ , then the equation (B.13c) can be rewritten as

$$E_b/N_0 = 10 \log_{10}\left(\frac{f_s}{2B}\Xi\right) \quad (\text{B.14})$$

For any two real numbers  $\varepsilon$  and  $\kappa$ , the relation  $\varepsilon = 10^\kappa$  is equivalent to  $\kappa = \log_{10}(\varepsilon)$ , where  $\varepsilon$  is positive and  $\varepsilon \neq 1$ . Then equation (B.14) becomes

$$10^{E_b/N_0} = \frac{f_s}{2B}\Xi \quad (\text{B.15})$$

Hence,  $N_0$  can be expressed as

$$N_0 = \frac{2E_b B}{f_s \Xi} \quad (\text{B.16})$$

# References

- [1] B. Rankov and A. Wittneben, “Achievable rate regions for the two-way relay channel,” *Information Theory, IEEE International Symposium on*, pp. 1668–1672, July 2006.
- [2] R. Ahlswede, N. Cai, S.-Y. Li, and R. W. Yeung, “Network information flow,” *Information Theory, IEEE Transactions on*, vol. 46, no. 4, pp. 1204–1216, 2000.
- [3] S. Zhang, S. C. Liew, and P. P. Lam, “Hot topic: physical-layer network coding,” *Proceedings of the 12th annual international conference on Mobile computing and networking (ACM)*, pp. 358–365, 2006.
- [4] W. Nam, S.-Y. Chung, and Y. H. Lee, “Capacity of the gaussian two-way relay channel to within 1/2 bit,” *Information Theory, IEEE Transactions on*, vol. 56, no. 11, pp. 5488–5494, Nov. 2010.
- [5] S. Zhang and S. C. Liew, “Applying physical-layer network coding in wireless networks,” *EURASIP Journal on Wireless Communications and Networking*, p. 1, 2010.
- [6] M. Wilson, K. Narayanan, H. Pfister, and A. Sprintson, “Joint physical layer coding and network coding for bidirectional relaying,” *Information Theory, IEEE Transactions on*, vol. 56, no. 11, pp. 5641–5654, Nov. 2010.
- [7] S. Katti, S. Gollakota, and D. Katabi, “Embracing wireless interference: analog network coding,” in *ACM SIGCOMM Computer Communication Review*, vol. 37, no. 4, 2007, pp. 397–408.
- [8] D. Tse and P. Vishwanath, *Fundamentals of Wireless Communications*. Cambridge University Press, 2005.

- 
- [9] R. Pickholtz, L. Milstein, and D. Schilling, "Spread spectrum for mobile communications," *Vehicular Technology, IEEE Transactions on*, vol. 40, no. 2, pp. 313–322, May 1991.
- [10] T. S. Rappaport, *Wireless Communications: Principles and practice*. Prentice Hall, 2nd edition, 2001.
- [11] E. C. V. D. Meulen, "Three-terminal communication channels," *Advances in Applied Probability*, vol. 3, no. 1, pp. 120–154, 1971.
- [12] T. Cover and A. Gamal, "Capacity theorems for the relay channel," *Information Theory, IEEE Transactions on*, vol. 25, no. 5, pp. 572–584, Sept. 1979.
- [13] J. Massey, "Coding and modulation in digital communications," in *International Zurich Seminar on Digital Communications, 3 rd, Zurich, Switzerland, 1974*.
- [14] G. Ungerboeck, "Channel coding with multilevel/phase signals," *Information Theory, IEEE Transactions on*, vol. 28, no. 1, pp. 55–67, Jan. 1982.
- [15] H. Imai and S. Hirakawa, "A new multilevel coding method using error-correcting codes," *Information Theory, IEEE Transactions on*, vol. 23, no. 3, pp. 371–377, May 1977.
- [16] U. Wachsmann, R. Fischer, and J. Huber, "Multilevel codes: theoretical concepts and practical design rules," *Information Theory, IEEE Transactions on*, vol. 45, no. 5, pp. 1361–1391, Jul 1999.
- [17] E. Zehavi, "8-psk trellis codes for a rayleigh channel," *Communications, IEEE Transactions on*, vol. 40, no. 5, pp. 873–884, May 1992.
- [18] G. Caire, G. Taricco, and E. Biglieri, "Bit-interleaved coded modulation," *Information Theory, IEEE Transactions on*, vol. 44, no. 3, pp. 927–946, May 1998.
- [19] C. Berrou, A. Glavieux, and P. Thitimajshima, "Near shannon limit error-correcting coding and decoding: Turbo-codes. 1," in *Communications, ICC '93 Geneva. Technical Program, Conference Record, IEEE International Conference on*, vol. 2, May 1993, pp. 1064–1070.

- 
- [20] J. Hagenauer, “The turbo principle: Tutorial introduction and state of the art.”
- [21] R. Gallager, “Low-density parity-check codes,” *Information Theory, IRE Transactions on*, vol. 8, no. 1, pp. 21–28, Jan. 1962.
- [22] D. J. C. MacKay and R. M. Neal, “Near shannon limit performance of low density parity check codes,” *Electronics Letters*, vol. 33, no. 6, pp. 457–458, Mar 1997.
- [23] X. Li and J. Ritcey, “Bit-interleaved coded modulation with iterative decoding,” *Communications Letters, IEEE*, vol. 1, no. 6, pp. 169–171, Nov 1997.
- [24] S. Ten Brink, J. Speidel, and R.-H. Yan, “Iterative demapping and decoding for multilevel modulation,” *Global Telecommunications Conference, GLOBECOM. The Bridge to Global Integration. IEEE*, vol. 1, pp. 579–584, 1998.
- [25] J. Lodge and M. Gertsman, “Joint detection and decoding by turbo processing for fading channel communications,” in *Proc. Int. Symp. on turbo codes and related topics, Brest, France*, pp. 88–95, Sept. 1997.
- [26] P. Hoeher, “On channel coding and multiuser detection for ds-cdma,” in *Universal Personal Communications, 1993. Personal Communications: Gateway to the 21st Century. Conference Record., 2nd International Conference on*, vol. 2, Oct 1993, pp. 641–646 vol.2.
- [27] J. Hagenauer, “Source-controlled channel decoding,” *Communications, IEEE Transactions on*, vol. 43, no. 9, pp. 2449–2457, Sep 1995.
- [28] C. Douillard, M. Jézéquel, C. Berrou, A. Picart, P. Didier, A. Glavieux, and E. de Bretagne, “Iterative correction of intersymbol interference turbo-equalization,” *European Trans. on Telecommunication*, vol. 6, pp. 507–511, Sep. 1995.
- [29] S. C. Liew, S. Zhang, and L. Lu, “Physical-layer network coding: Tutorial, survey, and beyond,” *Physical Communication*, vol. 6, pp. 4–42, 2013.
- [30] S. Zhang and S.-C. Liew, “Channel coding and decoding in a relay system operated with physical-layer network coding,” *Selected Areas in Communications, IEEE Journal on*, vol. 27, no. 5, pp. 788–796, June 2009.

- 
- [31] X. Lu, Q. Qiu, and H. Wu, "A joint design of network coding and channel coding for multiple access channel," Nov. 2010, pp. 214–217.
- [32] X. Wu, C. Zhao, and X. You, "Joint ldpc and physical-layer network coding for asynchronous bi-directional relaying," *Selected Areas in Communications, IEEE Journal on*, vol. 31, no. 8, pp. 1446–1454, Aug. 2013.
- [33] K. Xu, Z. Lv, Y. Xu, D. Zhang, X. Zhong, and W. Liang, "Joint physical network coding and ldpc decoding for two way wireless relaying," *Elsevier Physical Communication*, vol. 6, pp. 43–47, 2013.
- [34] D. Sui, C. Zhai, X. Zhang, and D. Yang, "Joint physical layer network-channel decoding for the multiple-access relay channel," Sept. 2009, pp. 1–5.
- [35] Z. Chen, B. Xia, and H. Liu, "Multi-level physical-layer network coding for gaussian two-way relay channels," Apr. 2013, pp. 2422–2427.
- [36] S. Benedetto, D. Divsalar, G. Montorsi, and F. Pollara, "Serial concatenation of interleaved codes: performance analysis, design, and iterative decoding," *Information Theory, IEEE Transactions on*, vol. 44, no. 3, pp. 909–926, May 1998.
- [37] T. Richardson and R. Urbanke, "The capacity of low-density parity-check codes under message-passing decoding," *Information Theory, IEEE Transactions on*, vol. 47, no. 2, pp. 599–618, Feb. 2001.
- [38] S. Ten Brink, "Convergence of iterative decoding," *Electronics Letters*, vol. 35, no. 10, pp. 806–808, May 1999.
- [39] E. Casas and C. Leung, "Ofdm for data communication over mobile radio fm channels. i. analysis and experimental results," *Communications, IEEE Transactions on*, vol. 39, no. 5, pp. 783–793, May 1991.
- [40] —, "Ofdm for data communication over mobile radio fm channels. ii. performance improvement," *Communications, IEEE Transactions on*, vol. 40, no. 4, pp. 680–683, Apr. 1992.
- [41] M. de-Ridder-de Groote, R. Prasad, and J. Bons, "Analysis of new methods for broadcasting digital data to mobile terminals over an fm-channel," *Broadcasting, IEEE Transactions on*, vol. 40, no. 1, pp. 29–37, Mar. 1994.

- 
- [42] P. Scalart, M. Leclerc, P. Fortier, and H. T. Huynh, "Performance analysis of a cofdm/fm in-band digital audio broadcasting system," *Broadcasting, IEEE Transactions on*, vol. 43, no. 2, pp. 191–198, June 1997.
- [43] K. Anwar, T. Hara, M. Okada, and H. Yamamoto, "Digital terrestrial television transmission over ofdm/fm using satellite communications system," *Electron. Comm. Jpn.*, no. Pt. II, pp. 74–84, 2007.
- [44] J. Sorensen, R. Krigslund, P. Popovski, T. Akino, and T. Larsen, "Physical layer network coding for fsk systems," *Communications Letters, IEEE*, vol. 13, no. 8, pp. 597–599, Aug. 2009.
- [45] M. Valenti, D. Torrieri, and T. Ferrett, "Noncoherent physical-layer network coding with fsk modulation: Relay receiver design issues," *Communications, IEEE Transactions on*, vol. 59, no. 9, pp. 2595–2604, Sept. 2011.
- [46] T. Ferrett, H. Ochiai, and M. Valenti, "Physical-layer network coding using fsk modulation under frequency offset," May 2012, pp. 1–5.
- [47] S. Thompson, J. Proakis, and J. Zeidler, "Constant envelope binary ofdm phase modulation," in *Military Communications Conference, 2003. MILCOM '03. 2003 IEEE*, vol. 1, Oct 2003, pp. 621–626.
- [48] A. Ahmed and J. Zeidler, "Novel low-complexity receivers for constant envelope ofdm," *Signal Processing, IEEE Transactions on*, vol. 63, no. 17, pp. 4572–4582, Sept 2015.
- [49] R. Koetter and F. Kschischang, "Coding for errors and erasures in random network coding," *Information Theory, IEEE Transactions on*, vol. 54, no. 8, pp. 3579–3591, Aug. 2008.
- [50] C. E. Shannon, "Two-way communication channels," *Proceedings of the Fourth Berkeley Symposium on Mathematical Statistics and Probability, University of California*, vol. 1, pp. 611–644, 1961.
- [51] W. Su, A. K. Sadek, and K. R. Liu, "Cooperative communication protocols in wireless networks: performance analysis and optimum power allocation," *Wireless Personal Communications*, vol. 44, no. 2, pp. 181–217, 2008.

- 
- [52] C. E. Shannon, "A mathematical theory of communication," *Bell System Technical Journal*, vol. 27, pp. 379–423, 1948.
- [53] T. M. Cover and J. A. Thomas, *Elements of Information Theory*. A John Wiley & Sons, Inc.: 2nd edition, 2006.
- [54] M. Tüchler and J. Hagenauer, "Exit charts of irregular codes," in *Proc. CISS 02 (Princeton University), NJ, USA*, pp. 748–753, 2002.
- [55] T. Richardson, M. Shokrollahi, and R. Urbanke, "Design of capacity-approaching irregular low-density parity-check codes," *Information Theory, IEEE Transactions on*, vol. 47, no. 2, pp. 619–637, Feb. 2001.
- [56] C. R. Cahn, "Combined digital phase and amplitude modulation communication systems," *Communications Systems, IRE Transactions on*, vol. 8, no. 3, pp. 150–155, Sept. 1960.
- [57] C. Campopiano and B. Glazer, "A coherent digital amplitude and phase modulation scheme," *Communications Systems, IRE Transactions on*, vol. 10, no. 1, pp. 90–95, Mar. 1962.
- [58] J. G. Proakis, *Digital Communications*. McGraw Hill: 4th edition, 2001.
- [59] S. Verdú, *Multiuser Detection*. Cambridge University Press: UK, 1998.
- [60] B. Nazer and M. Gastpar, "Reliable physical layer network coding," *Proceedings of the IEEE*, vol. 99, no. 3, pp. 438–460, Mar. 2011.
- [61] S. Benedetto, D. Divsalar, G. Montorsi, and F. Pollara, "Soft-input soft-output modules for the construction and distributed iterative decoding of code networks," pp. 155–172, 1998.
- [62] J. Proakis, "Coded modulation for digital communications over rayleigh fading channels," *Oceanic Engineering, IEEE Journal of*, vol. 16, no. 1, pp. 66–73, Jan. 1991.
- [63] R. W. Hamming, "Error detecting and error correcting codes," *Bell System Tech. J. (USA: AT&T)*, no. 2, pp. 147–160, Apr. 1950.
- [64] P. Elias, "Predictive coding-i," *Information Theory, IRE Transactions on*, vol. 1, no. 1, pp. 16–24, Mar. 1955.

- 
- [65] A. Viterbi, "Error bounds for convolutional codes and an asymptotically optimum decoding algorithm," *Information Theory, IEEE Transactions on*, vol. 13, no. 2, pp. 260–269, Apr. 1967.
- [66] L. Bahl, J. Cocke, F. Jelinek, and J. Raviv, "Optimal decoding of linear codes for minimizing symbol error rate (corresp.)," *Information Theory, IEEE Transactions on*, vol. 20, no. 2, pp. 284–287, Mar. 1974.
- [67] P. Robertson, P. Hoeher, and E. Villebrun, "Optimal and sub-optimal maximum a posteriori algorithms suitable for turbo decoding," *European Transactions on Telecommunications*, vol. 8, no. 2, pp. 119–125, 1997.
- [68] J. K. Cavers and P. Ho, "Analysis of the error performance of trellis-coded modulations in rayleigh-fading channels," *Communications, IEEE Transactions on*, vol. 40, no. 1, pp. 74–83, 1992.
- [69] X. Li and J. Ritcey, "Trellis-coded modulation with bit interleaving and iterative decoding," *Selected Areas in Communications, IEEE Journal on*, vol. 17, no. 4, pp. 715–724, Apr. 1999.
- [70] M. Luby, M. Mitzenmacher, A. Shokrollah, and D. Spielman, "Analysis of low density codes and improved designs using irregular graphs," *Proceedings of the thirtieth annual ACM symposium on Theory of computing*, pp. 249–258, 1998.
- [71] H. Jin, A. Khandekar, and R. McEliece, "Irregular repeat-accumulate codes," *Proc. 2nd Int. Symp. Turbo codes and related topics*, pp. 1–8, 2000.
- [72] X. Li and J. Ritcey, "Bit-interleaved coded modulation with iterative decoding using soft feedback," *Electronics Letters*, vol. 34, no. 10, pp. 942–943, May 1998.
- [73] S. Benedetto and G. Montorsi, "Design of parallel concatenated convolutional codes," *Communications, IEEE Transactions on*, vol. 44, no. 5, pp. 591–600, May 1996.
- [74] O. Acikel and W. Ryan, "Punctured turbo-codes for bpsk/qpsk channels," *Communications, IEEE Transactions on*, vol. 47, no. 9, pp. 1315–1323, Sep 1999.

- 
- [75] A. Al-Rubaie, C. Tsimenidis, M. Johnston, and B. Sharif, "Comparison of a physical-layer network coding system with iterative coding schemes," *Wireless and Mobile Networking Conference (WMNC), 6th Joint IFIP*, pp. 1–4, Apr. 2013.
- [76] S. Ten Brink, "Convergence behavior of iteratively decoded parallel concatenated codes," *Communications, IEEE Transactions on*, vol. 49, no. 10, pp. 1727–1737, Oct. 2001.
- [77] A. Grant, "Convergence of non-binary iterative decoding," *Global Telecommunications Conference, GLOBECOM '01. IEEE*, vol. 2, pp. 1058–1062, 2001.
- [78] P. Billingsley, *Probability and Measure*. New York, Toronto, London: John Wiley & Sons: 3rd edition, 1995.
- [79] F. Brannstrom, L. Rasmussen, and A. Grant, "Convergence analysis and optimal scheduling for multiple concatenated codes," *Information Theory, IEEE Transactions on*, vol. 51, no. 9, pp. 3354–3364, Sept. 2005.
- [80] M. Tuchler, S. T. Brink, and J. Hagenauer, "Measures for tracing convergence of iterative decoding algorithms," in *Proc. 4th IEEE/ITG Conf. on Source and Channel Coding*, pp. 53–60, 2002.
- [81] C. Shah, C. Tsimenidis, B. Sharif, and J. Neasham, "Exit chart analysis of bicm-id based receiver for shallow underwater acoustic communications," in *Wireless Communication Systems (ISWCS), 2010 7th International Symposium on*, Sept 2010, pp. 6–10.
- [82] S. ten Brink, G. Kramer, and A. Ashikhmin, "Design of low-density parity-check codes for modulation and detection," *Communications, IEEE Transactions on*, vol. 52, no. 4, pp. 670–678, Apr. 2004.
- [83] A. Ashikhmin, G. Kramer, and S. ten Brink, "Extrinsic information transfer functions: model and erasure channel properties," *Information Theory, IEEE Transactions on*, vol. 50, no. 11, pp. 2657–2673, Nov. 2004.
- [84] S.-Y. Chung, T. Richardson, and R. Urbanke, "Analysis of sum-product decoding of low-density parity-check codes using a gaussian approximation,"

- 
- Information Theory, IEEE Transactions on*, vol. 47, no. 2, pp. 657–670, Feb. 2001.
- [85] I. Land, P. A. Hoeher, and J. Huber, “Analytical derivation of exit charts for simple block codes and for ldpc codes using information combining,” *Information and Coding Theory Lab, Faculty of Engineering, University of Kiel, Germany*, 2004.
- [86] A. Al-Rubaie, C. Tsimenidis, M. Johnston, and B. Sharif, “Performance and exit chart analysis of bicm-id for physical layer network coding,” *Electronics, Circuits, and Systems (ICECS), IEEE 20th International Conference on*, pp. 205–208, Dec. 2013.
- [87] S. Haykin, *Communication Systems*. John Wiley & Sons, Inc., USA: 4th edition, 2000.
- [88] D. Gabor, “Theory of communication. part 1: The analysis of information,” *Electrical Engineers - Part III: Radio and Communication Engineering, Journal of the Institution of*, vol. 93, no. 26, pp. 429–441, Nov. 1946.
- [89] A. V. Oppenheim and R. W. Schaffer, *Discrete-Time Signal Processing*. Prentice-Hall International, Inc.: 3rd edition, 2010.
- [90] F. Castanie, *Digital Spectral Analysis*. John Wiley & Sons, Inc., 2011.
- [91] F. W. King, *Hilbert Transforms*. Cambridge university press: Volume-1, 2009.
- [92] B. P. Lathi, *Modern Digital and Analog Communication Systems*. Oxford university press: 3rd edition, 1998.
- [93] R. B. Randall, *Frequency Analysis*. Bruel & Kjaer, Naerum: 3rd edition, 1987.
- [94] S. L. Hahn, *Hilbert Transform in Signal Processing*, Artech House Signal Processing Library, 1996.
- [95] J. Marple, S.L., “Computing the discrete-time analytic signal via fft,” *Signal Processing, IEEE Transactions on*, vol. 47, no. 9, pp. 2600–2603, Sep. 1999.
- [96] R. N. Bracewell, *The Fourier Transform and Its Applications*. New York: McGraw-Hill, Inc., 1965.

- [97] R. L. Rabiner and B. Gold, *Theory and Application of Digital Signal Processing*. Englewood Cliffs, N. J.: Prentice-Hall, Inc., 1975.
- [98] R. Sadr and W. J. Hurd, *Detection of Signals by the Digital Integrate-and-Dump Filter with Offset Sampling*. Communication System Research Section: TDA Progress Report, 1987.
- [99] J. Tropp, J. Laska, M. Duarte, J. Romberg, and R. Baraniuk, “Beyond nyquist: Efficient sampling of sparse bandlimited signals,” *Information Theory, IEEE Transactions on*, vol. 56, no. 1, pp. 520–544, Jan. 2010.
- [100] S. Thompson, A. Ahmed, J. Proakis, and J. Zeidler, “Constant envelope ofdm phase modulation: spectral containment, signal space properties and performance,” in *Military Communications Conference, 2004. MILCOM 2004. 2004 IEEE*, vol. 2, Oct 2004, pp. 1129–1135.
- [101] W. Zhang and M. Miller, “Baseband equivalents in digital communication system simulation,” *Education, IEEE Transactions on*, vol. 35, no. 4, pp. 376–382, Nov. 1992.